REDOX PROPERTIES OF BIS-TRIARYLAMINES AND

LIGAND PROPERTIES OF THIANTHRENOPHANE

Dissertation zur Erlangung des

naturwissenschaftlichen Doktorgrades

der Bayerischen Julius-Maximilians-Universität Würzburg

vorgelegt von

STEPHAN AMTHOR

aus Schweinfurt

Würzburg 2005

Promotionsgesuch eingereicht am: _____

bei der Fakultät für Chemie und Pharmazie

1. Gutachter: _____

2. Gutachter: _____

der Dissertation

1. Prüfer: _____

2. Prüfer: _____

3. Prüfer: _____

des Öffentlichen Promotionskolloquiums

Tag des Öffentlichen Promotionskolloquiums:_____

Doktorurkunde ausgehändigt am: _____

Mein besonderer Dank gilt

Herrn Prof. Dr. Christoph Lambert

für die Vergabe des Themas, die Förderung und das mit vielen Anregungen und Diskussionen verbundene Interesse an dieser Arbeit.
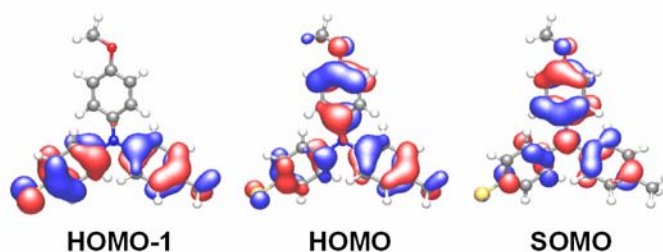
Abbreviations

14-ane-S4	1,4,8,11-tetrathiacyclotetradecane
AM1	*Austin* model 1
An	4-anisyl (= 4-methoxyphenyl)
BFGS	*Broyden-Fletcher-Goldfarb-Shanno* method
CISD	configuration interaction singles and doubles
CR	charge resonance
CT	charge transfer
CV	cyclic voltammetry / cyclic voltammogram
eq	equation
ESR	electron spin resonance
ET	electron transfer
Fc	ferrocene
GMH	generalized *Mulliken-Hush*
HOMO	highest occupied molecular orbital
HT	hole transfer
IVCT	inter-valence charge transfer
LUMO	lowest unoccupied molecular orbital
MV	mixed-valence
NIR	near infrared
NN	nearest neighborhood
PES	potential energy surface
sh	shoulder
SOMO	semi-occupied molecular orbital
TAPD	N,N,N',N'-tetra-(4-anisyl)phenylenediamine
Tara	triarylamine
TBAH	tetrabutylammonium hexafluorophosphate
UV	ultraviolet
Vis	visible

CONTENTS

INTRODUCTION

Photoinduced electron transfer plays a fundamental role in several biological processes as e.g. the photosynthesis. Bacteria and plants use photosynthesis to convert the energy of daylight to electrical energy which generates reactive molecules as energy store. The conversion of solar energy in electrical energy is of fundamental scientific interest. In this framework the study of photoinduced electron transfer in artificial model compounds which mimic biological systems is very essential.[1]

In this thesis I will focus on optically induced and photoinduced charge transfer processes of donor-bridge-donor D-B-D, donor-bridge-acceptor D-B-A as well as acceptor-bridge-acceptor A-B-A compounds. Such triads are generally composed of a bridging unit that connects two similar or different chromophores which are either electron withdrawing or electron donating. Redox active chromophores X that are stable in at least two redox states bear a great advantage in this context. If the neutral redox active chromophor X is a donor, it can in principle be transferred into an electron accepting cation X^+ unit by oxidation, if X^+ is sufficiently stable. This basic concept will be used in the framework of this thesis. A set of very similar X-B-X systems facilitate the investigation of all three kinds of triads by varying the oxidation states:

a) Neutral X-B-X triads can be understood as D-B-D compounds.
b) X^+-B-X^+ dications are A-B-A triads.
c) Singly oxidized species X-B-X^+ are a special type of a D-B-A triad.

The mono cations of the general type X-B-X^+ are so called mixed-valence (MV) compounds that are of considerable interest for studying intramolecular hole transfer processes. MV compounds generally show an intervalence charge transfer (IV-CT) transition in the optical absorption spectrum. By means of the *Mulliken-Hush* theory the analyses of IV-CT absorption bands directly yield electron transfer (ET) parameters which give an insight into the intramolecular ET processes.[2] The bridge may have a significant influence on the charge transfer processes in all three kinds of triads a), b) and c). If π-conjugated bridges are compared with partially saturated bridges with a broken conjugation, pronounced differences concerning charge transfer processes are expected. For example the [2.2]paracyclophane unit

has no direct conjugation but, nevertheless, interactions between the layered π-systems by through-space (π-π) and through-bond (σ) coupling may be significant as the two bent benzene rings are in very close contact.[3]

Although the investigation of [2.2]paracyclophanes started already more than fifty years ago, there is still an unabated attention to this compounds. Not only the chemical and physical properties of [2.2]paracyclophanes are very interesting, but also the industrial use e.g. for chemical vapour deposition polymerisation established new fields of applications. Nevertheless, cyclophane chemistry is of course not restricted to [2.2]paracyclophanes. A vast number of new compounds e.g. cyclophanes that consist of heterocycles instead of benzene rings have been synthesized. Furthermore, one has to notice that over the past years the focus in "cyclophane chemistry" has changed from pure electronic and structural properties to the investigation of the function and application of cyclophanes such as e.g. the host–guest chemistry.[3]

After this short preamble, the aims of this doctoral thesis will be presented in the following. This work is divided in five self-contained chapters that include separated introductions, that provide an insight into the corresponding topics. The most relevant literature is, therefore, cited in these introductions.

The first topic of this thesis was to get a detailed and fundamental insight into the linear optical properties of small triarylamines, which are potential redox chromophores for the synthesis of X-B-X triades. Therefore, the redox properties and the linear optical properties of neutral and oxidized triarylamines will be introduced in chapter I.[4]

The second intention of this thesis was to connect two triarylamine redox chromophores X via varying bridging units, in order to obtain neutral triads of the type X-B-X. These neutral compounds should be the starting point for the investigation of optically induced charge transfer processes in all three kinds of triads a), b) and c). Therefore, the neutral species X-B-X should be successively oxidized to the corresponding mono cations X-B-X$^+$ and to the dications X$^+$-B-X$^+$. The influence of the bridge on the optical properties of the triads in all three redox states ought to be investigated and analyzed. In particular, the [2.2]paracyclophane bridge should be compared with π-conjugated bridges as e.g. *p*-xylene. Furthermore, the properties of the triads should be compared with that of the corresponding dyads X-B^{n+} (n = 0, 1). Each chapter (II-IV) of this thesis attends to one of the three redox states: The neutral donor-bridge-donor compounds X-B-X will be discussed in chapter II,[5] the

donor-bridge-acceptor mono cations X-B-X$^+$ will be introduced in chapter III[6] and the acceptor-bridge-acceptor dications X$^+$-B-X$^+$ will be presented in chapter IV[7].

The third aim of this work was the investigation of the ligand properties of a cyclophane that is built up from two thianthrene units. The design of this thianthrenophane should offer both exohedral sulfur coordination sites to soft metal ions, as well as endohedral π-face coordination. Thus, the ligand properties of thianthrenophane to silver(I) ions ought to be probed by UV/Vis titration experiments. Furthermore, the transport capabilities of silver(I) ions through liquid membranes in comparison with other soft metal ions and in comparison with thianthrene parent compound and 1,4,8,11-tetrathiacyclotetradecane should be tested.[8]

References

(1)   Balzani, V., Ed. *Electron Transfer in Chemistry*; VCH: Weinheim, 2001; Vol. 1-5.

(2)   Brunschwig, B. S.; Sutin, N. In *Electron Transfer in Chemistry*; 1 ed.; Balzani, V., Ed.; VCH: Weinheim, 2001; Vol. 2, pp 583-617.

(3)   Gleiter, R.; Hopf, H., Eds. *Modern Cyclophane Chemistry*; VCH: Weinheim, 2004.

(4)   Amthor, S.; Noller, B.; Lambert, C. *Chem. Phys.* **2005**, *316*, 141-152.

(5)   Amthor, S.; Dümmler, S.; Fischer, I.; Lambert, C.; Schelter, J. *Excited Mixed-Valence States of Symmetrical Donor-Acceptor-Donor π-Systems* **2005**, manuscript submitted to *J. Phys. Chem. A*.

(6)   Amthor, S.; Lambert, C. *[2.2]Paracyclophane Bridged Mixed-Valence Compounds: Application of a GMH Three-Level Model* **2005**, manuscript submitted to *J. Phys. Chem. A*.

(7)   Amthor, S.; Lambert, C. *Dications of Bis-triarylamino-[2.2]paracyclophanes: Evaluation of Excited State Couplings by GMH Analysis* **2005**, manuscript submitted to *J. Phys. Chem. A*.

(8)   Amthor, S.; Lambert, C.; Graser, B.; Leusser, D.; Selinka, C.; Stalke, D. *Org. Biomol. Chem.* **2004**, *2*, 2897-2901.

UV/Vis/NIR Spectral Properties of Triarylamines and their Corresponding Radical Cations

CONTENTS

1 Introduction

Triarylamines possess a wide range of application due to their outstanding physical, photochemical and electrochemical properties. Being efficient hole conductors triarylamines (*Taras*) are commonly used as photoconductors in the Xerox® process in laser printers and photocopiers.[1-4] Aromatic amines also find application in organic light emitting devices[2-11], polymer batteries[12,13], photorefractive materials for optical data storage[14] and in electrochromic polymers[15], e.g., for anti-glare electrochromic mirrors. Furthermore, *Taras* are used as mild oxidation agents and as catalysts for redox reactions.[16]

The intermolecular electron-transfer between *Tara* and the corresponding *Tara*[•+] is another interesting property which was investigated by ESR measurements.[17] A relatively new field of research is the use of *Tara* redox centres in organic mixed-valence compounds in order to investigate intramolecular electron-transfer processes.[18-25] Thanks to the outstanding properties of *Taras* purely organic intervalence compounds have several advantages compared to, e.g., inorganic and organometallic mixed-valence compounds.[26,27] *Taras* with substituents in their *para*-position generally show reversible one electron oxidation behaviour.[16,28-30] Variation of the substituents at the aryl moieties of *Taras* allows the easy adjustment of the oxidation potential.[16,28,31] Another feature of *Taras* and their corresponding radical cations is that both species exhibit a very similar propeller-like structure (Fig. 1).[32,33] Thus, the inner reorganisation energy of bis(*Tara*) mixed-valence compounds is rather small compared to the reorganisation energy of many other redox systems.[34-36] Consequently, mixed-valence compounds based on bis(*Tara*) mono radical cations show a rather intense IV-CT band in the NIR region which is well separated from other absorption bands such as the localised π-π^* absorption of the oxidised *Tara*[•+] unit.[18-25] This facilitates the analysis of the optical electron transfer processes in bis(*Tara*) mixed-valence compounds and even allows the analysis of their electron transfer systems by a three-level model[37,38] which also takes bridge localised states into consideration.[24,25]

Thanks to their "stability" (persistence) several *Tara*[•+] radical cations are already described in the literature and characterised, e.g., by cyclic voltammetry[16,28-30], ESR[28,39-42] and UV/Vis-spectroscopy[16,30,31,39,41,42].

	R_1	R_2	R_3
1	OMe	OMe	OMe
2	Me	Me	Me
3	Me	OMe	OMe
4	Me	Cl	Cl
5	OMe	Me	Me
6	OMe	Cl	Cl
7	Cl	Me	Me
8	Cl	OMe	OMe
9	Cl	Cl	Cl
10	Cl	OMe	Me
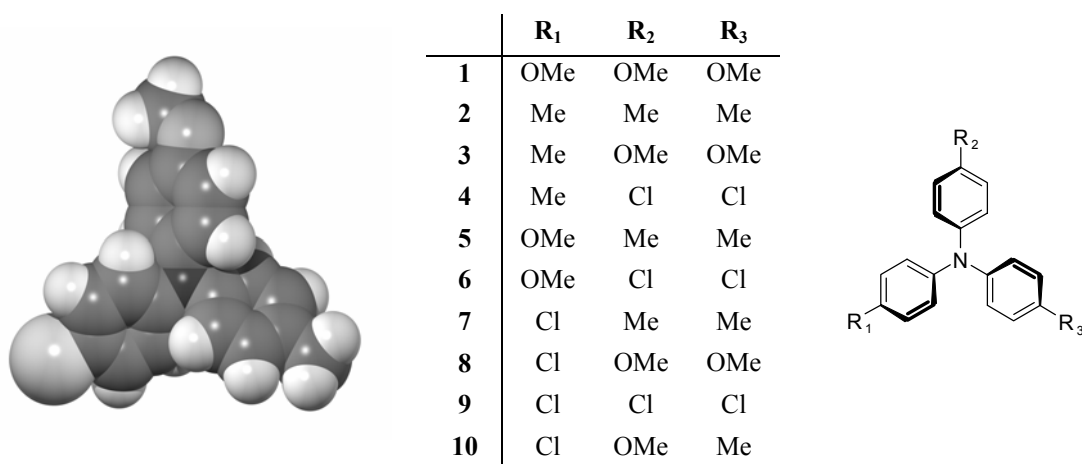
Fig. 1. AM1-calculated structure of **10** and *Taras* with all possible permutations of substituents Cl, OMe and Me in all *para*-postions.

However, a general picture of the electronic and optical properties of simple substituted triarylamines is still lacking. In order to gain a more detailed insight into the linear optical properties of *Taras* and their corresponding radical cations and dications and the dependence of these properties on weak perturbations by *para*-substituents, a set of triphenylamine derivatives with all permutations of Cl, OMe and Me in all three *para*-positions to the nitrogen atom (Fig. 1) was synthesised. The electrochemical behaviour and, in particular, the oxidation potential and the long-term reversibility of the oxidations of all ten *Taras* were investigated by cyclic voltammetry. The UV/Vis/NIR spectra of the neutral compounds and their corresponding radical cations were measured in CH_2Cl_2 and MeCN and the resulting absorption energies and oscillator strengths were compared to values obtained by AM1-CISD calculations. The UV/Vis/NIR spectrum of the dication 1^{2+} was measured by spectroelectrochemistry and the transition energy and oscillator strength of the lowest energy absorption was also compared to AM1-CISD computed values.

2   Synthesis and experimental methods

2.1   Synthesis

The *Taras* **1-9** have been synthesised by copper catalysed *Ullmann* coupling[43] of two equivalents of 4-iodobenzene derivatives with the 4-aniline derivatives shown in Scheme 1.

	R_1	R_2
1	OMe	OMe
2	Me	Me
3	Me	OMe
4	Me	Cl
5	OMe	Me
6	OMe	Cl
7	Cl	Me
8	Cl	OMe
9	Cl	Cl
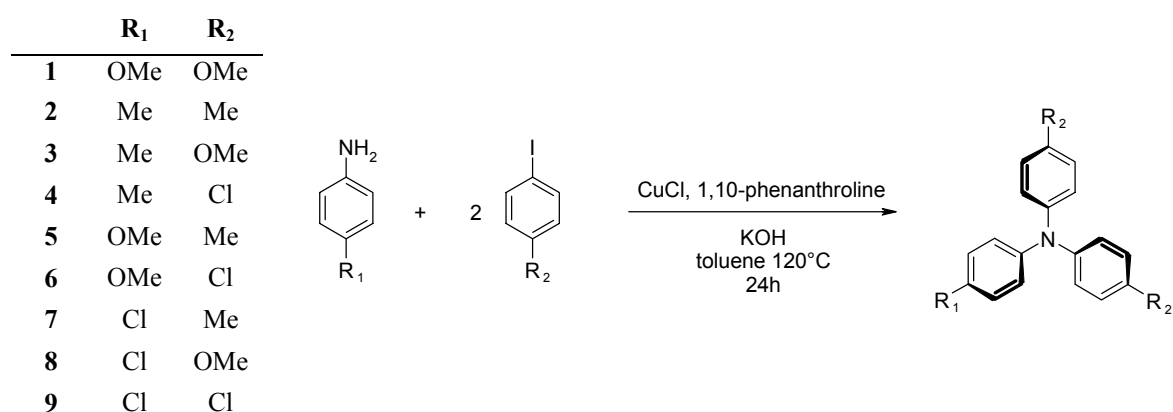
Scheme 1. Synthesis of *Taras* **1-9**.

In order to synthesise the *Tara* **10** with three different substituents in the *para*-positions, first 4-chloroaniline was coupled with only one equivalent of 4-iodotoluene which yields the diarylamine which was subsequently coupled with one equivalent of 4-iodoanisole (Scheme 2).
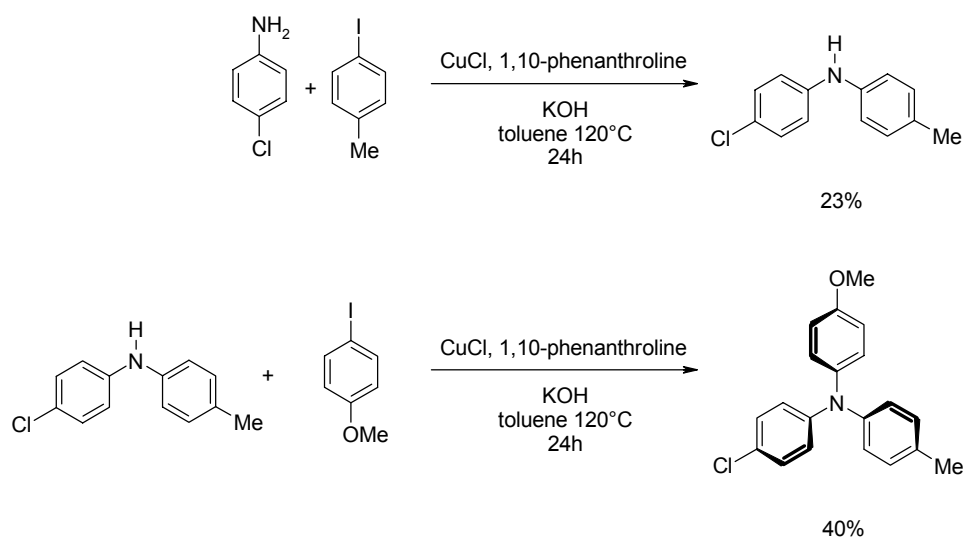
Scheme 2. Synthesis of *N*-(4-chlorophenyl)-*N*-(4-methoxyphenyl)-*N*-(4-methylphenyl)-amine (**10**).

2.2   Electrochemistry

The electrochemical experiments were performed in superdry, argon-saturated CH_2Cl_2 with 0.15 M tetrabutylammonium hexafluorophosphate (TBAH) as supporting electrolyte and ca. 0.002 M substrate using a conventional three-electrode set-up with platinum disk electrode (0.12 cm^2). The potentials are referenced against ferrocene (Fc/Fc$^+$). The long-term reversibility of the processes was checked by performing multi-cycle thin-layer measurements at 10 mV s^{-1} scanning speed.

2.3   Spectroelectrochemistry

The solution of the cyclic voltammetry experiment was transferred into a spectroelectrochemical optical transparent thin-layer cell (optical path length of 100 μm with a gold minigrid working electrode) described in ref. [44]. UV/Vis/NIR spectra were recorded at a constant potential in the thin layer arrangement referenced against a Ag/AgCl electrode. The potential was increased in 20 to 100 mV steps, and spectra were recorded until the two oxidative processes in CH_2Cl_2 were fully covered. Back reduction was also performed in order to prove the reversibility of the whole process. The UV/Vis/NIR spectra obtained were analysed by global least squares data fitting by the Levenberg-Marquardt method using SPECFIT/32^{TM} software.[45]

2.4   UV/Vis/NIR spectroscopy

The UV/Vis/NIR spectra of the radical cations $\mathbf{1^{\bullet+}}$-$\mathbf{10^{\bullet+}}$ in MeCN were obtained by stepwise addition of 10^{-2}-10^{-3} M NOBF$_4$/MeCN via a microlitre syringe to a solution of the *Taras* **1-10** (3 to 7·10^{-5} M). Because the electron transfer (ET) is rather slow using NOBF$_4$ in MeCN one has to wait approximately 30 min after each addition before the spectrum could be recorded. The extinction coefficients obtained in MeCN are too small due to the slight instability of the radical cations under the conditions employed. The spectra of $\mathbf{1^{\bullet+}}$-$\mathbf{10^{\bullet+}}$ in CH_2Cl_2 were

obtained by dropwise addition of 10^{-2}-10^{-3} M $SbCl_5$/CH_2Cl_2 in the same way. The quick oxidation process in CH_2Cl_2 allows very short periods between the addition of oxidation agent and spectrum measurement. The spectra of the neutral *Taras* in CH_2Cl_2 were analysed by integration of the absorption signal.

$$f = \frac{8 \ln(10) \cdot m_e \cdot c^2 \cdot \varepsilon_0}{2000 N \cdot e^2} \cdot \frac{9n}{(n^2 + 2)^2} \int \varepsilon d\tilde{\nu} \tag{1}$$

$$\tilde{\nu}_{abs} = \frac{\int \varepsilon d\tilde{\nu}}{\int \varepsilon \cdot \tilde{\nu}^{-1} d\tilde{\nu}} \tag{2}$$

The absorption bands of the *Tara*$^{\bullet+}$ radical cations in CH_2Cl_2 were analysed by fitting two gaussian bands to each transition. The oscillator strengths of all transitions recorded in CH_2Cl_2 were calculated by equation (1). The averaged reduced absorption energy $\tilde{\nu}_{abs}$ which is defined by equation (2) was also obtained from the band fits whereas $\tilde{\nu}_{max}$ is the wavenumber at maximum extinction.

2.5   *AM1-CISD calculations*

As AM1 computations proved to be a reasonably good and cost efficient alternative to DFT computations concerning triarylamine radical cations[46], semiempirical AM1 parameterisation implemented in the MOPAC97 program was used throughout this chapter.[47] The optimisation of **1**, **2**, **7-9** and the corresponding radical cations were performed with symmetry restrictions (see Table 2) by the BFGS method. The symmetry broken structures of **1**$^{\bullet+}$, **2**$^{\bullet+}$, **9**$^{\bullet+}$ were obtained by modification of the dihedral angles in the z-matrices of the corresponding higher symmetric structures. To examine the results of this geometry, a single SCF cycle was computed without further geometry optimisation. The remaining structures were optimised without symmetry restrictions in Cartesian coordinates by the BFGS method (**3-6**, **10** and their corresponding radical cations). The configuration interaction included singles and doubles excitations (CISD) within an active orbital window comprising the three highest doubly occupied, and the three lowest unoccupied orbitals for the neutral *Taras*; the four

highest doubly occupied, one singly occupied, and the two lowest unoccupied orbitals for the radical cations; and the five highest doubly occupied, and the five lowest unoccupied orbitals for 1^{2+}. Only the geometry optimisations of the radical cations were performed at CISD level while the geometries of the neutral *Taras* were performed at HF level.[48]

3   Results and Discussion

3.1   Cyclic voltammetry

The cyclic voltammograms of **1** and **10** in CH_2Cl_2 at 250 mV s^{-1} are shown in Fig. 2. The half wave potentials of the first oxidation wave observed for all ten compounds are given in Table 1; the second oxidation process was observed at $E_{1/2}(II)$ = 860 mV for tri-4-anisyl-amine **1** only.
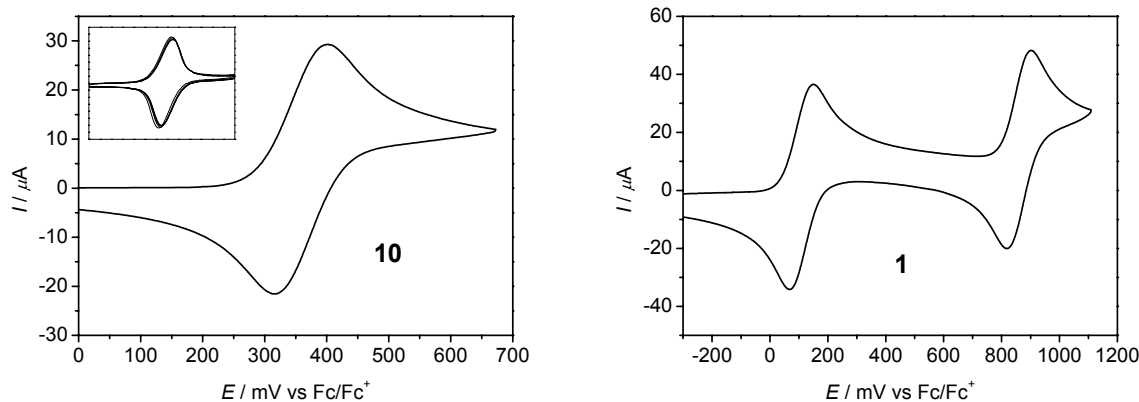
Fig. 2. Cyclic voltammograms in CH_2Cl_2 (TBAH) at v = 250 mV s^{-1} (inset: multi-cycle thin-layer CV of **10** at v = 10 mV s^{-1}).

All tris-*para*-substituted triphenylamines **1-10** show generally chemically and electrochemically reversible first oxidation waves in their cyclic voltammograms. This was shown by multi-cycle thin-layer cylovoltammetry.

Table 1

First oxidation potential of *Taras* **1-10** vs ferrocene (Fc/Fc$^+$) in CH_2Cl_2 (TBAH) at $v = 250$ mV s^{-1}.

	1	**2**	**3**	**4**	**5**	**6**	**7**	**8**	**9**	**10**
$E_{1/2}$(I) / mV	109	332	180	576	250	463	460	290	691	359

As expected the Cl-, OMe- and Me-substituents show a great influence on the redox potential $E_{1/2}$(I) of the first oxidation waves (see Table 1). Chloro substituents shift the oxidation potential to higher values while methoxy groups cause a shift to lower oxidation potentials. The redox potentials $E_{1/2}$(I) of the first oxidation waves correlate linearly with the number of Cl- and OMe-substituents (n[Cl] and n[OMe]). The empirical equation (3) is a good approximation for the calculation of $E_{1/2}$(I) values of **1** and **3-10** in comparison to tri-4-tolylamine **2**.

$$E_{1/2}(I) \approx 332 + 110 \cdot n[Cl] - 75 \cdot n[OMe] \tag{3}$$

This relationship proves additive electronic influence of the substituents on the oxidation potential of *Taras*. In the series investigated here tri-4-anisylamine **1** is the Tara with the lowest oxidation potential. From this compound one can also observe a second reversible oxidation process at 860 mV which yields **1**$^{2+}$.

3.2   Linear optical properties of neutral triarylamines

The absorption spectra of the neutral *Taras* **1** and **9** in CH_2Cl_2 are shown in Fig. 3 and are typical of *Taras*. The spectra of **1-10** are characterised by a single intense absorption between 32890 and 33980 cm^{-1} (Table 2) which is well separated from higher energy transitions.
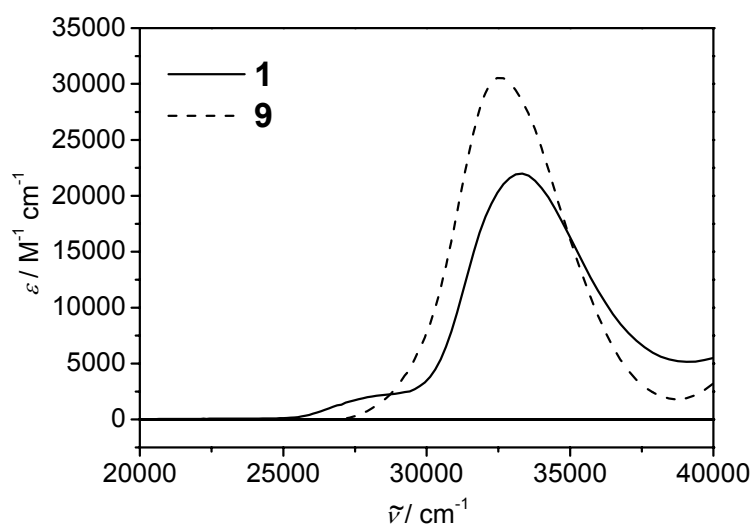
Fig. 3. UV/Vis absorption spectra of *Taras* **1** and **9** in CH_2Cl_2.

The full width at half maximum varies from 4300 to 5800 cm^{-1}. In general, the broader bands are observed in the more polar solvent MeCN and for asymmetrical compounds. This general tendency has two exceptions, **1** shows a relatively broad signal although C_3 symmetry is supposed while **5** exhibits a relatively small band width.

Concerning the substituent pattern the following tendencies can be observed. Starting from tri-4-tolylamine **2** each substitution of a methyl group by a methoxy group leads to a hypsochromic shift while the substitution by a chloro atom leads to a bathochromic shift of the absorption band. The oscillator strength f of the absorption band does not depend on the solvent but all absorption energies are slightly blue shifted (340-640 cm^{-1}) in MeCN relative to the energies in CH_2Cl_2 which suggests a minor CT character of the electronic transition. The experimental absorption energies are in good agreement with AM1-CISD calculated

transition energies while the computed oscillator strengths are more than twice the experimental oscillator strengths.

Table 2

Experimental excitation energies and full width at half maximum of the neutral *Taras* in MeCN and CH_2Cl_2 and oscillator strengths in CH_2Cl_2 in comparison to the AM1-CISD calculated values.

		experiment					theory		
		$\tilde{\nu}_{max}$ /cm^{-1} MeCN	$\Delta\tilde{\nu}_{1/2}$ /cm^{-1} MeCN	$\tilde{\nu}_{max}$ /cm^{-1} CH_2Cl_2	$\Delta\tilde{\nu}_{1/2}$ /cm^{-1} CH_2Cl_2	oscillator strength CH_2Cl_2	$\tilde{\nu}$ /cm^{-1}	oscillator strengh	transition
1	C_3	33780	4900	33330	4800	0.40	32100	1.04	$S_0(A){\rightarrow}S_1(E)$
2	C_3	33460	4600	33030	4500	0.43	31630	0.98	$S_0(A){\rightarrow}S_1(E)$
3	C_1	33820	5000	33280	4800	0.43	31920 32060	0.52 0.50	$S_0(A){\rightarrow}S_1(A)$ $S_0(A){\rightarrow}S_2(A)$
4	C_1	33230	5000	32890	4800	0.44	30900 32090	0.53 0.48	$S_0(A){\rightarrow}S_1(A)$ $S_0(A){\rightarrow}S_2(A)$
5	C_1	33640	4700	33180	4600	0.44	31800 32000	0.47 0.50	$S_0(A){\rightarrow}S_1(A)$ $S_0(A){\rightarrow}S_2(A)$
6	C_1	33370	5600	33090	5500	0.46	30750 32150	0.55 0.48	$S_0(A){\rightarrow}S_1(A)$ $S_0(A){\rightarrow}S_2(A)$
7	C_2	33490	4800	33080	4800	0.44	31130 32260	0.51 0.43	$S_0(A){\rightarrow}S_1(A)$ $S_0(A){\rightarrow}S_2(B)$
8	C_2	33980	5800	33340	5400	0.47	30760 32180	0.53 0.51	$S_0(A){\rightarrow}S_1(A)$ $S_0(A){\rightarrow}S_2(B)$
9	D_3	32900	4400	32530	4300	0.50	31380	1.02	$S_0(A_1){\rightarrow}S_1(E)$
10	C_1	33760	5300	33300	5200	0.43	30950 32260	0.52 0.48	$S_0(A){\rightarrow}S_1(A)$ $S_0(A){\rightarrow}S_2(A)$

The absorption properties of the neutral species with a C_3 symmetry axis (**1**, **2** and **9**)[49] can be explained by one intense HOMO$\rightarrow$LUMO ($S_0{\rightarrow}S_1$) excitation into a degenerate (E) S_1 state. Breaking the C_3 symmetry results in a splitting of the degenerate LUMO orbitals and, consequently, in a splitting of the degenerate S_1 state. Thus, all *Taras* without C_3 axis exhibit two transitions, one corresponding to a HOMO$\rightarrow$LUMO ($S_0{\rightarrow}S_1$) excitation and the other to a HOMO$\rightarrow$LUMO+1 ($S_0{\rightarrow}S_2$) excitation (see Fig. 4). The intensity of these two transitions approximately sums up to the one of the degenerate transition in **1**, **2**, and **9**.
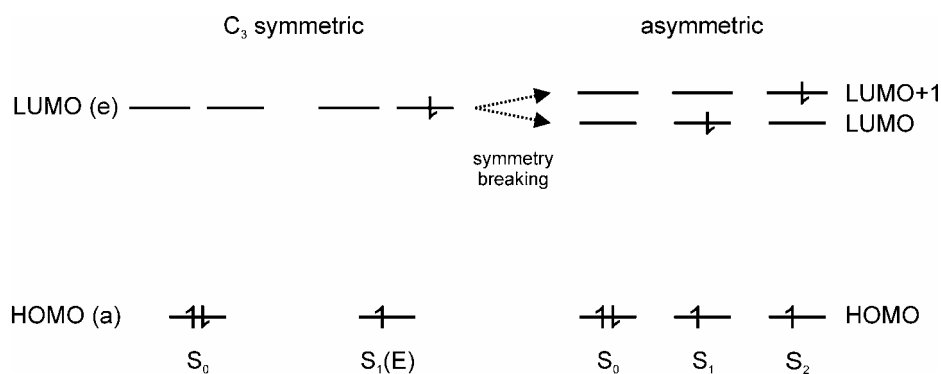
Fig. 4. Configuration diagram for the ground state and excited state of a neutral symmetric *Tara* and the ground state and excited states of an asymmetric *Tara*.

The experimental spectra of *Taras* **1**, **2**, **3**, **5**, **8**, and **10** show weak shoulders on the red edge of the main absorption signal. The AM1-CISD calculations within an active orbital window comprising the three highest doubly occupied, and the three lowest unoccupied orbitals give no explanation for the observed shoulders. The use of a larger active orbital window with the five highest doubly occupied, and the five lowest unoccupied orbitals causes an exchange of the energetic order of the CISD calculated states in some cases: The calculation of tri-4-anisylamine using the smaller active orbital window yields an S_1 state with a high oscillator strength (HOMO$\rightarrow$LUMO excitation) and an S_2 state with a weak oscillator strength. In contrast, the larger active orbital window results in the exchange of both states S_1 and S_2. This result would explain the weak shoulder in the absorption spectrum of **1**. However, the use of the larger active orbital window for the calculations of **2**, **3**, **5**, **8**, and **10** did not lead to an exchange of state energies which could explain shoulders in the corresponding spectra.

The band width of the spectra should give information about the character of the transitions. A single transition to a degenerate state should lead to smaller band width than two transitions with slightly different transition energies. The experimental half widths are generally in good agreement with these expectations since the symmetric molecules **2** and **9** with degenerate S_1 states show the narrowest UV absorption bands. However the third triarylamine **1** with C_3 symmetry axis shows a relatively broad signal. This may be explained by symmetry breaking in solution which leads to a splitting of the degenerate S_1 state, and, consequently, to a broadening of the absorption signal (see also 3.3). The UV spectrum of **5** exhibits a relatively narrow signal. This behaviour is explained by the small splitting between the S_1 and S_2 states which is only 200 cm^{-1} according to the computation.
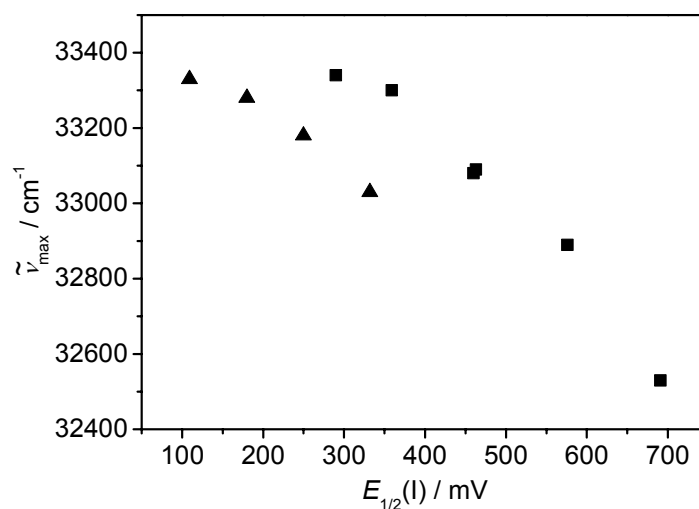
Fig. 5. Plot of the absorption energy of the neutral amines **1-10** versus oxidation potential $E_{1/2}(I)$. The *Taras* represented by squares have at least one chloro substituent while those represented by triangles have no chloro substituents.

A plot of the absorption energy versus the half wave potential $E_{1/2}(I)$ (Fig. 5) reveals two correlations: one for compounds **1**, **2**, **3** and **5** solely substituted with methyl and methoxy groups (triangles) and one for the remaining amines **4** and **6-10** (squares) with at least one chloro substituent. The half wave oxidation potential is approximately a relative measure for the energy of the HOMO of a compound and the transition energy is given by the difference between HOMO and LUMO/LUMO+1. Since chloro substituents as acceptors reveal the most significant influence presented by the decrease of the energies of LUMO and LUMO+1 the division into two groups of compounds with and without chloro substituents can be understood.

3.3 Linear optical properties of triarylamine radical cations

The absorption spectra of the mono radical cations **1**$^{•+}$ and **9**$^{•+}$ are shown in Fig. 6 as an example. All radical cations **1**$^{•+}$-**10**$^{•+}$ exhibit an intense absorption signal at 13100-14990 cm^{-1} and a second less intense and broader band at 15300-17570 cm^{-1}. A blue shift (170-660 cm^{-1}) of both absorption signals in MeCN relative to the energies in CH$_2$Cl$_2$ suggests a minor CT

character in the electronic transitions. Although all spectra were recorded in solution a very weak vibrational fine structure of both transitions can be observed (Fig. 6).

(a)   (b)
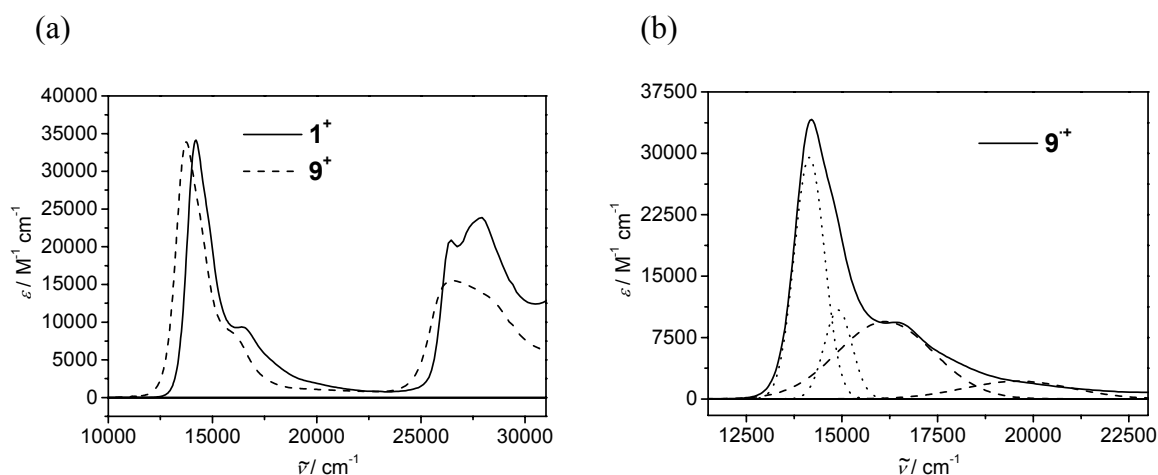
Fig. 6. (a) Experimental spectrum of $1^{\bullet+}$ and $9^{\bullet+}$ in CH_2Cl_2 and (b) deconvolution by four Gaussian functions ($D_0 \rightarrow D_1$ dotted lines, $D_0 \rightarrow D_2$ dashed lines).

In order to yield the oscillator strengths of the two absorption bands in total four Gaussian functions were used for fitting the spectra recorded in CH_2Cl_2.

In accordance with the literature both chloro substituents and methoxy groups shift the absorption maximum to lower energies caused by the extension of the π-system (Table 3).[16,39,41] The symmetrical *Tara* radical cations $1^{\bullet+}$ and $9^{\bullet+}$ are an exception to the general tendency because both radical cations show a longest wavelength absorption maximum at higher energies than expected.

Comparison of the experimental results with the AM1-CISD computed values shows that all theoretical oscillator strengths are distinctly higher but their general dependence on the substituent pattern is well described by the calculations. The experimental absorption energies are in reasonably good agreement with the theoretical energy values.

Table 3

Experimental excitation energies of the *Tara*[•+] radical cations in MeCN and CH_2Cl_2 and oscillator strengths in CH_2Cl_2 in comparison to the AM1-CISD calculated values.

		experiment				theory		
		$\widetilde{\nu}_{max}$ /cm^{-1} MeCN	$\widetilde{\nu}_{max}$ /cm^{-1} CH_2Cl_2	$\widetilde{\nu}_{abs}$ /cm^{-1} CH_2Cl_2	oscillator strength CH_2Cl_2	$\widetilde{\nu}$ /cm^{-1}	oscillator strength	transition
1[•+]	C_1[a]	13930	13740	13820	0.15	14550	0.25	$D_0(A) \rightarrow D_1(A)$
		15800	15300	15580	0.09	15610	0.23	$D_0(A) \rightarrow D_2(A)$
2[•+]	C_1[a]	14990	14820	14930	0.11	15570	0.25	$D_0(A) \rightarrow D_1(A)$
		17360	17150	17050	0.09	16650	0.21	$D_0(A) \rightarrow D_2(A)$
3[•+]	C_1	13790	13510	13670	0.17	13950	0.29	$D_0(A) \rightarrow D_1(A)$
		16950	16540	16470	0.10	17300	0.22	$D_0(A) \rightarrow D_2(A)$
4[•+]	C_1	14680	14380	14540	0.13	15610	0.27	$D_0(A) \rightarrow D_1(A)$
		17460	16800	17000	0.09	16050	0.26	$D_0(A) \rightarrow D_2(A)$
5[•+]	C_1	14170	13950	14150	0.14	14640	0.27	$D_0(A) \rightarrow D_1(A)$
		17400	17050	17580	0.10	17610	0.23	$D_0(A) \rightarrow D_2(A)$
6[•+]	C_1	13950	13580	13750	0.14	15250	0.28	$D_0(A) \rightarrow D_1(A)$
		17310	16910	17660	0.09	19180	0.17	$D_0(A) \rightarrow D_2(A)$
7[•+]	C_2	14770	14570	14680	0.10	15900	0.28	$D_0(B) \rightarrow D_1(A)$
		17570	16960	16960	0.12	16100	0.24	$D_0(B) \rightarrow D_2(B)$
8[•+]	C_2	13370	13100	13410	0.17	13760	0.32	$D_0(B) \rightarrow D_1(A)$
		16950	16600	17500	0.09	18140	0.18	$D_0(B) \rightarrow D_2(B)$
9[•+]	C_2[a]	14620	14200	14320	0.13	14990	0.28	$D_0(B) \rightarrow D_1(B)$
		16950	16390	16640	0.13	16090	0.24	$D_0(B) \rightarrow D_2(A)$
10[•+]	C_1	13990	13700	13960	0.16	14930	0.28	$D_0(A) \rightarrow D_1(A)$
		17310	17000	17680	0.09	18910	0.17	$D_0(A) \rightarrow D_2(A)$
TAPD[•+]	C_{2h}	10180	9480	9970	0.31	16270	0.26	$D_0(B_g) \rightarrow D_1(B_u)$
		18050	17540	18380	0.10	24140	0.14	$D_0(B_g) \rightarrow D_3(A_u)$

[a] symmetry broken geometry

For symmetry reasons only one excitation to a degenerate $D_1(E)$ state would be expected for all amines with a C_3 axis (**1**[•+], **2**[•+] and **9**[•+]). This $D_0 \rightarrow D_1$ excitation can be described by a HOMO→SOMO transition while the HOMO is a doubly degenerate orbital (Fig. 7).
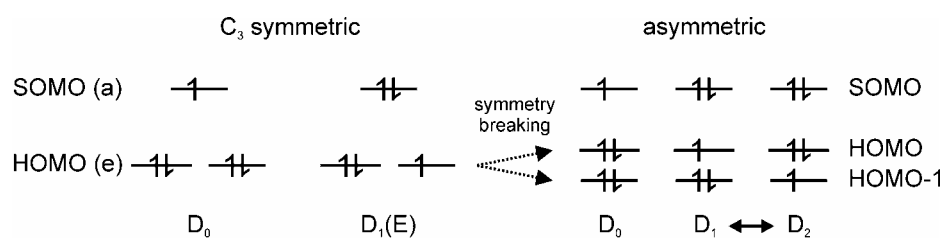
Fig. 7. Configuration diagram for the ground state and excited state of a symmetric *Tara*[•+] radical cation and the ground state and excited states of an asymmetric *Tara*[•+] radical cation.

Symmetry breaking either by exchange of one substituent or by interaction with the solvent causes a breaking of the degeneracy and the HOMO-1→SOMO transition is the second excitation visible. Owing to the small energy difference of HOMO and HOMO-1 the relative contribution of the HOMO→SOMO and HOMO-1→SOMO excitation to the D_0→D_1 and D_0→D_2 excitation may vary and even exchange. The iso-surface plots of the three orbitals of **10**[•+] which are involved in the two doublet excitations are shown Fig. 8 and are specified as π orbitals. Thus, these findings are in agreement with the former used simple description as π-π* band.
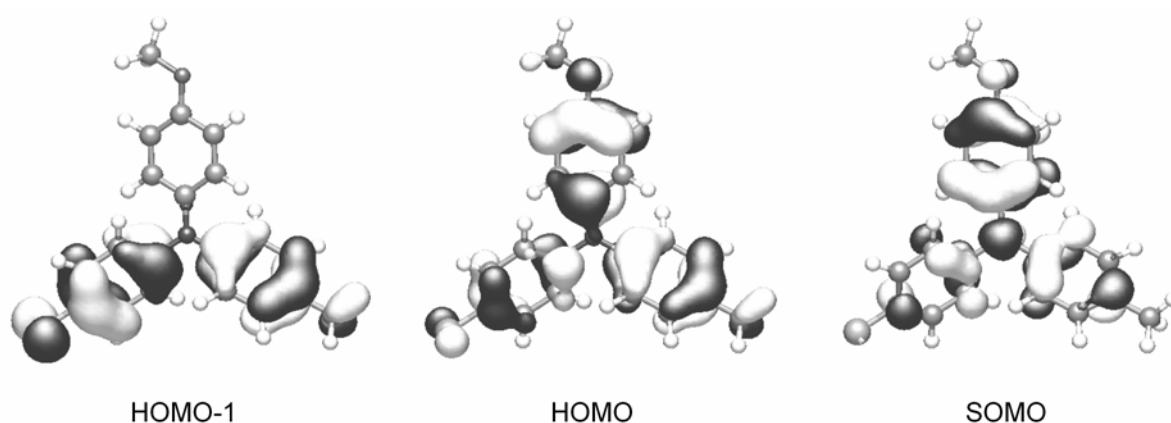
Fig. 8. Iso-surface plots of the HOMO-1 , HOMO and SOMO orbitals of **10**[•+] at the AM1-CISD level.

The experimental observation of a second absorption band even in the spectra of the symmetric molecules **1**[•+], **2**[•+] and **9**[•+] can be explained by symmetry breaking in solution as demonstrated for **9**[•+] in Fig. 9 and, consequently, a splitting of the degenerate D_1 state. The symmetry breaking is also facilitated by a *Jahn-Teller* distortion of the degenerate excited state. Thus, all AM1-CISD calculations for **1**[•+], **2**[•+] and **9**[•+] were carried out with one aryl moiety twisted in-plane as shown in Fig. 9.
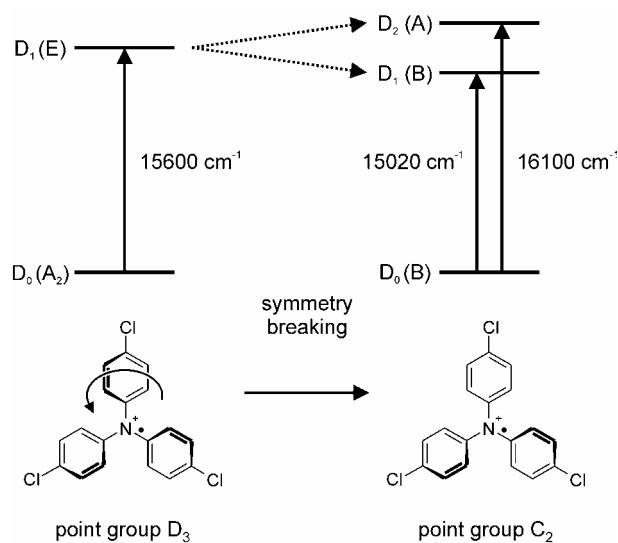
Fig. 9. Supposed symmetry breaking of **9**$^{\bullet+}$ in solution.

As shown in Fig. 10(a), a linear correlation between the experimental oscillator strength ($D_0 \to D_1$ excitation) and the absorption energy is observed. Even the delocalised intervalence system **TAPD**$^{\bullet+}$ (*N,N,N',N'*-tetra-(4-anisyl)phenylenediamine radical cation) which shows a rather strong charge resonance (CR) band in the NIR region at 9480 cm^{-1} fulfils this linear relationship.[21,46] In this system, the second dianisylamino group acts as a very strong donor and replaces one methoxy group in **1**. In addition the oscillator strengths of both excitations $D_0 \to D_1$ and $D_0 \to D_2$ calculated by AM1-CISD computations correlate linearly to the calculated absorption energies. As already mentioned, the degenerate state of a symmetrical compound can be considered as the origin of the D_1 and D_2 doublet states of the symmetry broken *Taras* which is the explanation for one linear relationship of both transitions. In contrast to the theoretical results the experimental values of the $D_0 \to D_2$ excitation show a large scattering and do not follow the same relationship of the experimental $D_0 \to D_1$ transitions. However, the absorption bands of the $D_0 \to D_2$ excitation are broad and less resolved compared to the intense $D_0 \to D_1$ excitation. Thus, the determination of the absorption energies and particularly the oscillator strengths of the $D_0 \to D_1$ excitation reflects a distinct tolerance.

(a)   (b)
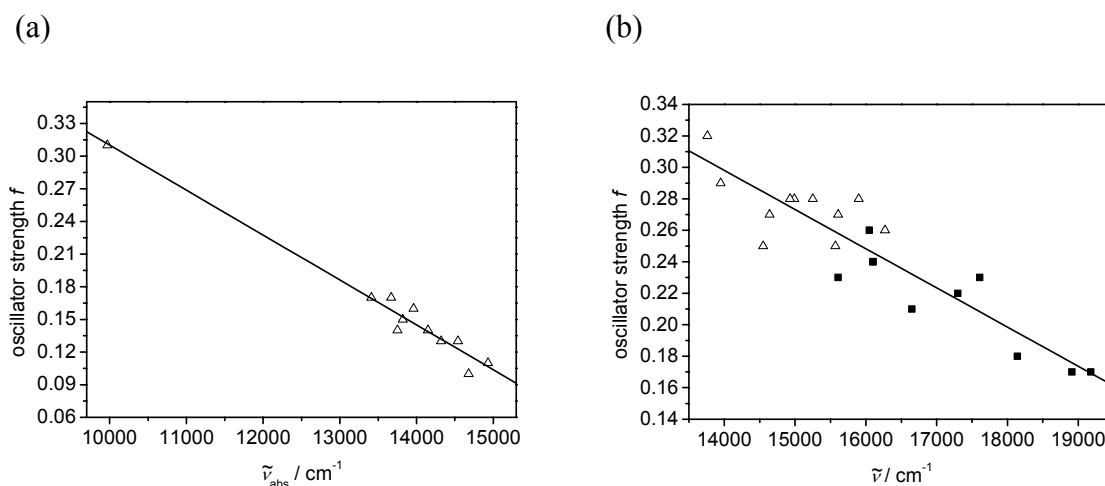
Fig. 10. Plot of the oscillator strength ($\triangle$, $D_0 \rightarrow D_1$ and $\blacksquare$, $D_0 \rightarrow D_2$ transition of *Tara* radical cations) versus averaged reduced absorption energy (a) values obtained from the experiments (b) AM1-CISD calculated values.

The oscillator strength f of a selected transition of a given molecule is directly proportional to the squared transition dipole moment μ_{eg}^2 (equation (4)).

$$f \cong \mu_{eg}^{\ 2} \tag{4}$$

According to *Mulliken*[50] and *Hush*[51], the transition dipole moment is approximately related to the mixing coefficient ξ and the transition dipole length r.

$$\mu_{eg} \cong \xi \cdot e \cdot r \tag{5}$$

The transition dipole length is supposed to be more or less constant for all *Tara* compounds examined in this study since the molecules are very similar in size. The mixing coefficient ξ is a measure for the degree of interaction of donor and acceptor units and, therefore, a measure for delocalisation of charge in the ground state of a molecule.[51] This means that more delocalised systems such as **TAPD**$^{\bullet+}$ show higher transition moments than more localised systems such as the radical cations **1**$^{\bullet+}$-**10**$^{\bullet+}$. Within the set of *Tara* radical cations **1**$^{\bullet+}$-**10**$^{\bullet+}$ radicals with more conjugating substituents chloro and/or methoxy show generally higher transition moments than tri-*para*-tolylamine radical cation **2**$^{\bullet+}$. In accordance with *Zhu* and *Wolf*[52] who obtained comparable results for (ferrocenylethynyl)oligothiophene complexes it

is supposed that the varying extent of charge delocalisation is the explanation for the linear relationship between the oscillator strength f and the absorption energy $\widetilde{\nu}_{abs}$.
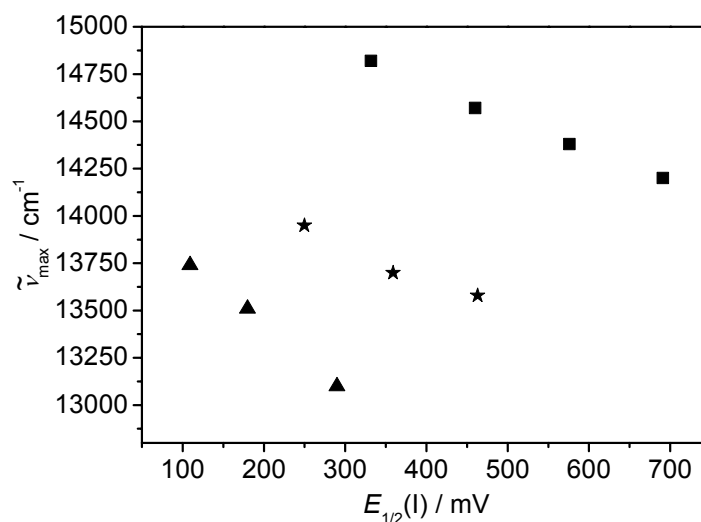
Fig. 11. Plot of the absorption energy of the radical cations $\mathbf{1}^{\bullet+}$-$\mathbf{10}^{\bullet+}$ versus oxidation potential $E_{1/2}$(I). The $Tara^{\bullet+}$s radical cations represented by squares have no methoxy substituent those represented by triangles have at least two methoxy substituents and those represented by stars have one methoxy substituent.

A plot of the absorption energy ($D_0 \rightarrow D_1$) versus the oxidation potential (Fig. 11) reflects three linear correlations. Thus, the radical cations are divided into three groups, one group with the electron richest compounds $\mathbf{1}^{\bullet+}$, $\mathbf{3}^{\bullet+}$ and $\mathbf{8}^{\bullet+}$ (triangles) with two or three methoxy substituents, a second set with the electron poorest radical cations $\mathbf{2}^{\bullet+}$, $\mathbf{4}^{\bullet+}$, $\mathbf{7}^{\bullet+}$ and $\mathbf{9}^{\bullet+}$ (squares) without any methoxy substituents, and a third lying in-between the two other groups with the molecules $\mathbf{5}^{\bullet+}$, $\mathbf{6}^{\bullet+}$ and $\mathbf{10}^{\bullet+}$ (stars) with only one methoxy group. Since the oxidation potential is a measure for the HOMO energy of the neutral compounds it correlates with the SOMO energy of the corresponding radical cations. The absorption energy is given by the gap between the HOMO and the SOMO energies. Due to the fact that the electron richness influences the energy of the HOMO the division into the three above-mentioned groups can be understood.

3.4   Linear optical properties of tri-4-anisylamine dication

The absorption spectrum of the dication 1^{2+} shown in Fig. 12 was obtained by global least squares data fitting of a spectroelectrochemical measurement in CH_2Cl_2 (TBAH) using SPECFIT/32[TM] software.[45] The spectroelectrochemical back reduction of the dication reveals that the second redox process is not completely reversible since only 83% of the neutral *Tara* could be recovered.[53] The dication 1^{2+} shows a broad and unsymmetrical absorption signal at 18800 cm^{-1} with an oscillator strength of 0.34. AM1-CISD calculation of 1^{2+} yields a transition energy of 15860 cm^{-1} and an oscillator strength of 0.90 which both show distinct deviation from the experimental data.
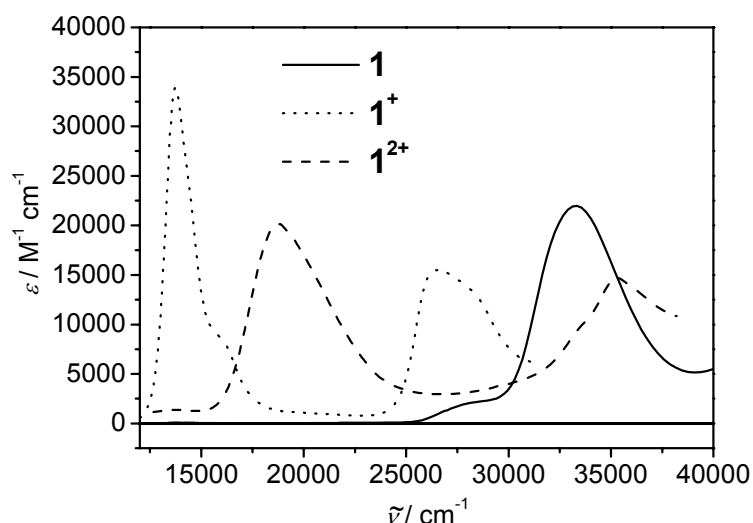
Fig. 12. Absorption spectra of 1, $1^{•+}$, 1^{2+} obtained by spectroelectrochemistry in CH_2Cl_2 (TBAH).

The absorption properties of the dication 1^{2+} can be explained by one intense HOMO→LUMO (S_0→S_1) excitation. The asymmetry of the signal can either be ascribed to symmetry breaking in solution as already discussed for the neutral and radical cationic species or be attributed to an unresolved vibrational fine structure.
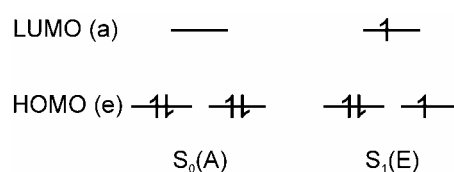
Fig. 13. Configuration diagram for the ground state and excited state of 1^{2+}.

4   Conclusions

The ten triaryalmines **1-10** with all permutations of chloro-, methoxy- and methyl-substituents in the three *para*-positions demonstrate a high long-term stability in multi-cycle thin-layer cyclic voltammetry at low scanning rates. The half wave potential $E_{1/2}$(I) of the first oxidation wave shows a linear correlation with the number of chloro- and methoxy-substituents (see equation (3)). This relationship proves additive electronic influence of the substituents on the oxidation potential of *Taras*.

AM1-CISD derived values of absorption energies are in good agreement with the experimental values of the neutral *Taras* and their corresponding radical cations but the theoretical value for the dication 1^{2+} differs strongly from the experimental absorption energy. All computed oscillator strengths show distinct deviations from experimental values. The experimental UV/Vis spectroscopy in CH_2Cl_2 and MeCN demonstrate only little solvent dependence of the transition energies and therefore a small charge transfer character of the absorption bands which is a single intense UV signal at 32890-33820 cm^{-1} ($S_0 \rightarrow S_1$ / HOMO$\rightarrow$LUMO and/or $S_0 \rightarrow S_2$ / HOMO$\rightarrow$LUMO+1) for the neutral triarylamines and two characteristic signals at 13100-14990 cm^{-1} ($D_0 \rightarrow D_1$ / HOMO$\rightarrow$SOMO) and 15300-17570 cm^{-1} ($D_0 \rightarrow D_2$ / HOMO-1$\rightarrow$SOMO) for the radical cations. The correlations between the absorption energy and the half wave oxidation potential of the neutral amines as well as for the radical cations demonstrate that the half wave potential $E_{1/2}$(I) is a good estimate for the HOMO energy of the neutral compounds and the SOMO energy of the radical cations. The two plots (Fig. 5 and Fig. 11) clearly demonstrate a division of the compounds into groups with comparable electron richness. This divisions can be understood since the absorption energy is characterised by the gap between two orbitals and the energy of the second orbital involved - which is not reflected by $E_{1/2}$(I) - depends on substituent effects. The two absorption signals of a radical cation with C_3 symmetry axis as $1^{\bullet+}$, $2^{\bullet+}$ and $9^{\bullet+}$ can be explained by symmetry breaking in solution which results in a splitting of the degenerate excited state. The oscillator strength f of the radical cations correlates linearly with the absorption energy for both experimental (only $D_0 \rightarrow D_1$) and AM1-CISD derived values. The charge delocalised intervalence system **TAPD$^{\bullet+}$** fulfils the same linear relationship which is a consequence of a varying extent of charge delocalisation in the ground state of the radical cations.

The experimental measurements and the AM1-CISD calculations of the neutral *Tara* species and the *Tara*[•+] radical cations give a consistent picture of the nature of their electronic and optical properties. These results will be important for the interpretation of the optical properties of molecular materials based on triarylamines such as hole conducting or mixed valence compounds.

5   Appendix

5.1   *Synthesis of N-(4-chlorophenyl)-N-(4-methylphenyl)amine*

CA-Nr. 21648-16-8

4-chloroaniline (788 mg, 6.18 mmol) and 4-iodotoluene (1.35 g, 6.18 mmol) were dissolved in 4.3 ml dry toluene. Copper(I) chloride (22.6 mg, 243 μmol), 1,10-phenanthroline (44.7 mg, 247 μmol) and powdered potassium hydroxide (2.71 g, 48.3 mmol) were added and the reaction mixture was heated to 120°C for one day. The solvent was removed in vacuum and the residue was dissolved in dichloromethane/water 1:1 (40 ml). The aqueous phase was extracted twice with dichloromethane (2×15 ml). The combined organic extracts were dried over magnesium sulphate and the solvent was removed after filtration. The residue was purified by flash-chromatography over silica gel with petroleum/CH_2Cl_2 5:1 as the eluent to give the colourless product 301 mg (1.38 mmol, 22 %); Spectral data matched that of the literature.[54]

5.2   *Synthesis of N-(4-chlorophenyl)-N-(4-methoxyphenyl)-N-(4-methylphenyl)amine (**10**)*

N-(4-chlorophenyl)-*N*-(4-methylphenyl)amine (301 mg, 1.38 mmol) and 4-iodoanisole (323 mg, 1.38 mmol) were dissolved in 1.5 ml dry toluene. Copper(I) chloride (5.04 mg, 54.3 μmol), 1,10-phenanthroline (9.98 mg, 55.2 μmol) and powdered potassium hydroxide (605 mg, 10.8 mmol) were added and the reaction mixture was heated to 120°C for one day. The solvent was removed in vacuum and the residue was dissolved in dichloromethane/water 1:1 (10 ml). The aqueous phase was extracted twice with dichloromethane (2×5 ml). The

combined organic extracts were dried over magnesium sulphate and the solvent was removed after filtration. The residue was purified by flash-chromatography over silica gel with petroleum/CH_2Cl_2 5:1 as the eluent to give the reddish product 179 mg (553 μmol, 40%); mp: 60-63°C; ^{1}H-NMR (400 MHz, [D_6]acetone, 27 °C): δ=7.19 (AA′, 2H), 7.11 (AA′, 2H), 7.04 (AA′, 2H), 6.96-6.86 (BB′, 6H), 3.79 (s, 3H; OMe), 2.28 (s, 3H; Me) ppm; {^{1}H}^{13}C-NMR (100 MHz, [D_6]acetone, 27 °C): δ=157.6, 148.5, 146.0, 141.1, 133.5, 130.9, 129.7, 128.1, 125.8, 125.1, 123.1, 115.8, 55.8 (OMe), 20.8 (Me) ppm; MS (70 eV, EI): m/z (%) 325 (36), 324 (21), 323.10764 (100) [M^+, $C_{20}H_{18}ClNO$ requires 323.10769], 310 (31) [M-Me]$^+$, 309 (18), 308 (89), 217 (12) [M-C_7H_7O]$^+$, 198 (6) [M-$C_{13}H_{11}NO$]$^+$, 128 (11) [C_6H_6NCl]$^+$; IR (KBr): $\tilde{\nu}$ =3088 (C=C-H), 1586 (C=C$_{Ar}$) cm^{-1}.

5.3 General procedure for the synthesis of the triarylamines 1-9

One equivalent of the *para*-substituted (Cl, OMe, Me) aniline derivative and 2.2 equivalents of the *para*-substituted (Cl, OMe, Me) iodobenzene derivative were dissolved in dry toluene (ca. 1 ml/mmol). Copper(I) chloride (3.9 mole percent), 1,10-phenanthroline (4 mole percent) and powdered potassium hydroxide (7.8 equivalents) were added and the reaction mixture was heated to 120°C for one day. The solvent was removed in vacuum and the residue was dissolved in dichloromethane/water 1:1. The aqueous phase was extracted twice with dichloromethane. The combined organic extracts were dried over magnesium sulphate and the solvent was removed after filtration. The residue was purified by flash-chromatography over silica gel with petroleum/CH_2Cl_2 as the eluent to give products **1-9**. If necessary the product was recrystallised from ethanol to obtain pure crystals. A full characterisation was done only if no NMR-spectroscopic data was found in the literature.

5.3.1 Isolation and characterisation of *N,N,N*-tri-(4-methoxyphenyl)amine (**1**)

CA-Nr.: 13050-56-1

The above general procedure was followed using 4-methoxyaniline (483 mg, 3.93 mmol), 4-methoxyiodobenzene (1.93 g, 8.24 mmol), copper(I) chloride (26.7 mg, 140 μmol), 2,2'-bipyridyl (43.7 mg, 140 μmol, instead of 1,10-phenanthroline), potassium *tert*-butoxide (1.32 g, 11.8 mmol, instead of potassium hydroxide) and 11.5 ml toluene. The residue was purified by flash-chromatography over silica gel with petroleum/CH_2Cl_2 1:1 as the eluent to give a brown solid which was crystallised from ethanol to give the pale yellow product 940 mg (2.80 mmol, 71%); ^{1}H-NMR (400 MHz, C_6D_6, 27 °C): δ=7.09 (AA′, 6H), 6.74 (BB′, 6H), 3.32 (s, 9H; OMe) ppm; $\{^1H\}^{13}$C-NMR (100 MHz, C_6D_6, 27 °C): δ=156.0, 142.9, 125.6, 115.3, 55.3 (OMe) ppm.

5.3.2 Isolation and characterisation of *N,N,N*-tri-(4-methylphenyl)amine (**2**)

CA-Nr.: 1159-53-1

The above general procedure was followed using 4-methylaniline (372 mg, 3.48 mmol), 4-methyliodobenzene (1.59 g, 7.31 mmol), copper(I) chloride (13.8 mg, 139 μmol), 1,10-phenanthroline (25.0 mg, 143 μmol), potassium hydroxide (1.52 g, 27.0 mmol) and 2.4 ml toluene. The residue was purified by flash-chromatography over silica gel with petroleum/CH_2Cl_2 8:1 as the eluent to give the colourless product 860 mg (2.96 μmol, 85%); mp: 114-115°C; ^{1}H-NMR (400 MHz, [D_6]acetone, 27 °C): δ=7.06 (AA′, 6H), 6.89 (BB′, 6H), 2.27 (s, 9H; Me) ppm; $\{^1H\}^{13}$C-NMR (100 MHz, [D_6]acetone, 27 °C): δ=146.7, 132.6, 130.6, 124.6, 20.8 (Me) ppm; MS (70 eV, EI): *m/z* (%) 287 (100) [M$^+$, $C_{21}H_{21}N$]; IR (KBr): $\tilde{\nu}$ =3022 (C=C-H), 2917 (C-H), 2857 (C-H), 1880-1600, 1607 (C=C_{Ar}), 1505 (C=C_{Ar}) cm^{-1}.

5.3.3 Isolation and characterisation of *N,N*-di-(4-methoxyphenyl)-*N*-(4-methylphenyl)-amine (**3**)

CA-Nr.: 156178-44-8

The above general procedure was followed using 4-methylaniline (335 mg, 3.13 mmol), 4-methoxyiodobenzene (1.54 g, 6.58 mmol), copper(I) chloride (12.4 mg, 118 μmol), 1,10-phenanthroline (22.5 mg, 129 μmol), potassium hydroxide (1.37 g, 24.4 mmol) and 2.2 ml toluene. The residue was purified by flash-chromatography over silica gel with petroleum/CH_2Cl_2 2:1 as the eluent to give a yellowish solid which was crystallised from ethanol to give the colourless product 101 mg (316 μmol, 10%); mp: 64-65°C; ^{1}H-NMR (400 MHz, [D$_6$]acetone, 27 °C): δ=7.01 (AA′, 2H), 6.96 (AA′, 4H), 6.86 (BB′, 4H), 6.80 (BB′, 2H), 3.77 (s, 6H; OMe), 2.24 (s, 3H; Me) ppm; {^{1}H}^{13}C-NMR (100 MHz, [D$_6$]acetone, 27 °C): δ=156.6, 147.4, 142.4, 131.2, 130.4, 126.7, 122.5, 115.5, 55.7 (OMe), 20.7 (Me) ppm; MS (70 eV, EI): *m/z* (%) 319.15701 (65) [M[+], $C_{21}H_{21}NO_2$ requires 319.15723], 304 (65) [M-Me][+], 214 (96), 199 (100), 171 (40); IR (KBr): $\tilde{v}$=3020 (C=C-H), 2930 (C-H), 1504 (C=C$_{Ar}$) cm^{-1}.

5.3.4 Isolation and characterisation of *N,N*-di-(4-chlorophenyl)-*N*-(4-methylphenyl)-amine (**4**)

CA-Nr.: 103052-38-6

The above general procedure was followed using 4-methylaniline (328 mg, 3.15 mmol), 4-chloro-iodobenzene (1.58 g, 6.61 mmol), copper(I) chloride (12.5 mg, 123 μmol), 1,10-phenanthroline (22.6 mg, 126 μmol), potassium hydroxide (1.37 g, 24.5 mmol) and 2.2 ml toluene. The residue was purified by flash-chromatography over silica gel with petroleum as the eluent to give the yellowish product 590 mg (1.80 mmol, 57%); mp: 91-93°C; ^{1}H-NMR (400 MHz, [D$_6$]acetone, 27 °C): δ=7.28 (AA′, 4H), 7.16 (AA′, 2H), 7.01 (BB′, 4H), 6.99 (BB′, 2H), 2.31 (s, 3H; Me) ppm; {^{1}H}^{13}C-NMR (100 MHz, [D$_6$]acetone, 27 °C): δ=131.1, 130.6, 129.5, 128.0, 127.2, 126.4, 125.6, 124.8, 29.8 (Me) ppm; MS (70 eV, EI): *m/z* (%) 329 (62) [M[+]], 327.05832 (100) [M[+], $C_{19}H_{15}Cl_2N$ requires 327.05816]; IR (KBr): $\tilde{v}$=3030 (C=C-H), 2918 (C-H), 1585 (C=C$_{Ar}$) cm^{-1}.

5.3.5   Isolation and characterisation of *N*-(4-methoxyphenyl)-*N,N*-di-(4-methylphenyl)-amine (**5**)

CA-Nr.: 61600-39-3

The above general procedure was followed using 4-methoxylaniline (403 mg, 3.27 mmol), 4-methyliodobenzene (1.50 g, 6.88 mmol), copper(I) chloride (12.9 mg, 128 μmol), 1,10-phenanthroline (23.5 mg, 130 μmol), potassium hydroxide (1.43 g, 25.4 mmol) and 2.0 ml toluene. The residue was purified by flash-chromatography over silica gel with petroleum/CH_2Cl_2 5:1 as the eluent to give the colourless product 650 mg (2.13 mmol, 65%); mp: 59-61°C; ^{1}H-NMR (400 MHz, [D_6]acetone, 27 °C): δ=7.04 (AA′, 4H), 6.98 (AA′, 2H), 6.88 (BB′, 4H), 6.85 (BB′, 2H), 3.78 (s, 3H; OMe), 2.26 (s, 6H; Me) ppm; {^{1}H}^{13}C-NMR (100 MHz, [D_6]acetone, 27 °C): δ=156.9, 146.9, 142.0, 132.0, 130.5, 127.3, 123.7, 115.5, 55.7 (OMe), 20.7 (Me) ppm; MS (70 eV, EI): *m/z* (%) 303.16239 (100) [M^+, $C_{21}H_{21}NO$ requires 303.16231], 288 (89); IR (KBr): $\tilde{\nu}$ =3022 (C=C-H), 2830 (C-H), 1606 (C=C_{Ar}) cm^{-1}.

5.3.6   Isolation and characterisation of *N,N*-di-(4-chlorophenyl)-*N*-(4-methoxyphenyl)-amine (**6**)

CA-Nr.: 103052-40-0

The above general procedure was followed using 4-methoxyaniline (358 mg, 2.90 mmol), 4-chloroiodobenzene (750 mg, 6.09 mmol), copper(I) chloride (11.5 mg, 114 μmol), 1,10-phenanthroline (20.8 mg, 116 μmol), potassium hydroxide (1.52 g, 27.0 mmol) and 2.0 ml toluene. The residue was purified by flash-chromatography over silica gel with petroleum/CH_2Cl_2 2:1 as the eluent to give the colourless solid which was crystallised from ethanol to give the colourless product 360 mg (1.05 mmol, 36%); mp: 56-59°C; ^{1}H-NMR (400 MHz, [D_6]acetone, 27 °C): δ=7.26 (AA′, 4H), 7.08 (AA′, 2H), 6.98 (BB′, 4H), 6.95 (BB′, 2H), 3.81 (s, 3H; OMe) ppm; {^{1}H}^{13}C-NMR (100 MHz, [D_6]acetone, 27 °C): δ=158.1, 147.7, 140.5, 130.1, 128.6, 127.4, 124.8, 116.0, 55.8 (OMe) ppm; MS (70 eV, EI): *m/z* (%) 345 (63) [M^+], 343.05332 (100) [M^+, $C_{19}H_{15}Cl_2NO$ requires 343.05307], 330 (51) [M-Me]$^+$, 328 (76) [M-Me]$^+$, 309 (46) [M-Cl]$^+$, 294 (42) [M-MeCl]$^+$; IR (KBr): $\tilde{\nu}$ =3020 (C=C-H), 2832 (C-H), 1584 (C=C_{Ar}) cm^{-1}.

5.3.7   Isolation and characterisation of *N*-(4-chlorophenyl)-*N,N*-di-(4-methylphenyl)-amine (**7**)

CA-Nr.: 58047-41-9

The above general procedure was followed using 4-chloroaniline (434 mg, 3.40 mmol), 4-methyl iodobenzene (1.56 g, 7.15 mmol), copper(I) chloride (13.5 mg, 133 μmol), 1,10-phenanthroline (24.5 mg, 136 μmol), potassium hydroxide (1.49 g, 26.5 mmol) and 2.5 ml toluene. The residue was purified by flash-chromatography over silica gel with petroleum/CH_2Cl_2 8:1 as the eluent to give the colourless product 736 mg (2.39 mmol, 74%); mp: 95-97°C; ^{1}H-NMR (400 MHz, [D_6]acetone, 27 °C): δ=7.22 (AA′, 2H), 7.12 (AA′, 4H), 6.95 (BB′, 4H), 6.92 (BB′, 2H), 2.29 (s, 6H; Me) ppm; {^{1}H}^{13}C-NMR (100 MHz, [D_6]acetone, 27 °C): δ=148.2, 145.9, 133.9, 130.9, 129.9, 126.7, 125.6, 124.2, 20.8 (Me) ppm; MS (70 eV, EI): *m/z* (%) 307.11263 (100) [M$^+$, $C_{20}H_{18}ClN$ requires 307.11278]; IR (KBr): $\tilde{\nu}$ =3023 (C=C-H), 2916 (C-H), 1605 (C=C_{Ar}), 1588 (C=C_{Ar}), 1508, 1486, 1319 cm^{-1}.

5.3.8   Isolation and characterisation of *N*-(4-chlorophenyl)-*N,N*-di-(4-methoxyphenyl)-amine (**8**)

CA-Nr.: 106614-61-3

The above general procedure was followed using 4-chloroaniline (383 mg, 3.00 mmol), 4-methoxyiodobenzene (1.47 g, 6.30 mmol), copper(I) chloride (11.9 mg, 118 μmol), 1,10-phenanthroline (21.6 mg, 120 μmol), potassium hydroxide (1.31 g, 23.3 mmol) and 2.4 ml toluene. The residue was purified by flash-chromatography over silica gel with petroleum/CH_2Cl_2 1:3 as the eluent to give the colourless product 910 mg (2.68 mmol, 89%); mp: 76-77°C; ^{1}H-NMR (400 MHz, [D_6]acetone, 27 °C): δ=7.16 (AA′, 2H), 7.05 (AA′, 4H), 6.91 (BB′, 4H), 6.80 (BB′, 2H), 3.79 (s, 6H; OMe) ppm; {^{1}H}^{13}C-NMR (100 MHz, [D_6]acetone, 27 °C): δ=157.4, 148.9, 141.3, 129.6, 127.7, 125.0, 121.8, 115.6, 55.7 (OMe) ppm; MS (70 eV, EI): *m/z* (%) 339.10265 (100) [M$^+$, $C_{20}H_{18}NClO_2$ requires 339.10261], 324 (92) [M-Me]$^+$; IR (KBr): $\tilde{\nu}$ =2995 (C=C-H), 2833 (C-H), 1504 cm^{-1} (C=C_{Ar}).

5.3.9 Isolation and characterisation of *N,N,N*-tri-(4-chlorophenyl)amine (**9**)
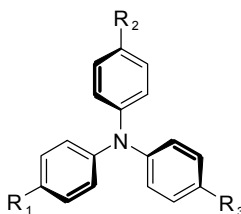
CA-Nr.: 16012-40-1

The above general procedure was followed using 4-chloroaniline (366 mg, 2.87 mmol), 4-chloroiodobenzene (1.44 g, 6.03 mmol), copper(I) chloride (11.3 mg, 112 μmol), 1,10-phenanthroline (22.3 mg, 114 μmol), potassium hydroxide (1.25 g, 22.3 mmol) and 2.0 ml toluene. The residue was purified by flash-chromatography over silica gel with petroleum as the eluent to give the pale yellow product 840 mg (2.41 mmol, 84%); mp: 146-148°C; ^{1}H-NMR (400 MHz, [D$_6$]acetone, 27 °C): δ=7.32 (AA′, 6H), 7.07 (BB′, 6H) ppm; {^{1}H}^{13}C-NMR (100 MHz, [D$_6$]acetone, 27 °C): δ=146.9, 130.4, 128.9, 126.4 ppm; MS (70 eV, EI): *m/z* (%) 347.00346 (97) [M$^+$, C$_{18}$H$_{12}$NCl$_3$ requires 347.00353], 347 (100), 277 (46) [M-Cl$_2$]$^+$, 121 (46); IR (KBr): $\tilde{\nu}$ =3088 (C=C-H), 1586 cm^{-1} (C=C$_{Ar}$)

5.4 *Experimental UV/Vis spectroscopy*

The experimental absorption spectra of all neutral triarylamines **1-10** and all corresponding radical cations recorded in CH$_2$Cl$_2$ as well as in MeCN are presented in Fig. 14.

	R$_1$	R$_2$	R$_3$
1	OMe	OMe	OMe
2	Me	Me	Me
3	Me	OMe	OMe
4	Me	Cl	Cl
5	OMe	Me	Me
6	OMe	Cl	Cl
7	Cl	Me	Me
8	Cl	OMe	OMe
9	Cl	Cl	Cl
10	Cl	OMe	Me

The extinction coefficients ε of the radical cartions **1$^{•+}$-10$^{•+}$** in MeCN are all supposed to be too small due to the slight instability of the radical cations under the conditions employed (see section 2.4 of this article).
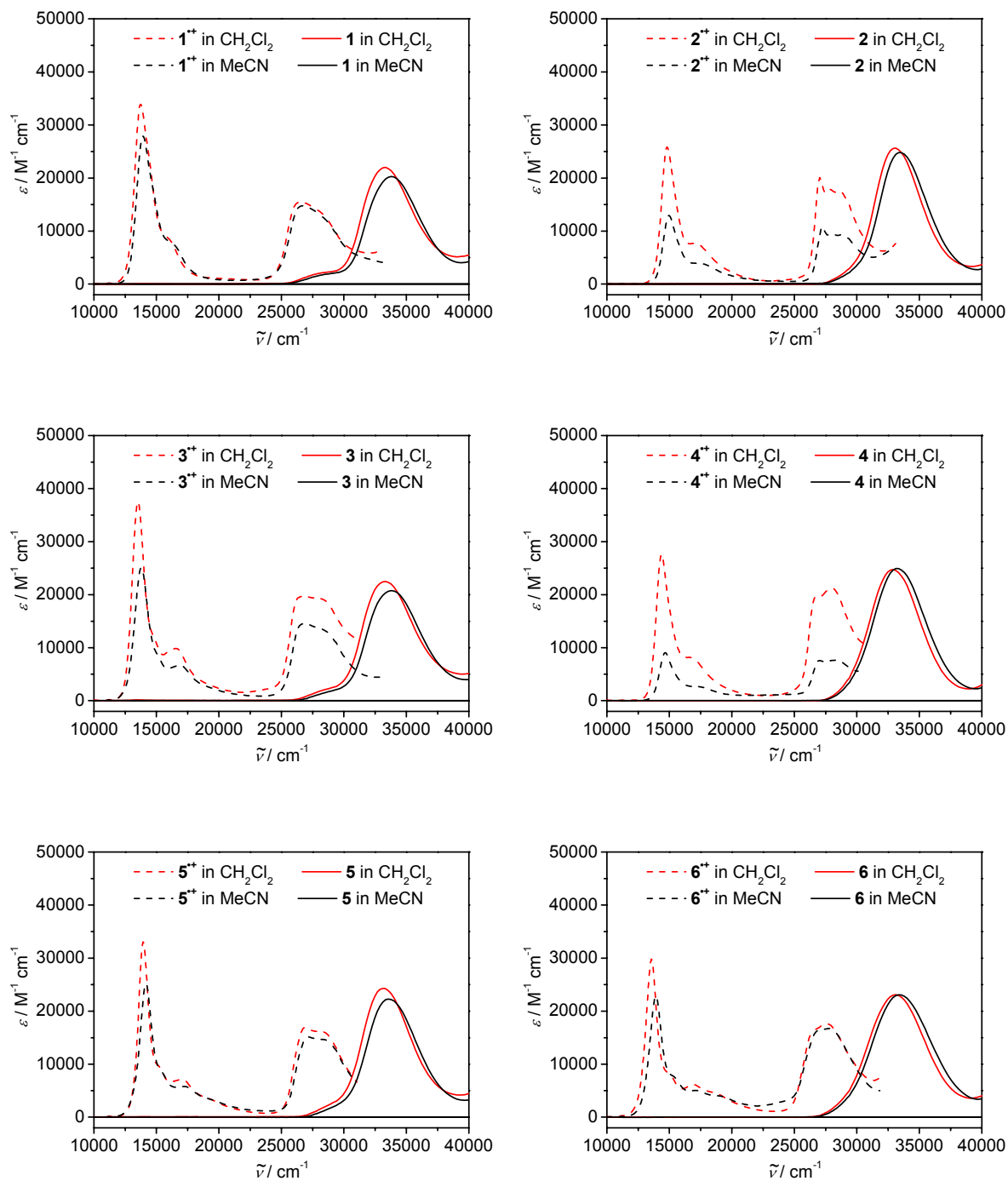
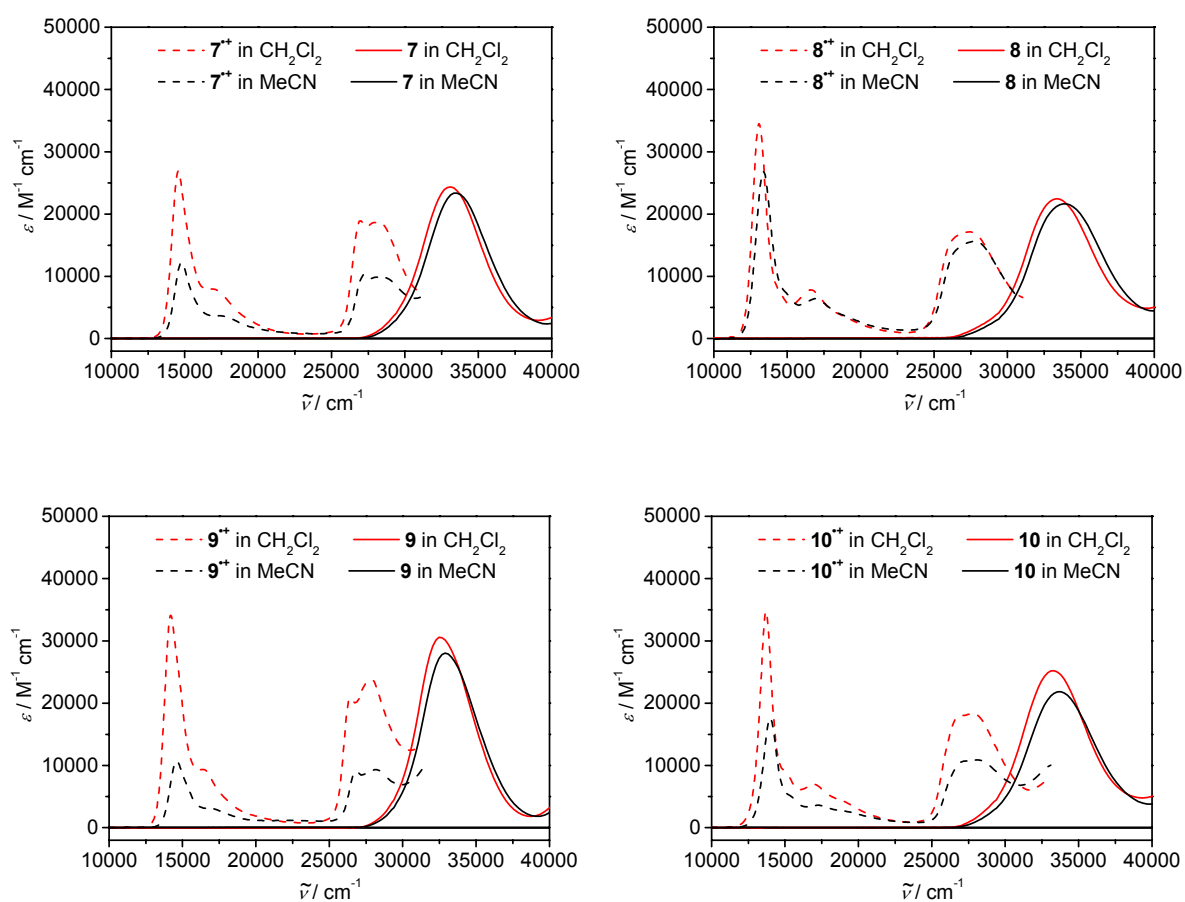Fig. 14. Experimental absorption spectra of all neutral triarylamines **1-10** and radical cations **1**$^{\bullet+}$-**10**$^{\bullet+}$ recorded in CH$_2$Cl$_2$ (red lines) as well as in MeCN (black lines).

6   References

(1)   Stolka, M.; Yanus, J. F.; Pai, D. M. *J. Phys. Chem.* **1984**, *88*, 4707.

(2)   Borsenberger, P. M.; Weiss, D. S. *Organic Photoreceptors for Imaging Systems*; Marcel Dekker: New York, 1993.

(3)   Thelakkat, M.; Fink, R.; Haubner, F.; Schmidt, H.-W. *Macromol. Symp.* **1998**, *125*, 157-164.

(4)   Thelakkat, M. *Macromol. Mater. Eng.* **2002**, *287*, 442-461.

(5)   Tang, C. W. *Appl. Phys. Lett.* **1986**, *48*, 183-185.

(6)   Tang, C. W.; van Slyke, S. A. *Appl. Phys. Lett.* **1987**, *51*, 913-915.

(7)   Kolb, E. S.; Gaudiana, R. A.; Mehta, P. G. *Macromolecules* **1996**, *29*, 2359-2364.

(8)   Fujikawa, H.; Tokito, S.; Taga, Y. *Synth. Met.* **1997**, *91*, 161-162.

(9)   Giebeler, C.; Antoniadis, H.; Bradley, D. D. C.; Shirota, Y. *Appl. Phys. Lett.* **1998**, *72*, 2448-2450.

(10) Redecker, M.; Bradley, D. D. C.; Inbasekaran, M.; Wu, W. W.; Woo, E. P. *Adv. Mater.* **1999**, *11*, 241-246.

(11) Braig, T.; Müller, D. C.; Groß, M.; Meerholz, K.; Nuyken, O. *Macromol. Rapid Commun.* **2000**, *21*, 583-589.

(12) Takeuchi, M.; Kobayashi, M.; Shishikawa, R.; Sakai, T.; Nakamura, H.; Konuma, H. *Jpn. Kokai Tokkyo Koho* **1986**.

(13) Kaeriyama, K.; Suda, M.; Sato, M.; Osawa, Y.; Ishikawa, M.; Kawai, M. *Jpn. Kokai Tokkyo Koho* **1988**.

(14) Moerner, W. E.; Silence, S. M. *Chem. Rev.* **1994**, *94*, 127-155.

(15) Nishikitani, Y.; Kobayashi, M.; Uchida, S.; Kubo, T. *Electrochim. Acta* **2001**, *46*, 2035-2040.

(16) Dapperheld, S.; Steckhan, E.; Grosse Brinkhaus, K. H.; Esch, T. *Chem. Ber.* **1991**, *124*, 2557-2567.

(17) Koshechko, V. G.; Titov, V. E.; Pokhodenko, V. D. *Teor. Eksp. Khim.* **1983**, *19*, 161-169.

(18) Bonvoisin, J.; Launay, J.-P.; Verbouwe, W.; Van der Auweraer, M.; De Schryver, F. C. *J. Phys. Chem.* **1996**, *100*, 17079-17082.

(19) Lambert, C.; Stadler, S.; Bourhill, G.; Bräuchle, C. *Angew. Chem., Int. Ed.* **1996**, *35*, 644-646.

(20) Lambert, C.; Nöll, G. *Angew. Chem., Int. Ed.* **1998**, *37*, 2107-2110.

(21) Lambert, C.; Nöll, G. *J. Am. Chem. Soc.* **1999**, *121*, 8434-8442.

(22) Lambert, C.; Gaschler, W.; Schmälzlin, E.; Meerholz, K.; Bräuchle, C. *J. Chem. Soc., Perkin Trans. 2* **1999**, 577-588.

(23) Lambert, C.; Nöll, G.; Hampel, F. *J. Phys. Chem. A* **2001**, *105*, 7751-7758.

(24) Lambert, C.; Nöll, G.; Schelter, J. *Nat. Mater.* **2002**, *1*, 69–73.

(25) Lambert, C.; Amthor, S.; Schelter, J. *J. Phys. Chem. A* **2004**, *108*, 6474-6486.

(26) Creutz, C. *Prog. Inorg. Chem.* **1983**, *30*, 1-73.

(27) Crutchley, R. J. *Adv. Inorg. Chem.* **1994**, *41*, 273-325.

(28) Seo, E. T.; Nelson, R. F.; Fritsch, J. M.; Marcoux, L. S.; Leedy, D. W.; Adams, R. N. *J. Am. Chem. Soc.* **1966**, *88*, 3498-3503.

(29) Nelson, R. F.; Adams, R. N. *J. Am. Chem. Soc.* **1968**, *90*, 3925-3930.

(30) Schmidt, W.; Steckhan, E. *Chem. Ber.* **1980**, *113*, 577-585.

(31) Hagopian, L.; Kohler, G.; Walter, R. I. *J. Phys. Chem.* **1967**, *71*, 2290-2296.

(32) Freeman, G. R.; Levy, H. A.; Brown, G. M. *Acta Crystallogr., Sect. A: Found. Crystallogr.* **1969**, *25*, S145-S146.

(33) Brown, G. M.; Freeman, G. R.; Walter, R. I. *J. Am. Chem. Soc.* **1977**, *99*, 6910-6915.

(34) Eberson, L. *Electron transfer reactions in organic chemistry*; Springer: Berlin Heidelberg, 1987; Vol. 25.

(35) Malagoli, M.; Brédas, J.-L. *Chem. Phys. Lett.* **2000**, *327*, 13-17.

(36) Lin, B. C.; Cheng, C. P.; Lao, Z. P. M. *J. Phys. Chem. A* **2003**, *107*, 5241-5251.

(37) Brunschwig, B. S.; Creutz, C.; Sutin, N. *Chem. Soc. Rev.* **2002**, *31*, 168-184.

(38) Rust, M.; Lappe, J.; Cave, R. J. *J. Phys. Chem. A* **2002**, *106*, 3930-3940.

(39) Neugebauer, F. A.; Bamberger, S.; Groh, W. R. *Chem. Ber.* **1975**, *108*, 2406-2415.

(40) Pearson, G. A.; Rocek, M.; Walter, R. I. *J. Phys. Chem.* **1978**, *82*, 1185-1192.

(41) Walter, R. I. *J. Am. Chem. Soc.* **1966**, *88*, 1923-1930.

(42) Mohammad, M.; Sundheim, B. R. *Theoret. Chim. Acta* **1968**, *10*, 222-230.

(43) Goodbrand, H. B.; Hu, N.-X. *J. Org. Chem.* **1999**, *64*, 670-674.

(44) Salbeck, J. *Anal. Chem.* **1993**, *65*, 2169-2173.

(45) Binstead, R. A.; Jung, B.; Zuberbühler, A. D. SPECFIT/32™ V3.0.33, Program for Multivariate Data Analysis; Spectrum Software Associates: 1993.

(46) Lambert, C.; Risko, C.; Coropceanu, V.; Schelter, J.; Amthor, S.; Gruhn, N. E.; Durivage, J.; Brédas, J.-L. *J. Am. Chem. Soc.* **2005**, *127*, 8508-8516.

(47) Stewart, J. J. P. MOPAC97; Fujitsu Limited: 1997.

(48) The computation of transition energies and transition moments under consideration of the environmental effect of the solvent by the inclusion of COSMO method does not improve the agreement of the theory with the experiment.

(49) **1** and **2** with molecular point group C_3 have a C_3 axis which goes through the trigonal planar N centre and is perpendicular to the plane surrounding the N while **9** with point group D_3 has three additional C_2 axis along each connection line between N and the rotationally symmetric Cl substituents.

(50) Mulliken, R. S. *J. Am. Chem. Soc.* **1952**, *74*, 811-824.

(51) Hush, N. S. *Prog. Inorg. Chem.* **1967**, *8*, 391-444.

(52) Zhu, Y.; Wolf, M. O. *J. Am. Chem. Soc.* **2000**, *122*, 10121-10125.

(53) The shift of the baseline can be explained by decomposition of the compound at high potentials which is followed by deposition of solid material; It is supposed that the decomposition has only little influence on the shape of the absorption spectrum but certainly reduces the experimental oscillator strength.

(54) Katritzky, A. R.; Cozens, A. J. *J. Chem. Soc., Perkin Trans. 1* **1983**, 2611-2615.

Excited Mixed-Valence States of Symmetrical

Donor-Acceptor-Donor π-Systems

CONTENTS

1 Introduction

The donor-π-bridge-donor (D-π-D) motive plays an increasingly important role in conjugated π-electron systems for two photon absorption applications which is a *nonlinear* optical property.[1-9] For a rational design of optoelectronic properties it is necessary to develop models that are capable to describe most if not all of the ground and excited state features of these D-π-D chromophores. Therefore, this chapter presents the *linear* optical properties of a number of D-π-D systems in which the donors are triarylamine groups at a constant separation while the π-bridge vary. The excited state potential energy surfaces for these D-π-D chromophores will be constructed within the framework of a three-state model and explain the photophysical behavior concerning the absorption and fluorescence properties. Furthermore, it will be shown that the electronic nature of the first excited state can be explained analogously to the ground state of mixed-valence compounds.

Chart 1
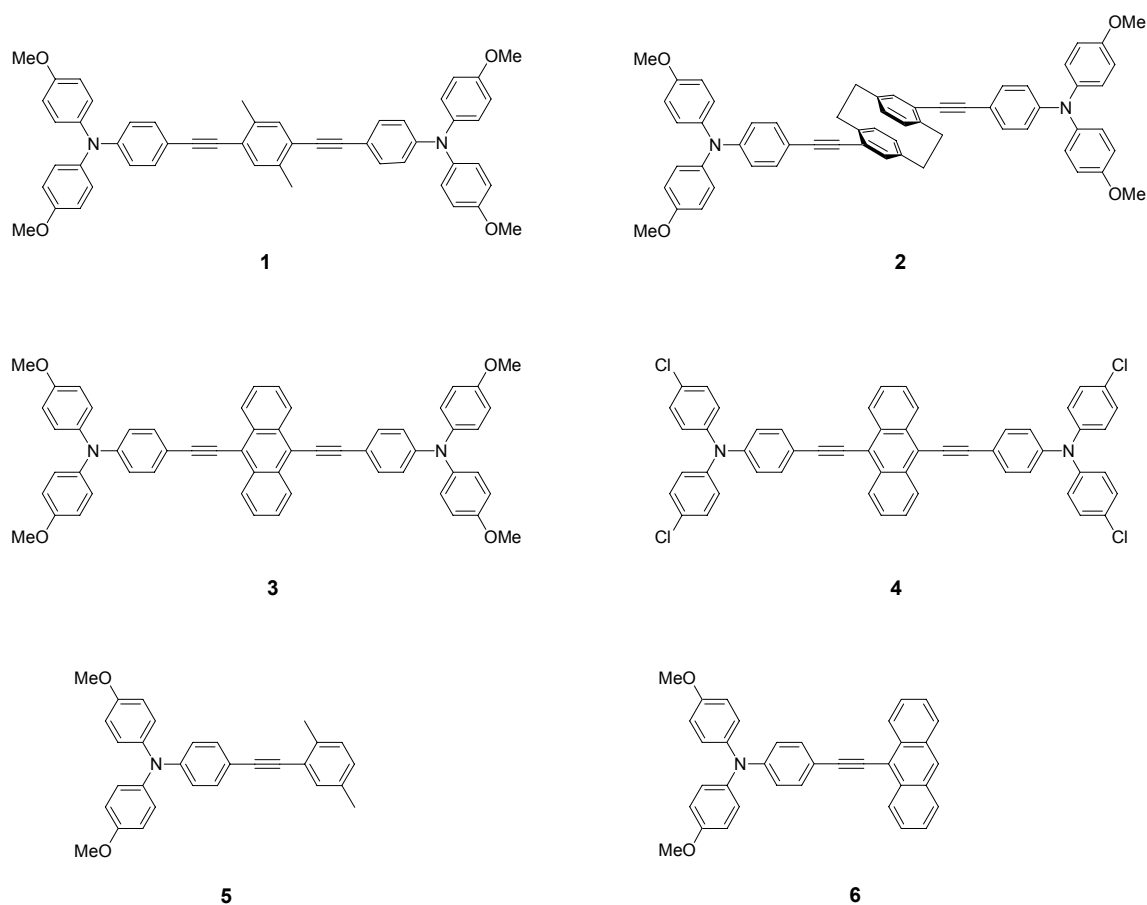
In Chart 1 four different D-π-D systems (hereafter called "dimers") with a conjugated bridge are displayed. They have been synthesized recently[9-11] and their radical cations have been studied in detail[10-12]. While **1** has a *p*-xylene bridge, this is replaced in **3** by anthracene which has a smaller HOMO-LUMO gap. In compound **4** the dianisylamino groups are replaced by di(*p*-chlorophenyl)amimo groups which possess a higher oxidation potential and, thus, are somewhat weaker electron donors.[13] Systems containing anthracene as the bridge moiety attracted considerable attention in recent years due to their unusual properties in "molecular wire" systems.[14-21] The fourth systems **2** has a formally broken π-conjugation although it is well known that the [2.2]paracyclophane bridge includes distinct direct orbital overlap between the π-planes.[22-34] This effect was used in novel extended π-systems for organic semiconductor applications.[35-47] For comparison with the D-π-D dimers, the D-π reference systems **5** and **6** hereafter called "monomers" will also be included in the discussion. The aim of this investigation is to clarify whether the photophysical properties of **1-4** can be deduced from the asymmetric analogous or whether cooperative effects play a role, that is, whether the properties are additive (weak coupling of asymmetric subunits) or whether the coupling of subunits is strong. The problem of symmetry breaking which might play an important role in the photophysics of these symmetric D-π-D systems, particularly in polar solvent environment will also be addressed.[48-57]

2   Methods

2.1 *Experimental*

Absorption spectra were measured in spectrograde solvents using a JASCO V570 spectrometer with 2 nm resolution. Fluorescence spectra were recorded at very low concentrations (c < 2×10^{-6}) in degassed spectrograde solvents and corrected for the wavelength dependence of the detector sensitivity using a PTI QuantaMaster[TM] Model QM-2000-4 spectrometer. The fluorescence quantum yield was determined relative to Rhodamine 101.[58] The fluorescence lifetime was determined using a PTI TimeMaster[TM] TM-2/2003 spectrometer with a flash lamp charged with a 1:1 H_2/N_2 mixture. The instrument response function (ca. 2.1 ns) was measured by a Ludox scatterer. For excitation energy the

N$_2$ band at 358 nm was employed. The fluorescence decay was single-exponential in all cases; the quality of the fit was judged by the χ^2 values, the Durbin-Wattson parameter, the autocorrelation function and the residuals.

The experimental setup of the picosecond time resolved transient absorption measurement is similar to the one published in ref.[59,60]. For sample excitation either the second (3-5 mJ) or third (1 mJ) harmonic of a mode-locked Nd:YAG laser (Continuum PY61C-10) was used. A white-light probe beam was generated by focusing the Nd:YAG laser fundamental at 1064 nm into a D$_2$O filled cell. The white light continuum was split in two parts that were directed into the sample cell by quartz fibres at an angle of 90° with respect to the excitation beam. One part served as the reference beam, the other one was overlapped with the pump beam. The two white-light beams were further directed by fibres into a spectrograph with a diode array for spectral analysis. The delay time between the pump beam and the white probe beam was adjusted by a computer controlled motorized delay stage. Each data points (i.e. a complete spectrum at each time delay) usually consists of an average of hundred shots. Although concentrations were varied, typically between 5×10^{-5} mol/l and 1×10^{-4} mol/l were employed. Measurements of β-carotene in C$_2$H$_4$Cl$_2$ were used to derive the zero in time as well as the instrument response function (FWHM = 35–40 ps).

2.2   Data evaluation

As the origin transition is not accurately discernible in all experimental absorption and fluorescence spectra, the averaged reduced absorption and fluorescence energy were calculated, which are given in eq. 1 and 2 where I_f is the fluorescence intensity *vs* wavenumber.[61] These reduced energies deviate from the apparent absorption and fluorescence maxima $\tilde{\nu}_{\text{abs-max}}$ and $\tilde{\nu}_{\text{fl-max}}$, respectively.

$$\tilde{\nu}_{\text{abs}} = \int \varepsilon \, \mathrm{d}\tilde{\nu} / \int \varepsilon \tilde{\nu}^{-1} \mathrm{d}\tilde{\nu} \tag{1}$$

$$\tilde{\nu}_{\text{fl}} = \int \tilde{\nu}^{-2} I_f \, d\tilde{\nu} / \int \tilde{\nu}^{-3} I_f \, d\tilde{\nu} \tag{2}$$

The transition moment μ_{abs} for the absorption process is given in eq. 3 where n is the index of refraction of the solvent and the integration has to be performed over the reduced absorption spectrum.[61,62]

$$\mu_{abs}^2 = \frac{3hc\varepsilon_0 \ln 10}{2000\pi^2 N} \frac{9n}{(n^2+2)^2} \int \frac{\varepsilon}{\tilde{\nu}} d\tilde{\nu} \tag{3}$$

The oscillator strength was calculated as

$$f_{abs,fl} = \frac{8\pi^2 m_e c \tilde{\nu}_{abs,fl}}{3he^2} \mu_{abs,fl}^2 \tag{4}$$

where μ is the transition moment for absorption or fluorescence, respectively.[61]

If there is no change in the nature of the excited state transition moment the transition moment for the absorption (μ_{abs}) and fluorescence (μ_{fl}) should be equal.

The fluorescence transition moment μ_{fl} can be evaluated by the Strickler-Berg relation (eq. 5) where the averaged cubic fluorescence energy (eq. 6) is used and g_e and g_g are the degree of degeneracy of the ground and excited state.[63]

$$k_f = \frac{16 \times 10^6 \pi^3}{3h\varepsilon_0} \frac{n(n^2+2)^2}{9} \frac{g_g}{g_e} \left\langle \tilde{\nu}_{fl}^{-3} \right\rangle_{av}^{-1} \mu_{fl}^2 \tag{5}$$

with $\left\langle \tilde{\nu}_{fl}^{-3} \right\rangle_{av}^{-1} = \int I_f d\tilde{\nu} / \int \tilde{\nu}^{-3} I_f d\tilde{\nu}$ $\tag{6}$

The fluorescence rate constant k_f was determined experimentally from the fluorescence quantum yield Φ and the fluorescence lifetime τ by $k_f = \Phi/\tau$. The rate constant for nonradiative processes was calculated by $k_{nr} = 1/\tau - k_f$.[61]

In a purely classical model with parabolic ground and excited state potentials for a combined solvent and molecular mode the free energy difference ΔG_{class}^{00} between the ground and excited state can be calculated by eq. 7 and the total reorganization for the absorption and fluorescence process energy $\lambda = \lambda_v + \lambda_o$ is given by eq. 8.

$$\Delta G_{class}^{00} = \frac{\tilde{\nu}_{abs} + \tilde{\nu}_{fl}}{2} \tag{7}$$

$$\lambda = \lambda_v + \lambda_o = \frac{\widetilde{V}_{abs} - \widetilde{V}_{fl}}{2} \tag{8}$$

The dipole moment differences between the ground and excited state was estimated by the method of Lippert and Mataga (eq. 9) using a plot of the Stokes shift vs. the Onsager solvent parameter.[64,65]

$$\widetilde{V}_{abs} - \widetilde{V}_{fl} = \frac{(\vec{\mu}_e - \vec{\mu}_g)^2}{2\pi\varepsilon_0 hca_0^3}\left(f(\varepsilon) - f(n^2)\right) + (\widetilde{v}_{abs}^{gas} - \widetilde{v}_{fl}^{gas}) \tag{9}$$

$$\text{with } f(\varepsilon) = \frac{\varepsilon - 1}{2\varepsilon + 1} \text{ and } f(n^2) = \frac{n^2 - 1}{2n^2 + 1}$$

where μ_e and μ_g is the excited and ground state dipole moment, respectively. The slope of the plot yields the dipole moment difference.

3   Results

3.1   Stationary Spectroscopy

The absorption spectra and fluorescence spectra of **1-6** are given in Figure 1. All compounds show a distinct lowest energy absorption which in the cases of **3** and **4** is almost base-line separated. For the anthracene compounds **3**, **4** and **6** this band is at distinctly lower energy than in the other compounds which is due to a stronger CT character of this transition owing to the stronger acceptor properties of anthracene. The absorption spectra of the anthracene compounds **3**, **4** and **6** only show a weak vibronic structure both in apolar and in polar solvents. It is immediately obvious that while the absorption spectra are only slightly solvent dependent the fluorescence spectra show a pronounced bathochromic solvatochromism. Thus, all compounds show strong Stokes shifts in polar solvents.
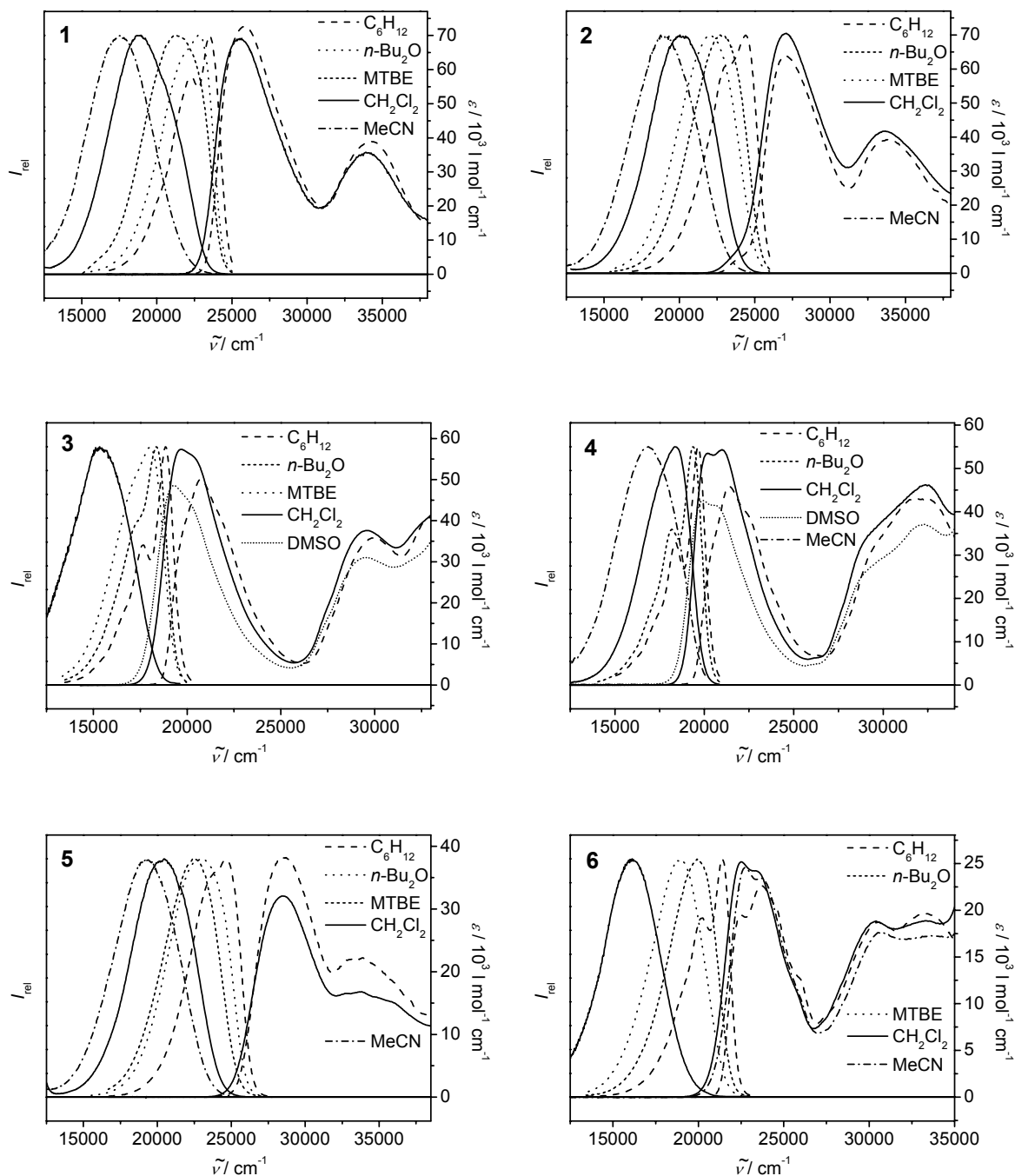
Figure 1. Absorption and fluorescence spectra of **1-6** in selected solvents.

The fluorescence spectra of all compounds display vibronic structure in apolar solvents while they are completely diffuse in the more polar solvents. For the symmetric anthracene containing species **3** and **4** the vibrational fine structure is very pronounced in cyclohexane, even more pronounced than in the asymmetric analogue **6**. In no case an exact mirror relationship of reduced absorption and fluorescence spectra was observed.

The transition moments for absorption μ_{abs} and the related oscillator strength f were calculated by eqs. 3 and 4. The symmetric D-π-D compounds **1**, **2** and **3** have an oscillator strength twice as high as their asymmetric analogues **5** and **6**, respectively.

The total reorganization energy λ for the absorption and fluorescence process was calculated by eq. 8. It increases strongly on going from apolar to polar solvents for all compounds. However, this effect is less pronounced for the anthracene compounds **3** and **4**. The free energy difference between the relaxed excited state and the relaxed ground state was calculated by eq. 7. This free energy difference decreases with increasing solvent polarity. Both trends - for λ and for ΔG_{class}^{00} - cancel out for the absorption but add for the fluorescence process which explains the different solvatochromic behavior.

The *Lippert-Mataga* plots of $\tilde{\nu}_{abs} - \tilde{\nu}_{fl}$ versus the *Onsager* solvent parameter (Figure 2) shows distinct differences for nonpolar and polar solvents, i.e. for the weakly polar solvents a linear correlation with small slope is observed while for polar solvents a much steeper slope is found. This behavior indicates a major molecular reorganization in the excited state. The solute radii a_0 were estimated as one fourth of the maximum molecular dimension of the dimers which was obtained from the AM1 optimized dimer structures. For the monomers **5** and **6** similar radii of the corresponding dimers **1** and **3** were used to calculate the dipole moment differences between the excited and the ground state in both sets of solvents (see Table 1). From the differences of slopes it is evident that the dipole moment differences are small in apolar solvents and much higher in the set of polar solvents.

Table 1. Dipole moment differences of **1-6** (nonpolar/polar) estimated by the method of *Lippert-Mataga* (eq. 9).

	1	**2**	**3**	**4**	**5**	**6**
$a_0/10^{-10}$m	7.61	7.83	7.60	6.82	7.61	7.60
$\Delta\mu$ /D	17.8/36.2	20.1/35.0	13.6/35.8	3.0/20.4	19.2/33.8	20.5/43.2
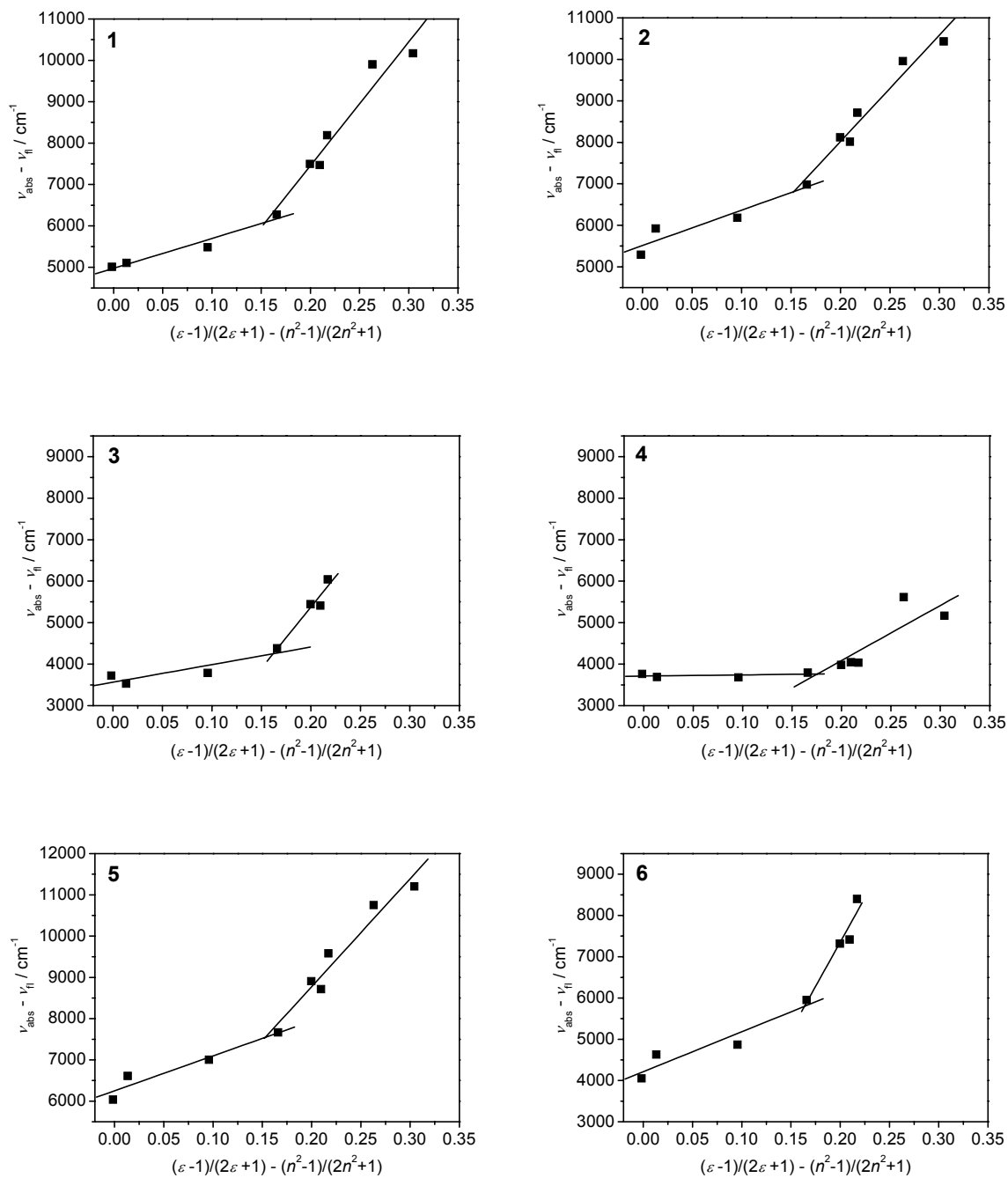
Figure 2. *Lippert-Mataga* plots for **1**-**6**. The solvents are from left to right: C_6H_{12}, toluene, *n*-Bu$_2$O, MTBE, EtOAc, THF, CH_2Cl_2, DMSO and MeCN.

3.2   Time-resolved fluorescence spectroscopy

Fluorescence quantum yields Φ are generally high for all compounds (see Table 2 and Table 3). However, there are significant differences between the symmetric D-π-D compounds and their asymmetric analogues: Both, the species with the *p*-xylene (**1**) and the paracyclophane bridge (**2**) show distinctly higher quantum yields than **5** in most solvents. Much in contrast, the anthracene compound **3** has a lower quantum yield than **6**. The quantum yields of the latter approach unity in many solvents while those of **4** are unity in most solvents.

The fluorescence lifetimes of all compounds are between ca. 1 and 5 ns. Even for the anthracene containing species the lifetime is is only 2-3 ns in apolar solvents which demonstrates that there is a strong mixing of anthracene excited states with those of the other molecular parts because anthracene itself has a longer lifetime (5.2 ns in cyclohexane)[66]. In the literature a "phane" state is frequently discussed which is the first excited state of pseudo-*p*-[2.2]paracyclophane with small substituents.[25,28] These states are generally characterized by relatively long lifetimes. However, the electronic situation is different for larger substituents as for [2.2]paracyclophane **2** where the fluorescence lifetimes are much smaller.

From the fluorescence rate constants, the fluorescence transition moment μ_{fl} was calculated by eq. 5 and the oscillator strength by eq. 4. The oscillator strengths f_{abs} for absorption for the dimers **1**, **2** and **3** are approximately twice as high as these of their corresponding monomers **5** and **6**. Analogously to the absorption, the fluorescence oscillator strength for **2** is twice as high as that of its asymmetric analogue **5**. However, compounds **1** and **3** show much different behaviors: While f_{fl} of **1** is three to four times as high as f_{fl} of **5**, that of **3** is about the same as of **6**. This fact points towards strong interactions in the chromophore branches in the excited states of **1** and of **3**.

Table 2. Linear optical properties of **1**, **2** and **5**.

	$\widetilde{\nu}_{abs}$ /cm^{-1}	μ_{abs} /D	f_{abs}	$\widetilde{\nu}_{fl}$ /cm^{-1}	Φ	τ_{fl} / ns	k_f / ns^{-1}	k_{nr} / ns^{-1}	μ_{fl} /D	f_{fl}	λ /cm^{-1}	ΔG^{00}_{class} /cm^{-1}
1												
C_6H_{12}	26860	9.3	1.09	21860	0.81	0.8	1.03	0.24	10.9	1.22	2510	24360
toluene	26350	9.1	1.03	21240	0.80						2550	23790
n-Bu$_2$O	26670	9.8	1.20	21190	0.93	1.2	0.79	0.06	10.3	1.06	2740	23930
MTBE	26690	10.5	1.38	20420	0.82	1.5	0.55	0.12	9.4	0.85	3140	23560
EtOAc	26590	9.7	1.18	19100	0.65						3750	22840
THF	26510	9.9	1.22	19040	0.87	2.2	0.40	0.06	8.5	0.65	3740	22780
CH$_2$Cl$_2$	26400	9.7	1.17	18220	0.70	2.7	0.26	0.11	7.3	0.46	4100	22310
DMSO	26210			16310	0.33						4950	21260
MeCN	26650	10.5	1.38	16480	0.36	1.4	0.25	0.45	8.9	0.61	5090	21570
2												
C_6H_{12}	28040	8.8	1.02	22750	0.52	1.1	0.48	0.44	7.0	0.52	2650	25390
toluene	27590	9.1	1.07	21670	0.71						2960	24630
n-Bu$_2$O	27900	9.6	1.21	21710	0.72	1.7	0.44	0.17	7.4	0.56	3090	24800
MTBE	27980	9.9	1.29	21000	0.63	1.7	0.38	0.22	7.5	0.56	3490	24490
EtOAc	28090	10.6	1.48	19970	0.70						4060	24030
THF	27900	9.5	1.18	19880	0.91	3.3	0.27	0.03	6.6	0.41	4010	23890
CH$_2$Cl$_2$	28030	9.8	1.27	19320	0.92	4.0	0.23	0.02	6.2	0.35	4360	23680
DMSO	27910	9.5	1.18	17960	0.76						4980	22930
MeCN	28480	9.9	1.31	18050	0.77	3.7	0.22	0.06	7.1	0.43	5220	23270
5												
C_6H_{12}	29220	6.9	0.65	23180	0.35	1.1	0.32	0.60	5.6	0.34	3020	26200
toluene	28810	6.3	0.54	22200	0.44						3310	25500
n-Bu$_2$O	29000	6.3	0.54	21990	0.39	1.5	0.26	0.41	5.6	0.32	3500	25490
MTBE	29140	6.1	0.51	21480	0.58	2.7	0.21	0.15	5.4	0.29	3830	25310
EtOAc	29200	6.8	0.63	20300	0.50						4450	24750
THF	29030	6.9	0.65	20310	0.70	3.9	0.18	0.08	5.2	0.26	4360	24670
CH$_2$Cl$_2$	29090	6.5	0.58	19510	0.71	5.0	0.14	0.06	4.8	0.21	4790	24300
DMSO	28960	6.5	0.58	18210	0.75						5380	23590
MeCN	29470	6.7	0.62	18260	0.46	5.0	0.09	0.11	4.6	0.18	5600	23870

Table 3. Linear optical properties of **3**, **4** and **6**.

	$\tilde{\nu}_{abs}$ /cm^{-1}	μ_{abs} /D	f_{abs}	$\tilde{\nu}_{fl}$ /cm^{-1}	Φ	τ_{fl} / ns	k_f / ns^{-1}	k_{nr} / ns^{-1}	μ_{fl} /D	f_{fl}	λ /cm^{-1}	ΔG^{00}_{class} /cm^{-1}
3												
C$_6$H$_{12}$	21370	7.3	0.54	17650	0.74	2.4	0.31	0.11	8.2	0.56	1860	19510
toluene	20770	8.4	0.69	17240	0.78						1760	19000
n-Bu$_2$O	21000	6.8	0.46	17210	0.80	2.0	0.40	0.10	10.1	0.83	1890	19100
MTBE	21230	7.5	0.56	16850	0.84	3.2	0.27	0.05	8.7	0.60	2190	19040
EtOAc	21130	8.8	0.77	15690	0.52						2720	18410
THF	20830	8.7	0.74	15420	0.47	3.2	0.15	0.17	7.1	0.37	2700	18130
CH$_2$Cl$_2$	20640	8.6	0.72	14590	0.31	2.3	0.14	0.30	7.3	0.37	3020	17610
DMSO	20230	7.8	0.58									
MeCN						0.9						
4												
C$_6$H$_{12}$	22140	7.3	0.55	18380	0.94	2.4	0.40	0.03	8.8	0.67	1880	20260
toluene	21580	7.7	0.60	17890	1.00						1840	19740
n-Bu$_2$O	21810	8.0	0.66	18130	1.00	2.8	0.36	0.00	8.8	0.66	1840	19970
MTBE	21910	8.5	0.74	18110	1.00	2.6	0.39	0.00	9.4	0.75	1900	20010
EtOAc	21670	8.8	0.79	17690	0.89						1990	19680
THF	21570	8.5	0.73	17520	1.00	2.5	0.41	0.00	9.7	0.78	2020	19550
CH$_2$Cl$_2$	21410	8.3	0.69	17380	1.00	2.6	0.38	0.00	9.5	0.74	2020	19390
DMSO	21080	7.2	0.51	15470	0.83						2810	18280
MeCN	21170			16000	0.78	3.2	0.24	0.07	9.1	0.62	2580	18580
6												
C$_6$H$_{12}$	23960	5.3	0.32	19910	0.97	2.6	0.37	0.01	9.0	0.76	2030	21930
toluene	23600	5.7	0.36	18970	0.99						2310	21290
n-Bu$_2$O	23800	5.6	0.35	18930	0.96	3.1	0.31	0.01	8.9	0.70	2440	21360
MTBE	23960	5.7	0.37	18010	0.89	3.4	0.26	0.03	8.7	0.64	2980	20980
EtOAc	23810	5.7	0.36	16490	0.73						3660	20150
THF	23680	5.7	0.36	16270	0.82	5.1	0.16	0.04	7.4	0.42	3710	19970
CH$_2$Cl$_2$	23650	5.7	0.36	15250	0.54	4.5	0.12	0.10	6.8	0.33	4200	19450
DMSO	23960											
MeCN	23600	5.7	0.36			0.2						

3.3   Picosecond time-resolved transient absorption spectroscopy

Picosecond time-resolved transient absorption spectra of compounds **1-6** were recorded in apolar toluene as well as in the polar solvent benzonitrile (PhCN). A solvent-dependent investigation of the excited state dynamics of compounds **1-6** is of interest, because the *Lippert-Mataga* plots already indicate that the nature of the first excited state of all compounds depends on the solvent polarity. In most experiments the samples were excited with a pump wavelength of 355 nm (28200 cm^{-1}), with the exception of **3** in toluene and **4** in toluene and PhCN which were excited at 532 nm (18800 cm^{-1}). The spectra recorded approximately around the zero in time are given in Figure 3. Beside the transient absorption bands negative absorption due to ground-state bleaching or steady–state emission caused by the excitation laser is visible in some experiments. The most important spectral features of compounds **1-6** in the transient absorption spectra recorded around time zero (see Figure 3) are summarized in Table 4.

Table 4. Transient absorption maxima of **1-6** in cm^{-1} (sh = shoulder, br = broad) and lifetimes τ in ns.

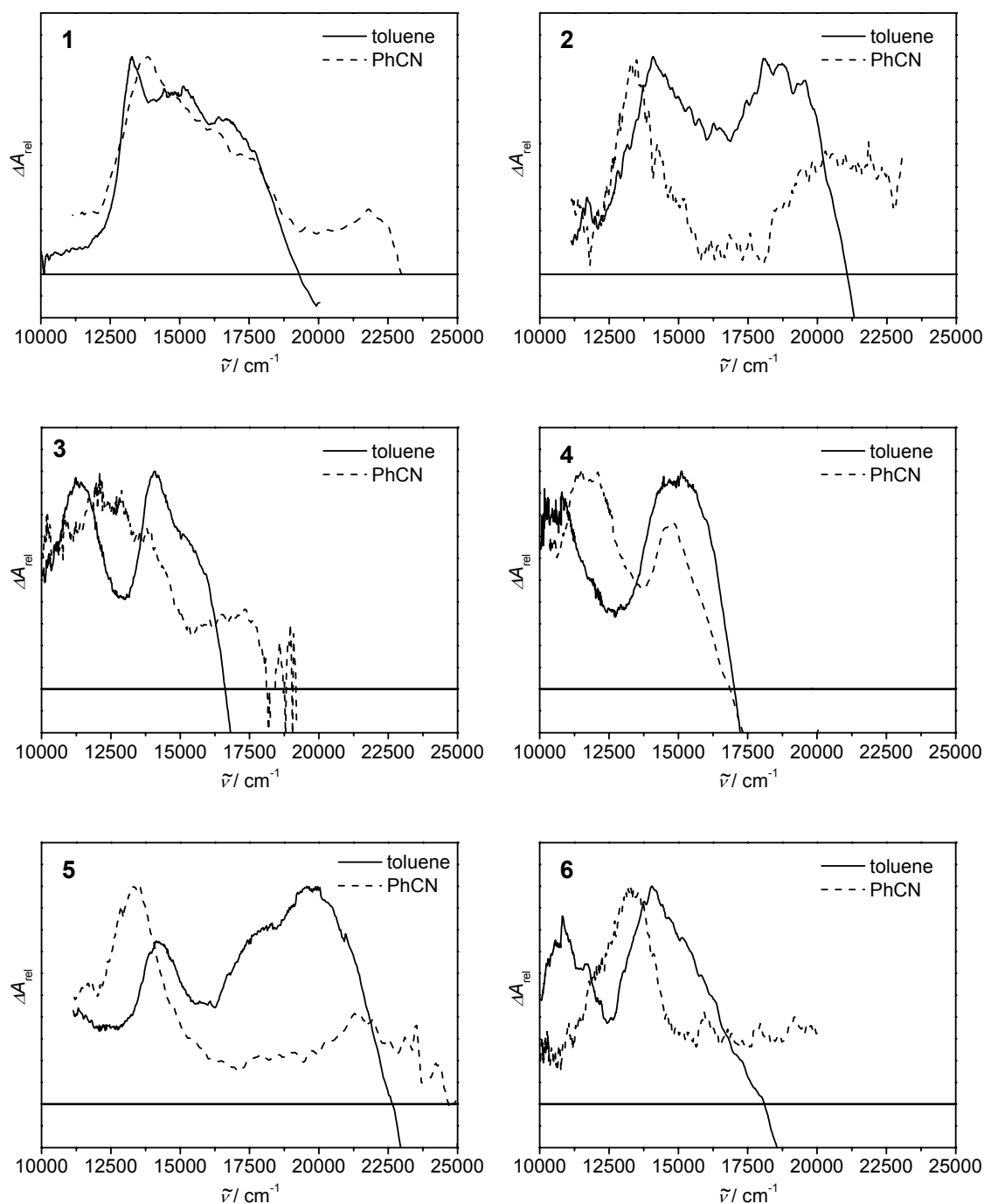|	**1**	**2**	**3**	**4**	**5**	**6**
PhCN	14000 (br)	13500	10000 -	11500	13500	12000 (sh)
	16000 (sh)	22000	14500	14000	18500 (sh)	13500
	22000		17000	18000 (bleach)	21500	
τ / ns	2.8	3.4	0.5	2.4	4.5	1.5
toluene	13500	14000	11500	10500	14500	11000
	15000	18500	14000	15000	17500 (sh)	14000
	16500		15500 (sh)		19500	
	>20000 (bleach)	23000 (emission)	18000 (bleach)	18500 (bleach)	24000 (emission)	19500 (em/bleach)
τ / ns	1.2	1.5	2.0	2.5	2.4	3.2

Figure 3. Transient absorption spectra of **1-6** in benzonitrile and toluene.

An intense absorption band between 13000 cm^{-1} and 15000 cm^{-1} is typical of triarylamine radical cations.[13] For example, in the transient absorption of neutral diansiylphenylamine a signal around 14500 cm^{-1} was observed.[67] In the same energy region a transient absorption was also found for acridine-triarylamine donor-acceptor compounds,[67] acridine-triarylamine redox cascades[67] and neutral triarylmethyl-triarylamine mixed-valence compounds[68]. In the

present study this π-π^* band being typical of triarylamine radical cations is expected for all compounds that form a charge separated excited CT state. In fact, absorptions in this region are visible in the spectra of all compounds in both solvents. The positive solvatochromism observed for the corresponding transitions in compounds **2**, **4**, and **5** supports this assignment. Even compound **4** with its more delocalized first excited state shows the typical triarylamine radical cation π-π^* band.[13] This observation reflects that the degree of charge separation does not significantly influence the absorption caused by a triarylamine moiety. A similar conclusion has been drawn recently for acridine-triarylamine redox cascades.[67]

Based on the *Lippert-Mataga* plots a charge separated excited CT state is expected for the *p*-xylenes **1** and **5** and the [2.2]paracyclophane **2** and, therefore, as already mentioned one absorption typical of the triarylamine radical cation and another absorption of the radical anion of the corresponding bridge. The unsubstituted [2.2]paracyclophane radical anion itself shows one absorption band at 12200 cm^{-1} and a second at 26000 cm^{-1} in MTHF[69], while the unsubstituted benzene radical anion is characterized by only one band at ca. 26000 cm^{-1} in MTHF.[70] As the conjugating substitutents in excited *p*-xylenes **1** and **5** may shift the *p*-xylene anion absorption band to smaller wavenumbers, it is supposed that the absorptions of **1** and **5** above 16000 cm^{-1} can be traced back to this *p*-xylene radical anion absorption. In contrast, the cyclophane **2** does not show the typical absorption bands of the [2.2]paracyclophane radical anion at 12200 cm^{-1} and 26000 cm^{-1} (the latter might be hidden by strong stimulated emission in toluene).[69] This might also be due to the fact that the substituents at the cyclphane moiety shift both bands significantly to the red and, thus, the absorption bands of **2** at 18500 cm^{-1} in toluene and 20000 cm^{-1} in PhCN are the corresponding radical anion bands. Interestingly, the transient absorption of the donor substituted paracyclophane **2** shows significant differences compared to the transient absorption of pseudo-*p*-distyryl-[2.2]paracyclophane. The dimer **2** shows two maxima, while pseudo-*p*-distyryl-[2.2]paracyclophane shows an intense and broad, but featureless transient absorption between 8000 and 22000 cm^{-1}.[71] This indicates that the triarylamine donor groups have significant influence on the nature of the excited states. It is supposed that the different absorption properties can be explained by a completely delocalized first excited state without charge separation of pseudo-*p*-distyryl-[2.2]paracyclophane while a charge separated excited CT state of D-π-D compound **2** is observed. The *p*-xylene **1** shows a broad transient absorption in both solvents which has three maxima in toluene but only a shoulder on the high energy side in PhCN. It is assumed that the absorption of **1** is the result of at least two electronic transitions. On the one hand the *p*-xylene radical anion band is

observed at wave numbers larger than ~16000 cm^{-1} and on the other hand there is a triarylamine excited-state absorption at 13500 cm^{-1} (toluene) and 14000 cm^{-1} (PhCN), respectively.

Comparison of the transient absorption spectra in toluene and PhCN shows for all compounds with exception of **4** significant differences of the absorption properties upon changing the solvent polarity. In toluene, the first excited state of the anthracenes **3**, **4** and **6** shows an absorption at low energy between 10500 and 11500 cm^{-1}. The remaining compounds with either a *p*-xylene bridge (**1** and **5**) or the [2.2]paracyclophane bridge (**2**) do not show any transient absorption below 13500 cm^{-1} neither in toluene nor in PhCN. This indicates that this absorption at low energy is due to a transition closely related with the anthracene bridge itself. From the *Lippert-Mataga* plots (Figure 2) a charge separated CT state is expected only for the anthracenes **3** and **6**. These CT states should be characterized by a partial positive charge one the triarylamine moiety and a partial negative charge on the anthracene bridge. Although, as judged from the *Lippert-Mataga* plots in Figure 2, the CT character is less pronounced for the chloro-substituted anthracene bridged compound **4** the absorption bands for all anthracenes in toluene are very similar. However, the influence of the solvent polarity on the transient absorption spectra is much more pronounced for compounds **3** and **6** than for **4**. It is supposed that this fact is a consequence of the distinctly more delocalized first excited state of **4**. The signals of **4** and **6** at smaller wavenumbers (related with the anthracene bridge) show negative solvatochromism while the signals of **4** and **6** at higher energy (related with the triarylamine) show positive solvatochromism. An even more pronounced effect of the solvent polarity on the transient absorption was found for anthracene **3** which shows a very broad and featureless transient absorption in PhCN between 10000 and 14500 cm^{-1} and an additional weak absorption at 17000 cm^{-1}.

With exception of **3** in PhCN (τ=500 ps), lifetimes on the order of a few ns were observed (Table 4). Similar decay times were derived for all spectral features (absorption bands and ground state bleach) in a given spectrum. Within the experimental error they are in good agreement with the fluorescence lifetimes (Table 2 and 3) in nonpolar media and polar solvents, respectively.

Several transient spectra show additional negative absorptions. In all spectra recorded with an excitation at 532 nm (**3** and **4** in toluene, **4** in PhCN), as well as the spectrum of **1** in toluene a signal is visible that can be assigned to a ground state bleach. The time constant for ground state recovery is similar to the absorption decay time. This confirms that the excited state decay is due to a return to the electronic ground state with no additional intermediate

state. On the other hand, in compounds **2** and **5** the negative absorption in toluene is due to a probe-independent emission caused by the excitation laser. At least in compound **6** it seems that such an emission conceals an additionally present ground state bleach.

4   Discussion

For the interpretation of the photophysical properties of the D-π-D compounds the ground and excited state potential energy surfaces (PES) were constructed by mixing three diabatic (formally noninteracting) states in a two-mode (one asymmetric (x) and one symmetric mode (y)) approximation similar to the one used for analogous ground state mixed-valence radical cations.[10-12] The three diabatic states are the ground state and two degenerate excited CT states. In the latter the excitation is localized in only one half of the D-π-D chromophore, (D$^+$-π^--D) or (D-π^--D$^+$), respectively (see Figure 4).

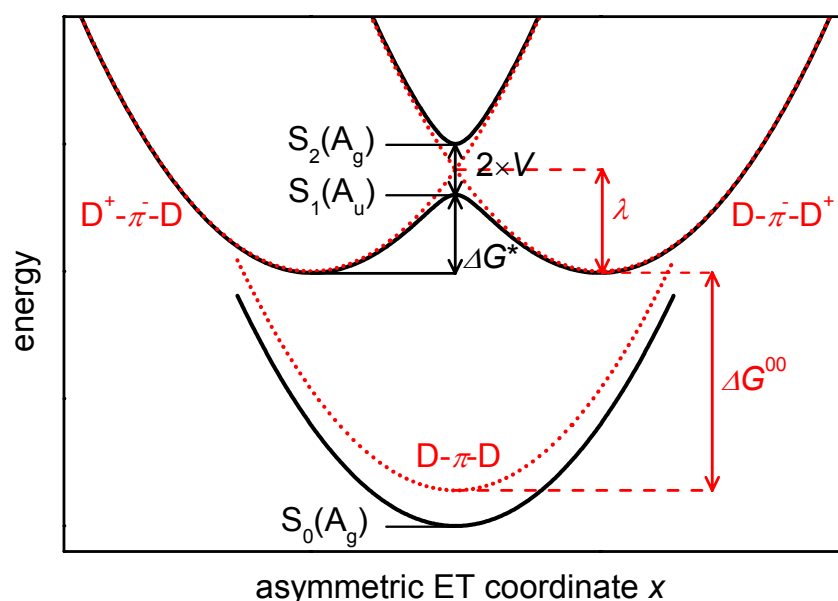Figure 4. One-dimensional projection of diabatic (red) and adiabatic PES (black) of a D-π-D excited state mixed-valence system.

These states have local CT character as proved by the solvatochromism of the fluorescence (see above). Coupling of these two excited diabatic states yields the two excited states S$_1$ and S$_2$. For the excited state electronic coupling V half the energy splitting between the S$_1$ and the

S_2 state as determined by two-photon absorption measurements were used (Table 5).[9] The couplings between the ground and the two degenerate excited CT states are neglected ($V_{12}=V_{23}=0$ cm^{-1}) in this model.

Table 5. S_1-S_2 splitting and electronic couplings from two-photon absorption measurements and relative shift of $\tilde{\nu}_{abs}$ vs. these of the reference compound **5** (for **1** and **2**) and **6** (for **3**) in C_6H_{12} (all values in cm^{-1}).

	1	**2**	**3**	**4**
S_2-S_1 $^{\text{two-photon}}$	2300	480	3400	3600
V	1200	240	1700	1800
$\tilde{\nu}_{abs} - \tilde{\nu}_{abs}$ (**5/6**)	2400	1200	2600	

The above evaluated electronic couplings and harmonic potentials with reorganization energies λ were used for constructing the PES. The minima of the three diabatic potentials are chosen in a way that they form a regular triangle on a two-dimensional potential map, that is, the (dimensionless) reaction coordinates connecting the three states are unity.

$$\begin{vmatrix} \lambda\left[\left(-\dfrac{1}{2}-x\right)^2+\left(\dfrac{\sqrt{3}}{2}-y\right)^2\right]+\Delta G^{00}-\varepsilon & 0 & V \\ 0 & \lambda(x^2+y^2)-\varepsilon & 0 \\ V & 0 & \lambda\left[\left(\dfrac{1}{2}-x\right)^2+\left(\dfrac{\sqrt{3}}{2}-y\right)^2\right]+\Delta G^{00}-\varepsilon \end{vmatrix}=0 \qquad (14)$$

Diagonalization of matrix (14) yields the adiabatic PES with the three states S_0, S_1 and S_2 (see Figure 5). If one assumes C_i symmetry to be the highest symmetry in all compounds **1-4** the electronic state S_0 possesses A_g symmetry, S_1 is A_u symmetric and S_2 has again A_g symmetry. The reorganization energies λ as well as the free energy difference ΔG^{00} between the diabatic ground state and the diabatic degenerate excited states were optimized in order to reproduce the experimentally observed absorption and fluorescence energies as indicated by yellow arrows in Figure 5. Owing to the crudeness of this model the resulting λ, ΔG^{00} and ΔG^* values may only be treated as qualitative and are given in Table 6.

Table 6. Optimized ΔG^{00}, λ values, calculated ET-barriers ΔG^* and transient IVCT absorption energies S_2-S_1^{trans} in cm^{-1}.

		λ	ΔG^{00}	ΔG^*	S_2-S_1^{trans}
1	C_6H_{12}	3100	24950	40	3080
	MeCN	5700	22150	480	5660
2	C_6H_{12}	2800	25500	480	2570
	MeCN	5350	23350	1110	4840
3	C_6H_{12}	2450	20600	0	3400
	CH_2Cl_2	3900	18450	20	3920
4	C_6H_{12}	2550	21400	0	3600
	MeCN	3450	19500	0	3600

In the following the photophysical processes in the symmetrical *p*-xylene **1** will be interpreted using the three-level approximation described above. Dimer **1** can formally be divided into two subunits **5** which are electronically coupled: Excitation of **1** yields an initially symmetrical excited Franck-Condon state as indicated by the lack of solvatochromism in the absorption process. This Franck-Condon state is at the ridge between two minima. The transition into the S_1 state is symmetry allowed while the transition into the S_2 state is one-photon forbidden and only allowed in a two-photon process, see ref.[9]. As evident from Figure 5 the S_1 state is distorted by a second order *Jahn-Teller* effect. It relaxes into one of two minima which represent a symmetry broken locally excited CT state in which a partial positive charge is localized on the triarylamine donor and the negative charge on the π-bridge. From this symmetry broken CT state the molecule might return to the ground state by fluorescence. The large excited-state geometry relaxation also explains the large Stokes-shift.

On the excited state potential energy surface the optical excitation from the relaxed S_1 state to a Franck-Condon S_2 state can be viewed as an excited state intervalence charge transfer (cyan arrow in Figure 5) because it essentially refers to the transfer of a positive charge from one triarylamine over the negatively charged π-bridge to the other triarylamine moiety (D^+-$\bar{\pi}$-D $\rightarrow$ D-$\bar{\pi}$-D^+). This excited state intervalence charge transfer (IVCT) may in principle be observed in the transient absorption spectra of compounds **1-4**. The energy of this excited IVCT transition S_2-S_1^{trans} (Table 6) was estimated from the adiabatic PES to lie between 2570 and 5660 cm^{-1} for all compounds. Unfortunately, this energy is too low to be measurable in the present experimental set-up.
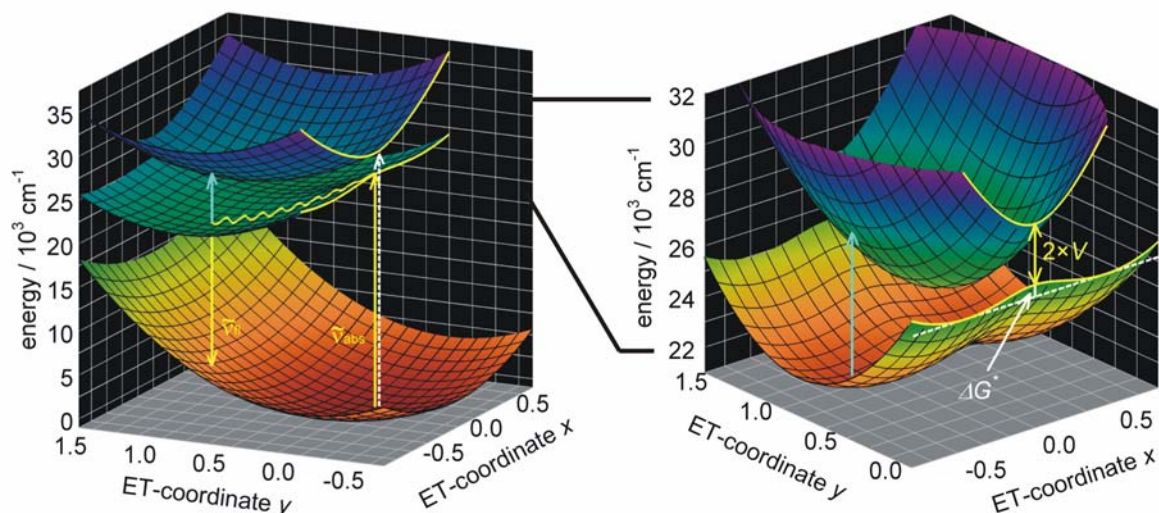
Figure 5. Adiabatic potential energy surfaces of **1** in MeCN (yellow arrows: absorption and fluorescence; dashed white arrow: two-photon absorption; cyan arrow: transient IVCT transition). The diagram on the right is a close-up of the S_1 and S_2 PES.

For the weakly coupled paracyclophane **2** as well as the *p*-xylene **1** the S_1 potential energy surface shows a double minimum potential in both apolar and polar media. This situation is reflected by the considerable magnitude of the barrier along the *x*-coordinate ΔG^* (which is *y*-coordinate independent) of the excited intervalence electron transfer (see Figure 5) as estimated from the adiabatic PES (Table 6). Generally this barrier is large for weak coupling as well as for small solvent reorganization energy. In fact, only **1** and **2** have a CT-barrier in both apolar and polar solvents. Based on the theoretical analysis paracyclophane **2** shows the weakest coupling and, therefore, the adiabatic locally excited CT state at the minimum of the S_1 potential energy surface can be considered to be similar to the localized diabatic state (D^+-π^--D). Thus, this symmetry broken diabatic state of paracyclophane **2** can directly be compared with the first excited state (D^+-π^-) of the asymmetric subunit **5**. This close analogy explains that both the transient absorption spectra of **5** and **2** and the dipole moment differences $\Delta\mu$ derived from the linear correlations in the *Lippert-Mataga* plots of **5** and **2** are very similar. Furthermore, the weak interactions of the subunits (diabatic states) in **2** are the reason for the additive behavior of the fluorescence oscillator strengths f_{fl}. As the paracyclophane **2** is composed of two subunits **5** the oscillator strengths f_{fl} of the dimer **2** are approximately twice that of the corresponding monomer **5** (see Table 2).

The stronger coupling of the *p*-xylene dimer **1** has, in contrast to the weak coupling of **2**, a significant influence on the optical properties. This is demonstrated, in particular, by the non-additive behavior of f_{fl} which is three to four times as high as for the dimer **1** in comparison to f_{fl} of **5**. The fluorescence quantum yields ϕ of the dimers **1** and **2** are larger than that of monomer **5** in most solvents. This cooperative effect of the dimers **1** and **2** can be understood as an exciton superradiant emission:[72] In a weakly coupled dimer chromophore the absorption oscillator strength f_{abs} of the dimer is twice that of the monomer. Consequently, if there is no change in the nature of the excited state transition moment the fluorescence oscillator strength f_{fl} of the dimer is twice that of the monomer. As the fluorescence rate constant k_f is linearly correlated to the fluorescence oscillator strength f_{fl} (see eqs. 4 and 5) k_f of the dimer is twice that of the monomer. The fluorescence quantum yield is given by $\phi = k_f/(k_f+k_{nr})$. Provided that $k_{nr} > k_f$ and the rate constant of nonradiative processes k_{nr} being constant it follows $\phi = k_f/k_{nr,const}$. Thus, it follows that the quantum yield of the dimer is also twice that of the monomer. Consequently, the significantly larger fluorescence quantum yields of dimers **1** and **2** compared to **5** will be interpreted as an exciton superradiance of these dimers.

In contrast to **1** and **2**, the strongly coupled chloro-substituted anthracene **4** shows, independent of solvent polarity, no CT-barrier ($\Delta G^* = 0$ cm^{-1}). Thus, the S$_1$ state is characterized by a single minimum potential. The excitation of **4** to the S$_1$ state is not followed by symmetry breaking because the S$_1$ state relaxes solely along the symmetric *y*-coordinate to the symmetrically delocalized minimum. It is supposed that the delocalized S$_1$ state of **4** explains the relatively weak solvent effect both in the absorption and fluorescence spectra as well as the similar appearance of the transient absorption spectra of anthracene **4** in both solvents. Furthermore, the small dipole moment differences $\Delta\mu$ derived from the *Lippert-Mataga* plots of **4** can be traced back to this delocalized character of the S$_1$ state. The single minimum potential of the S$_1$ state in apolar as well as polar media is also the explanation for the large and solvent independent fluorescence quantum yields ϕ as there is no significant reorganization (only along symmetric coordinate *y*) in the first excited state of **4**. A consequence of the single minimum PES of the first excited state is that the S$_0$ and S$_1$ potentials have either no intersection or at much higher energy and, therefore, the rate constant k_{nr} for nonradiative processes is small and the fluorescence quantum yield ϕ approaches unity.

The situation is different for the S$_1$ potential energy surface of the methoxy-substituted anthracene **3** which has a single minimum potential in a nonpolar medium but a double

minimum potential with a small barrier in a polar solvent. Therefore, the fluorescence quantum yields of **3** are larger in apolar media in comparison to polar media because there is no significant reorganization of the S_1 state in apolar medium as mentioned above (for anthracene **4**). As the excited state S_1 is solvent dependent the relaxation leads to a symmetry broken locally excited CT state only in a polar medium, but to a symmetrically delocalized excited state in an apolar solvent. This fact accounts for the strong solvent influence on the transient absorption of **3**. The different behavior of **3** and **4** in apolar media is due to the influence of the methoxy and chloro substituents. The latter destabilize a polar symmetry broken CT state. The strong coupling in **3** leads to significant differences of the spectral properties of dimer **3** and monomer **6**. In particular, these differences become clear considering the oscillator strengths for fluorescence f_{fl} of **3** and **6** which are about the same and, thus, are not additive. Furthermore, the estimated dipole moment differences $\Delta\mu$ derived from the *Lippert-Mataga* plots of dimer **3** differ significantly from $\Delta\mu$ of **6**. The fluorescence quantum yields of the anthracene monomer **6** is close to unity in the most solvents and, therefore, k_{nr} is small. The quantum yields of the corresponding anthracene dimer **3** show no cooperative effect because they are even smaller than that of the monomer unit **6** in all solvents. This observation reflects that superradiant emission is found only if in the monomer k_{nr} is large and the quantum yield is small. Thus, superradiance is not possible for strongly coupled dimers such as **3** and **4** because the strong coupling results in non-additive behavior of f_{fl} as demonstrated for **3**.

The excited state mixed-valence compounds **1-4** as well as their corresponding monomers **5** and **6** investigated in this study show significantly different spectroscopic behavior in apolar and polar solvents. The *Lippert-Mataga* plots cannot be fitted by a single linear function over the complete polarity range. Not only the dimers **1-4** show two different linear correlations, one for weakly polar and one for polar solvents, but also the corresponding monomers **5** and **6**. Consequently, this behavior can not be traced back to interactions of the subunits in the dimers. Comparable results with bilinear *Lippert-Mataga* plots have already been described in the literature.[53,73-75] The bilinear *Lippert-Mataga* plots as well as the transient absorption properties of compounds **1-6** clearly indicate a major molecular reorganization in the first excited states.[76]

5   Conclusions

In this study a set of bistriarylamine compounds **1-4** composed of two asymmetric subunits was investigated. Although superficially symmetrical the bistriarylamines **1** and **2** undergo a strong symmetry breaking in the excited state in both apolar and polar solvent environments. This is due to a weak electronic coupling of the monomeric subchromophores and a strong coupling to solvent modes which increases the reorganization energy. Reactions on the excited state PES can be conceived as being excited state hole transfer processes from one triarylamine unit to the other, i.e. as excited state mixed-valence compounds. A further consequence of the weak electronic coupling is the superradiant behavior particularly of **2** which leads to an up to threefold enhancement of fluorescence quantum yield compared to monomer **5**. Much in contrast the anthracene derivatives **3** and **4** show a different behavior. While both, **3** and **4**, exhibit a much stronger electronic coupling than **1** and **2** the PES is solvent dependent in a more subtle way: anthracene **3** with methoxy substituents attached to the triarylamine moieties shows a double minimum PES of the S_1 state in polar solvents while in apolar solvents the barrier vanishes and the excited state is delocalized. This shows that solvent influence is the symmetry breaking factor in these cases. Compound **4** with chloro substituents instead of methoxy exhibits a delocalized barrierless PES in all solvents. This observation demonstrates very nicely that even small modifications in the chromophore periphery may strongly influence the fluorescence behavior.

The excited state PES of the anthracene compounds show a solvent dependence very similar to the ground state PES of **3**$^+$ and **4**$^+$ mixed-valence radical cations. This observation demonstrates the close analogy of excited state mixed-valence behavior of neutral chromophores and the ground state mixed-valence behavior of the radical cations derived thereof.

6   References

(1)   Hreha, R. D.; George, C. P.; Haldi, A.; Domercq, B.; Malagoli, M.; Barlow, S.; Brédas, J.-L.; Kippelen, B.; Marder, S. R. *Adv. Funct. Mater.* **2003**, *13*, 967-973.

(2)   Albota, M.; Beljonne, D.; Brédas, J.-L.; Ehrlich, J. E.; Fu, J.-Y.; Heikal, A. A.; Hess, S. E.; Kogej, T.; Levin, M. D.; Marder, S. R.; McCord-Maughon; Dianne, P.; Joseph, W.; Rockel, H.; Rumi, M.; Subramaniam, G.; Webb, W. W.; Wu, X.-L.; Xu, C. *Science* **1998**, *281*, 1653-1656.

(3)   Reinhardt, B. A.; Brott, L. L.; Clarson, S. J.; Dillard, A. G.; Bhatt, J. C.; Kannan, R.; Yuan, L. X.; He, G. S.; Prasad, P. N. *Chem. Mater.* **1998**, *10*, 1863-1874.

(4)   Rumi, M.; Ehrlich, J. E.; Heikal, A. A.; Perry, J. W.; Barlow, S.; Hu, Z.; McCord-Maughon, D.; Parker, T. C.; Roeckel, H.; Thayumanavan, S.; Marder, S. R.; Beljonne, D.; Brédas, J.-L. *J. Am. Chem. Soc.* **2000**, *122*, 9500-9510.

(5)   Chung, S. J.; Lin, T. C.; Kim, K. S.; He, G. S.; Swiatkiewicz, J.; Prasad, P. N.; Baker, G. A.; Bright, F. V. *Chem. Mater.* **2001**, *13*, 4071-4076.

(6)   Cho, B. R.; Piao, M. J.; Son, K. H.; Lee, S. H.; Yoon, S. J.; Jeon, S. J.; Cho, M. H. *Chem.-Eur. J.* **2002**, *8*, 3907-3916.

(7)   Pond, S. J. K.; Rumi, M.; Levin, M. D.; Parker, T. C.; Beljonne, D.; Day, M. W.; Brédas, J. L.; Marder, S. R.; Perry, J. W. *J. Phys. Chem. A* **2002**, *106*, 11470-11480.

(8)   Ortiz, R. P.; Delgado, M. C. R.; Casado, J.; Hernandez, V.; Kim, O. K.; Woo, H. Y.; Navarrete, J. T. L. *J. Am. Chem. Soc.* **2004**, *126*, 13363-13376.

(9)   Strehmel, B.; Amthor, S.; Schelter, J.; Lambert, C. *ChemPhysChem* **2005**, *6*, 893-896.

(10)   Lambert, C.; Nöll, G.; Schelter, J. *Nat. Mater.* **2002**, *1*, 69–73.

(11)   see chapter III

(12)   Lambert, C.; Amthor, S.; Schelter, J. *J. Phys. Chem. A* **2004**, *108*, 6474-6486.

(13)   Amthor, S.; Noller, B.; Lambert, C. *Chem. Phys.* **2005**, *316*, 141-152.

(14)   Fraysse, S.; Coudret, C.; Launay, J. P. *Tetrahedron Lett.* **1998**, *39*, 7873-7876.

(15)   Schlicke, B.; De Cola, L.; Belser, P.; Balzani, V. *Coord. Chem. Rev.* **2000**, *208*, 267-275.

(16)   Schenning, A. P. H. J.; Tsipis, A. C.; Meskers, S. C. J.; Beljonne, D.; Meijer, E. W.; Brédas, J. L. *Chem. Mater.* **2002**, *14*, 1362-1368.

(17)   Fraysse, S.; Coudret, C.; Launay, J.-P. *J. Am. Chem. Soc.* **2003**, *125*, 5880-5888.

(18) Zareie, M. H.; Ma, H.; Reed, B. W.; Jen, A. K. Y.; Sarikaya, M. *Nano Letters* **2003**, *3*, 139-142.

(19) Giacalone, F.; Segura, J. L.; Martin, N.; Guldi, D. M. *J. Am. Chem. Soc.* **2004**, *126*, 5340-5341.

(20) Kang, S. H.; Ma, H.; Kang, M. S.; Kim, K. S.; Jen, A. K. Y.; Zareie, M. H.; Sarikaya, M. *Angew. Chem., Int. Ed.* **2004**, *43*, 1512-1516.

(21) Walter, D.; Neuhauser, D.; Baer, R. *Chem. Phys.* **2004**, *299*, 139-145.

(22) Heilbronner, E.; Maier, J. P. *Helv. Chim. Acta* **1974**, *57*, 151-159.

(23) Canuto, S.; Zerner, M. C. *Chem. Phys. Lett.* **1989**, *157*, 353-358.

(24) Canuto, S.; Zerner, M. C. *J. Am. Chem. Soc.* **1990**, *112*, 2114-2120.

(25) Bazan, G. C.; Oldham Jr., J.; Lachicotte, R. J.; Tretiak, S.; Chernyak, V.; Mukamel, S. *J. Am. Chem. Soc.* **1998**, *120*, 9188-9204.

(26) Verdal, N.; Godbout, J. T.; Perkins, T. L.; Bartholomew, G. P.; Bazan, G. C.; Kelley, A. M. *Chem. Phys. Lett.* **2000**, *320*, 95-103.

(27) Zyss, J.; Ledoux, I.; Volkov, S.; Chernyak, V.; Mukamel, S.; Bartholomew, G. P.; Bazan, G. C. *J. Am. Chem. Soc.* **2000**, *122*, 11956-11962.

(28) Bartholomew, G. P.; Bazan, G. C. *Acc. Chem. Res.* **2001**, *34*, 30-39.

(29) Bartholomew, G. P.; Bazan, G. C. *J. Am. Chem. Soc.* **2002**, *124*, 5183-5196.

(30) Moran, A. M.; Bartholomew, G. P.; Bazan, G. C.; Kelley, A. M. *J. Phys. Chem. A* **2002**, *106*, 4928-4937.

(31) Bartholomew, G. P.; Rumi, M.; Pond, S. J. K.; Perry, J. W.; Tretiak, S.; Bazan, G. C. *J. Am. Chem. Soc.* **2004**, *126*, 11529-11542.

(32) Stefan Grimme *Chem.-Eur. J.* **2004**, *10*, 3423-3429.

(33) Hong, J. W.; Woo, H. Y.; Liu, B.; Bazan, G. C. *J. Am. Chem. Soc.* **2005**, *127*, 7435-7443.

(34) Woo, H. Y.; Hong, J. W.; Liu, B.; Mikhailovsky, A.; Korystov, D.; Bazan, G. C. *J. Am. Chem. Soc.* **2005**, *127*, 820-821.

(35) Guyard, L.; Nguyen Dinh An, M.; Audebert, P. *Adv. Mater.* **2001**, *13*, 133-136.

(36) Guyard, L.; Audebert, P. *Electrochem. Commun.* **2001**, *3*, 164-167.

(37) Morisaki, Y.; Chujo, Y. *Macromolecules* **2002**, *35*, 587-589.

(38) Morisaki, Y.; Ishida, T.; Chujo, Y. *Macromolecules* **2002**, *35*, 7872-7877.

(39) Morisaki, Y.; Chujo, Y. *Chem. Lett.* **2002**, 194-195.

(40) Salhi, F.; Lee, B.; Metz, C.; Bottomley, L. A.; Collard, D. M. *Org. Lett.* **2002**, *4*, 3195-3198.

(41) Salhi, F.; Collard, D. M. *Adv. Mater.* **2003**, *15*, 81-85.

(42) Morisaki, Y.; Chujo, Y. *Macromolecules* **2003**, *36*, 9319-9324.

(43) Morisaki, Y.; Fujimura, F.; Chujo, Y. *Organometallics* **2003**, *22*, 3553-3557.

(44) Morisaki, Y.; Chujo, Y. *Macromolecules* **2004**, *37*, 4099-4103.

(45) Morisaki, Y.; Ishida, T.; Tanaka, H.; Chujo, Y. *J. Polym. Sci., Part A: Polym. Chem.* **2004**, *42*, 5891-5899.

(46) Morisaki, Y.; Chujo, Y. *Bull. Chem. Soc. Jpn.* **2005**, *78*, 288-293.

(47) Morisaki, Y.; Wada, N.; Chujo, Y. *Polymer* **2005**, *46*, 5884-5889.

(48) Miller, D. S.; Leffler, J. E. *J. Phys. Chem.* **1970**, *74*, 2571-2574.

(49) Leroy, E.; Lami, H. *Chem. Phys. Lett.* **1976**, *41*, 373-377.

(50) Yao, H.; Okada, T.; Mataga, N. *J. Phys. Chem.* **1989**, *93*, 7388-7394.

(51) Lueck, H. B.; McHale, J. L.; Edwards, W. D. *J. Am. Chem. Soc.* **1992**, *114*, 2342-2348.

(52) Lewis, L. M.; Indig, G. L. *Dyes Pigm.* **2000**, *46*, 145-154.

(53) Piet, J. J.; Schuddeboom, W.; Wegewijs, B. R.; Grozema, F. C.; Warman, J. M. *J. Am. Chem. Soc.* **2001**, *123*, 5337-5347.

(54) Zhang, F. S.; Lynden-Bell, R. M. *Phys. Rev. Lett.* **2003**, *90*, 185505.

(55) Cisnetti, F.; Ballardini, R.; Credi, A.; Gandolfi, M. T.; Masiero, S.; Negri, F.; Pieraccini, S.; Spada, G. P. *Chemistry-a European Journal* **2004**, *10*, 2011-2021.

(56) Ortiz, R. P.; Delgado, M. C. R.; Casado, J.; Hernández, V.; Kim, O. K.; Woo, H. Y.; Navarrete, J. T. L. *J. Am. Chem. Soc.* **2004**, *126*, 13363-13376.

(57) Thompson, A. L.; Gaab, K. M.; Xu, J. J.; Bardeen, C. J.; Martínez, T. J. *J. Phys. Chem. A* **2004**, *108*, 671-682.

(58) Karstens, T.; Kobs, K. *J. Phys. Chem. A* **1980**, *84*, 1871-1872.

(59) Gurzadyan, G. G.; Steenken, S. *Chem.-Eur. J.* **2001**, *7*, 1808-1815.

(60) Gurzadyan, G.; Gorner, H. *Chem. Phys. Lett.* **2000**, *319*, 164-172.

(61) Birks, J. *Photophysics of Aromatic Molecules*; Wiley-Interscience: London, 1970.

(62) Lewis, J. E.; Maroncelli, M. *Chem. Phys. Lett.* **1998**, *282*, 197-203.

(63) Strickler, S. J.; Berg, R. A. *J. Chem. Phys.* **1962**, *37*, 814.

(64) Mataga, N.; Kaifu, Y.; Koizumi, M. *Bull. Chem. Soc. Jpn.* **1956**, *29*, 465-470.

(65) Lippert, E. *Z. Elektrochem.* **1957**, *61*, 962-975.

(66) Lampert, R. A.; Chewter, L. A.; Phillips, D.; O'Connor, D. V.; Roberts, A. J.; Meech, S. R. *Anal. Chem.* **1983**, *55*, 68-73.

(67) Lambert, C.; Schelter, J.; Fiebig, T.; Mank, D.; Trifonov, A. *J. Am. Chem. Soc.* **2005**, *127*, 10600-10610.

(68) Dümmler, S.; Roth, W.; Fischer, I.; Heckmann, A.; Lambert, C. *Chem. Phys. Lett.* **2005**, *408*, 264-268.

(69) Badger, B.; Brocklehurst , B. *Trans. Faraday Soc.* **1969**, *65*, 2582-2587.

(70) Shida, T. *Electronic Absorption Spectra of Radical Ions*; Elsevier: Amsterdam, 1988; Vol. 34.

(71) Ruseckas, A.; Namdas, E. B.; Lee, J. Y.; Mukamel, S.; Wang, S. J.; Bazan, G. C.; Sundström, V. *J. Phys. Chem. A* **2003**, *107*, 8029-8034.

(72) Rehler, N. E.; Eberly, J. H. *Phys. Rev. A* **1971**, *3*, 1735-1751.

(73) Verbeek, G.; Depaemelaere, S.; Van der Auweraer, M.; De Schryver, F. C.; Vaes, A.; Terrell, D.; De Meutter, S. *Chem. Phys.* **1993**, *176*, 195-213.

(74) Catalán, J.; Díaz, C.; López, V.; Perez, P.; Claramunt, R. M. *J. Phys. Chem.* **1996**, *100*, 18392-18398.

(75) Onkelinx, A.; DeSchryver, F. C.; Viaene, L.; VanderAuweraer, M.; Iwai, K.; Yamamoto, M.; Ichikawa, M.; Masuhara, H.; Maus, M.; Rettig, W. *J. Am. Chem. Soc.* **1996**, *118*, 2892-2902.

(76) In eq. 9 the polarizability α of the molecule is neglected and the dipole is approximated as a point-dipole in a spherical cavity of the solvent which is described by a dielectric continuum model.[64,65] These approximations and the fact that the molecules investigated here are all not spherical may be the explanation that the solvent influence on the first excited state is not described well and the plots are, thus, bilinear. A similar behavior was found for other organic molecules and in this context modified polarity scales were tested to improve the Lippert-Mataga equation.[73-75] In fact, what was found in this study is that the use of an other polarity scale still results in bilinear plots.

Bis-triarylamino-[2.2]paracyclophanes I:
Mixed-Valence Mono-Radical Cations

## CONTENTS

1   Introduction

Both intermolecular and intramolecular charge transfer in π-conjugated molecules are of fundamental interest for the development of conducting and semiconducting materials for organic electronic devices. While charge transfer along conjugated backbones is usually quite fast, it is the charge transfer between the conjugated systems that limits the overall charge transfer rate. In this chapter, the synthesis and investigation of the optically induced hole transfer processes of model systems, in which the π-faces of two triarylamine moieties are brought in close contact by a [2.2]paracyclophane unit are presented.

The [2.2]paracyclophane moiety is a simple scaffold to bring chromophores in close contact even beyond the *van der Waals* distance, in order to examine interactions based on through-bond (σ) and through-space (π-π) couplings without having direct π-conjugation.[1-10] It has been demonstrated by *Heilbronner* and *Maier*, that both couplings, through-bond and through-space are of importance for electronic interactions in [2.2]paracyclophanes.[11] In this context, the investigation of charged cyclophane systems is of great interest for studying charge transfer processes over the [2.2]paracyclophane moiety. While the oxidation of unsubtituted [2.2]paracyclophane to the corresponding radical cation is irreversible in solution[12] the radical anion of [2.2]paracyclophane is more persistent.[13-16] *Badger* and *Brocklehurst* reported absorption spectra of both the radical anion and the radical cation of [2.2]paracyclophane which were generated by γ-radiolysis of glassy solutions at low temperatures.[17] The absorption spectrum of the radical cation was compared with the photoelectron spectrum of neutral [2.2]paracylophane by *Heilbronner et al..*[18] It was shown by ESR and ENDOR spectroscopy, that a substitution of [2.2]paracyclophane by electron donating groups such as methyl or methoxy substituents leads to a stabilization of the corresponding radical cations.[16,19-22] By these methods, a strong intramolecular electronic coupling between the two aromatic subunits was found, which is in agreement with the interpretation of the absorption signal of the [2.2]paracyclophane radical cation as a charge resonance band by *Badger* and *Brocklehurst*.[17] The *Mulliken-Hush* theory was recently applied to the absorption spectra of dinitro-[2.2]paracyclophane radical anions.[23] In this study, the authors found that the *pseudo-para* isomer is a class III mixed valence system where the charge is completely delocalized over the hole cyclophane while the *pseudo-ortho* isomer is

supposed to be at the class II / class III borderline where, depending on the solvent polarity, the charge is either localized (class II) on one molecular half or delocalized (class III).

Triarylamine moieties have recently been used as redox centers in a number of mixed-valence (MV) compounds[24-51] and redox cascades[52] in order to study hole transfer processes. MV species are generally characterized by at least two redox centers with unequal formal oxidation states. In the study presented here, the cyclophane moiety is used as the bridging unit between two triarylamine redox centers (see Chart 1). In the resulting MV radical ions, [N-B-N]$^+$ the distance between the two charge bearing units N was varied from $1^{\bullet+}$ over $4^{\bullet+}$ to $9^{\bullet+}$. The two isomers *pseudo-para* [2.2]paracyclophane $4^{\bullet+}$ and *pseudo-ortho* isomer $5^{\bullet+}$ were used to investigate the influence of the connectivity on hole transfer (HT) processes. For the comparison of the through-bond and through-space interactions of the [2.2]paracyclophane bridge with direct π-conjugation the *p*-xylene bridge was used in compound $6^{\bullet+}$. The Vis/NIR spectra of the MV compounds were analyzed by a generalized *Mulliken-Hush* (GMH)[53-55] three-level model using both experimental transition energies and transition moments as well as AM1-CISD computed values in order to calculate the diabatic electronic coupling matrix elements which yield information about the electronic interactions of the MV species.

Chart 1.

An = 4-methoxyphenyl
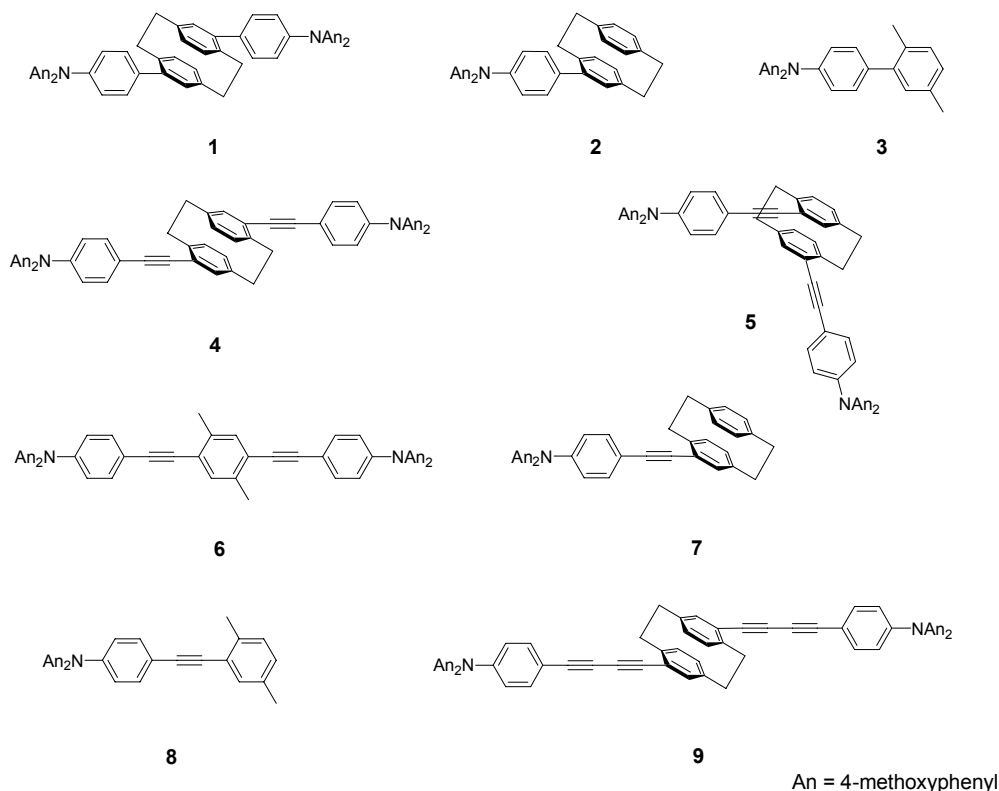
In the three-level GMH model, which was recently applied for similar MV compounds,[34,44] two transitions are taken into account: on the one hand the inter-valence charge transfer (IV-CT) band which is assigned to an optically induced hole transfer from one redox center to the second and, on the other hand, a second band associated with a triarylamine radical cation to bridge hole transfer hereafter called "bridge band". Therefore, three levels have to be used for a proper description of the MV properties: the ground state (g), the first excited IV-CT state (a) and the second excited bridge state (b) (see Figure 1).
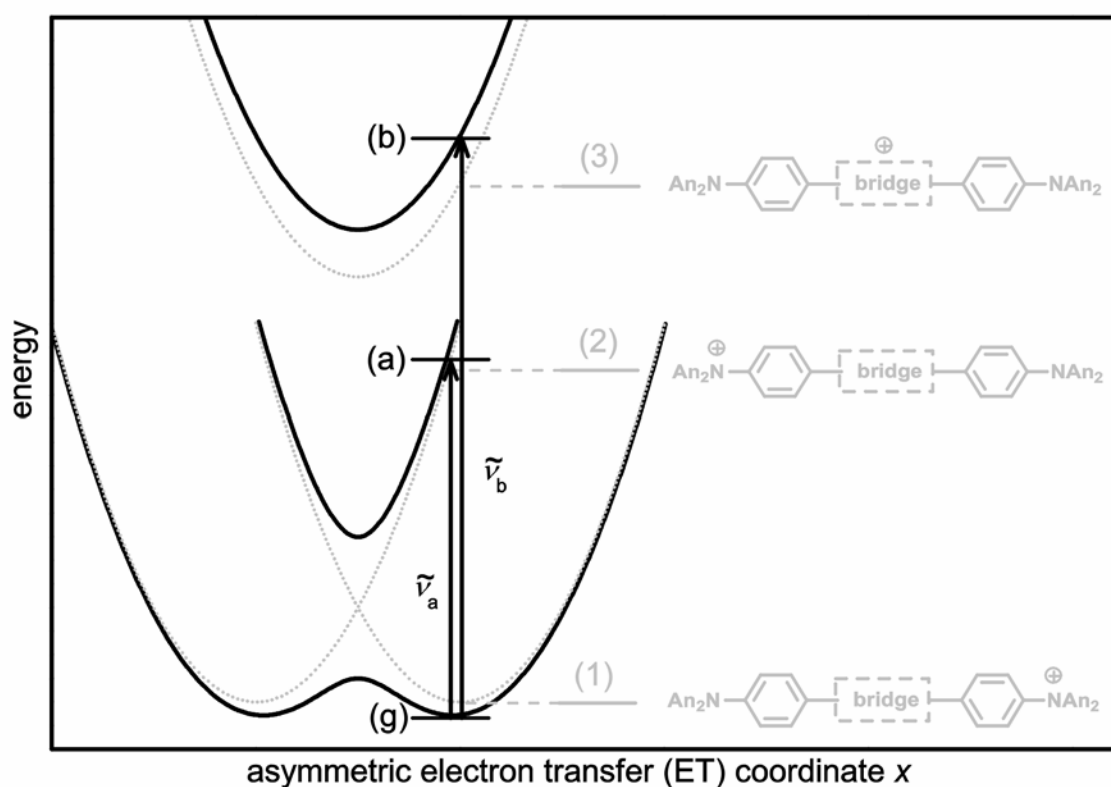
Figure 1. Adiabatic (black solid) and diabatic (grey dotted) states within a GMH three-level model.

Taking the bridge band into account is particularly necessary, if the MV species show an intense bridge band and the dipole moment difference between the ground (g) and the first excited (a) IV-CT state are relatively small.[44] In this paper, the results of the GMH analysis of the MV compounds will be used to evaluate potential energy surfaces (PES) of the three states within a semiclassical two-mode model.

2   Results and Discussion

2.1   Synthesis

Compounds **1-9** were synthesized by palladium and copper catalyzed C-C cross coupling reactions (Scheme 1). K$_3$PO$_4$ as the base for the *Suzuki* reaction[56,57] allows the protected boronic acid ester to be used in the synthesis of the biaryl compounds **1-3** from the corresponding aryl bromides.

Scheme 1.
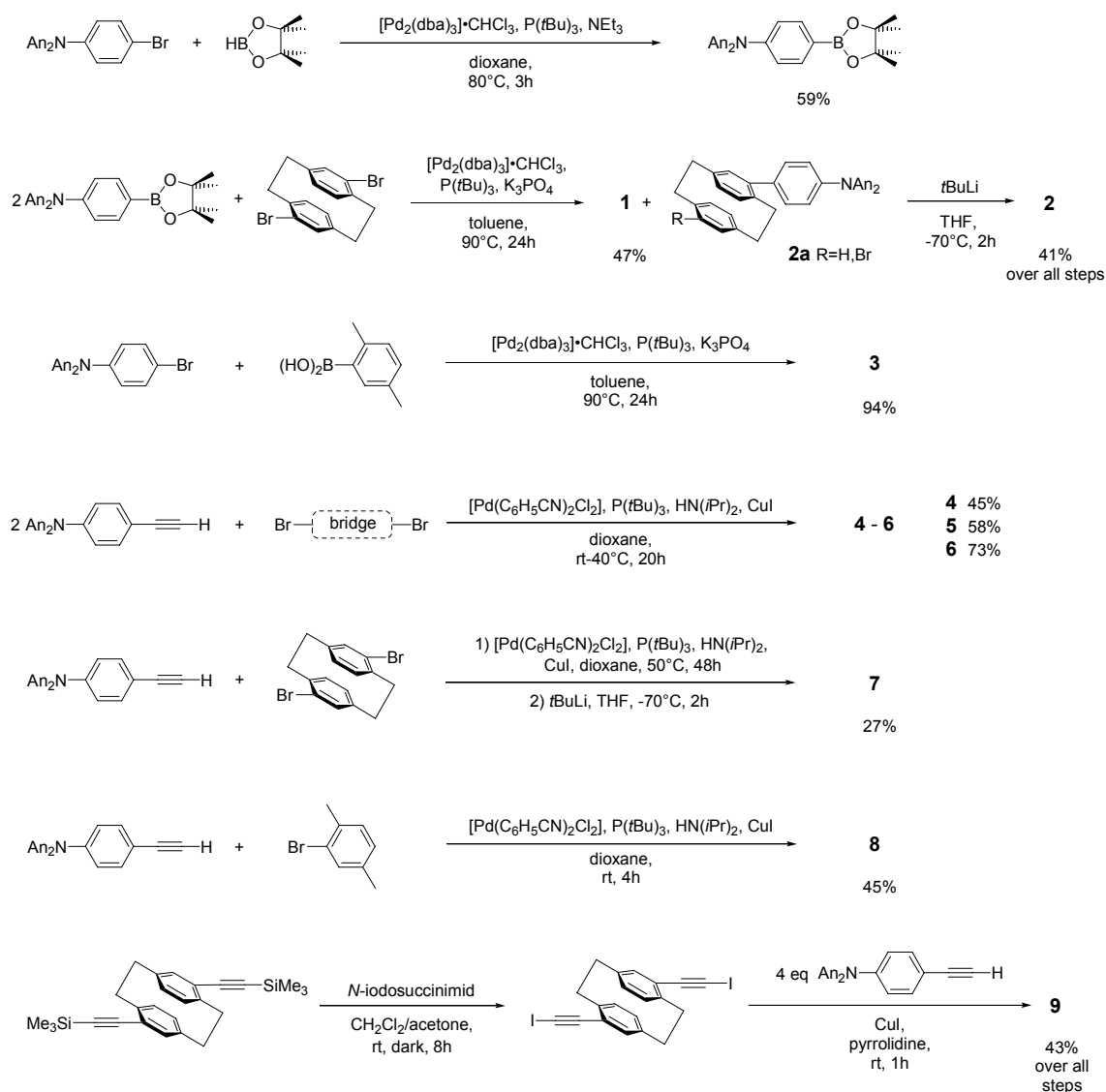
The protected boronic acid (see Scheme 1) was synthesized by palladium catalyzed cross coupling of aryl bromide with pinacol borane.[58,59] Compounds **4-8** with one acetylene unit between the aromatic building blocks were synthesized by *Sonogashira* coupling[60] of the acetylene compound with the corresponding aryl bromides. A one-pot synthesis of 4,16-bis-(iodoethynyl)-[2.2]paracyclophane from the bis(trimethylsilylacetylene)[61] and a convenient copper catalyzed coupling reaction of iodoacetylenes with unprotected acetylenes[62] made it possible to synthesize the bis-butadiyne **9** in good yield.

2.2   Evaluation of Diabatic Electronic Couplings (V) by GMH Theory

GMH theory developed by *Newton* and *Cave*[54] can be applied for the description of charge-transfer excitations in a system with any number of excited states *n* and has often been used within a two-level model for the analysis of IV-CT absorption properties from experimental or computational data.[63-69] Within the two-level approach the GMH is equivalent to the well-known *Mulliken-Hush* formalism (eq 1) with the experimental transition moment μ_{ga} (see eq 2) and the transition energy $\tilde{\nu}_a$ and the diabatic dipole moment difference $\Delta\mu_{12}$. The latter quantity can be traced back to purely adiabatic quantities (eq 3), where μ_{gg} and μ_{aa} are the dipole moments of the ground and the excited IV-CT state, respectively.

$$V_{\text{two-level}} = \frac{\mu_{ga}\tilde{\nu}_a}{\Delta\mu_{12}} \tag{1}$$

$$\mu_{ga} = 0.09584\sqrt{\frac{\int \varepsilon(\tilde{\nu})\mathrm{d}\tilde{\nu}}{\tilde{\nu}_a}} \tag{2}$$

$$\Delta\mu_{12} = \mu_{22} - \mu_{11} = \sqrt{(\mu_{aa} - \mu_{gg})^2 + 4\mu_{ga}^2} \tag{3}$$

In this study a three-level model which takes into account the ground state (g), the IV-CT state (a) and the bridge state (b) was used. The transition moments and dipole moments of these states yield the adiabatic matrix $\mu_{\mathbf{adiab}}$ (eq 4).[70] The transition moments for the IV-CT

excitation (μ_{ga}) and the bridge excitation (μ_{gb}) can both be obtained by band integration of the experimental spectrum (eq 2). In contrast, the transition moment μ_{ab} between these excited states (a) and (b) as well as the dipole moments μ_{gg}, μ_{bb} and μ_{aa} of the three levels (g), (a) and (b) are difficult to evaluate experimentally, and, therefore, are calculated by quantum chemical methods in the present study.

$$\boldsymbol{\mu}_{\text{adiab}} = \begin{pmatrix} \mu_{gg} & \mu_{ga} & \mu_{gb} \\ \mu_{ga} & \mu_{aa} & \mu_{ab} \\ \mu_{gb} & \mu_{ab} & \mu_{bb} \end{pmatrix} \qquad (4)$$

$$\boldsymbol{\mu}_{\text{diab}} = \begin{pmatrix} \mu_{11} & 0 & 0 \\ 0 & \mu_{22} & 0 \\ 0 & 0 & \mu_{33} \end{pmatrix} \qquad (5)$$

The GMH theory defines diabatic (model) levels which are strictly localized, and therefore have vanishing transition dipole moments between all states. Thus, all off-diagonal elements of the diabatic transition moment matrix $\boldsymbol{\mu}_{\text{diab}}$ (eq 5) are zero. Within this assumption the GMH theory uses a unitary transformation of the adiabatic transition moment matrix into the corresponding diabatic matrix according to $\boldsymbol{\mu}_{\text{diab}} = \mathbf{C}^{t} \boldsymbol{\mu}_{\text{adiab}} \mathbf{C}$. This is done by applying the diagonalization matrix $\mathbf{C}$ which consists of the normalized eigenvectors of $\boldsymbol{\mu}_{\text{adiab}}$. The same unitary transformation with identical matrix $\mathbf{C}$ is then applied to the adiabatic energy matrix $\mathbf{H}_{\text{diab}} = \mathbf{C}^{t} \mathbf{H}_{\text{adiab}} \mathbf{C}$. The adiabatic energy matrix (eq 6) consists of adiabatic energy differences between the ground state (a) and the first excited state (b) as well as the ground state (g) and the second excited state (b). These values are measurable quantities, since they correspond to the transition energies of the IV-CT band ($\tilde{\nu}_{a}$) and the bridge band ($\tilde{\nu}_{b}$).

$$\mathbf{H}_{\text{adiab}} = \begin{pmatrix} 0 & 0 & 0 \\ 0 & \tilde{\nu}_{a} & 0 \\ 0 & 0 & \tilde{\nu}_{b} \end{pmatrix} \qquad (6)$$

The resulting diabatic energy matrix (eq 7) then contains the energies of the diabatic states (1)-(3) as the diagonal elements H_{11}, H_{22} and H_{33} and, in addition, the electronic couplings V_{12}, V_{13} and V_{23} between these states as the off-diagonal elements.

$$\mathbf{H}_{diab} = \begin{pmatrix} H_{11} & V_{12} & V_{13} \\ V_{12} & H_{22} & V_{23} \\ V_{13} & V_{23} & H_{33} \end{pmatrix} \qquad (7)$$

These couplings are a measure for the electronic interactions between the diabatic states and, therefore, important for the description of the opto-electronic properties of MV systems. At this point, it has to be mentioned, that the couplings V in general depend on the nuclear motion but are evaluated here using the *Condon* approximation.

2.3   Electrochemical properties

All compounds **1-9** show a first oxidation wave between 200 mV and 300 mV versus ferrocene/ferrocenium (Fc/Fc^+) as the internal standard in CH_2Cl_2/0.15 M tetrabutyl-ammonium hexafluorophosphate (TBAH) (see Table 1).

Table 1. Redox potentials of **1-9** measured by cyclic voltammetry in CH_2Cl_2/0.15 TBAH vs Fc/Fc^+. The redox potentials of **1**, **4**, **5**, **6**, and **9** were determined by digital simulation of the voltammograms.

	$E_{1/2}(I)$ / mV	$E_{1/2}(II)$ / mV	ΔE
1	200	250	50
2	205	925	
3	225		
4	240	290	50
5	250	300	50
6	270	320	50
7	265	1000[a]	
8	270		
9	290	340	50

[a] Peak potential of an irreversible oxidation process

This first oxidation wave is reversible for all molecules even under thin layer conditions and is associated with a one-electron oxidation of the nitrogen center of mono-triarylamines and with a sequence of two one-electron oxidations of the first and the second nitrogen center of the bis-triarylamines. Because the peak separation is invisibly small for all bis-triarylamines, digital simulations of the voltammograms were used in order to determine the absolute values of the two redox potentials (see Figure 2 and Table 1).
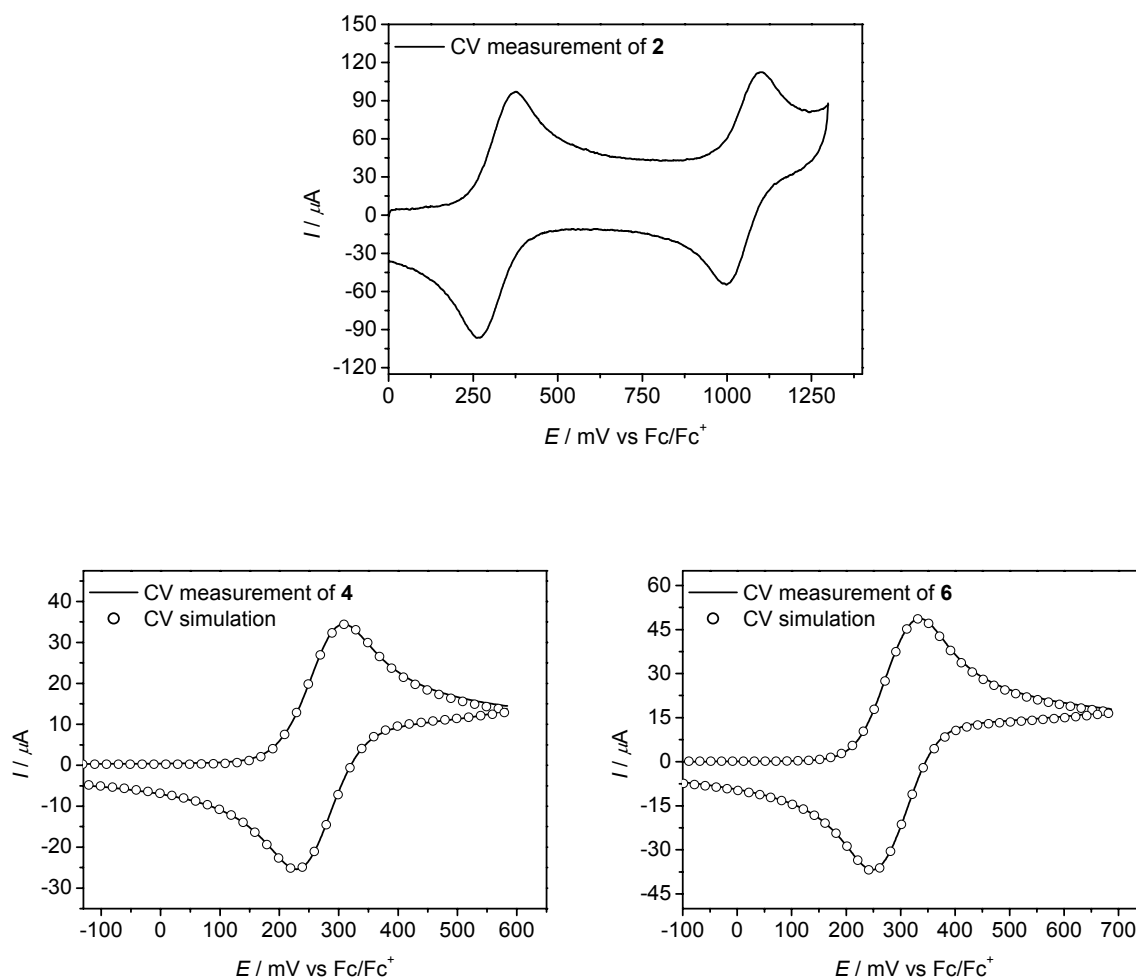
Figure 2. Cyclic voltammograms of **2** ($v = 5000$ mVs^{-1}), **4** and **6** (both $v = 250$ mVs^{-1}) in CH$_2$Cl$_2$/0.15 TBAH and digital simulations of the CVs of **4** and **6**.

The first oxidation potential of biaryl compounds **1-3** is within a 200-225 mV range, while molecules containing acetylene spacer show higher redox potentials between 240 and 270 mV and **9** with two butadiyne spacers shows the highest redox potential at 290 mV. The potential splittings between the first and the second oxidation are small due to the large distance

between the two triarylamine redox centers in **1**, **4**, **5**, **6** and **9**. The absolute $\mathit{\Delta E}$ values of all bis-triarylamines are similar within the experimental error. The fact, that all $\mathit{\Delta E}$ values are somewhat larger than the statistical value of 35.6 mV for non-interacting redox centers, is a hint that all the two redox centers in MV species interact weakly. Thus, the mono radical cations **1**$^{\bullet+}$, **4**$^{\bullet+}$, **5**$^{\bullet+}$, **6**$^{\bullet+}$ and **9**$^{\bullet+}$ are expected to be IV-CT systems of *Robin-Day* class II. For mono-triarylamine **2**, a second oxidation wave at 925 mV which is reversible only at high scan rates ($v = 5000$ mV s^{-1}) was observed, as well as a third irreversible oxidation at E_p(III) = 1305 mV. For compound **7**, there is a second oxidation peak at 1000 mV which proved to be irreversible. The second oxidation wave of **2** and **7** is associated with a second one-electron oxidation of the nitrogen center, while the third oxidation wave of **2** is interpreted as an irreversible oxidation of the paracyclophane moiety.

2.4 Experimental Vis/NIR spectra

The absorption spectra of the MV species $1^{\bullet+}$, $4^{\bullet+}$, $5^{\bullet+}$, $6^{\bullet+}$ and $9^{\bullet+}$ in CH_2Cl_2 and in MeCN (except $9^{\bullet+}$) were obtained by stepwise chemical oxidation of the corresponding neutral compounds and are shown in Figure 3 and Figure 4. For comparison, the spectra of the mono-triarylamine radical cations $2^{\bullet+}$, $3^{\bullet+}$, $7^{\bullet+}$ and $8^{\bullet+}$ in CH_2Cl_2 obtained in an analogous manner are also presented.
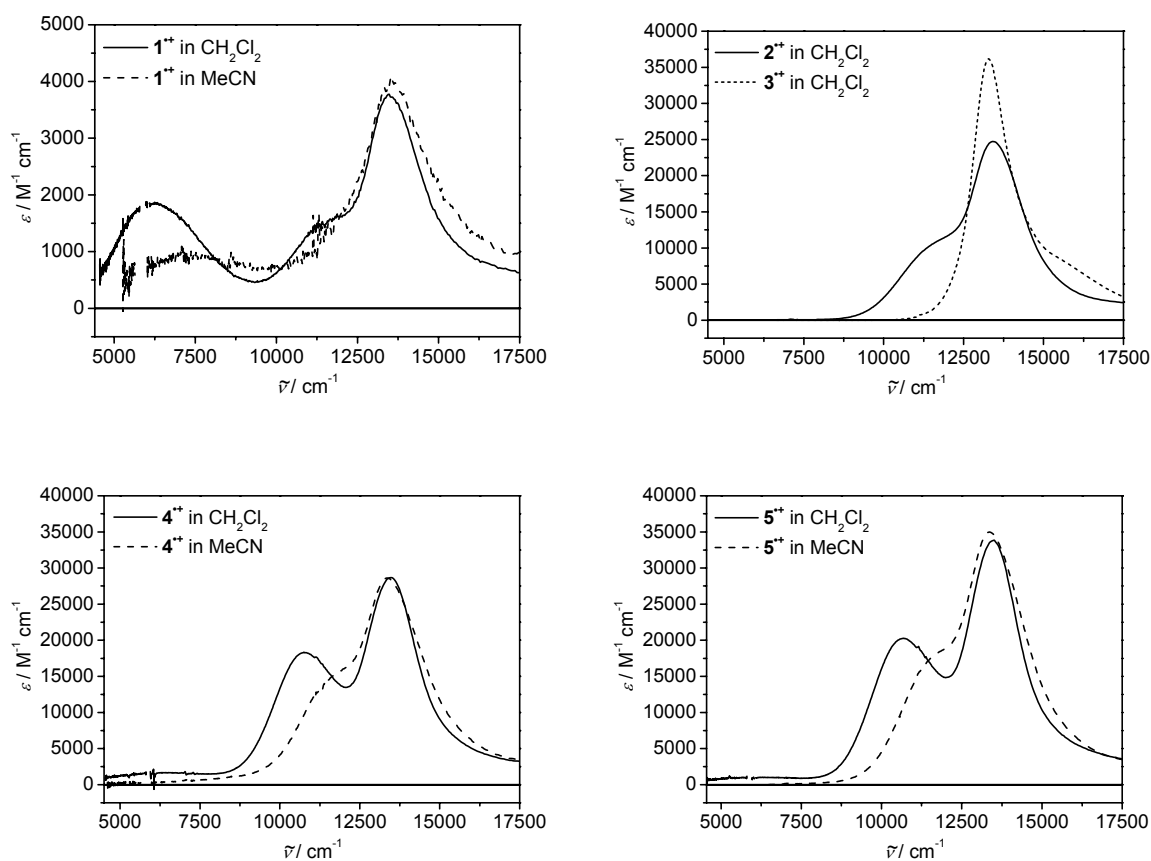
Figure 3. Experimental absorption spectra of mixed-valence species $1^{\bullet+}$, $4^{\bullet+}$ and $5^{\bullet+}$ in CH_2Cl_2 and in MeCN and spectrum of mono-triarylamine radical cations $2^{\bullet+}$ and $3^{\bullet+}$ in CH_2Cl_2.
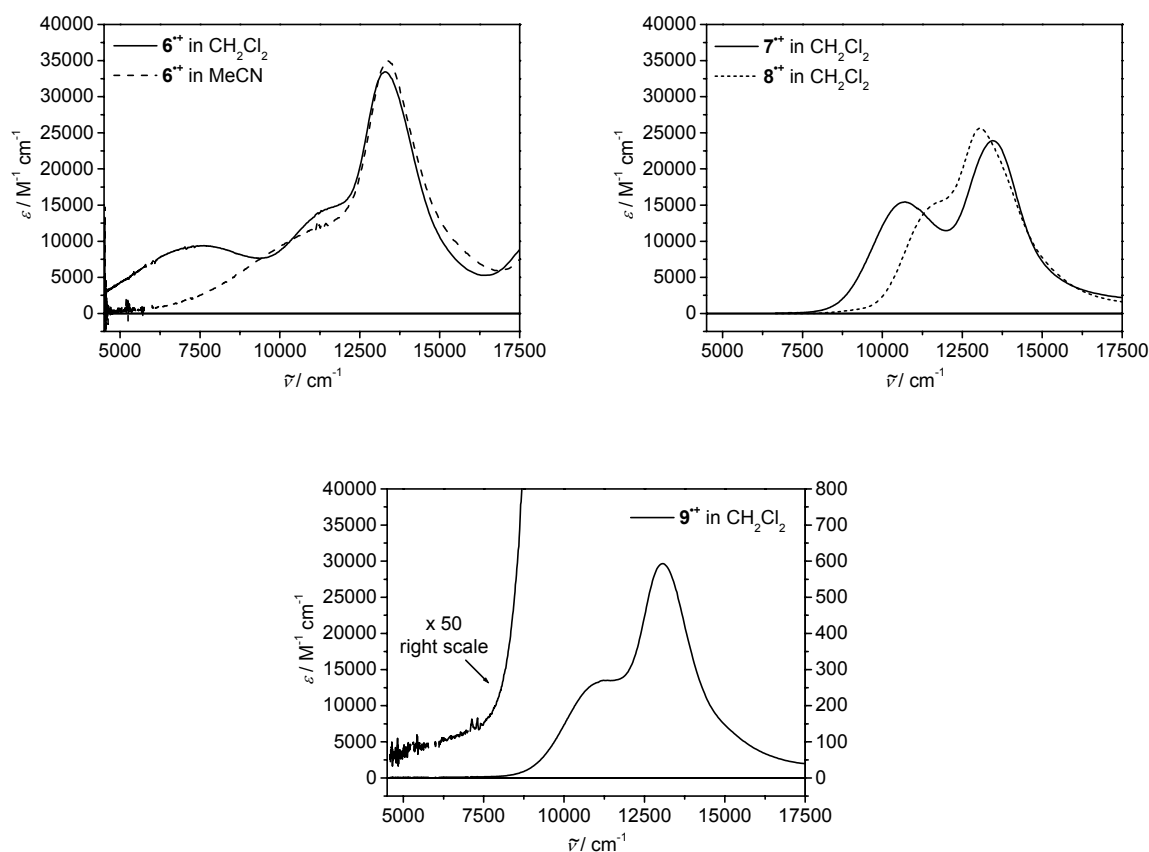
Figure 4. Experimental absorption spectra of mixed-valence species $6^{\bullet+}$ and $9^{\bullet+}$ in CH_2Cl_2 and of $6^{\bullet+}$ in MeCN and spectra of mono-triarylamine radical cations $7^{\bullet+}$ and $8^{\bullet+}$ in CH_2Cl_2.

All MV species show a typical absorption band in the NIR region between 6230 cm^{-1} and 7500 cm^{-1} which is associated with an optically induced intramolecular hole transfer from the oxidized triarylamine moiety to the second neutral triaryalmine unit. This IV-CT absorption shows a distinct blue shift in MeCN compared to the less polar CH_2Cl_2. This solvatochromism proves the pronounced CT character of the transition and can be explained by an increase of solvent reorganization energy in MeCN versus CH_2Cl_2. Accordingly, in the Vis/NIR spectra of the mono-triarylamine radical cations, no absorption signals in the NIR region are found as no intramolecular charge transfer can occur. The second absorption band of the MV compounds lies between 10680 cm^{-1} and 11870 cm^{-1} and is assigned to a hole transfer from the oxidized triarylamine moiety to the bridging unit. This bridge band also appears in the spectra of the mono-triarylamine radical cations $2^{\bullet+}$, $3^{\bullet+}$, $7^{\bullet+}$ and $8^{\bullet+}$. It is obvious, that compounds with identical spacers and "bridging" units as, e.g., $1^{\bullet+}$ and $2^{\bullet+}$ have nearly identical transition energies $\tilde{\nu}_b$ in CH_2Cl_2. The bridge band of all MV species also

shows a distinct blue shift in MeCN which is again explained by an increase of the solvent reorganization energy. In addition to the IV-CT and the bridge band, all MV species, as well as the mono-triarylamine radical cations, exhibit an additional band between 13000 and 13500 cm^{-1} which lacks any pronounced solvatochromism. This so called π-π* band is typical of triarylamine radical cations $\mathbf{1^{\bullet+}}$-$\mathbf{9^{\bullet+}}$. It can be assigned to a dianisylamine localized charge resonance transition.[71] For a more detailed analysis of the absorption bands of the MV compounds the spectra in CH$_2$Cl$_2$ were deconvoluted by four (five for $\mathbf{1^{\bullet+}}$) *Gaussian* functions. A single *Gaussian* function was fitted to the IV-CT band and this function was used for the calculation of the transition moment μ_{ga} according to eq 2 for all MV compounds. Because the IV-CT band of $\mathbf{1^{\bullet+}}$ is slightly asymmetric, an additional function was fitted to the high-energy side of this band. The bridge band was fitted in a similar way by a second single *Gaussian* function, which was used to obtain the transition energy $\tilde{\nu}_b$ as well as the transition moment μ_{gb} (see Table 2). Two further *Gaussian* functions were combined to fit the π-π* band of the spectra. The strong overlap of the absorption signals in MeCN precludes deconvolution by *Gaussian* functions and made a GMH analysis of the MV systems in the more polar solvent MeCN impossible.

Table 2. Experimental data obtained from Vis/NIR spectra recorded in CH$_2$Cl$_2$ and spectra deconvolution by Gaussian functions.

	$\tilde{\nu}_a$[a] / cm^{-1}	$\Delta\tilde{\nu}_{1/2}$[b] / cm^{-1}	ε[c] / cm^{-1}	μ_{ga} / D	$\tilde{\nu}_b$[a] / cm^{-1}	$\Delta\tilde{\nu}_{1/2}$[b] / cm^{-1}	ε[c] / cm^{-1}	μ_{gb} / D	$\tilde{\nu}_{\pi-\pi^*}$[a] / cm^{-1}	ε[c] / cm^{-1}
$\mathbf{1^{\bullet+}}$	6230	2700	1900	2.8±0.1	11870 (sh)	3240	1600	2.0±0.1	13480	3800
$\mathbf{1^{\bullet+}_{corr}}$ [d]	6230	2700	13900	7.6±0.3	11870 (sh)	3240	11700	5.4±0.3	13480	27800
$\mathbf{2^{\bullet+}}$	-	-	-	-	11500	2490	10500	4.6±0.3	13400	24700
$\mathbf{3^{\bullet+}}$	-	-	-	-	15500 (sh)	2840	8600	3.9±0.2	13260	36200
$\mathbf{4^{\bullet+}}$	6600	4570	1700	3.4±0.1	10700	2120	18300	5.9±0.3	13480	28700
$\mathbf{5^{\bullet+}}$	6280	4340	1000	2.6±0.1	10680	2150	20300	6.3±0.3	13510	33900
$\mathbf{6^{\bullet+}}$	7500	4660	9400	7.6±0.3	11590 (sh)	2580	14600	5.3±0.3	13300	33400
$\mathbf{7^{\bullet+}}$	-	-	-	-	10680	2180	15400	5.3±0.3	13440	23900
$\mathbf{8^{\bullet+}}$	-	-	-	-	11500 (sh)	1670	14900	4.1±0.2	13050	25600
$\mathbf{9^{\bullet+}}$	7500	4890	150	0.9±0.03	11100	2350	13400	5.2±0.3	13050	29700

[a] ±200 cm^{-1}. [b] ±200 cm^{-1}. [c] ±5%. [d] estimated under the assumption that the mono-radical cation $\mathbf{1^{\bullet+}}$ shows a π-π* band half as intense as the dication $\mathbf{1^{2+}}$.

The Vis/NIR absorption spectra of the mono-triarylamines $2^{\bullet+}$, $7^{\bullet+}$ and $8^{\bullet+}$ were fitted by three *Gaussian* functions. A single function was fitted to the bridge band and two *Gaussian* functions were fitted to the π-π^* absorption signal. For the radical cation $3^{\bullet+}$, two functions were fitted to each absorption signal.

The extinction coefficient ε and, thus, the transition moment μ_{ga} of the MV compound with the largest N-N distance $9^{\bullet+}$ is much smaller than that of the three paracyclophane bridged MV compounds $1^{\bullet+}$, $4^{\bullet+}$ and $5^{\bullet+}$. The π-conjugated compound $6^{\bullet+}$ shows the most intense IV-CT band with the largest transition moment μ_{ga}. Therefore, the strongest electronic interactions are expected in $6^{\bullet+}$ and the weakest interactions in $9^{\bullet+}$.

For $4^{\bullet+}$-$6^{\bullet+}$ and $9^{\bullet+}$, similar bridge band transition moments μ_{gb} were obtained, but $1^{\bullet+}$ is an exception with a very weak absorption signal. The π-π^* band is also unusually weak in $1^{\bullet+}$. It can definitely be ruled out decomposition processes or kinetically hindered, and, thus slow oxidation processes, because the dication 1^{2+} shows a π-π^* band twice as intense as the mono radical cation $2^{\bullet+}$ and $3^{\bullet+}$, and similar to those of 4^{2+}, 5^{2+}, 6^{2+} and 9^{2+}.[72] In order to calculate the extinction coefficients of the radical cation spectrum, it is necessary to estimate the comproportionation constant K_{co}. In general, K_{co} is calculated by $K_{co} = 10^{(\Delta E/0.059)}$ using the redox potential splittings ΔE obtained by fitting the cyclic voltammogram. The unexpectedly weak π-π^* band of $1^{\bullet+}$ may thus be a consequence of an error in ΔE which leads to wrong extinction coefficients of the absorption spectrum. Therefore, the extinction coefficients of $1^{\bullet+}_{corr}$ were calculated alternatively under the assumption that the mono radical cation $1^{\bullet+}$ shows a π-π^* band half as intense as the dication 1^{2+}. From the resulting extinction coefficients it was inferred that the corresponding comproportionation constant $K_{co} = 2.8 \times 10^{-3}$ and $\Delta E = -91$ mV. Negative ΔE values which were determined, e.g., for 2,5-disubstituted furans[73] are found, if the second redox process occurs a more negative potential than the first, i.e. if the second oxidation is facilitated and the dication is particularly stabilized. The CV signal of $1^{\bullet+}$ has a peak width at half-height = 70 mV; however, for negative ΔE values, a peak width at half-height < 57 mV is expected.[73] On the other, the experimental CV could be broadened by a remaining uncompensated resistance particularly in the low polarity CH_2Cl_2. Thus, a definite conclusion about the origin of the unusually small extinction coefficients of $1^{\bullet+}$ is still lacking. Therefore, in the following both sets of extinction coefficients for the absorption bands were used: the ones as determined experimentally and the ones as calculated

(hereafter called "corrected spectra"), if it is assumed that the $\pi-\pi^*$ transition has half the intensity as the one in the dication.

In chapter I of this thesis a linear relationship between the oscillator strength and the absorption energy $\tilde{\nu}$ of a series of triarylamine radical cations was found.[71] Therefore, the oscillator strengths f_{gb} of the MV species and mono-triarylamines $2^{\bullet+}$, $7^{\bullet+}$ and $8^{\bullet+}$ were calculated by eq 9 and the resulting f_{gb} values were plotted versus the absorption energy $\tilde{\nu}_b$ (see Figure 5).

$$f_{gb} = \frac{4.7014 \times 10^{-7}\ \tilde{\nu}_b\ \mu_{gb}^2}{cm^{-1}\ D^2} \qquad (9)$$

Compound $3^{\bullet+}$ was neglected, because it is difficult to determine the energy $\tilde{\nu}_b$ as well as the oscillator strength exactly due to strong overlap of the absorption bands (see Figure 3).
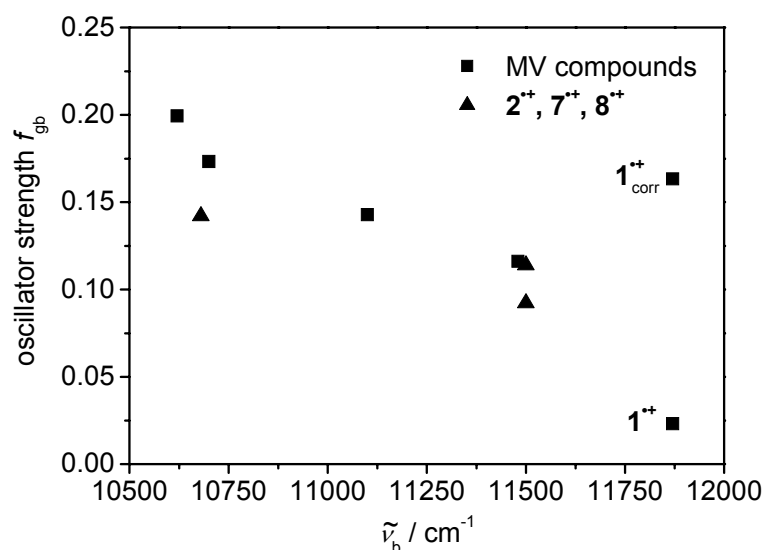
Figure 5. Plot of the oscillator strength f_{gb} of the bridge band versus the corresponding absorption energy of the MV compounds (■) and mono cations $2^{\bullet+}$, $7^{\bullet+}$ and $8^{\bullet+}$ (▲).

Figure 5 clearly demonstrates that the oscillator strength of the bridge band f_{gb} decreases approximately linearly with increasing transition energy $\tilde{\nu}_b$. As the bridge band of $1^{\bullet+}$ has the highest absorption energy $\tilde{\nu}_b$, compound $1^{\bullet+}$ has the smallest oscillator strength f_{gb}, and

consequently the smallest transition moment μ_{ga}. This is the case only for the spectrum of $\mathbf{1^{\bullet+}}$ derived from the electrochemical ΔE value, but not for the corrected spectrum $\mathbf{1^{\bullet+}_{corr}}$ with a π-π^* band half as intense as the π-π^* band of dication $\mathbf{1^{2+}}$. At present, there is no quantitative description, nor a physical interpretation for the linear correlation of f_{gb} and $\tilde{\nu}_b$. Nevertheless, this finding is in accordance with that in chapter I of a series of triarylamine radical cations[71] and also in agreement with a study of *Zhu* and *Wolf*[74], who also obtained a linear relationship between the oscillator strength f and the transition energy $\tilde{\nu}$ for (ferrocenylethynyl)-oligothiophene complexes.

2.5   AM1-CISD computations and evaluation of electronic couplings by GMH theory

In a recent work, the GMH three-level model was used for a general analysis of electronic couplings depending on the transition moments and the relative transition energies of IV-CT and bridge bands.[44] It was demonstrated that the three-level model is necessary for a more precise description of MV systems, if they show an intense bridge band and if the dipole moment difference between the ground μ_{gg} and the first excited IV-CT state μ_{aa} are relatively small. In order to examine the dependence of the couplings on the relative energy of the bridge state $\tilde{\nu}_b$, a given set of parameters was used (see Figure 6) and the following simplified adiabatic transition moment matrix (eq 10) was used as input for a GMH analysis. In this matrix, the dipole moment μ_{gg} is subtracted from the diagonal elements and, as a reasonable approximation, the difference μ_{bb}-μ_{gg} was set to $(\mu_{aa}$-$\mu_{gg})/2$. The set of parameters used applies to a strongly localized MV compound.

$$\mu_{adiab} = \begin{pmatrix} 0 & \mu_{ga} & \mu_{gb} \\ \mu_{ga} & \Delta\mu_{ag} = \mu_{aa} - \mu_{gg} & \mu_{ab} \\ \mu_{gb} & \mu_{ab} & \Delta\mu_{ag}/2 \end{pmatrix} \qquad (10)$$

As shown in Figure 6 a), the couplings calculated by the three-level model reveal a linear correlation to $\tilde{\nu}_b$, if the transition moment for the bridge state μ_{gb} is kept constant. Therefore, the deviation of V_{12} from $V_{two\text{-}state}$ (eq 1) increases with increasing energy of the bridge

state $\tilde{\nu}_b$.[44] However, a more realistic set of parameters should also consider the empirically found correlation between μ_{gb} and $\tilde{\nu}_b$ (Figure 5). Thus, because $\mu_{gb} \sim \sqrt{f_{gb}} / \tilde{\nu}_b$ the relation $\mu_{gb} = \sqrt{25 - 5\tilde{\nu}_b} / \tilde{\nu}_b$ was implied in the general GMH analysis which is shown in Figure 6 b). The given empirical relation for μ_{gb} was chosen so that μ_{gb} has a realistic value (4.5) for $\tilde{\nu}_b = 1$ and that μ_{gb} becomes zero for the limit of the plot $\tilde{\nu}_b = 5$.
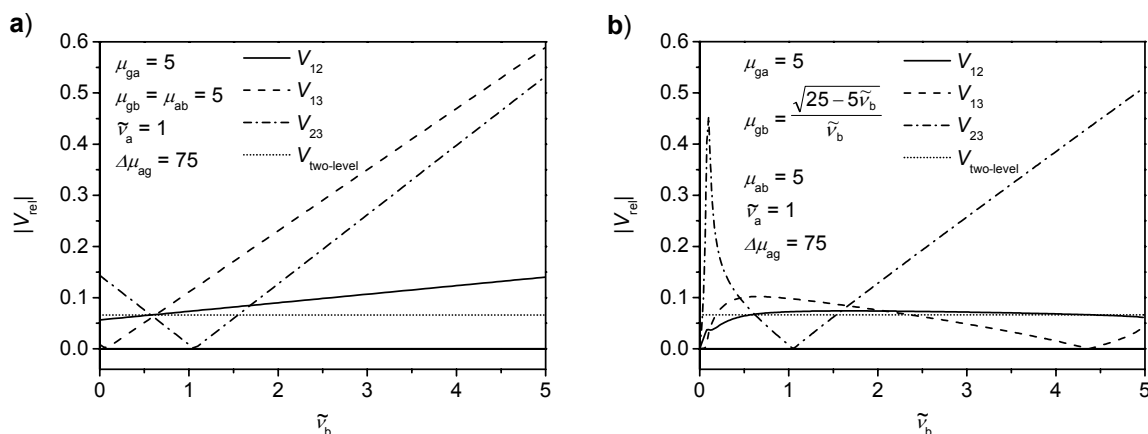

Figure 6. Plots of the absolute values of the electronic couplings derived by GMH three-level model and GMH two-level model versus $\tilde{\nu}_b$. At positions with $|V_{rel}| = 0$ a change of sign of the relative electronic coupling V_{rel} occurs.

In this more sophisticated representation, only the coupling V_{23} shows a linear correlation at $\tilde{\nu}_b > 1$, while V_{12} is very similar to $V_{two-state}$ even at high $\tilde{\nu}_b$ energy values, due to the fact that the transition moment μ_{gb} approaches zero. Thus, for strongly localized MV systems, V_{12} depends only weakly on the energy of the bridge state $\tilde{\nu}_b$, while V_{13} and V_{23} show a more pronounced dependence on $\tilde{\nu}_b$. It is supposed that including the relationship between μ_{gb} and $\tilde{\nu}_b$ gives a more realistic model to predict the behavior of coupling values as a function of the energy of the bridge state.

To analyze the MV compounds $1^{\bullet+}$, $4^{\bullet+}$-$6^{\bullet+}$ and $9^{\bullet+}$ by the GMH three-level model data for μ_{gg}, μ_{aa}, μ_{bb} and μ_{ab} are required additionally to the experimental values for $\tilde{\nu}_a$, $\tilde{\nu}_b$, μ_{ga} and μ_{gb}. It was previously demonstrated that AM1-CISD computations may be used for the evaluation of these four missing data and that the results are physically reasonable.[44] Thus, the ground state geometry was optimized at AM1-CISD level with an active orbital window

consisting of four doubly occupied orbitals, one singly occupied orbital and two unoccupied orbitals. In order to calculate the transition moments and dipole moments, the gas phase optimized ground state structures were used and single SCF cycles were calculated at the AM1-CISD level. For the simulation of a solvent environment with $\varepsilon = 2.0$, the conductor-like screening model (COSMO) was used and single points were calculated at the gas phase optimized structures in the same way. The computational results are collected in Table 3 and in Table 4.

Table 3. Adiabatic (calculated and experimental)[70] and diabatic transition moments calculated by GMH three-level model in D.

		μ_{gg}	μ_{aa}	μ_{bb}	μ_{ga}	μ_{gb}	μ_{ab}	μ_{11}	μ_{22}	μ_{33}
	AM1-CISD[a]	-33.4	33.2	7.3	18.5	1.0	9.4	-38.2	40.6	4.7
$1^{\bullet+}$	+ COSMO[a]	-34.1	30.8	7.7	2.3	2.1	7.7	-34.3	33.2	5.4
	exp.[a, b]	-	-	-	2.8	2.0	-	-34.3	33.3	5.4
$1_{corr}^{\bullet+}$ [c]	exp.[a, b]	-	-	-	7.6	5.4	-	-35.5	34.3	5.6
	AM1-CISD[a]	-35.5	33.7	-14.3	22.2	6.3	12.7	-42.2	43.6	-17.4
$4^{\bullet+}$	+ COSMO[a]	-36.9	29.1	-6.1	6.5	8.9	7.1	-39.6	31.5	-5.8
	exp.[a, b]	-	-	-	3.4	5.9	-	-38.1	30.8	-6.6
	AM1-CISD[a]	-20.0	22.6	3.7	10.8	2.0	2.1	-22.7	25.5	3.5
$5^{\bullet+}$	+ COSMO[a]	-20.7	21.7	-0.6	0.5	2.5	0.9	-21.0	21.7	-0.3
	exp.[a, b]	-	-	-	2.6	3.2	-	-21.3	21.9	-0.2
	AM1-CISD[a]	-21.3	18.6	-5.8	5.6	1.0	4.3	-22.1	20.1	-6.5
$6^{\bullet+}$	+ COSMO[a]	-32.2	20.2	-2.9	4.7	1.3	3.4	-32.7	21.1	-3.4
	exp.[a, b]	-	-	-	7.5	5.4	-	-34.0	21.9	-2.8
	AM1-CISD[a]	-50.0	51.2	-8.2	27.3	8.2	9.7	-57.5	60.0	-9.5
$9^{\bullet+}$	+ COSMO[a]	-51.2	47.5	0.9	3.6	9.7	10.2	-53.0	49.9	0.2
	exp.[a, b]	-	-	-	0.9	5.2	-	-51.7	49.7	-0.8

[a] Odd number of positive off-diagonal transition moments. [b] For the three-level GMH analysis the experimental values and, where lacking, the COSMO ($\varepsilon = 2.0$) values were used. [c] extinction coefficients were estimated under the assumption that the mono radical cation $1^{\bullet+}$ shows a π-π^* band half as intense as the dication 1^{2+}.

The adiabatic transition moments derived from AM1-CISD calculation in the gas phase and with the COSMO solvent model and the experimental values (exp.) are given in Table 3, where the diagonal elements of the diabatic transition moment matrix $\mu_{\mathbf{diab}}$ (eq 5) derived from the GMH three-level model are also presented.

Table 4. Transition energies (computed and experimental) and diabatic electronic couplings (GMH) in cm^{-1}.

		$\widetilde{\nu}_a$	$\widetilde{\nu}_b$	$V_{12}{}^a$	$V_{13}{}^a$	$V_{23}{}^a$	$V_{\text{two-level}}{}^b$
	AM1-CISD^c	10730	16120	2410	1180	1650	2600
1$^{\bullet+}$	+ COSMO^d	11900	16700	560	600	1320	420
	exp.$^{d,\,e}$	6230	11870	370	390	1560	270
1$^{\bullet+}_{\text{corr}}$ ^{f}	exp.$^{d,\,e}$	6230	11870	970	990	1550	710
	AM1-CISD^d	8640	11310	2380	480	540	2330
4$^{\bullet+}$	+ COSMO^d	10030	13060	1320	2850	340	970
	exp.$^{d,\,e}$	6600	10710	570	1760	720	340
	AM1-CISD^d	9850	16330	2280	620	670	2230
5$^{\bullet+}$	+ COSMO^d	10370	16390	180	1970	230	120
	exp.$^{d,\,e}$	6280	10620	430	1550	150	380
	AM1-CISD^d	4160	9930	590	160	950	560
6$^{\bullet+}$	+ COSMO^d	5620	11380	530	310	810	500
	exp.$^{d,\,e}$	7500	11590	1220	1590	510	1030
	AM1-CISD^d	9190	12790	2280	1040	420	2180
9$^{\bullet+}$	+ COSMO^d	10790	14570	730	2390	680	390
	exp.$^{d,\,e}$	7500	11100	220	1070	710	70

^{a} Obtained by the GMH three-level model. ^{b} Obtained by the GMH two-level model (eq 1). ^{c} Even number of positive coupling values. ^{d} Odd number of positive coupling values. ^{e} For the three-level GMH analysis the experimental values and, where lacking, the COSMO (in the solvent) values were used. ^{f} extinction coefficients were estimated using corrected spectra under the assumption that the mono radical cation **1**$^{\bullet+}$ shows a π-π^* band half as intense as the dication **1**$^{2+}$.

All given transition dipole moments are the projections of the respective vectors on the vector connecting the two nitrogen redox centers. The computed and experimental adiabatic transition energy values and the electronic couplings V (off-diagonal elements of the diabatic energy matrix $\mathbf{H_{diab}}$ (eq 7)) derived from the GMH three-level model and, in addition, the couplings $V_{\text{two-level}}$ of the GMH two-level model estimated by eq 1 are given in Table 4. The AM1-CISD +COSMO computed values were used for μ_{gg}, μ_{aa}, μ_{bb} and μ_{ab} to complete the given experimental values for the GMH three-level analysis. As absolute dipole moments of ions are origin dependent,[70] the discussion in the following rests on dipole moment differences projected on the N-N axis of the molecules (see Table 5). The dipole moment differences $\Delta\mu_{ag} = \mu_{aa}-\mu_{gg}$ in a solvent with $\varepsilon = 2.0$ for all MV compounds is between 42.4 D (**5**$^{\bullet+}$) and 98.7 D (**9**$^{\bullet+}$). The dipole moment differences $\Delta\mu_{bg} = \mu_{bb}-\mu_{gg}$ is roughly half of $\Delta\mu_{ag}$ (e.g. 20.1 D for **5**$^{\bullet+}$ and 52.1 D for **9**$^{\bullet+}$). Thus, the corresponding states can easily be identified as the IV-CT state and the bridge state, respectively. From the values above it is clear that the

assumption made in Figure 6 to set $\Delta\mu_{bg} = \Delta\mu_{ag}/2$ is quite reasonable. Deviations from this relation are due to invalidity of *Condon* approximation. As expected, the diabatic dipole moment differences $\Delta\mu_{12} = \mu_{22}-\mu_{11}$ and $\Delta\mu_{13} = \mu_{33}-\mu_{11}$ are all somewhat larger than the corresponding adiabatic values. The diabatic differences $\Delta\mu_{12}$ correspond to unit charge transfer distances of 14.1 Å for $1^{\bullet+}$, 9.0 Å for $5^{\bullet+}$ and 21.1 Å for $9^{\bullet+}$ which is somewhat smaller than the geometric N-N distances (15.1 Å $1^{\bullet+}$, 9.9 Å $5^{\bullet+}$ and 25.0 Å $9^{\bullet+}$). The corresponding diabatic unit charge transfer distances are even distinctly smaller in the MV compounds $4^{\bullet+}$ (14.4 Å, N-N = 19.9 Å) and $6^{\bullet+}$ (11.7 Å, N-N = 19.3 Å). This behavior reflects stronger charge delocalization into the bridge in the latter cases, in particular in the π-conjugated system $6^{\bullet+}$.

Table 5. Dipole moment differences in D.

	$\Delta\mu_{ag}$ [a]	$\Delta\mu_{bg}$ [a]	$\Delta\mu_{12}$ [b]	$\Delta\mu_{13}$ [b]
$1^{\bullet+}$	64.9	41.8	67.6	39.7
$4^{\bullet+}$	66.0	30.8	68.9	31.5
$5^{\bullet+}$	42.4	20.1	43.2	21.1
$6^{\bullet+}$	52.4	29.3	55.9	31.2
$9^{\bullet+}$	98.7	52.1	101.4	50.9

[a] Differences of the AM1-CISD +COSMO dipole moments. [b] Differences of the diabatic GMH transition moments derived from experimental input (see Table 3).

The gas phase computed transition moments μ_{ga} and μ_{gb} are in bad agreement with the experimental transition moments. In general, transition moments are difficult to calculate even at a much higher level of theory. However, including the COSMO solvent model in our computation yields transition moments which are in significantly better agreement for all compounds with exception of *p*-xylene $6^{\bullet+}$. The fact that μ_{ga} and μ_{ab} are different, suggests that the *Condon* approximation (μ independent of the nuclear coordinates) is invalid. The computed transition energies $\tilde{\nu}_a$ and $\tilde{\nu}_b$ of the paracyclophane derivatives are all significantly larger than the experimental values, while both computed energies $\tilde{\nu}_a$ and $\tilde{\nu}_b$ of the *p*-xylene derivative $6^{\bullet+}$ are somewhat smaller than the experimental values. In general, the inclusion of the COSMO solvent model does not improve the agreement.

The GMH analysis yields the electronic couplings V_{12}, V_{13} and V_{23} given in Table 4. Those values, that are derived only from computed energies and transition dipole moments, show a

distinct deviation from the couplings derived from experimental in combination with computed values (= exp. in Table 3 and Table 4). This is due to the fact that the computed transition energies are too large compared to the experimental values. In the discussion below therefore exclusively the values obtained from the combination of experimental and computed data are considered.

The diabatic coupling V_{12} is a measure for the electronic interaction between the diabatic states (1) and (2) and characteristic for the inter-valence charge transfer. The couplings V_{13} between the diabatic states (1) and (3) as well as V_{23} between the states (2) and (3) are both attributed to triarylamine to bridge charge transfer. As expected the smallest V_{12} was found for MV compound $9^{\bullet+}$ with the largest N-N distance.[29] For the two compounds with different connectivity, the *pseudo-para* isomer $4^{\bullet+}$ and the *pseudo-ortho* isomer $5^{\bullet+}$, a somewhat larger coupling was obtained for $4^{\bullet+}$ although the N-N distance is much larger in this case. However, for these two isomers the number of bondings between the two redox centers is the same and the similar couplings for $4^{\bullet+}$ and $5^{\bullet+}$ prove that the coupling is provided by the bond pathway and not directly between the triarylamine moieties. In contrast, the cyclophane $1^{\bullet+}$ with the shortest N-N distance and the smallest number of bonds between the triarylamine redox centers shows a weaker coupling than $4^{\bullet+}$ and $5^{\bullet+}$, if the coupling derived from the spectrum with the smaller extinction coefficients (see $1^{\bullet+}$ Table 4) is regarded. The steric strain in the biaryl moieties of $1^{\bullet+}$ results in large twist (AM1 computed: 58° in $1^{\bullet+}$ compared to 46° in $3^{\bullet+}$) which may explain the weak electronic interaction. But if the larger extinction coefficients of $1^{\bullet+}_{\text{corr}}$ derived from the corrected spectra is used for the GMH analysis, the coupling V_{12} is, as expected, higher than these of $4^{\bullet+}$ and $5^{\bullet+}$ and smaller than V_{12} of $6^{\bullet+}$. For the π-conjugated *p*-xylene $6^{\bullet+}$ the largest V_{12} was obtained. Thus, direct conjugation obviously leads to stronger electronic interactions than the through-bond and through-space interactions provided by [2.2]paracyclophane. Nevertheless, from the order of magnitude of the couplings of the [2.2]paracyclophane derivatives, it is assumed that this bridge is able to mediate significant through-space and through-bond interactions.

The through-space interaction of the [2.2]paracyclophane moiety occurs via direct overlap of the π-orbitals of the two unsaturated rings and the through-bond interactions occur via the σ-orbitals of the two ethanediyl bridges. In order to separate these two interactions, a calculation of $4^{\bullet+}$ with the modification that the two ethanediyl bridges were replaced by four hydrogen atoms with a fixed carbon hydrogen distance of 1.1 Å was performed. All other

atoms remained as in the optimized geometry of $4^{\bullet+}$. The CISD results are given in Table 6 where $4^{\bullet+}_{\mathbf{mod}}$ is the modified cyclophane without the ethanediyl bridges.

Table 6. AM1-CISD+COSMO results of $4^{\bullet+}$ in comparison to $4^{\bullet+}_{\mathbf{mod}}$.

|	$4^{\bullet+}$	$4^{\bullet+}_{\mathbf{mod}}$
$\tilde{\nu}_a$ / cm^{-1}	10030	9540
$\tilde{\nu}_b$ / cm^{-1}	13060	13080
μ_{gg} / D	-36.9	-37.5
μ_{aa} / D	29.1	20.6
μ_{bb} / D	-6.1	15.6
μ_{ga} / D	6.5	11.8
μ_{gb} / D	8.9	6.3
μ_{ab} / D	7.1	11

The transition energies $\tilde{\nu}_a$ and $\tilde{\nu}_b$ and the dipole moment of the ground state μ_{gg} do not vary greatly after removal of the ethanediyl bridges, but all transition moments and particularly the dipole moments μ_{aa} and μ_{bb} are affected by this modification. Hence, it was inferred that both the through-space as well as the through-bond interactions have significant influence on the electronic properties of MV compounds and, thus, on the communication between the two redox centers.

The couplings $V_{\text{two-level}}$ derived from the GMH two-level model are somewhat smaller than the V_{12} values but they show similar trends. Because the couplings V_{12} and $V_{\text{two-level}}$ depend on the N-N distance (see $9^{\bullet+}$ vs $4^{\bullet+}$), it was concluded that the [2.2]paracyclophane moiety is not the limiting factor which governs the intramolecular charge transfer.

At this point the question arises what are the determining factors for the electronic couplings. In order to elucidate this aspect, McConnell's superexchange model was used in the formulation by *Newton et al.* (eq 11).[75,76] This model is valid in the perturbation limit with $|H/E|<1$, where $H_{i,j}$ are the electronic coupling elements between states localized at adjacent centres and E is the respective energy relative to the ground state. Only nearest neighborhood (NN) interactions are being considered. This approximation cannot be directly compared to our GMH three level model presented above, because the GMH model considers only those states which are experimentally accessible, i.e. the states which are visible in the absorption spectra and where a dominating direct donor acceptor interaction is involved which invalidates the NN approximation.

A general model system was considered consisting of a donor D, an acceptor A and a number of bridge sites S being connected by both $n+1$ saturated spacers "-" (saturated bridge sites) and $m+1$ unsaturated spacers "----" (unsaturated bridge sites). Those sites being connected by saturated spacers (weak coupling), all have site energy E_1, those being connected by unsaturated spacers, all shall have site energy E_2. The electronic coupling between donor and first bridge site is $H_{1,2}$, that between the last bridge site and the acceptor is $H_{4+m+n,5+m+n}$. The electronic coupling between the equivalent bridge sites connected by saturated spacers is $H_{2,3}$ and that between unsaturated spacers is $H_{3+n,4+n}$ (Chart 1).

Chart 1.

1   2   2+n   3+n 3+m+n 4+m+n 5+m+n

$$D\text{———}S\text{——}\{S\}_n\text{——}S\text{---}\{S\}_m\text{---}S\text{———}A$$
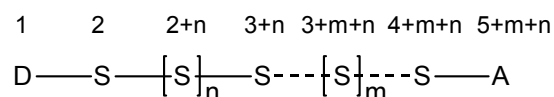
Then the effective electronic coupling V_{eff} follows from eq 11.

$$V_{\text{eff}} = \frac{H_{1,2}}{E_1} \cdot H_{4+m+n,5+m+n} \left(\frac{H_{2,3}}{E_1}\right)^{n+1} \left(\frac{H_{3+n,4+n}}{E_2}\right)^{m+1} \tag{11}$$

The $\ln(V_{\text{eff}})$ (eq 12) shows a linear relation with both the number $n+1$ of sites connected by saturated spacers and/or with the number of unsaturated spacers $m+1$.

$$\ln(V_{\text{eff}}) = \ln\left(\frac{H_{1,2}}{E_1}\right) + \ln(H_{4+m+n,5+m+n}) + (n+1)\ln\left(\frac{H_{2,3}}{E_1}\right) + (m+1)\ln\left(\frac{H_{3+n,4+n}}{E_2}\right) \tag{12}$$

As $|H/E|<1$ the third and fourth term of eq 12 have a negative slope as expected for a superexchange model. From eq 12 it is obvious that because $H_{3+n,4+n}$ is much larger than $H_{2,3}$, varying the number $n+1$ of saturated bridge sites yields a linear correlation with a steep but negative slope, while varying the number $m+1$ of unsaturated bridge sites yields a much smaller negative slope in agreement with enumerable experimental and theoretical findings.[77-81] For, e.g., varying unsaturated bridge sites the onset of the correlation is $\ln(H_{1,2}/E_1) + \ln(H_{4+m+n,5+m+n}) + (n+1)\ln(H_{2,3}/E_1)$, that is, a higher number n of saturated bridge sites shifts the correlation vertically to smaller values V_{eff}. For varying saturated bridge

sites   the   onset   is $\ln\left(H_{1,2}/E_1\right)+\ln\left(H_{4+m+n,5+m+n}\right)+(m+1)\ln\left(H_{3+n,4+n}/E_2\right)$.   As

$\left|(m+1)\ln\left(H_{3+n,4+n}/E_2\right)\right| < \left|(n+1)\ln\left(H_{2,3}/E_1\right)\right|$ for $m=n$ the onset shift is smaller for the correlation of varying saturated bridge sites than for varying unsaturated bridge sites.

Coming back to the real system $\mathbf{6}^{\bullet+}$ and, in addition, to the known systems $\mathbf{10}^{\bullet+}\text{-}\mathbf{13}^{\bullet+29}$ (see Chart 3) where only unsaturated bridges of different length (i.e. varying m) separate the triarylamines, and the systems $\mathbf{1}^{\bullet+}$, $\mathbf{4}^{\bullet+}$, $\mathbf{5}^{\bullet+}$ and $\mathbf{9}^{\bullet+}$ where an additional unsaturated cyclophane is incorporated, one would expect from the above stated arguments that both series of systems exhibit linear correlations with the same negative slope but that the series $\mathbf{1}^{\bullet+}$, $\mathbf{4}^{\bullet+}$, $\mathbf{5}^{\bullet+}$, $\mathbf{9}^{\bullet+}$ has a smaller onset than the series $\mathbf{6}^{\bullet+}$, $\mathbf{10}^{\bullet+}\text{-}\mathbf{13}^{\bullet+}$.

Chart 3.

| 10 | 11 | 12 | 13 |
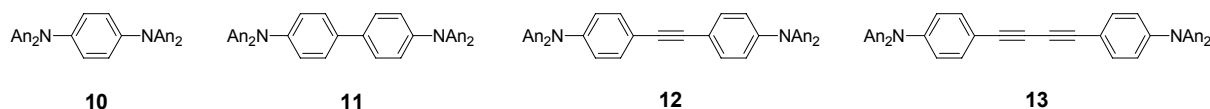
In fact, a logarithmic plot of V vs the number of bonds n separating the N centers is linear for $\mathbf{1}^{\bullet+}_{\mathbf{corr}}$, $\mathbf{4}^{\bullet+}$, $\mathbf{5}^{\bullet+}$ and $\mathbf{9}^{\bullet+}$ (see Figure 7). The coupling derived from the smaller transition moments of $\mathbf{1}^{\bullet+}$ is much weaker than expected from the linear correlations (for both $V_{\text{two-level}}$ and V_{12}) in Figure 7. This indicates that using the corrected spectrum of $\mathbf{1}^{\bullet+}_{\mathbf{corr}}$ results in a more realistic coupling V_{12} consistent with the other values in this series. In Figure 7 the couplings V of π-conjugated MV compounds with smaller bridges $\mathbf{10}^{\bullet+}\text{-}\mathbf{13}^{\bullet+}$ (see Chart 3) are also presented. The electronic couplings V_{vc} of $\mathbf{10}^{\bullet+}\text{-}\mathbf{12}^{\bullet+}$ were obtained by band shape analysis. The analyses of MV species $\mathbf{10}^{\bullet+48}$ and $\mathbf{11}^{\bullet+47}$ were recently described. Applying an analogous procedure to analyze the spectrum of tolane $\mathbf{12}^{\bullet+29}$ yields $V_{\text{vc}} = 2400$ cm^{-1}. The coupling $V_{\text{two-level}}$ of $\mathbf{13}^{\bullet+}$ was obtained using the Mulliken-Hush formalism (eq 1) with $\Delta\mu_{12}$ derived from TD-DFT calculations.[39] As shown in Figure 7 the couplings of the π-conjugated MV systems $\mathbf{6}^{\bullet+}$ (V_{12} and $V_{\text{two-level}}$) and $\mathbf{10}^{\bullet+}\text{-}\mathbf{13}^{\bullet+}$ also correlate linearly with n, but the slope is somewhat smaller.
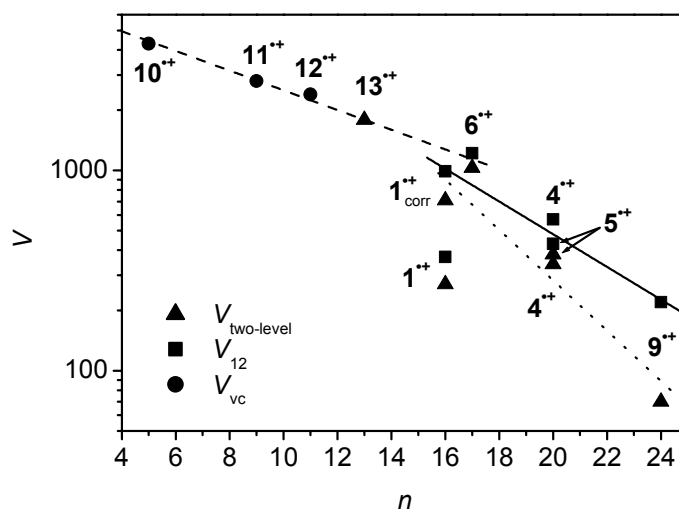
Figure 7. Logarithmic plot of electronic couplings V_{12}, $V_{\text{two-model}}$ and V_{vc} vs the number of bonds n separating the N centers and linear fits of the data as described in the text.

A simpler model that takes only one coupling value into account (eq 13) also reflects the exponential dependence of the coupling V on the distance r separating the redox centers. If it is assumed that the interactions occur through the bonds, the number of bonds n can be set in relation with the distance r. In the following it will be approximated that $r = 1.4$ Å $\times n$.

$$V = V_0 \cdot e^{-(\frac{\beta \cdot r}{2})} \quad \text{or} \quad \ln(V) = \ln(V_0) - (\frac{\beta \cdot r}{2}) \qquad (13)$$

The slope of the linear fits can, thus, be correlated to the β factor of eq 13. It was reported that this factor is ~1 Å^{-1} for saturated bridges[77,78,80] and significantly smaller (e.g. 0.46 Å^{-1})[81] for conjugated bridges[79,81]. The β values were calculated for the three linear fits in Figure 7. The conjugated MV systems $6^{\bullet+}$ (V_{12} and $V_{\text{two-level}}$) and $10^{\bullet+}$-$13^{\bullet+}$ show $\beta = 0.16$ Å^{-1}, while the linear fit of V_{12} ($1^{\bullet+}_{\text{corr}}$, $4^{\bullet+}$, $5^{\bullet+}$ and $9^{\bullet+}$) yields $\beta = 0.27$ Å^{-1} and the linear fit of $V_{\text{two-level}}$ ($1^{\bullet+}_{\text{corr}}$, $4^{\bullet+}$, $5^{\bullet+}$ and $9^{\bullet+}$) results $\beta = 0.41$ Å^{-1}. Thus, the β values are all significantly smaller than 1 Å^{-1} and β of the π-conjugated compounds is somewhat smaller than both β values of $1^{\bullet+}_{\text{corr}}$, $4^{\bullet+}$, $5^{\bullet+}$ and $9^{\bullet+}$. As mentioned above, from the McConnell's superexchange model in the formulation by *Newton et al.* eq 11 similar β values for both series $1^{\bullet+}$, $4^{\bullet+}$, $5^{\bullet+}$, $9^{\bullet+}$ and the π-conjugated

species $6^{\bullet+}$, $10^{\bullet+}$-$13^{\bullet+}$ were expected. This prediction is not fulfilled, but the difference of the slope of $6^{\bullet+}$, $10^{\bullet+}$-$13^{\bullet+}$ in comparison to the slope of $1_{corr}^{\bullet+}$, $4^{\bullet+}$, $5^{\bullet+}$, $9^{\bullet+}$ (V_{12}) is small. Thus, the cyclophane bridge behaves more like an unsaturated spacer rather than a saturated bridge.

As the β value is small for the present type of π-conjugated MV compounds, it is supposed that a larger number of bonds n and, therefore, longer π-conjugated bridges should still reveal a significant coupling in bis-triarylamine MV compounds. Therefore, it is supposed that the bridge of a π-conjugated MV compound can, in principle, be significantly elongated and, the MV compound will nevertheless have an analyzable IV-CT band.

The two couplings V_{13} and V_{23}, which affect the bridge state, show significant differences and this again reflects that the *Condon* approximation is not valid in these cases.
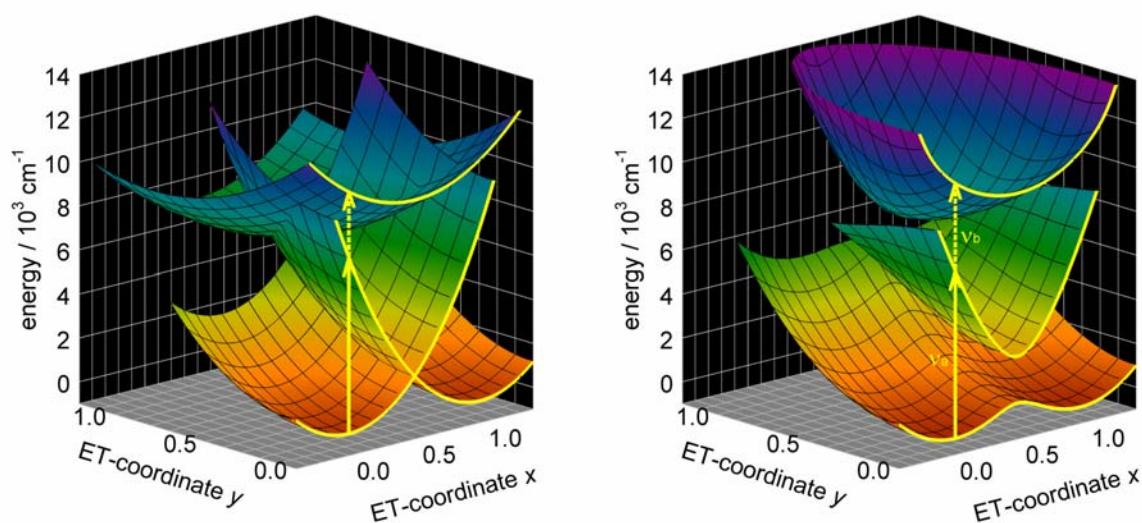
2.6   PES parameter fitting by spectra simulation

In the previous section it was demonstrated how to estimate electronic coupling values from linear optical characteristics of MV species. These evaluated GMH couplings can be used to calculate potential energy surfaces of the adiabatic states by solving the secular determinant (eq 14).

$$
\begin{vmatrix}
\lambda_1 \left[\dfrac{x^2 + Cx^4 + y^2 + Cy^4}{1+C} \right] - \varepsilon & V_{\mathrm{IV}} & V_{\mathrm{br}} \\[3ex]
V_{\mathrm{IV}} & \lambda_1 \left[\dfrac{(1-x)^2 + C(1-x)^4 + y^2 + Cy^4}{1+C} \right] - \varepsilon & V_{\mathrm{br}} \\[3ex]
V_{\mathrm{br}} & V_{\mathrm{br}} & \lambda_2 \left[(\tfrac{1}{2}-x)^2 + (\tfrac{\sqrt{3}}{2}-y)^2 \right] + \Delta G^0 - \varepsilon
\end{vmatrix} = 0 \qquad (14)
$$

The construction of the adiabatic PES starts off with three diabatic (diagonal elements of eq 14) energy surfaces described by two dimensional parabolic functions which were augmented by quartic terms (adjusted by parameter C). In this model, which was introduced in two recent papers,[34,44] two independent average modes x (asymmetric vibrational mode) and y (symmetric vibrational mode) were used. The minima of the diabatic potential functions of the states (1) and (2) each with the hole localized at one of the triarylamine redox centers (see Figure 1) are placed at $(x,y) = (0,0)$ and at $(x,y) = (1,0)$. The minimum of state (3) with the hole localized at the bridge is positioned at $(x,y) = (0.5, \sqrt{3}/2)$. Thus, the minima of the three diabatic states are located at the corners of an equilateral triangle with an edge length of unity. The bridge state (3) is shifted energetically by ΔG^0 relative to (1) while (2) and (1) are degenerate states. Two different *Marcus* reorganization energies are used within this model. One reorganization energy λ_1 is associated with (1) and (2) and a second reorganization energy λ_2 is associated with the bridge state (3). These two force constants are assumed to be equal for the x-mode and the y-mode. For the calculation of the adiabatic PES the GMH derived coupling V_{12} was used for V_{IV} between states (1) and (2) as well as the averaged GMH couplings $V_{\mathrm{br}} = (|V_{13}|+|V_{23}|)/2$ were used for the coupling between the triarylamine localized states and the bridge state (3). Thus, within this model it is assumed that the couplings are coordinate independent (*Condon* approximation).

Figure 8. Diabatic (left) and adiabatic (right) potential energy surfaces of $\mathbf{6^{\bullet+}}$.

The simulations of the IV-CT absorption and the bridge band were done in a classical manner with a *Boltzmann* distribution of the adiabatic ground state and vertical transitions to the IV-CT state and to the bridge state, respectively. The PES were modeled by tuning the parameters λ_1, λ_2, ΔG^0 and C to give the best fit to the *Gaussian* bands (IV-CT and bridge) of the deconvoluted experimental absorption spectrum. As the parameters display no significant dependence on each other only one parameter set is suitable for a stable fit and, therefore, the PES fitting procedure yields reliable values for λ_1, λ_2 and ΔG^0 (see Table 7).

Table 7. ET parameters for all MV compounds in CH_2Cl_2 derived from GMH analysis and PES fits.

	V_{IV} [a]/ cm^{-1}	V_{br} [a]/ cm^{-1}	λ_1 [b]/ cm^{-1}	λ_2 [b]/ cm^{-1}	C	ΔG^0 [b]/ cm^{-1}	ΔG^* [c]/ cm^{-1}
$\mathbf{1^{\bullet+}}$	370	980	6300	5900	-0.15	5800	1510
$\mathbf{1^{\bullet+}_{corr}}$	970	1270	6400	6000	-0.15	5400	1090
$\mathbf{4^{\bullet+}}$	570	1240	7000	3200	0.16	6800	1180
$\mathbf{5^{\bullet+}}$	430	850	6400	3300	0.13	7050	1110
$\mathbf{6^{\bullet+}}$	1220	1050	8000	4500	0.10	6500	900
$\mathbf{9^{\bullet+}}$	220	890	7700	3800	0.16	7000	1580

[a] $\pm$ 50 cm^{-1}. [b] $\pm$ 300 cm^{-1}. [c] $\pm$ 100 cm^{-1}.

The diabatic and the modeled adiabatic PES of $\mathbf{6^{\bullet+}}$ are presented in Figure 8. The yellow lines represent the two dimensional one-mode model which takes only the asymmetric

electron transfer coordinate *x* into account. The IV-CT and bridge absorption band simulated for the resulting PES are shown in Figure 9 where the experimental Vis/NIR spectra in CH_2Cl_2 and the spectra deconvolution by *Gaussian* functions of $1^{•+}$, $4^{•+}$, $5^{•+}$, $6^{•+}$ and $9^{•+}$ are also presented.
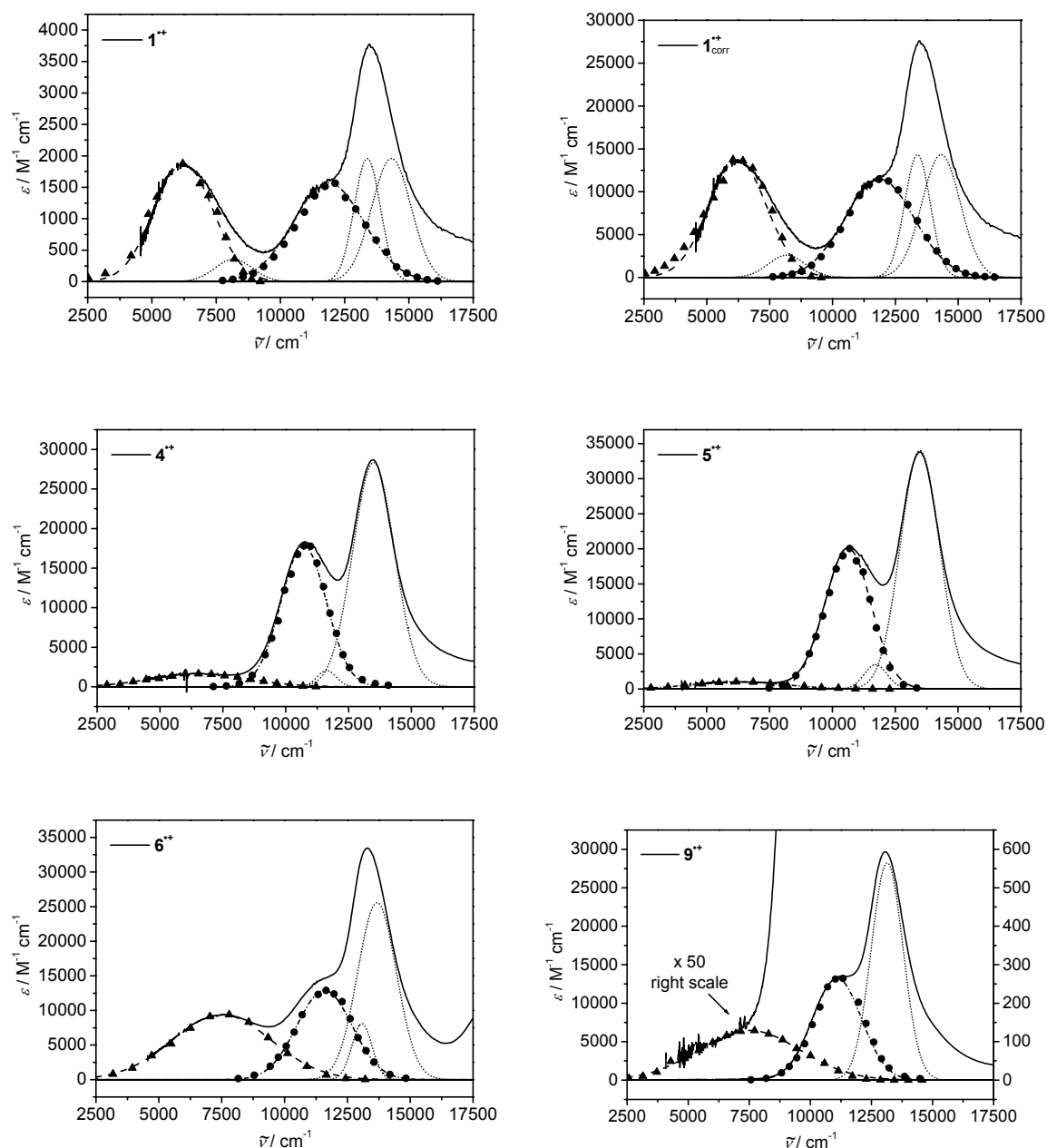
Figure 9. Absorption spectra of MV compounds $1^{•+}$, $4^{•+}$, $5^{•+}$, $6^{•+}$ and $9^{•+}$ in CH_2Cl_2 (solid), spectra deconvolution by Gaussian functions (IV-CT: dashed; bridge: dash-dotted; π-π*: dotted) and PES spectra simulation (IV-CT: solid triangles; bridge: solid circles).

The negative parameter C of the PES fit of $\mathbf{1}^{\bullet+}$ and $\mathbf{1}^{\bullet+}_{corr}$ is a consequence of the unexpectedly narrow IV-CT band (see above). The remaining PES fits yield positive values for parameter C as a result of broad IV-CT bands. In general, the reorganization energy λ_1 varies little within the set of MV compounds (λ_1 = 6300–8000 cm^{-1}). The MV compounds $\mathbf{4}^{\bullet+}$, $\mathbf{5}^{\bullet+}$, $\mathbf{6}^{\bullet+}$ and $\mathbf{9}^{\bullet+}$ show small λ_2 values between 3200 and 4500 cm^{-1}, while $\mathbf{1}^{\bullet+}$ has a significant larger λ_2 = 5900 cm^{-1} and λ_2 = 6000 cm^{-1} derived from the π-π^* corrected spectrum, respectively. The higher value for $\mathbf{1}^{\bullet+}$ might be due to the twisted biaryl moiety. The relative free energy ΔG^0 is very similar for all MV compounds (6500-7050 cm^{-1}), except for $\mathbf{1}^{\bullet+}$ and where the PES fitting procedure yields a somewhat smaller value (5800 and 5400 cm^{-1}).
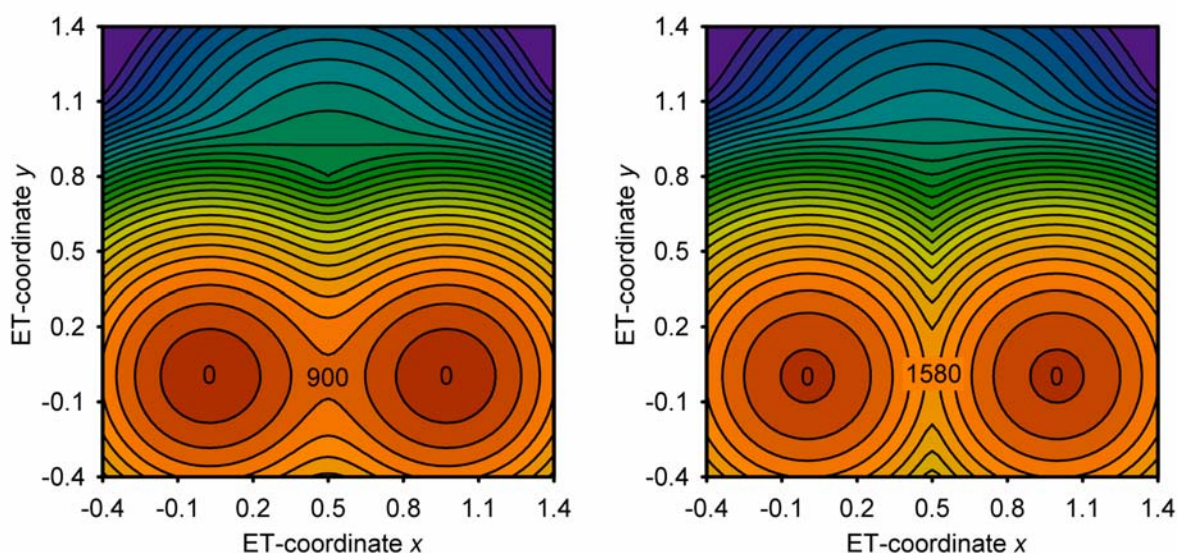
Figure 10. Contour plots of the adiabatic ground state PESs of $\mathbf{6}^{\bullet+}$ (left) and $\mathbf{9}^{\bullet+}$ (right). 350 cm^{-1} contour spacing.

Contour plots of the adiabatic ground state PESs of $\mathbf{6}^{\bullet+}$ and $\mathbf{9}^{\bullet+}$ are depicted in Figure 10. These PESs are representative for all MV species investigated in this study and they all exhibit a double minimum. All adiabatic ground state PESs show a weak impression at the position of the diabatic bridge state potential, but without provoking an additional minimum. In a recent study it was shown that a third minimum in the PES is obtained for more electron-rich p-dimethoxybenzene bridge and, thus, in such a system electron hopping and superexchange may be two coexisting thermal ET mechanisms.[34,44] Depending on the free enthalpy difference ΔG^0, the bay is more or less profound for the MV compounds $\mathbf{4}^{\bullet+}$, $\mathbf{5}^{\bullet+}$, $\mathbf{6}^{\bullet+}$ and $\mathbf{9}^{\bullet+}$. A small ΔG^0 value results in a deeper impression, while larger ΔG^0 values cause a

less pronounced smooth bay in the adiabatic ground state PES. Nevertheless, these findings preclude a hopping mechanism for the thermal ET and, therefore, ET can occur solely by a superexchange mechanism.

As all the λ_1 values are very similar for the MV compounds, the adiabatic ET barrier ΔG^* between the two minima of the adiabatic PES decreases with increasing coupling V_{IV}. Consequently, ΔG^* is relatively small for the π-conjugated MV compound $6^{\bullet+}$ (900 cm^{-1}) and largest for $9^{\bullet+}$ (1580 cm^{-1}).

3   Conclusions

The bis-triarylamines **1**, **4-6** and **9** were synthesized by palladium and copper catalyzed C-C cross coupling reactions (see Scheme 1). The Vis/NIR spectra of the MV radical cations $1^{\bullet+}$, $4^{\bullet+}$-$6^{\bullet+}$ and $9^{\bullet+}$ were analyzed by GMH model developed by *Newton* and *Cave*[54]. A GMH three-level model was used which takes into account two transitions: the inter-valence charge transfer (IV-CT) transition and the bridge band which is associated with a triarylamine radical cation to bridge hole transfer. The model was applied to the MV species using both experimental transition energies and transition moments as well as AM1-CISD computed values in order to calculate the diabatic electronic coupling matrix elements. The diabatic coupling V_{12} is a measure for the electronic interaction between the triarylamine localized diabatic states (1) and (2) and is, therefore, characteristic for the inter-valence charge transfer. This coupling V_{12} increases from $9^{\bullet+}$ over the cyclophanes $5^{\bullet+}$, $4^{\bullet+}$ and $1^{\bullet+}_{\text{corr}}$ (if the analysis based on the corrected spectrum of $1^{\bullet+}$ is considered) to the π-conjugated p-xylene $6^{\bullet+}$. Thus, within this set of [2.2]paracyclophanes the coupling increases with increasing number of bonds. The similar couplings of the two isomers $5^{\bullet+}$ and $4^{\bullet+}$ which have the same numbers of bonds between the redox centers but different N-N distances prove that the hole transfer is always provided by the bond pathway and not directly between the two triarylamine moieties. The direct π-conjugation of $6^{\bullet+}$ leads to a stronger electronic coupling $V_{12} = 1220$ cm^{-1} than the through-bond and through-space interactions provided by the [2.2]paracyclophane bridge. Nevertheless, it is assumed that the [2.2]paracyclophane bridge is able to mediate significant through-space and through-bond interactions because the [2.2]paracyclophane derivatives show still significant couplings V_{12} between 220 and 970 cm^{-1}. The electronic couplings

$V_{\text{two-level}}$ derived from the GMH two-level model (eq 1) are somewhat smaller than V_{12}, but they show similar trends.

AM1-CISD calculations on the MV species $4_{\text{mod}}^{\bullet+}$ which is similar to $4^{\bullet+}$, but with the ethanediyl bridges of the [2.2]paracyclophane moiety being replaced by hydrogen atoms, reveal that both the through-space interaction which occurs via direct overlap of the π-orbitals of the two unsaturated rings of the cyclophane and the through-bond interactions which occur via the σ-orbitals of the two ethanediyl bridges have significant influence on the communication between the two triarylamine units of the cyclophane bridged MV species.

The *McConnell*'s superexchange model predicts a linear correlation of $\ln(V)$ to the number of bridge sites with similar slopes for both series the cyclophanes $1^{\bullet+}$, $4^{\bullet+}$, $5^{\bullet+}$, $9^{\bullet+}$ and π-conjugated species as $6^{\bullet+}$, $10^{\bullet+}$-$13^{\bullet+}$. However, the slope of the latter series is only slightly steeper than that of the conjugated series. Therefore, it is concluded that the cyclophane bridge acts more like an unsaturated bridge than like a saturated spacer. These findings will have implications for the design of molecular materials based on cyclophane bridges.

The couplings derived from the GMH three-level model were used to calculate the potential energy surfaces of the adiabatic states of $1^{\bullet+}$, $4^{\bullet+}$-$6^{\bullet+}$ and $9^{\bullet+}$. The ground state potential energy surfaces of $1^{\bullet+}$, $4^{\bullet+}$-$6^{\bullet+}$ and $9^{\bullet+}$ all show a double minimum which is typical for localized MV compounds. This finding confirms that HT solely occurs by a superexchange mechanism in these cases and a hopping mechanism for the thermal HT can be precluded.

4   Experimental Section

4.1   Cyclic voltammetry

The electrochemical experiments were performed in superdry, argon-saturated CH_2Cl_2 with 0.15 M tetrabutylammonium hexafluorophosphate (TBAH) as supporting electrolyte and ca. 0.002 M substrate using a conventional three-electrode set-up with platinum disk electrode (0.12 cm^2). The potentials are referenced against ferrocene (Fc/Fc$^+$). The long-term

reversibility of the processes was checked by performing multi-cycle thin-layer measurements at 10 mV s^{-1} scan rate.

4.2   UV/Vis/NIR spectroscopy

The UV/Vis/NIR spectra of the radical cations and dications in MeCN were obtained by stepwise addition of 10^{-2}-10^{-3} M NOBF$_4$/MeCN via a microliter syringe to a solution of the compounds (3 to 7·10^{-5} M). Because the electron transfer (ET) is rather slow, using NOBF$_4$ in MeCN one has to wait approximately 30 min, before the spectrum after each addition could be recorded. The extinction coefficients obtained in MeCN are too small due to the slight instability of the radical cations under the conditions employed. The spectra in CH$_2$Cl$_2$ were obtained by dropwise addition of 10^{-2}-10^{-3} M SbCl$_5$/CH$_2$Cl$_2$ in the same way. The quick oxidation process in CH$_2$Cl$_2$ allows very short periods between the addition of oxidation agent and spectrum measurement. The extinction coefficients of the MV species in CH$_2$Cl$_2$ were obtained as already described in ref.[29]. For the analysis of the absorption bands of the MV compounds deconvolution of these spectra by four (five for 1$^{•+}$) *Gaussian* functions were performed as described in the text above.

4.3   Semiempirical calculations

All calculation were done using the AM1 parameterization implemented in the MOPAC97 program.[82] All optimization were performed without symmetry restrictions in Cartesian coordinates by the eigenvector following (EF) routine. The configuration interaction included singles and doubles excitations (CISD) within an active orbital window consisting of the four highest doubly occupied, one singly occupied and the two lowest unoccupied orbitals. The *Pulay*'s procedure was used as the self consistent field (SCF) converger of all calculations. The effect of the solvent (CH$_2$Cl$_2$) was simulated using the conductor-like screening model (COSMO) including the parameters $\varepsilon = 2.0$ and a radius of the solvent of 2.5 Å at the CISD optimized gas phase structures. The experimental permittivity of CH$_2$Cl$_2$ is 8.9, but a previous study revealed that a smaller empirical permittivity yields more reliable results. The use of the

experimental permittivity for the COSMO method results in an overestimation of the solvent influence on the CT absorption energies.[44]

4.4   Syntheses

All transition-metal catalyzed reactions were done under inert gas atmosphere in dry, degassed solvents.

4.4.1   *N,N*-Bis-(4-methoxyphenyl)-*N*-[4-(4,4,5,5-tetramethyl-[1,3,2]dioxaborolan-2-yl)-phenyl]-amine

N-(4-Bromphenyl)-*N,N*-bis-(4-methoxyphenyl)-amine   (300   mg,   780 μmol), [Pd$_2$(dba)$_3$]•CHCl$_3$ (20 mg, 20 μmol, 2.5 mol%), triethylamine (240 mg, 320 μl, 2.3 mmol), pinacol borane (149 mg, 170 μl, 1.17 mmol) and tri-*tert*-butylphosphine (16 mg, 7.8 μmol, 10 mol%, solution 10% in hexane) were dissolved in dry dioxane (1.5 ml) and heated at 80°C for 3 h. The solvent was removed in vacuum and the residue was purified by flash chromatography (silica gel, gradient PE/CH$_2$Cl$_2$ 2:1 → 1:1) to yield a colorless solid (200 mg, 464 μmol, 59%). M.p. 113°C; ^{1}H-NMR (250 MHz, CDCl$_3$)**:** δ = 7.60 (AA′, 2 H; H-3, H-5, dioxoborolan-2-ylphenyl), 7.06 (AA′, 4 H; H-3, H-5, methoxyphenyl), 6.88 - 6.81 (2 BB′, 6 H), 3.80 (s, 6 H; OMe), 1.32 (s, 12 H; Me); ^{13}C-NMR (63 MHz, CDCl$_3$)**:** δ = 156.3, 151.5, 140.6, 135.9, 127.3, 118.8, 114.9, 83.5, 55.61 (OMe), 23.0 (Me); MS (EI): *m/z* (%): 431.22695 (100; C$_{26}$H$_{30}$BNO$_4$ requires 431.22679) [M$^+$], 416 (46) [M$^+$-Me].

4.4.2 4,16-Bis-{4-amino-[*N,N*-di-(4-methoxyphenyl)]-phenyl}-[2.2]paracyclophane (**1**)

4,16-Dibromo-[2.2]paracyclophane (75.0 mg, 205 μmol), *N,N*-bis-(4-methoxyphenyl)-*N*-[4-(4,4,5,5-tetramethyl-[1,3,2]dioxaborolan-2-yl)-phenyl]-amine (194 mg, 451 μmol, 2.2 eq), [Pd$_2$(dba)$_3$]•CHCl$_3$ (6 mg, 6 μmol, 3 mol%), potassium phosphate (174 mg, 820 μmol, 4 eq) and tri-*tert*-butylphosphane (3.0 mg, 1.5 μmol, 7.2 mol%, solution 10% in hexane) were dissolved in dry toluene (1 ml), the mixture was degassed with N$_2$ for 10 minutes and heated at 90°C for 24 h. The solvent was removed in vacuum and the residue was purified by flash chromatography (silica gel, gradient PE/CH$_2$Cl$_2$ 1:1 → CH$_2$Cl$_2$) to yield a pale yellow solid (77.0 mg, 9.45 μmol, 47%). M.p. 254°C; ^{1}H-NMR (250 MHz, CD$_2$Cl$_2$)**:** δ = 7.37 (AA′, 4 H; phenylene), 7.13 (AA′, 8 H; H-3, H-5, 4-anisyl), 7.00 (BB′, 4 H; phenylene), 6.88 (BB', 8 H; H-2, H-6, 4-anisyl), 6.60-6.57 (6 H; [2.2]paracyclophane), 3.81 (s, 12 H; OMe), 3.54-3.43 (2 H; CH$_2$), 3.01-2.79 (6 H; CH$_2$); ^{13}C-NMR (63 MHz, CD$_2$Cl$_2$)**:** δ = 156.5, 148.1, 142.2, 141.3, 140.3, 137.1, 137.1, 135.1, 133.9, 132.2, 130.6, 129.0, 127.1, 120.4, 115.0, 55.9 (OMe), 35.0 (CH$_2$), 34.3 (CH$_2$); IR (KBr)**:** $\tilde{\nu}$ = 2929 wbr (C-H), 1603 m, 1504 vs, 1240vs, 1034 s, 828 s cm^{-1}; MS (EI): *m/z* (%): 814.38033 (100; C$_{56}$H$_{50}$N$_2$O$_4$ requires 814.37706) [M$^+$], 407 (41) [M^{2+}].

4.4.3 4-{4-Amino-[*N,N*-di-(4-methoxyphenyl)]-phenyl}-[2.2]paracyclophane (**2**)

The slower running fractions of the flash chromatography of **1** contained a mixture (85 mg) of 4-bromo-16-{4-amino-[*N,N*-di-(4-methoxyphenyl)]-phenyl}-[2.2]paracyclophane and **2** which was dissolved in THF (3 ml), cooled to -70°C and *t*BuLi (0.5 ml, 0.8 mmol) was slowly added. The mixture was stirred for 2 h at -70°C, hydrolyzed with water (2 ml) and, after warming up to rt, was extracted with MTBE. The organic layer was washed with water and the solvent was removed in vacuum to yield a colorless solid (43 mg), which can be precipitated from CH$_2$Cl$_2$/MeOH. M.p. 121°C; ^{1}H-NMR (400 MHz, (CD$_3$)$_2$CO)**:** δ = 7.35 (AA′, 2 H; phenylene), 7.12 (AA′, 4 H; H-3, H-5, 4-anisyl), 7.00-6.93 (2 BB′, 6 H; phenylene, 4-anisyl), 6.66-6.49 (7 H; [2.2]paracyclophane), 3.81 (s, 6 H; OMe), 3.52-2.60 (8 H; CH$_2$); ^{13}C-NMR (101 MHz, (CD$_3$)$_2$CO)**:** δ = 157.3, 148.7, 142.5, 141.7, 140.52, 140.46,

140.3, 137.6, 136.8, 134.4, 134.0, 133.5, 133.0, 132.7, 132.5, 131.1, 130.6, 127.8, 120.6, 115.7, 55.8 (OMe), 36.0 (CH_2), 35.8 (CH_2), 35.4 (CH_2), 35.1 (CH_2); MS (EI): m/z (%): 511.25149 (100; $C_{36}H_{33}NO_2$ requires 511.25113) [M^+], 496 (12) [M^+-Me].

4.4.4 N-(2',5'-Dimethylbiphenyl-4-yl)-N,N-bis-(4-methoxyphenyl)-amine (3)

N-(4-Bromphenyl)-N,N-bis-(4-methoxyphenyl)-amine (100 mg, 260 μmol), 2,5-dimethyl-phenylboronic acid (58.5 mg, 390 μmol, 1.5 eq), [$Pd_2(dba)_3$]•$CHCl_3$ (4.0 mg, 3.9 μmol, 1.5 mol%), potassium phosphate (110 mg, 0.520 mmol, 2 eq) and tri-*tert*-butylphosphane (1.6 mg, 7.8 μmol, 3 mol%, solution 10% in hexane) were dissolved in dry toluene (1.5 ml), the mixture was degassed with N_2 for 10 minutes and heated at 90°C for 24 h. The solvent was removed in vacuum and the residue was purified by flash chromatography (silica gel, eluent PE/CH_2Cl_2 2:1) to yield a colorless solid (100 mg, 244 μmol, 94%). M.p. 130°C; ^{1}H-NMR (400 MHz, C_6D_6): δ = 7.20 (AA′, 2 H; phenylene), 7.15 (AA′, 4 H; 4-anisyl), 7.09 (d, $^3J(H,H)$ = 7.7 Hz, 1 H; H-3, 4-xylene), 6.97 (dd, $^3J(H,H)$ = 7.6 Hz, $^4J(H,H)$ = 1.4 Hz, 1 H; H-4, 4-xylene), 6.73 (BB′, 4 H; 4-anisyl), 3.31 (s, 6 H, OMe), 2.29 (s, 3 H, Me), 2.18 (s, 3 H, Me); ^{13}C-NMR (101 MHz, $(CD_3)_2CO$): δ = 157.2, 148.6, 142.4, 141.8, 135.8, 134.9, 132.7, 131.2, 131.1, 130.5, 128.3, 127.6, 120.5, 115.7, 55.8 (OMe), 21.0 (Me), 20.3 (Me); MS (EI): m/z (%):409.20476 (100; $C_{28}H_{27}NO_2$ requires 409.20418) [M^+], 204.6 (11) [M^{2+}].

4.4.5   4,16-Bis-{4-[N,N-bis-(4-methoxyphenyl)-amino]-phenylethynyl}-
   [2.2]paracyclophane (4)

4,16-Dibromo-[2.2]paracyclophane (300 mg, 819 μmol), N,N-bis-(4-methoxyphenyl)-(4-ethynylphenyl)-amine (594 mg, 1.80 mmol, 2.2 eq), [$Pd(C_6H_5CN)_2Cl_2$] (18.9 mg, 49.2 μmol, 6 mol%), tri-*tert*-butylphosphane (19.9 mg, 98.3 μmol, 12 mol%, solution 10% in hexane), copper (I) iodide (6.24 mg, 32.8 μmol, 4 mol%) and di-*iso*-propylamine (182 mg, 1.80 mmol) were dissolved in dry dioxane (3.5 ml) and heated at 40°C for 20 h. The solvent was removed in vacuum and the residue was purified by flash chromatography (silica gel,

eluent PE/CH$_2$Cl$_2$ 1:1) to yield a yellow solid (320 mg, 371 μmol, 45%). M.p. >215°C; ^{1}H-NMR (400 MHz, CD$_2$Cl$_2$)**:** δ = 7.37 (AA′, 4 H; phenylene), 7.09 (AA′, 8 H; 4-anisyl), 6.99 (dd, ^3J(H,H) = 7.8 Hz, ^4J(H,H) = 1.6 Hz, 2 H; H-7, H-13, [2.2]paracyclophane), 6.89-6.86 (2 BB′, 12 H; phenylene and 4-anisyl), 6.53 (d, ^4J(H,H) = 1.5 Hz, 2 H; H-5, H-15, [2.2]paracyclophane), 6.48 (d, ^3J(H,H) = 7.8 Hz, 2 H; H-8, H-12, [2.2]paracyclophane), 3.80 (12 H; OMe), 3.67-3.60 (2 H; CH$_2$), 3.23-3.16 (2 H; CH$_2$), 3.05-2.99 (2 H; CH$_2$), 2.93-2.86 (2 H; CH$_2$); ^{13}C-NMR (101 MHz, CD$_2$Cl$_2$)**:** δ = 157.0, 149.3, 142.2, 140.5, 140.0, 137.3, 133.5, 130.2, 127.6, 125.5, 119.4, 115.2, 114.7, 93.8, 88.8, 55.8 (OMe), 34.4 (CH$_2$), 34.2 (CH$_2$); MS (EI): m/z (%): 862 (7) [M$^+$], 431 (20) [M^{2+}]; elemental analysis calcd (%) for C$_{60}$H$_{50}$N$_2$O$_4$ (863.1): C 83.50, H 5.84, N 3.25; found: C 83.31, H 5.98, N 3.20.

4.4.6 4,12-Bis-{4-[*N,N*-bis-(4-methoxyphenyl)-amino]-phenylethynyl}-[2.2]paracyclophane (**5**)

4,16-Dibromo-[2.2]paracyclophane (100 mg, 273 μmol), *N,N*-bis-(4-methoxyphenyl)-(4-ethynylphenyl)-amine (198 mg, 601 μmol, 2.2 eq), [Pd(C$_6$H$_5$CN)$_2$Cl$_2$] (6.28 mg, 16.4 μmol, 6 mol%), tri-*tert*-butylphosphane (6.63 mg, 32.8 μmol, 12 mol%, solution 10% in hexane), copper (I) iodide (2.08 mg, 10.9 μmol, 4 mol%) and di-*iso*-propylamine (60.8 mg, 601 μmol) were dissolved in dry dioxane (3.5 ml) and heated at 40°C for 20 h. The solvent was removed in vacuum and the residue was purified by flash chromatography (silica gel, gradient PE/EtOAc 10:1 $\rightarrow$ 2:1) to yield a yellow solid (137 mg, 159 μmol, 58%). M.p. 118°C; ^{1}H-NMR (400 MHz, CD$_2$Cl$_2$)**:** δ = 7.37 (AA′, 4 H; phenylene), 7.10-7.07 (10 H; 4-anisyl and [2.2]paracyclophane), 6.88-6.85 (2 BB′, 12 H; phenylen and 4-anisyl), 6.56 (d, ^3J(H,H) = 8.1 Hz, 2 H; H-8, H-16, [2.2]paracyclophane), , 6.54 (d, ^4J(H,H) = 1.5 Hz, 2 H; H-5, H-13, [2.2]paracyclophane), 3.80 (12 H; OMe), 3.62-3.59 (2 H; CH$_2$), 3.21-3.13 (2 H; CH$_2$), 3.09-3.02 (2 H; CH$_2$), 2.91-2.84 (2 H; CH$_2$); ^{13}C-NMR (101 MHz, CD$_2$Cl$_2$)**:** δ = 156.9, 149.2, 142.2, 140.6, 140.1, 134.0, 133.8, 133.0, 132.6, 127.5, 126.6, 119.6, 115.2, 115.0, 94.0, 88.7, 55.8 (OMe), 34.7 (CH$_2$), 34.0 (CH$_2$); MS (EI): *m/z* (%): 862 (23) [M$^+$], 431 (31) [M^{2+}]; elemental analysis calcd (%) for C$_{60}$H$_{50}$N$_2$O$_4$ (863.1)**:** C 83.50, H 5.84, N 3.25; found: C 83.33, H 5.97, N 3.20.

4.4.7 1,4-Bis-{4-[*N,N*-bis-(4-methoxyphenyl)-amino]-phenylethynyl}-
2,5-dimethylbenzene (**6**)

1,4-Dibromo-2,5-dimethyl-benzene (64.7 mg, 245 μmol), *N,N*-bis-(4-methoxyphenyl)-(4-ethynylphenyl)-amine (178 mg, 540 μmol, 2.2 eq), [Pd(C$_6$H$_5$CN)$_2$Cl$_2$] (12.4 mg, 32.4 μmol, 13 mol%), tri-*tert*-butylphosphane (13.1 mg, 64.8 μmol, 26 mol%, solution 10% in hexane), copper (I) iodide (4.11 mg, 21.6 μmol, 9 mol%) and di-*iso*-propylamine (54.6 mg, 540 μmol) were dissolved in dry dioxane (3.5 ml) and stirred at rt for 20 h. The solvent was removed in vacuum and the residue was purified by flash chromatography (silica gel, eluent PE/EtOAc 5:1) to yield a yellow solid (136 mg, 179 μmol, 73%). M.p. 97°C; ^{1}H-NMR (400 MHz, C$_6$D$_6$)**:** δ = 7.48 (AA′, 4 H; phenylene), 7.41 (s, 2 H; 4-xylene), 7.03 (AA′, 8 H; 4-anisyl), 6.99 (BB′, 4 H; phenylene), 6.71 (BB′, 2 H; 4-anisyl). 3.30 (s, 12 H; OMe), 2.40 (s, 6 H; Me); ^{13}C-NMR (101 MHz, C$_6$D$_6$)**:** δ = 157.0, 149.4, 140.8, 137.4, 133.1, 133.0, 128.3 (DEPT), 127.5, 123.8, 120.0, 115.3, 96.0, 88.2, 55.0 (OMe), 20.2 (Me); MS (ESI): *m/z* (%): 760.33569 (C$_{52}$H$_{44}$N$_2$O$_4$ requires 760.33286) [M$^+$]; elemental analysis calcd (%) for C$_{52}$H$_{44}$N$_2$O$_4$ (760.9): C 82.08, H 5.83, N 3.68; found: C 81.47, H 5.95, N 3.67.

4.4.8 4-{4-[*N,N*-Bis-(4-methoxyphenyl)-amino]-phenylethynyl}-[2.2]paracyclophane (**7**)

4,16-Dibromo-[2.2]paracyclophane (100 mg, 273 μmol), *N,N*-bis-(4-methoxyphenyl)-(4-ethynylphenyl)-amine (89.9 mg, 273 μmol), [Pd(C$_6$H$_5$CN)$_2$Cl$_2$] (6.28 mg, 16.4 μmol, 6 mol%), tri-*tert*-butylphosphane (6.63 mg, 32.8 μmol, 12 mol%, solution 10% in hexane), copper (I) iodide (2.0 mg, 11 μmol, 4 mol%) and di-*iso*-propylamine (60.8 mg, 601 μmol) were dissolved in dry dioxane (2 ml) and heated at 50°C for two days. The solvent was removed in vacuum and the residue was purified by flash chromatography (silica gel, gradient PE/CH$_2$Cl$_2$ 1:1 → 1:2) to yield a pale green solid (72 mg). The solid was dissolved in THF (3 ml) and cooled to -70°C and *t*BuLi (0.5 ml, 0.8 mmol) was slowly added to the solution and the mixture was stirred for 2 h at -70°C. The mixture was hydrolyzed with water (2 ml) and, after warming up to rt, was extracted with MTBE. The organic layer was washed with water and the solvent was removed in vacuum to yield a pale green solid (40 mg), which can be

precipitated from CH$_2$Cl$_2$/MeOH. M.p 130°C (decomposition); ^{1}H-NMR (400 MHz, (CD$_3$)$_2$CO): δ = 7.41 (AA′, 2 H; phenylene), 7.13 (AA′, 4 H; H-3, H-5, 4-anisyl), 6.99 (dd, ^3J(H,H) = 7.9 Hz, ^4J(H,H) = 1.7 Hz, 1 H; [2.2]paracyclophane), 6.96 (BB′, 4 H; 4-anisyl), 6.84 (BB′, 2 H; phenylene), 6.59-6.53 (5 H; [2.2]paracyclophane), 6.48 (dd, ^3J(H,H) = 7.8 Hz, ^4J(H,H) = 1.6 Hz, 1 H; [2.2]paracyclophane), 3.81 (s, 6 H; OMe), 3.65-3.59 (1 H; CH$_2$), 3.25-2.87 (7 H, CH$_2$); ^{13}C-NMR (101 MHz, (CD$_3$)$_2$CO): δ = 157.8, 150.0, 142.9, 140.9, 140.8, 140.3, 140.2, 137.6, 134.8, 134.3, 133.7, 133.3, 133.2, 133.0, 130.6, 128.3, 126.3, 119.6, 115.8, 115.2, 94.3, 89.2, 55.8 (OMe), 36.0 (CH$_2$), 35.6 (CH$_2$), 35.1 (CH$_2$), 34.9 (CH$_2$); MS (EI): m/z (%): 535.25133 (76; C$_{38}$H$_{33}$NO$_2$ requires 535.25113) [M$^+$], 431 (100) [M$^+$-p-xylylene].

4.4.9 N-[4-(2,5-Dimethyl-phenylethynyl)-phenyl]-N,N-bis-(4-methoxyphenyl)-amine (**8**)

2-Bromo-1,4-dimethylbenzene (100 mg, 540 μmol), N,N-bis-(4-methoxyphenyl)-(4-ethynylphenyl)-amine (178 mg, 540 μmol), [Pd(C$_6$H$_5$CN)$_2$Cl$_2$] (12.4 mg, 32.4 μmol, 6 mol%), tri-$tert$-butylphosphane (13.1 mg, 64.8 μmol, 12 mol%, solution 10% in hexane), copper (I) iodide (4.11 mg, 21.6 μmol, 4 mol%) and di-iso-propylamine (54.6 mg, 540 μmol) were dissolved in dry dioxane (2 ml) and stirred at rt for 4 h. The solvent was removed in vacuum and the residue was purified by flash chromatography (silica gel, gradient PE/EtOAc 10:1 → 4:1) to yield a colorless solid (105 mg, 242 μmol, 45%). M.p. 88°C; ^{1}H-NMR (400 MHz, (CD$_3$)$_2$CO): δ = 7.33 (AA′, 2 H; phenylene), 7.26 (m, 1 H; H-6, 4-xylene), 7.14 (d, ^3J(H,H) = 7.8 Hz, 1 H; H-3, 4-xylene), 7.11 (AA′, 4 H; 4-anisyl), 7.06 (m, 1 H; H-4 4-xylene), 6.94 (BB′, 4 H; 4-anisyl), 6.79 (BB′, 2 H; phenylene). 3.80 (s, 6 H; OMe), 2.41 (s, 3 H; Me), 2.28 (s, 3 H, Me); ^{13}C-NMR (101 MHz, (CD$_3$)$_2$CO): δ = 157.8, 150.1, 140.9, 137.3, 136.0, 133.1 ,132.7, 130.3, 129.7, 128.3, 124.2, 119.4, 115.8, 114.7, 94.6, 87.7, 55.8 (OMe), 20.7 (Me), 20.3 (Me); MS (EI): m/z (%): 433.20458 (100; C$_{30}$H$_{27}$NO$_2$ requires 433.20418) [M$^+$], 216.7 (11) [M^{2+}].

4.4.10   4,16-Bis-(4-{4-[N,N-bis-(4-methoxyphenyl)-amino]-phenyl}-buta-1,3-diynyl)-[2.2]-paracyclophane (**9**)

Silver(I) nitrate (8.96 mg, 52.7 μmol) and N-iodosuccinimide (356 mg, 1.58 mmol) were added to a solution of 4,16-bis-(trimethylsilylethynyl)-[2.2]paracyclophane (150 mg, 374 μmol) in CH_2Cl_2/acetone (4 ml/4 ml) and stirred in the dark for 8h. The mixture was cooled to 0°C, hydrolyzed with water and extracted with CH_2Cl_2. The combined organic extracts were washed twice with water, twice with brine and dried over sodium sulfate. The solvent was removed in vacuum and the residue was purified by flash chromatography (silica gel, gradient PE/CH_2Cl_2 19:1 $\rightarrow$ 9:1) to yield a colorless solid (79 mg, 0.16 mmol, 42%). The product 4,16-bis-(iodoethynyl)-[2.2]paracyclophane was not fully characterized and was used for the synthesis of **9** without further purification due to its sensitivity to light and instability in solution. ^{1}H-NMR (400 MHz, CDCl$_3$)**:** δ = 6.92 (dd, [3]J(H,H) = 7.8 Hz, [4]J(H,H) = 1.8 Hz, 2H), 6.49 (d, [4]J(H,H) = = 1.8 Hz, 2H), 6.44 (d, [3]J(H,H) = 7.7 Hz, 2H), 3.53 (m, 2H), 3.14 (m, 2H), 2.97 (m, 2H), 2.85 (m, 2H). 4,16-Bis(iodethynyl)-[2.2]paracyclophane (75 mg, 148 μmol) and N,N-bis-(4-methoxyphenyl)-(4-ethynylphenyl)-amine (194 mg, 590 μmol, 4 eq) were suspended in pyrrolidine (1.5 ml) and degassed with N$_2$ for 5 minutes. Copper(I) iodide (5.62 mg, 29.5 μmol, 20 mol%) was added and the mixture was stirred at rt for 1h. The solvent was removed in vacuum and the residue was purified by flash chromatography (silica gel, gradient PE/EtOAc 15:1 $\rightarrow$ 5:1) to yield a yellow solid (80 mg, 88 μmol, 59%). M.p. 278°C (decomposition); ^{1}H-NMR (400 MHz, CD$_2$Cl$_2$)**:** δ = 7.33 (AA′, 4H; phenylene), 7.10 (AA′, 8H; 4-anisyl), 7.01 (dd, [3]J(H,H) = 7.8 Hz, [4]J(H,H) = 1.8 Hz, 2H), 6.88 (BB′, 8H; 4-anisyl), 6.78 (BB′, 4H; phenylene), 6.59 (d, [4]J(H,H) = 1.8 Hz, 2H), 6.48 (d, [3]J(H,H) = 7.8 Hz, 2H), 3.80 (s, 12H; OMe), 3.56 (m, 2H; CH$_2$), 3.21 (m, 2H; CH$_2$), 3.02 (m, 2H; CH$_2$), 2.91 (m, 2H; CH$_2$); It was not possible to measure ^{13}C-NMR due to low solubility and decomposition in solution; MS (ESI): m/z (%): 910.37793 ($C_{64}H_{50}N_2O_4$ requires 910.37651) [M$^+$]; elemental analysis calcd (%) for $C_{64}H_{50}N_2O_4$ (911.1): C 84.37, H 5.53, N 3.07; found: C 84.71, H 5.59, N 2.98.

5   References

(1)   Bazan, G. C.; Oldham Jr., J.; Lachicotte, R. J.; Tretiak, S.; Chernyak, V.; Mukamel, S. *J. Am. Chem. Soc.* **1998**, *120*, 9188-9204.

(2)   Verdal, N.; Godbout, J. T.; Perkins, T. L.; Bartholomew, G. P.; Bazan, G. C.; Kelley, A. M. *Chem. Phys. Lett.* **2000**, *320*, 95-103.

(3)   Zyss, J.; Ledoux, I.; Volkov, S.; Chernyak, V.; Mukamel, S.; Bartholomew, G. P.; Bazan, G. C. *J. Am. Chem. Soc.* **2000**, *122*, 11956-11962.

(4)   Bartholomew, G. P.; Bazan, G. C. *Acc. Chem. Res.* **2001**, *34*, 30-39.

(5)   Bartholomew, G. P.; Bazan, G. C. *J. Am. Chem. Soc.* **2002**, *124*, 5183-5196.

(6)   Moran, A. M.; Bartholomew, G. P.; Bazan, G. C.; Kelley, A. M. *J. Phys. Chem. A* **2002**, *106*, 4928-4937.

(7)   Utz, N.; Koslowski, T. *Chem. Phys.* **2002**, *282*, 389-397.

(8)   Bartholomew, G. P.; Rumi, M.; Pond, S. J. K.; Perry, J. W.; Tretiak, S.; Bazan, G. C. *J. Am. Chem. Soc.* **2004**, *126*, 11529-11542.

(9)   Hong, J. W.; Woo, H. Y.; Liu, B.; Bazan, G. C. *J. Am. Chem. Soc.* **2005**, *127*, 7435-7443.

(10)   Woo, H. Y.; Hong, J. W.; Liu, B.; Mikhailovsky, A.; Korystov, D.; Bazan, G. C. *J. Am. Chem. Soc.* **2005**, *127*, 820-821.

(11)   Heilbronner, E.; Maier, J. P. *Helv. Chim. Acta* **1974**, *57*, 151-159.

(12)   Sato, T.; Torizuka, K. *J. Chem. Soc., Perkin Trans. 2* **1978**, 1199-1204.

(13)   Gerson, F.; Martin Jr., W. B. *J. Am. Chem. Soc.* **1969**, *91*, 1883-1891.

(14)   Gerson, F.; Martin, W. B.; Wydler, C. *J. Am. Chem. Soc.* **1976**, *98*, 1318-1320.

(15)   Gerson, F.; Lopez, J.; Boekelheide, V.; Hopf, H. *Helv. Chim. Acta* **1982**, *65*, 1391-1397.

(16)   Bruhin, J.; Gerson, F.; Ohyanishiguchi, H. *J. Chem. Soc., Perkin Trans. 2* **1980**, 1045-1050.

(17)   Badger, B.; Brocklehurst , B. *Trans. Faraday Soc.* **1969**, *65*, 2582-2587.

(18)   Kovac, B.; Mohraz, M.; Heilbronner, E.; Boekelheide, V.; Hopf, H. *J. Am. Chem. Soc.* **1980**, *102*, 4314-4324.

(19)   Gerson, F.; Lopez, J.; Hopf, H. *Helv. Chim. Acta* **1982**, *65*, 1398-1403.

(20) Ohyanishiguchi, H.; Terahara, A.; Hirota, N.; Sakata, Y.; Misumi, S. *Bull. Chem. Soc. Jpn.* **1982**, *55*, 1782-1789.

(21) Wartini, A. R.; Valenzuela, J.; Staab, H. A.; Neugebauer, F. A. *Eur. J. Org. Chem.* **1998**, 139-148.

(22) Wartini, A. R.; Staab, H. A.; Neugebauer, F. A. *Eur. J. Org. Chem.* **1998**, 1161-1170.

(23) Nelsen, S. F.; Konradsson, A. E.; Telo, J. P. *J. Am. Chem. Soc.* **2005**, *127*, 920-925.

(24) Bonvoisin, J.; Launay, J.-P.; Van der Auweraer, M.; De Schryver, F. C. *J. Phys. Chem.* **1994**, *98*, 5052-5057, **Erratum: 1996,** *100(45)*, 18006.

(25) Bonvoisin, J.; Launay, J.-P.; Verbouwe, W.; Van der Auweraer, M.; De Schryver, F. C. *J. Phys. Chem.* **1996**, *100*, 17079-17082.

(26) Stickley, K. R.; Blackstock, S. C. *Tetrahedron Lett.* **1995**, *36*, 1585-1588.

(27) Lambert, C.; Nöll, G. *Angew. Chem., Int. Ed.* **1998**, *37*, 2107-2110.

(28) Lambert, C.; Nöll, G.; Schmalzlin, E.; Meerholz, K.; Bräuchle, C. *Chem.-Eur. J.* **1998**, *4*, 2129-2135.

(29) Lambert, C.; Nöll, G. *J. Am. Chem. Soc.* **1999**, *121*, 8434-8442.

(30) Lambert, C.; Nöll, G.; Hampel, F. *J. Phys. Chem. A* **2001**, *105*, 7751-7758.

(31) Coropceanu, V.; Malagoli, M.; Andre, J. M.; Brédas, J.-L. *J. Chem. Phys.* **2001**, *115*, 10409-10416.

(32) Lambert, C.; Nöll, G. *Chem.-Eur. J.* **2002**, *8*, 3467-3477.

(33) Coropceanu, V.; Malagoli, M.; Andre, J. M.; Brédas, J.-L. *J. Am. Chem. Soc.* **2002**, *124*, 10519-10530.

(34) Lambert, C.; Nöll, G.; Schelter, J. *Nat. Mater.* **2002**, *1*, 69–73.

(35) Lambert, C.; Nöll, G. *J. Chem. Soc., Perkin Trans. 2* **2002**, 2039-2043.

(36) Nelsen, S. F.; Konradsson, A. E.; Weaver, M. N.; Telo, J. P. *J. Am. Chem. Soc.* **2003**, *125*, 12493-12501.

(37) Lambert, C.; Nöll, G.; Zabel, M.; Hampel, F.; Schmalzlin, E.; Bräuchle, C.; Meerholz, K. *Chem.-Eur. J.* **2003**, *9*, 4232-4239.

(38) Lambert, C. *ChemPhysChem* **2003**, *4*, 877-880.

(39) Coropceanu, V.; Lambert, C.; Nöll, G.; Brédas, J.-L. *Chem. Phys. Lett.* **2003**, *373*, 153-160.

(40) Yano, M.; Ishida, Y.; Aoyama, K.; Tatsumi, M.; Sato, K.; Shiomi, D.; Ichimura, A.; Takui, T. *Synth. Met.* **2003**, *137*, 1275-1276.

(41) Yano, M.; Aoyama, K.; Ishida, Y.; Tatsumi, M.; Sato, K.; Shiomi, D.; Takui, T. *Polyhedron* **2003**, *22*, 2003-2008.

(42) Jones, S. C.; Coropceanu, V.; Barlow, S.; Kinnibrugh, T.; Timofeeva, T.; Brédas, J. L.; Marder, S. R. *J. Am. Chem. Soc.* **2004**, *126*, 11782-11783.

(43) Coropceanu, V.; Gruhn, N. E.; Barlow, S.; Lambert, C.; Durivage, J. C.; Bill, T. G.; Nöll, G.; Marder, S. R.; Brédas, J.-L. *J. Am. Chem. Soc.* **2004**, *126*, 2727-2731.

(44) Lambert, C.; Amthor, S.; Schelter, J. *J. Phys. Chem. A* **2004**, *108*, 6474-6486.

(45) Szeghalmi, A. V.; Erdmann, M.; Engel, V.; Schmitt, M.; Amthor, S.; Kriegisch, V.; Nöll, G.; Stahl, R.; Lambert, C.; Leusser, D.; Stalke, D.; Zabel, M.; Popp, J. *J. Am. Chem. Soc.* **2004**, *126*, 7834-7845.

(46) Heckmann, A.; Lambert, C.; Goebel, M.; Wortmann, R. *Angew. Chem., Int. Ed.* **2004**, *43*, 5851-5856.

(47) Low, P. J.; Paterson, M. A. J.; Puschmann, H.; Goeta, A. E.; Howard, J. A. K.; Lambert, C.; Cherryman, J. C.; Tackley, D. R.; Leeming, S.; Brown, B. *Chem.-Eur. J.* **2004**, *10*, 83-91.

(48) Lambert, C.; Risko, C.; Coropceanu, V.; Schelter, J.; Amthor, S.; Gruhn, N. E.; Durivage, J.; Brédas, J.-L. *J. Am. Chem. Soc.* **2005**, *127*, 8508-8516.

(49) Barlow, S.; Risko, C.; Coropceanu, V.; Tucker, N. M.; Jones, S. C.; Levi, Z.; Khrustalev, V. N.; Antipin, M. Y.; Kinnibrugh, T. L.; Timofeeva, T.; Marder, S. R.; Brédas, J. L. *Chem. Commun.* **2005**, 764-766.

(50) Chiu, K. Y.; Su, T. H.; Huang, C. W.; Liou, G. S.; Cheng, S. H. *J. Electroanal. Chem.* **2005**, *578*, 283-287.

(51) Dümmler, S.; Roth, W.; Fischer, I.; Heckmann, A.; Lambert, C. *Chem. Phys. Lett.* **2005**, *408*, 264-268.

(52) Lambert, C.; Schelter, J.; Fiebig, T.; Mank, D.; Trifonov, A. *J. Am. Chem. Soc.* **2005**, *127*, 10600-10610.

(53) Creutz, C.; Newton, M. D.; Sutin, N. J. *J. Photochem. Photobiol. A* **1994**, *82*, 47-59.

(54) Cave, R. J.; Newton, M. D. *Chem. Phys. Lett.* **1996**, *249*, 15-19.

(55) Newton, M. D. *Adv. Chem. Phys.* **1999**, *106*, 303-375.

(56) Littke, A. F.; Dai, C.; Fu, G. C. *J. Am. Chem. Soc.* **2000**, *122*, 4020-4028.

(57) Littke, A. F.; Fu, G. C. *Angew. Chem., Int. Ed.* **1998**, *37*, 3387-3388.

(58) Murata, M.; Watanabe, S.; Masuda, Y. *J. Org. Chem.* **1997**, *62*, 6458-6459.

(59)   Murata, M.; Oyama, T.; Watanabe, S.; Masuda, Y. *J. Org. Chem.* **2000**, *65*, 164-168.

(60)   Hundertmark, T.; Littke, A. F.; Buchwald, S. L.; Fu, G. C. *Org. Lett.* **2000**, *2*, 1729-1731.

(61)   Nishikawa, T.; Shibuya, S.; Hosokawa, S.; Isobe, M. *Synlett* **1994**, 485-486.

(62)   Alami, M.; Ferri, F. *Tetrahedron Lett.* **1996**, *37*, 2763-2766.

(63)   Cave, R. J.; Newton, M. D.; Kumar, K.; Zimmt, M. B. *J. Phys. Chem.* **1995**, *99*, 17501-17504.

(64)   Cave, R. J.; Newton, M. D. *J. Chem. Phys.* **1997**, *106*, 9213-9226.

(65)   Nelsen, S. F.; Newton, M. D. *J. Phys. Chem. A* **2000**, *104*, 10023-10031.

(66)   Newton, M. D. *Theoretical Chemistry Accounts* **2003**, *110*, 307-321.

(67)   Shin, Y. G. K.; Newton, M. D.; Isied, S. S. *J. Am. Chem. Soc.* **2003**, *125*, 3722-3732.

(68)   Lappe, J.; Cave, R. J.; Newton, M. D.; Rostov, I. V. *J. Phys. Chem. B* **2005**, *109*, 6610-6619.

(69)   Nadeau, J. M.; Liu, M.; Waldeck, D. H.; Zimmt, M. B. *J. Am. Chem. Soc.* **2003**, *125*, 15964-15973.

(70)   The GMH theory uses the projection of the transition dipole moment vectors in one defined direction. In this paper, we use the projections of all vectors on the N-N axis of each molecule. For the dipole moment of ions we used the centre of mass as the origin.

(71)   Amthor, S.; Noller, B.; Lambert, C. *Chem. Phys.* **2005**, *316*, 141-152.

(72)   Chapter IV of this doctoral thesis.

(73)   Salbeck, J.; Schoberl, U.; Rapp, K. M.; Daub, J. *Z. Phys. Chem.* **1991**, *171*, 191-212.

(74)   Zhu, Y.; Wolf, M. O. *J. Am. Chem. Soc.* **2000**, *122*, 10121-10125.

(75)   Newton, M. D. *Chem. Rev.* **1991**, *91*, 767-792.

(76)   Newton, M. D.; Cave, R. J. In *Molecular Electronics*; Jortner, J., Ratner, M., Eds.: Blackwell, Malden, MA, 1997.

(77)   Closs, G. L.; Calcaterra, L. T.; Green, N. J.; Penfield, K. W.; Miller, J. R. *J. Phys. Chem.* **1986**, *90*, 3673-3683.

(78)   Johnson, M. D.; Miller, J. R.; Green, N. S.; Closs, G. L. *J. Phys. Chem.* **1989**, *93*, 1173-1176.

(79) Creager, S.; Yu, C. J.; Bamdad, C.; O'Connor, S.; MacLean, T.; Lam, E.; Chong, Y.;
      Olsen, G. T.; Luo, J. Y.; Gozin, M.; Kayyem, J. F. *J. Am. Chem. Soc.* **1999**, *121*,
      1059-1064.

(80) Smalley, J. F.; Finklea, H. O.; Chidsey, C. E. D.; Linford, M. R.; Creager, S. E.;
      Ferraris, J. P.; Chalfant, K.; Zawodzinsk, T.; Feldberg, S. W.; Newton, M. D. *J. Am.
      Chem. Soc.* **2003**, *125*, 2004-2013.

(81) Weiss, E. A.; Ahrens, M. J.; Sinks, L. E.; Gusev, A. V.; Ratner, M. A.; Wasielewski,
      M. R. *J. Am. Chem. Soc.* **2004**, *126*, 5577-5584.

(82) Stewart, J. J. P. MOPAC97; Fujitsu Limited: 1997.

Bis-triarylamino-[2.2]paracyclophanes II:

Excited State Couplings in the Diradical Dications

CONTENTS

1 Introduction

The linear optical properties of bis-triarylamine dications are presented in this article. The understanding of the physical and chemical properties of triarylamines and their oxidized counterparts are of fundamental interest, since they were widely used as hole conducting materials in organic light emitting devices,[1-10] polymer batteries,[11,12] photorefractive materials for optical data storage[13] and in electrochromic polymers[14], e.g., for anti-glare electrochromic mirrors as well as in the Xerox® process[3,6,10,15] of laser printers and photocopiers. Bis-triarylamines with two nitrogen N redox centers that are connected by varying bridging units B are well known and the corresponding mono-cationic mixed valence (MV) species [N-B-N]$^+$ are of great importance for studying hole transfer (HT) processes from one redox center to the other redox center.[16-43] In this context, a profound influence of the bridge on the HT properties has been demonstrated for several examples.[21,22,26,31,35,36] In addition to the triarylamine to triarylamine hole transfer in MV species, it has been shown that for some systems an additional HT to the bridge B has to be taken into account for a more detailed description of the MV system.[26,36] In this context, bridge localized MV species with excited state mixed-valence character were described and analyzed.[26,36,44] A dihydrazine diradical dication with excited MV states was described by a similar model.[45] Apart from MV compounds, it was quite recently demonstrated that triarylamines can be used to investigate hole transfer processes along redox cascades, since the redox potential of the triarylamine redox centers can easily be tuned.[46]

While MV species [N-B-N]$^+$ are now reasonably well understood, detailed studies of the optical properties of neutral bis-triarylamines [N-B-N] are still quite rare.[47-54] In two previous articles, the linear and nonlinear optical properties of some bis-triarylamines with varying bridging moieties including compounds **4** and **6** presented here (Chart 1) were investigated and analyzed by a three-level model.[54,55] In this chapter of the present thesis, the linear optical properties of bis-triarylamine dications [N-B-N]$^{2+}$ **1^{2+}**, **4^{2+}**, **6^{2+}** and **9^{2+}** are presented and analyzed by an exciton coupling model. The results are compared to the photophysical properties of the "monomeric" triarylamine radical cations **2$^{•+}$**, **3$^{•+}$**, **7$^{•+}$** and **8$^{•+}$**.

In **1^{2+}**, **4^{2+}**, **5^{2+}**, and **9^{2+}** the [2.2]paracyclophane moiety was used to bring two chromophores in close contact. This moiety provides no direct π-conjugation, but allows through-space (π–π) and through-bond (σ) interactions.[56] It was already demonstrated by

Bazan et al. that these interactions are responsible for significant π–electron delocalization between aromatic polymer chains[57-59] as well as between donor and acceptor groups[60-65]. The [2.2]paracyclophane systems, therefore, might serve as model compounds to study interchromophore interactions between two π-conjugated strands as they might occur in π-conjugated oligomers or polymers.[66,67]

The replacement of the [2.2]paracyclophane moiety in 4^{2+} by a *p*-xylyl unit in 6^{2+} allows for the comparison of through-space and through-bond interactions with direct π-conjugation. Different arrangements of the two triarylamine chormophores as in the isomers 4^{2+} (*pseudo-para*) and 5^{2+} (*pseudo-ortho*) and their influence on exciton coupling will be investigated. Furthermore, a comparison of 1^{2+}, 4^{2+} and 9^{2+} will provide insight into the influence of the distance between the two N redox centers on the spectral features of bis-triarylamine dications with a [2.2]paracyclophane bridge.

Chart 1.

An = 4-methoxyphenyl
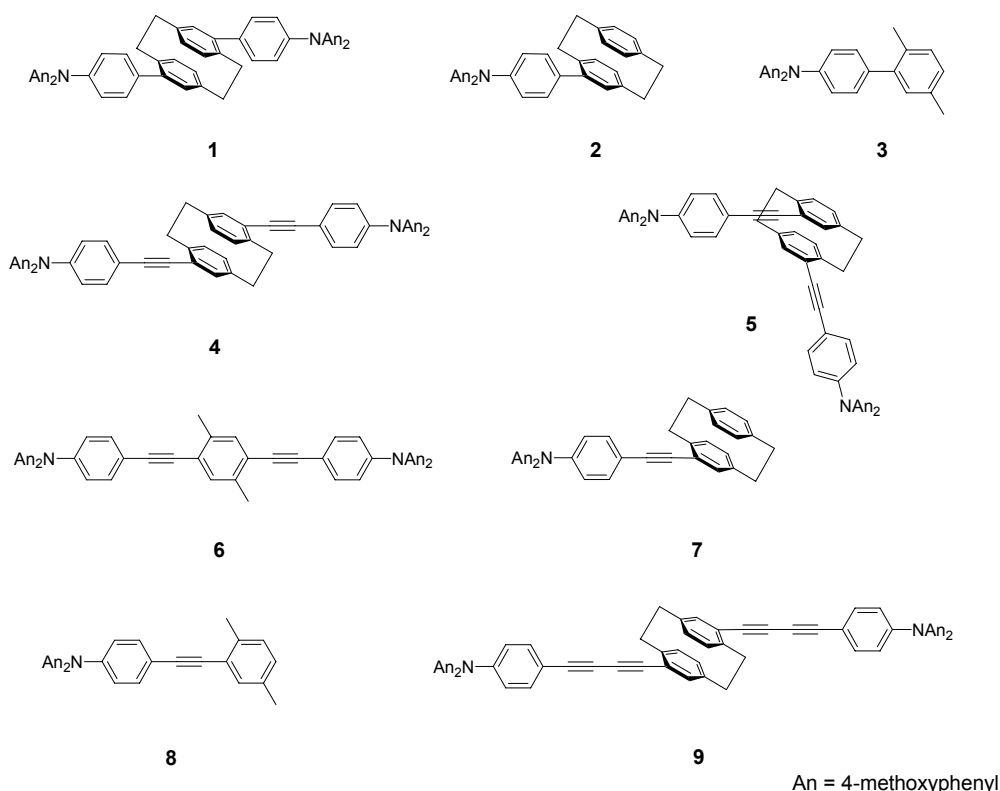
The experimental spectral characteristics will be compared with AM1-CISD computations. These computational results will complement the observed experimental data in order to analyze the above mentioned dications by a generalized *Mulliken-Hush* (GMH)[68-70]

model to yield couplings V_{23}(GMH), which are a measure for electronic interactions of the mixed-valence (MV) excited states.

2   Results and Discussion

2.1   *Experimental UV/Vis/NIR spectra*

The absorption spectra of all cations and dications were obtained by chemical oxidation of the neutral precursors in CH_2Cl_2 and MeCN, respectively. The diradical dications of bis-triarylamine compounds **1**, **4**, **5**, **6** and **9** and the mono radical cations of **2**, **3**, **7** and **8** show a rather intense absorption band at 13000-13440 cm^{-1} in CH_2Cl_2 (Figure 1 and Table 1).
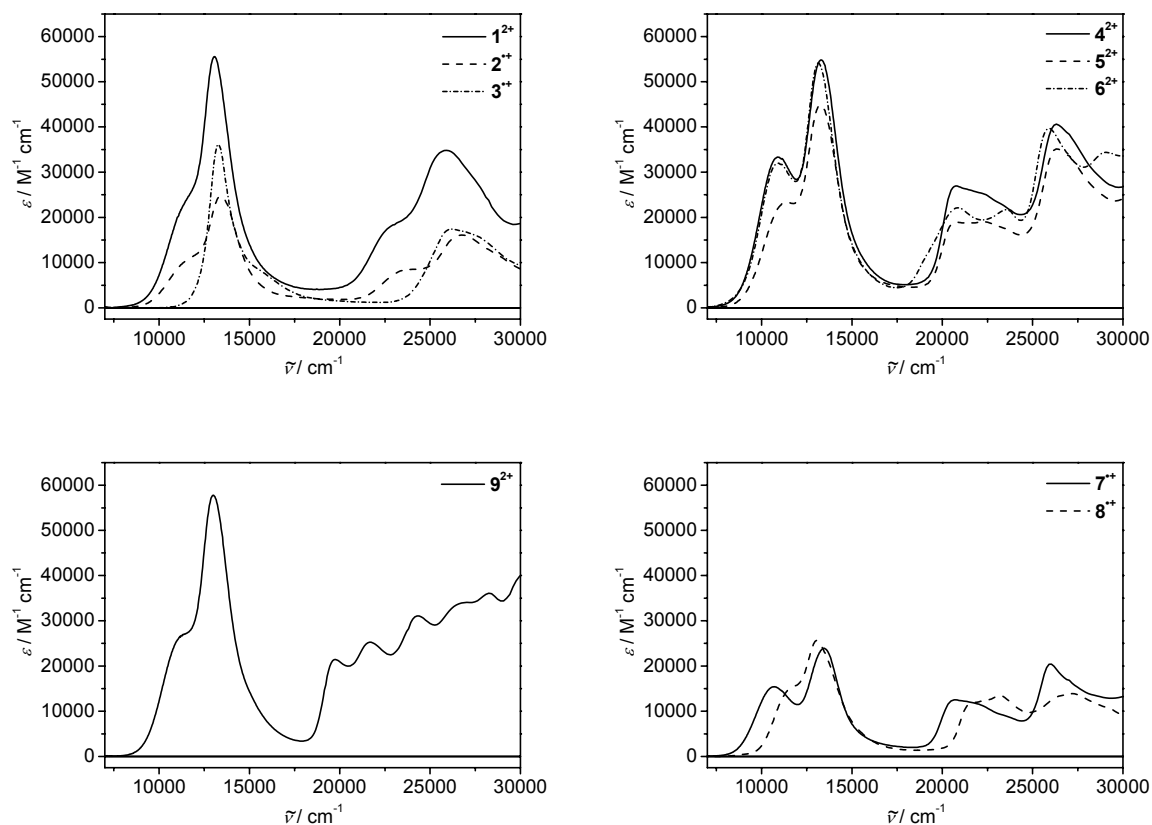
Figure 1. UV/Vis/NIR spectra of radical cations and diradical dications in CH_2Cl_2.

This band is not solvent dependent and is due to a π-π^* excitation localized within the triarylamine radical cation moiety.[71] This intense triarylamine radical cation π-π^* excitation is accompanied by a second less intense absorption reflected by a distinct shoulder or even by a separated band (**4²⁺**, **5²⁺**, **7•⁺**). This weaker absorption is at lower energies than the intense main signal for all compound, except **3•⁺** for which a shoulder at the higher energy side of the π-π^* excitation band is observed.

Table 1. Experimental absorption energies and extinction coefficients between parentheses in $M^{-1}\ cm^{-1}$.

	$\widetilde{\nu}_{NIR}$ / cm^{-1}	$\widetilde{\nu}_{vis}$ / cm^{-1}
1²⁺	11300 sh (22000),	13090 (55600), 22800 sh (18000), 25900 (34800)
2•⁺	11500 sh (10500),	13400 (24700), 23600 sh (8400), 26740 (16100)
3•⁺	13260 (36200),	15500 sh (8600), 26180 (17400), 27600 sh (15800)
4²⁺	10900 (33300),	13300 (54800), 20750 (26900)
5²⁺	11260 (23300),	13260 (44900), 20750 (19000)
6²⁺	10870 (32000),	13160 (54100), 20830 (22100), 23580 (21700)
7•⁺	10680 (15400),	13440 (23900), 20660 (12500)
8•⁺	11500 sh (14900),	13050 (25600), 21700 sh (11900), 23150 (13500)
9²⁺	11100 sh (26300),	13000 (57800), 19760 (21500), 21650 (25300), 24390 (31100)

As can be seen from Figure 2, there is only little influence of the solvent polarity (MeCN vs CH₂Cl₂) on the position of the intense π-π^* band. However, the second weaker band shows a distinct blue shift which suggests a certain CT (charge transfer) character. It is supposed that the small blue shift of the intense main peak of **1²⁺** in MeCN relative to the peak in CH₂Cl₂ results from the strong overlap with the CT band.
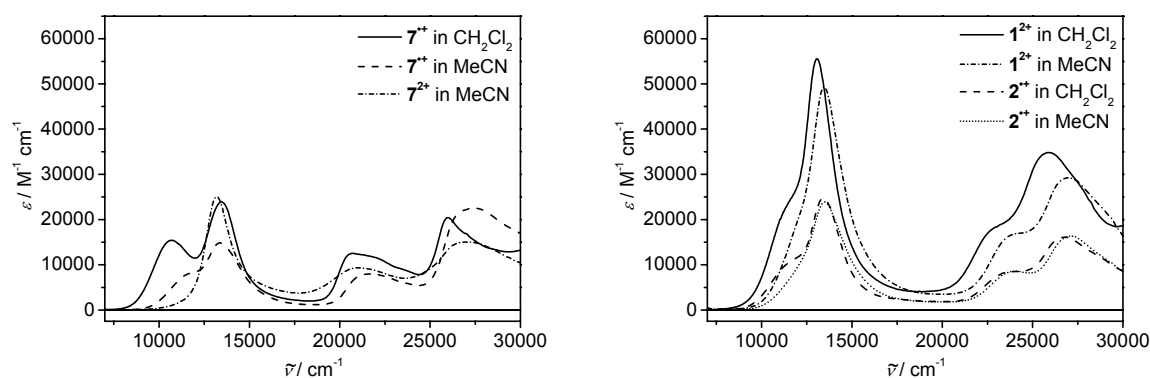
Figure 2. UV/Vis/NIR spectra of **1²⁺**, **2•⁺** and **7•⁺** recorded in CH₂Cl₂ in comparison to spectra recorded in MeCN and spectrum of **7²⁺** in MeCN.

While for biaryls 1^{2+} and $2^{\bullet+}$ with the same cyclophane "bridge" the CT band causes a shoulder at similar energy, this band is significantly blue-shifted in $3^{\bullet+}$ by about 4000 cm^{-1} in CH$_2$Cl$_2$. This shift is due to the weaker electron donor character of the *p*-xylene group compared to the [2.2]paracyclophane group. Comparison of the spectra of 4^{2+}, 6^{2+} and $7^{\bullet+}$ shows that the CT signal of these acetylenes is well separated from the triarylamine radical cation π-π* band and appears at similar absorption energies for all three cations. In contrast, the CT signal of the *pseudo-ortho* paracylophane 5^{2+} and the *p*-xylene derivative $8^{\bullet+}$ is little blue-shifted compared to the CT bands of 4^{2+}, 6^{2+} and $7^{\bullet+}$. The observation of this shift of the CT absorption of *p*-xylene $8^{\bullet+}$ versus cyclophanes $7^{\bullet+}$ and 4^{2+} is in accordance with the findings for 1^{2+}, $2^{\bullet+}$ and $3^{\bullet+}$. This is also due to the weaker electron donor character of the *p*-xylene group compared to the [2.2]paracyclophane group. The π-π* and CT absorption signals of the mono-triarylamine cations $2^{\bullet+}$, $3^{\bullet+}$, $7^{\bullet+}$, and $8^{\bullet+}$ show approximately half the intensity of the absorption bands of the bis-triarylamine diradical dications 1^{2+}, 4^{2+}, 5^{2+}, 6^{2+} and 9^{2+}. Since the oxidized triarylamine unit is predominantly responsible for the absorption properties, a doubling of the absorption intensities is expected for the symmetrical dications compared to their "monomeric" counterparts.

2.2   Exciton coupling model

The absorption signals of the mono-triarylamine radical cations in the Vis/NIR region can be interpreted in terms of a transition polarized along the molecular principal axis z and a transition polarized along the x-axis (see Figure 4). The transition polarized along z has a distinct CT character, because charge can be transferred from the triarylamine to the bridge. The transition which is x-polarized has vanishing CT character, since the charge is localized at the dianisylamino groups. Thus, the intense signals at ca. 13000 cm^{-1} can be interpreted as x-polarized transitions which are described as localized π-π* transitions.[71] The solvent dependent second weaker absorption is attributed to the transition polarized along z termed hereafter bridge CT band (CT$_{bridge}$). Surprisingly, the bis-triarylamine dications reveal a negative solvatochromism, although the dipole moment of the ground and the *Franck-Condon* excited states is expected to be zero for symmetry reasons. This behavior can be explained by the following model: According to *Marcus-Hush* theory[72,73] the adiabatic potential energy surfaces of the ground and the two excited CT states are described by the following 3×3 secular determinant (eq 1) which couples three diabatic (model) states (diagonal elements) by the off-diagonal elements (electronic couplings).

$$\begin{vmatrix} \lambda\,x^2 - \varepsilon & 0 & 0 \\ 0 & \lambda\,(-\frac{1}{2}-x)^2 + \Delta G^0 - \varepsilon & V_{23} \\ 0 & V_{23} & \lambda\,(\frac{1}{2}-x)^2 + \Delta G^0 - \varepsilon \end{vmatrix} = 0 \qquad (1)$$

Within this model, the diabatic potentials are specified as parabolic functions depending on the asymmetric electron transfer coordinate x with the minimum of the ground state located at $x = 0$ and the minima of the degenerate excited states at $x = -0.5$ and $x = 0.5$, respectively. In principle, a symmetric coordinate would also be required for a reasonable description of the potential energy surfaces, but because the necessary experimental or computational information is lacking, the simplest one-dimensional model was used in this case. The two degenerate excited states are shifted in energy by ΔG^0 versus the ground state. The electronic couplings which are a measure for the interactions between the diabatic ground

and the two excited states are neglected for simplicity ($V = 0$) and only the interactions between the excited MV states are taken into account.

As the diabatic excited states of the "dimers" 1^{2+}, 4^{2+}, 5^{2+}, 6^{2+} and 9^{2+} have mixed-valence character, an increase of the solvent polarity leads to an increase of the solvent reorganization energy and, consequently, to an increase of the transition energy i.e. to a blue shift as shown in Figure 3. The negative solvatochromism of $2^{•+}$, $3^{•+}$, $7^{•+}$, and $8^{•+}$ can be explained analogously.
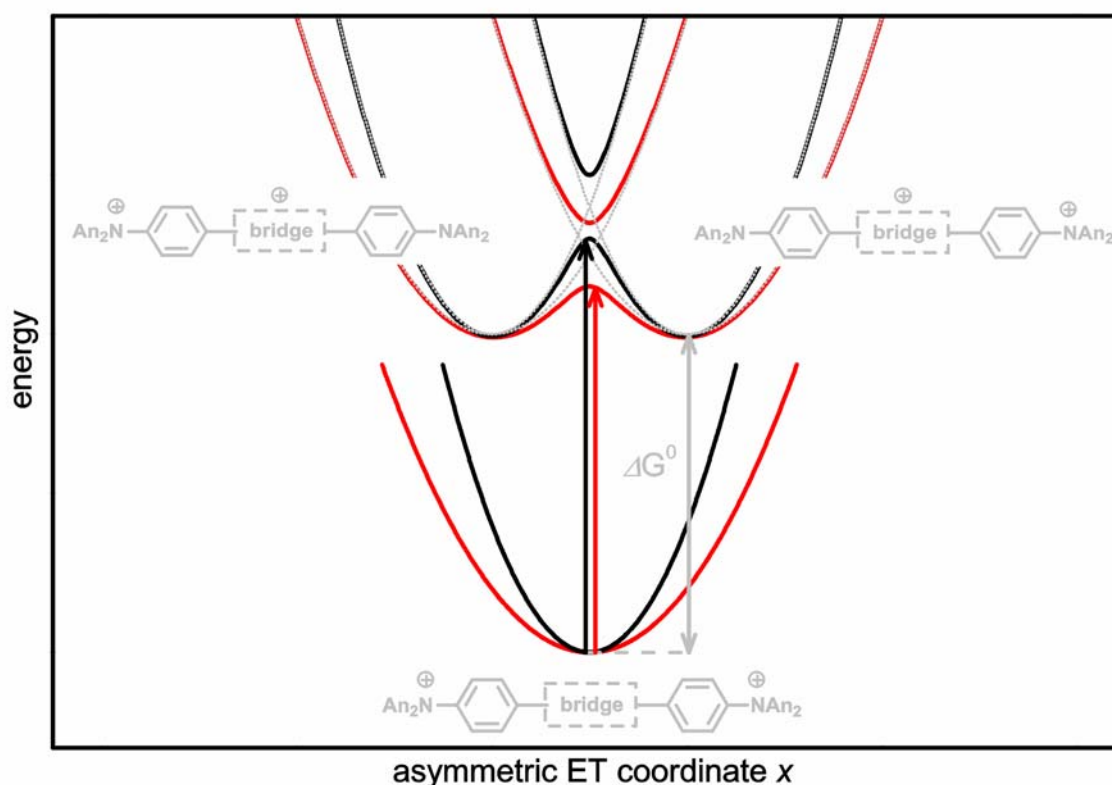
Figure 3. Adiabatic (solid) and diabatic (grey and dotted) potential energy surfaces of the "dimeric" dications with differing reorganization energies (red: small for, e.g., CH_2Cl_2; black: large for MeCN). One fixed set of parameters V_{23} and ΔG^0 was used to calculate the potential energy surfaces.

For the interpretation of the linear optical properties of the bis-triarylamines, a simple exciton coupling model[74-78] can be used. Two "monomeric" subunits, e.g. $8^{•+}$, with the z-polarized CT_{bridge} state (2) and the x-polarized π-π^* state (3) are combined with an 180° angle to yield the C_i symmetric *pseudo-para* isomer 4^{2+} and, with an 60° angle, to form the C_2 symmetric *pseudo-ortho* isomer 5^{2+} (Figure 4).
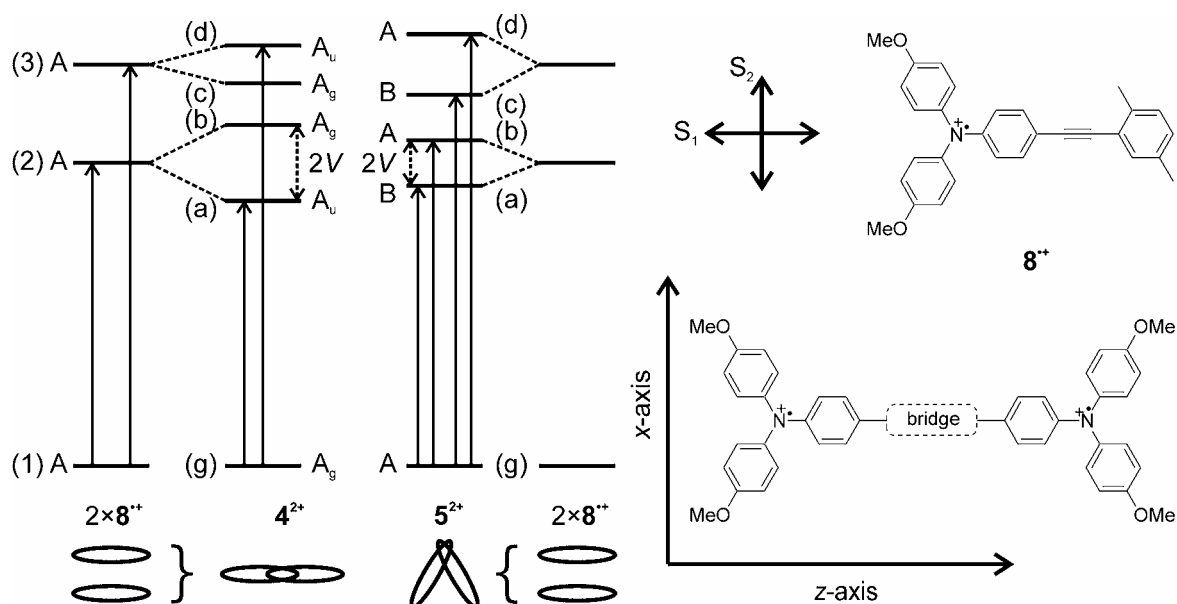
Figure 4. Exciton energy diagrams for molecular dimers 4^{2+} and 5^{2+}.

Within the point-dipole approximation exciton coupling theory, yields eq 2 for the coupling integral V. This model uses the transition moments $\mu_{12}^{(m1)}$ and $\mu_{12}^{(m2)}$ from the ground state (1) to the CT$_{bridge}$ state (2) of the two monomeric subunits (m1) and (m2), the distance $r_{m1, m2}$ of the centers of the two point-dipole transition moment vectors in the dimer, the angle between the two transition moment vectors α and the two angles $\theta^{(m1)}$ and $\theta^{(m2)}$ between each transition moment vector and $\vec{r}_{m1, m2}$.

$$V = \frac{\mu_{12}^{(m1)} \cdot \mu_{12}^{(m2)}}{r_{m1, m2}^{3}} (\cos\alpha - 3\cos\theta^{(m1)} \cdot \cos\theta^{(m2)}) \qquad (2)$$

Coupling of two monomer excited states (2) results in two excited states (a) and (b) (see Figure 4) of the dimer with a splitting energy of $2\,V$. Thus, if ground state interactions are neglected, the coupling can in principle be obtained directly from the absorption spectra, since V equals the difference of the transition energies of the monomer and the dimer.[79] The trigonometric correlation of eq 2 was used as an estimate for the relative couplings in Figure 4. An explicit calculation of couplings V by eq 2 was not done, since r has a great influence on the calculated result, but it can not be determined exactly. The transition moments of the ground state excitation of the dimer $\mu_{ga}^{(d)}$ to the first excited state (a) and $\mu_{gb}^{(d)}$ to the second

excited state (b) can be calculated from the transition moment of the monomers $\mu_{12}^{(m1)}$ or $\mu_{12}^{(m2)}$ by the following eq 3 and eq 4.[80]

$$\mu_{ga}^{(d)} = \sqrt{2}\mu_{12}^{(m1)} \cos\theta^{(m1)} = \sqrt{2}\mu_{12}^{(m2)} \cos\theta^{(m2)} \qquad (3)$$

$$\mu_{gb}^{(d)} = \sqrt{2}\mu_{12}^{(m1)} \sin\theta^{(m1)} = \sqrt{2}\mu_{12}^{(m2)} \sin\theta^{(m2)} \qquad (4)$$

These two relations can also be applied to calculate the transition moments $\mu_{gc}^{(d)}$ and $\mu_{gd}^{(d)}$ of the higher lying two excited states of the dimer (c) (compare eq 3) and (d) (compare eq 4) starting from the transition moment of the second excited state (3) of the monomers $\mu_{13}^{(m1)}$ or $\mu_{13}^{(m2)}$.

For C_i symmetric dications such as $\mathbf{4^{2+}}$, the linear combination of the z-polarized transition moments $\mu_{12}^{(m1)}$ and $\mu_{12}^{(m2)}$ of $\mathbf{8^{\bullet+}}$ results in only one allowed transition to state (a) of the dimer with a transition moment $\mu_{ga}^{(d)} = \sqrt{2}\mu_{12}^{(m1)}$ derived by eq 3. According to eq 4, the transition moment $\mu_{gb}^{(d)}$ of the second excited state (b) of the dimer vanishes and, thus, the second excitation is forbidden. The coupling of the π-π^* states (3) of two monomeric subunits with $\mu_{13}^{(m1)}$ and $\mu_{13}^{(m2)}$ again results in one allowed transition to state (d) of the dimer with $\mu_{gd}^{(d)} = \sqrt{2}\mu_{13}^{(m1)}$ and one forbidden transition to state (c) of the dimer, because the transition moment $\mu_{gc}^{(d)}$ also vanishes. Thus, for the linear dications the exciton coupling model predicts two allowed transitions, one to the stabilized excited CT_{bridge} state (a) and a second to the destabilized excited π-π^* state (d). Both states (a) and (d) have A_u symmetry. The two transitions to the excited states (c) and (b) with A_g symmetry are forbidden. Consequently, a red shift of the CT_{bridge} excitation and a small blue shift of the localized π-π^* transition is predicted by the model.[79] The latter shift is smaller, because of the weaker coupling of the x-polarized transition. Both predictions are fulfilled in the experimental spectra as demonstrated by the shifts of the bridge band ($\mathbf{4^{2+}}$: -600 cm^{-1} and $\mathbf{6^{2+}}$: -630 cm^{-1}) and π-π^* band ($\mathbf{4^{2+}}$: +250 cm^{-1} and $\mathbf{6^{2+}}$: +110 cm^{-1}) of $\mathbf{4^{2+}}$ and $\mathbf{6^{2+}}$ compared to the absorption signals of $\mathbf{8^{\bullet+}}$.

In principle, a similar model can be used to explain the differences in the spectra of the paracyclophane $\mathbf{1^{2+}}$ and the molecular half $\mathbf{3^{\bullet+}}$. As already mentioned, the "monomeric" fragment $\mathbf{3^{\bullet+}}$ shows a reversed order of the π-π^* state (2) and the CT_{bridge} state (3) in

comparison to $\mathbf{1^{2+}}$. In fact, what was obtained experimentally is a distinct red shift of the bridge band (4200 cm^{-1}) and a small red shift of the π-π* band (170 cm^{-1}) of the bis-triarylamine $\mathbf{1^{2+}}$compared to the molecular half $\mathbf{3^{\bullet+}}$. The shift of the bridge band is unexpectedly large, while the spectra of $\mathbf{1^{2+}}$ and $\mathbf{2^{\bullet+}}$ with identical bridges are very similar. Therefore, it is supposed that $\mathbf{3^{\bullet+}}$ can not reasonably be used as a "monomeric" subunit for the exciton coupling model. In a recent study, it was demonstrated that the sterical hindrance of *ortho* and *meta* methyl groups may have a distinct influence on the optical properties of biaryls.[81] The [2.2]paracyclophane moiety of $\mathbf{1^{2+}}$ and the *p*-xylene bridge of $\mathbf{3^{\bullet+}}$ exhibit different sterical influence and induce different torsion angles around the biaryl axes. Thus, it is assumed that the pronounced shift of the CT$_{bridge}$ band of $\mathbf{3^{\bullet+}}$ versus $\mathbf{1^{2+}}$ can be traced back to the different torsional angles and, consequently, to a different extent of π-conjugation in the [2.2]paracyclophane and the *p*-xylene bridges.

The coupling of the bridge states (2) with the corresponding transition moment vectors $\mu_{12}^{(m1)}$ and $\mu_{12}^{(m2)}$ of two monomers $\mathbf{8^{\bullet+}}$ to the kinked C$_2$ symmetric dimer $\mathbf{5^{2+}}$ results according to eq 3 and eq 4 in two allowed transitions to the states (a) and (b) of the dimer. The stabilized bridge state (a) of the dimer has B symmetry, while the destabilized bridge state (b) possess A symmetry. The corresponding exciton coupling of π-π* states (3) of $\mathbf{8^{\bullet+}}$ also yields two allowed transitions to the π-π* states (c) and (d) of the dimer $\mathbf{5^{2+}}$. Here, the stabilized state (c) has B symmtery, while the destabilized state (d) is A symmetric. The splitting energy 2 V of the CT$_{bridge}$ transition is expected to be slightly smaller compared to the splitting of the CT$_{bridge}$ state of $\mathbf{4^{2+}}$, but the splitting energy of the π-π* transition should be somewhat larger than the splitting of the π-π* states of $\mathbf{4^{2+}}$ due to the 60° orientation of the chromophores (see eq 2).[82] For symmetry reasons, the resulting transition moments of the A$\rightarrow$A excitations are polarized along the C$_2$ axis and the transition moments of A$\rightarrow$B excitations are perpendicularly polarized to the symmetry axis. This model predicts only little influence on the transition energies, but a broadening of both absorption signals in the spectrum of the V-shaped paracyclophane $\mathbf{5^{2+}}$ compared to the molecular half $\mathbf{8^{\bullet+}}$. In fact, experimentally, a small red shift of the CT$_{bridge}$ band (-240 cm^{-1}) and a small blue shift of the π-π* band (+210 cm^{-1}) is obtained, while a broadening is not recognized.

2.3 Semiempirical calculation

Mopac AM1-CISD calculations were performed for all radical cations and diradical dications.[83] The resulting transition energies, transition moments and the character of the transitions are collected in Table 2.

Table 2. AM1-CISD computed absorption energies and transition moments (using the active orbital window with the specified MOPAC keywords "c.i." and "open").

	c.i. open	sym.	$\tilde{\nu}$ / cm⁻¹	$\tilde{\nu}_{exp}$ / cm⁻¹	μ_{exp} / D	μ / D	assignment
1²⁺	(11,7) (2,2)	A_u	20160	11300	5.6	7.6	CT_{bridge}
		A_g	20400	-	-	-	CT_{bridge}
		A_g	20160	-	-	-	π-π*
		A_u	14100	13090	7.8	11.8	π-π*
2·⁺	(8,5) -	A	14390	11500	4.1	6.7	CT_{bridge}
		A	15740	13400	5.1	7.7	π-π*
3·⁺	(8,5) -	A	14590	15500	3.4	7.4	CT_{bridge}
		A	14460	13260	5.3	6.6	π-π*
4²⁺	(11,7) (2,2)	A_u	16100	10900	7.4	9.0	CT_{bridge}
		A_g	16190	-	-	-	CT_{bridge}
		A_g	14490	-	-	-	π-π*
		A_u	14540	13300	8.4	12.7	π-π*
5²⁺	(11,7) (2,2)	B	15370	11260	5.9	6.5	CT_{bridge}
		A	15600			8.8	CT_{bridge}
		B	14620	13260	7.7	12.2	π-π*
		A	14490			2.6	π-π*
6²⁺	(11,7) (2,2)	A_u	16140	10870	7.3	9.7	CT_{bridge}
		A_g	15270	-	-	-	CT_{bridge}
		A_g	14430	-	-	-	π-π*
		A_u	14520	13160	7.9	12.8	π-π*
7·⁺	(8,5)	A	12960	10680	4.8	12.3	CT_{bridge}
		A	14970	13440	5.7	6.6	π-π*
8·⁺	(8,5)	A	11780	11500	3.7	10.8	CT_{bridge}
		A	15500	13050	5.8	5.9	π-π*
9²⁺	(11,7) (2,2)	A_u	17740	11100	6.2	7.9	CT_{bridge}
		A_g	17720	-	-	-	CT_{bridge}
		A_g	14360	-	-	-	π-π*
		A_u	14390	13000	8.3	12.8	π-π*

The geometry optimizations of the mono radical cations were performed at CISD level. All dications were described as diradicals and not as the closed shell quinoide like systems, since the optimization with solely doubly filled levels yielded somewhat larger heat of formations than the optimization as diradicals with two singly occupied levels. The computations generally yield two symmetrically allowed transitions in the Vis/NIR region. One transition is polarized along the (CT_{bridge}) z-axis and the second along the x-axis (π-π*). The calculation of

the C_2 symmetric $\mathbf{5^{2+}}$ yields four allowed transitions with transition moments directed along the C_2 axis for A→A excitations and perpendicular to the C_2 axis for A→B excitations.

The energy of the localized π-π^* transition of the diradical dications is generally described well, while the energy of the bridge band is much larger than the experimental values. The corresponding computed transition moments of the π-π^* band are much larger than the experimental values. Except for $\mathbf{5^{2+}}$, the transition moments of the bridge band of the dications are in good agreement with the experimental values.

The calculated transition energies of the mono radical cations are generally too large compared with the experimental values. Here the calculated transition moments of the π-π^* excitation fits well with the values obtained from the experiment, but the transition moments of the bridge band are estimated too large in comparison to the experimental values.

2.4   Application of GMH Theory

The coupled CT_{bridge} states (a) (A_u or B symmetry) and (b) (A_g or A symmetry) of the bis-triaryalmine diradical dications can be conceived as excited mixed-valence (MV) states (see Figure 5).
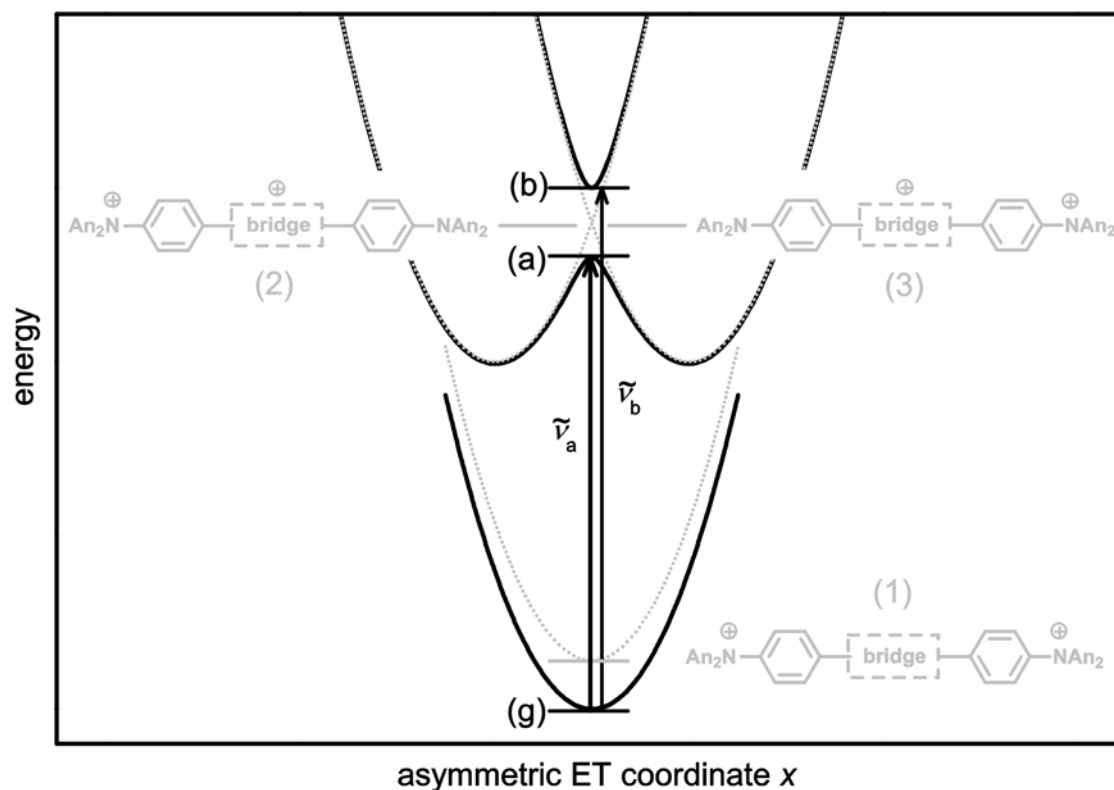
Figure 5. Adiabatic (solid) potential energy surfaces of ground state (g) and MV excited CT_{bridge} states (a) and (b) as well as diabatic (grey and dotted) potential energy surfaces (1) – (3) of bis-triarylamine diradical dications.

The difference between the absorption energies of the molecular halves and the corresponding "dimers" is only a rough estimate for the coupling between the first and the second excited CT_{bridge} state. The exciton coupling model used is a simple two-state model which neglects interactions with the ground state. Therefore, a GMH three-level model[84] was applied to estimate the electronic couplings using experimental and computational data. This model was used previously to analyze a valence delocalized bis-triarylamine radical cation MV system.[36] Here the GMH comprises the following adiabatic (observable) states: the

electronic ground state (g) and the two CT_{bridge} *Franck-Condon* states (a) and (b) as shown in Figure 5 (black bars).

The transition moments between the three levels (g), (a) and (b) as well as the dipole moments of these three states constitute the adiabatic transition moment matrix (eq 5). Before the elements of this matrix are explained, it should be mentioned that according to *Newton et al.*[68-70] the projections of the transition moment vectors and the dipole moment vectors on an arbitrary axis have to be used for the GMH analysis. Here the axis that connects the two nitrogen redox centers was used and, therefore, the adiabatic transition moment matrix consists of the components of the transition moment vectors as well as the components of the dipole moment vectors directed along this chosen axis. Thus, only the transition moment μ_{ga} between the ground state (g) and the first excited CT_{bridge} state (a) and the transition moment μ_{ab} between both excited CT_{bridge} states (a) and (b) differ from zero for symmetry reasons. For the C_i symmetric species the transition moment between the ground state (g) and the second excited CT_{bridge} state (b) μ_{gb} is zero, because the excitation is symmetry forbidden ($A_g \rightarrow A_g$). The transition moment vector component μ_{gb} along the N-N axis also vanishes for the C_2 symmetric molecule $\mathbf{5^{2+}}$ since A$\rightarrow$A transitions are polarized along the C_2 axis which is perpendicular to the N-N axis. The diagonal elements of the adiabatic transition moment matrix represent the dipole moment μ_{gg} of the ground state (g), the dipole moment μ_{aa} of state (a) and the dipole moment μ_{bb} of state (b). These moments are all zero for C_i symmetric molecules and they are directed along the C_2 axis for a C_2 symmetric molecule and, therefore, the dipole moment projection on the N-N axis vanishes.

$$\mu_{adiab} = \begin{pmatrix} 0 & \mu_{ga} & 0 \\ \mu_{ga} & 0 & \mu_{ab} \\ 0 & \mu_{ab} & 0 \end{pmatrix} \qquad (5)$$

$$\mu_{diab} = \begin{pmatrix} 0 & 0 & 0 \\ 0 & \mu_{22} & 0 \\ 0 & 0 & \mu_{33} = -\mu_{22} \end{pmatrix} \qquad (6)$$

Within GMH theory, strictly localized diabatic (model) levels (1)-(3) (see gray bars and structures in Figure 5) are defined with the consequence that all off-diagonal elements of the

diabatic transition moment matrix $\boldsymbol{\mu}_{\text{diab}}$ (eq 6) become zero.[68-70] The GMH theory uses a unitary transformation of the adiabatic transition moment matrix into the corresponding diabatic matrix according to $\boldsymbol{\mu}_{\text{diab}} = \mathbf{C}^{\mathbf{t}}\boldsymbol{\mu}_{\text{adiab}}\mathbf{C}$. This diagonalization is done by applying the matrix $\mathbf{C}$ which consists of the normalized eigenvectors of $\boldsymbol{\mu}_{\text{adiab}}$. The same unitary transformation with identical matrix $\mathbf{C}$ is then applied to the adiabatic energy matrix $\mathbf{H}_{\text{diab}} = \mathbf{C}^{\mathbf{t}}\mathbf{H}_{\text{adiab}}\mathbf{C}$. This adiabatic energy matrix (eq 7) consists of adiabatic energy differences between the ground and the first excited state $\tilde{\nu}_{\text{a}}$ as well as the ground and the second excited state $\tilde{\nu}_{\text{b}}$. If the electronic couplings are small, it can be approximated $\tilde{\nu}_{\text{a}} \approx \tilde{\nu}_{\text{b}}$.[84] This approximation has to be done, because $\tilde{\nu}_{\text{b}}$ can neither be measure, nor can it be computed accurately enough.

$$\mathbf{H}_{\text{adiab}} = \begin{pmatrix} 0 & 0 & 0 \\ 0 & \tilde{\nu}_{\text{a}} & 0 \\ 0 & 0 & \tilde{\nu}_{\text{b}} = \tilde{\nu}_{\text{a}} \end{pmatrix} \qquad (7)$$

The resulting diabatic energy matrix (eq 8) includes the energies of the diabatic states (1)-(3) as the diagonal elements H_{11}, H_{22} and H_{33} and, in addition, the electronic couplings V_{12}, V_{13} and V_{23} as the off-diagonal elements. The coupling V_{23} between the degenerate states (2) and (3) is a direct measure for the electronic interaction between these two diabatic states.[85]

$$\mathbf{H}_{\text{diab}} = \begin{pmatrix} H_{11} & V_{12} & V_{13} \\ V_{12} & H_{22} & V_{23} \\ V_{13} & V_{23} & H_{33} \end{pmatrix} \qquad (8)$$

The GMH analysis was performed for the compounds $\mathbf{1^{2+}}$, $\mathbf{4^{2+}}$, $\mathbf{5^{2+}}$, $\mathbf{6^{2+}}$ and $\mathbf{9^{2+}}$ using the available experimental transition energies $\tilde{\nu}_{\text{a}}$(exp.) and transition moments μ_{ga}(exp.) and AM1-CISD computational values for the missing data μ_{ab}(calc.) to estimate the coupling $V_{23}^{(\text{d})}$. The transition moment μ_{ga}(exp.) of $\mathbf{5^{2+}}$ was estimated as one half of the transition moment obtained from spectrum deconvolution (see experimental section), since the two CT_{bridge} transitions to (a) and (b) which are expected can not be analyzed separately due to strong

overlap of these signals. The input values and the GMH results of all bis-triarylamine diradical dications are given in Table 3.

Table 3. Input for GMH analysis μ_{ga}(exp.), μ_{ab}(calc.) and $\tilde{\nu}_a$ (exp.) and resulting GMH coupling values V_{23} of excited MV compounds $\mathbf{1^{2+}}$, $\mathbf{4^{2+}}$, $\mathbf{5^{2+}}$, $\mathbf{6^{2+}}$ and $\mathbf{9^{2+}}$.

	μ_{ga}(exp.) / D	$\Delta\mu_{12}^{(ma)}$ (calc.)^a / D	$\Delta\mu_{12}^{(mb)}$ (calc.)^b / D	μ_{ab}(calc.) / D	$\tilde{\nu}_a$ (exp.) / cm^{-1}	$V_{23}^{(d)\,c}$ / cm^{-1}	$V_{23}^{(m)\,d}$ / cm^{-1}
$\mathbf{1^{2+}}$	5.6	10.4 ($\mathbf{3^{•+}}$)	27.1 ($\mathbf{2^{•+}}$)	22.2	11300	340	460
$\mathbf{4^{2+}}$	7.4	11.0 ($\mathbf{8^{•+}}$)	26.5 ($\mathbf{7^{•+}}$)	23.5	10900	490	790
$\mathbf{5^{2+}}$	3.0	6.5 ($\mathbf{8^{•+}}$)^e	13.3 ($\mathbf{7^{•+}}$)^e	16.1	11260	200	550
$\mathbf{6^{2+}}$	7.3	11.0 ($\mathbf{8^{•+}}$)	-	16.4	10870	900	3320
$\mathbf{9^{2+}}$	6.2	21.7 ($\mathbf{11^{•+}}$)	28.2 ($\mathbf{10^{•+}}$)	33.1	11100	190	510

^{a} *p*-xylenes as monomers. ^{b} cyclophanes as monomers. ^{c} calculated with μ_{ab}(calc.). ^{d} calculated from $\Delta\mu_{12}^{(ma)}$ for $\mathbf{6^{2+}}$ and from $\Delta\mu_{12}^{(mb)}$ for the remaining dications. ^{e} projection on the N-N axis of the corresponding dimer $\mathbf{5^{2+}}$ calculated by multiplication of the dipole moment difference with cos 60° = 0.5.

The bis-butadiyne $\mathbf{9^{2+}}$ with the longest N-N distance shows the smallest coupling $V_{23}^{(d)} = 190$ cm^{-1} and the acetylene $\mathbf{4^{2+}}$ shows a medium coupling $V_{23}^{(d)} = 490$ cm^{-1}, while the conjugated *p*-xylyl derivative $\mathbf{6^{2+}}$ has the largest coupling $V_{23}^{(d)} = 900$ cm^{-1}. Thus, the GMH couplings $V_{23}^{(d)}$ of the "linear" *para*- and *pseudo-para* compounds are large for small bridges and, especially, for molecules with direct π-conjugation between the redox centers ($\mathbf{6^{2+}}$). Compound $\mathbf{1^{2+}}$ is an exception from this general trend, because the coupling $V_{23}^{(d)} = 340$ cm^{-1} is smaller than the coupling of acetylene $\mathbf{4^{2+}}$ although the AM1 calculated N-N distance (15.2 Å) of $\mathbf{1^{2+}}$ is significantly smaller compared to that of $\mathbf{4^{2+}}$ (20.1 Å). It is supposed, that this is a consequence of the steric hindrance which results in larger torsion angle around the biaryl axes (AM1 computed: 59° of $\mathbf{1^{2+}}$ and 46° of $\mathbf{3^{•+}}$) and, therefore, in weaker interactions of the π-systems. The kinked *pseudo-ortho* isomer $\mathbf{5^{2+}}$ shows a coupling $V_{23}^{(d)} = 200$ cm^{-1} which is much smaller in comparison to that of the linear *pseudo-para* isomer $\mathbf{4^{2+}}$ owing to the 60° orientation of the chromophores.

After having performed the GMH analysis of the excited MV states, now a new definition of the diabatic states will be used in the GMH in order to demonstrate the similarities between GMH theory and exciton coupling theory. In contrast to the assumption that the diabatic states

are strictly localized, *Kryachko* introduced a modified GMH model which allows non-zero off-diagonal elements of the diabatic transition moment matrix.[86] Instead of diagonalizing the adiabatic matrices to yield the diabatic matrices, *Kryachko* generated the diabatic states by rotating the adiabatic states. This means that a *Jacobi* transformation of the adiabatic matrices yields the corresponding diabatic matrices (see eqs 9-11).

$$
\mathbf{J}_{ga} = \begin{pmatrix} \cos\alpha & \sin\alpha & 0 \\ -\sin\alpha & \cos\alpha & 0 \\ 0 & 0 & 1 \end{pmatrix} \quad
\mathbf{J}_{gb} = \begin{pmatrix} \cos\beta & 0 & \sin\beta \\ 0 & 1 & 0 \\ -\sin\beta & 0 & \cos\beta \end{pmatrix} \quad
\mathbf{J}_{ab} = \begin{pmatrix} 1 & 0 & 0 \\ 0 & \cos\gamma & \sin\gamma \\ 0 & -\sin\gamma & \cos\gamma \end{pmatrix} \quad (9)
$$

$$
\boldsymbol{\mu}_{diab} = \mathbf{J}_{ab}^t \mathbf{J}_{gb}^t \mathbf{J}_{ga}^t \boldsymbol{\mu}_{adiab} \mathbf{J}_{ga} \mathbf{J}_{gb} \mathbf{J}_{ab} \qquad (10)
$$

$$
\mathbf{H}_{diab} = \mathbf{J}_{ab}^t \mathbf{J}_{gb}^t \mathbf{J}_{ga}^t \mathbf{H}_{adiab} \mathbf{J}_{ga} \mathbf{J}_{gb} \mathbf{J}_{ab} \qquad (11)
$$

In the following, the adiabatic GMH labels will be kept rather than the labels introduced for the exciton coupling model. In order to find the analogies between GMH theory and exciton coupling theory, one has to remember that the exciton coupling model starts off with two monomeric subunits. The transition moments of these two subunits can be derived from the transition moment of the dimer by transposed eqs 3 and 4. Accordingly, the transition moments of the two monomers is $\mu_{12}^{(m)} = \mu_{ga}/\sqrt{2}$. A *Jacobi* transformation of the adiabatic transition moment matrix (5) by using the mixing angles $\alpha = 0$, $\beta = 0$ and $\gamma = 45°$ yields newly defined diabatic states with the corresponding transition moment matrix (12) (see Scheme 1). This matrix reveals that this GMH model yields transition moments that have the same value as the transition moments evaluated for the exciton coupled monomers $\mu_{12}^{(m)}$. Thus, on the one hand, matrix (12) can be conceived as the combination of the transition moments and dipole moments μ_{ab} of two monomeric subunits of the exciton coupling model and, on the other hand, as being derived from two coupled two-level systems[36]. An additional outcome of this modified GMH model, is that the transition moments μ_{ab} connecting the two excited states (a) and (b) of the dimer equals the adiabatic dipole moment difference $\Delta\mu_{12}^{(m)} = \mu_{11}^{(m)} - \mu_{22}^{(m)}$ between the ground state (1) and the CT$_{bridge}$ excited state (2) of the monomer. This dipole moment difference could in principle be determined experimentally or computationally more accurately than the transition moment μ_{ag} of the dimer.

Scheme 1.

$$\mu_{\text{adiab}} = \begin{pmatrix} 0 & \mu_{\text{ga}} & 0 \\ \mu_{\text{ga}} & 0 & \mu_{\text{ab}} \\ 0 & \mu_{\text{ab}} & 0 \end{pmatrix} \xrightarrow[\text{exciton coupling}]{45° \text{ rotation}} \mu_{\text{diab}} = \begin{pmatrix} 0 & \dfrac{\mu_{\text{ga}}}{\sqrt{2}} & \dfrac{\mu_{\text{ga}}}{\sqrt{2}} \\ \dfrac{\mu_{\text{ga}}}{\sqrt{2}} & -\mu_{\text{ab}} & 0 \\ \dfrac{\mu_{\text{ga}}}{\sqrt{2}} & 0 & \mu_{\text{ab}} \end{pmatrix}$$

(5)   (12)

$$\mathbf{H}_{\text{adiab}} = \begin{pmatrix} 0 & 0 & 0 \\ 0 & \tilde{\nu}_{\text{a}} & 0 \\ 0 & 0 & \tilde{\nu}_{\text{b}} \end{pmatrix} \xrightarrow[\text{exciton coupling}]{45° \text{ rotation}} \mathbf{H}_{\text{diab}} = \begin{pmatrix} 0 & 0 & 0 \\ 0 & \dfrac{\tilde{\nu}_{\text{a}} + \tilde{\nu}_{\text{b}}}{2} & \dfrac{\tilde{\nu}_{\text{a}} - \tilde{\nu}_{\text{b}}}{2} \\ 0 & \dfrac{\tilde{\nu}_{\text{a}} - \tilde{\nu}_{\text{b}}}{2} & \dfrac{\tilde{\nu}_{\text{a}} + \tilde{\nu}_{\text{b}}}{2} \end{pmatrix}$$

(7)   (13)

The 45° rotation is equivalent to a block diagonalization of matrix (5).[87] If now the 45° rotation is applied to the adiabatic energy matrix, the corresponding diabatic energy matrix (13) is obtained (Scheme 1). This matrix consists of the energies of the diabatic states as the diagonal elements and of the electronic couplings as the off-diagonal elements. As shown in Scheme 1, this matrix (13) exhibits no coupling between the ground and the excited states, but only a coupling between the two excited states. The energy of the diabatic states equals the midpoint between the two transition energies $\tilde{\nu}_{\text{a}}$ and $\tilde{\nu}_{\text{b}}$ of the dimer. The result of the *Jacobian* transformation of the adiabatic energy matrix (7) is equivalent to a two-level model where only the interactions between the two excited states are taken into account. Again, this is equivalent to the exciton coupling model where the exciton splitting energy equals twice the exciton coupling energy.

In order to proof the finding that μ_{ab} of the dimer equals the adiabatic dipole moment difference $\Delta\mu_{12}^{(\text{m})}$ of the monomer, further AM1-CISD calculations were performed to compare the dipole moment differences of the monomers with the calculated transition moments μ_{ab} of the corresponding dimers. The differences $\Delta\mu_{12}^{(\text{ma})}$ of the *p*-xylene derivatives **3·+**, **8·+** and **11·+** as well as the differences $\Delta\mu_{12}^{(\text{mb})}$ of the [2.2]paracyclophanes **2·+**, **7·+** and **10·+**

are given in Table 3. The compounds $10^{\bullet+}$ and $11^{\bullet+}$ (see Chart 2) -which have not been synthesized- are the two corresponding monomers of 9^{2+}.

Chart 2.

10   **11**
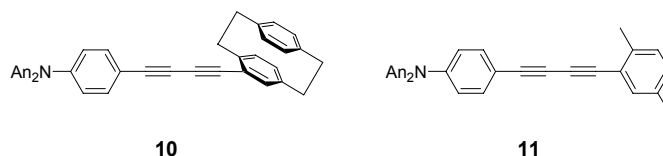
For the [2.2]paracyclophanes 1^{2+}, 4^{2+}, 5^{2+} and 9^{2+} the calculated dipole moment difference $\Delta\mu_{12}^{(ma)}$ of the corresponding *p*-xylene derivatives $3^{\bullet+}$, $8^{\bullet+}$ and $11^{\bullet+}$ is significantly smaller than the transition moment μ_{ab} while smaller deviation of $\Delta\mu_{12}^{(ma)}$ and μ_{ab} are found for the *p*-xylene 6^{2+}. Since the [2.2]paracyclophane moiety is a stronger donor than the *p*-xylene moiety, all $\Delta\mu_{12}^{(mb)}$ values are significantly larger than $\Delta\mu_{12}^{(ma)}$. The differences $\Delta\mu_{12}^{(mb)}$ of the [2.2]paracyclophanes $2^{\bullet+}$, $7^{\bullet+}$ and $10^{\bullet+}$ are in good agreement with the corresponding transition moments μ_{ab} of 1^{2+}, 4^{2+}, 5^{2+} and 9^{2+}. Thus, this comparison indicates that the [2.2]paracyclophane monomers $2^{\bullet+}$, $7^{\bullet+}$ and $10^{\bullet+}$ are more suitable monomeric building blocks for the corresponding dications 1^{2+}, 4^{2+}, 5^{2+} and 9^{2+}, while 6^{2+} can be traced back to the *p*-xylene monomer $8^{\bullet+}$.

The dipole moment differences $\Delta\mu_{12}^{(ma)}$ and $\Delta\mu_{12}^{(mb)}$ of the adequate monomers were used instead of μ_{ab} of the GMH analysis according to eqs 5 to 7. The resulting couplings $V_{23}^{(m)}$ are given in Table 3. These couplings are all larger than the couplings $V_{23}^{(d)}$, in particular for 6^{2+}, where $V_{23}^{(m)}$ is more than three times larger than $V_{23}^{(d)}$. These deviations reveal that the GMH analysis shows a pronounced dependence on the transition moment μ_{ag} or $\mu_{12}^{(m)}$, respectively. However, the trends of $V_{23}^{(m)}$ and $V_{23}^{(d)}$ are similar with the exception that the couplings $V_{23}^{(m)}$ of 5^{2+} and 9^{2+} are somewhat larger than $V_{23}^{(m)}$ of 1^{2+}.

As demonstrated above, the exciton coupling model is suitable for the interpretation of the energetic shifts of the absorption bands of 4^{2+} and 6^{2+} versus the corresponding absorption bands of *p*-xylene $8^{\bullet+}$. But as discussed in this section, the monomer $8^{\bullet+}$ is not a good model to fulfill the relation between $\Delta\mu_{12}^{(m)}$ of the monomer and μ_{ag} of the corresponding dimer 4^{2+}.

This relation demonstrates nicely that choosing the proper monomeric model compound is crucial for a correct analysis.

3   Conclusion

Although the differences in the Vis/NIR spectra of the [2.2]paracyclophanes $\mathbf{1^{2+}}$, $\mathbf{2^{\bullet+}}$, $\mathbf{4^{2+}}$, $\mathbf{5^{2+}}$, $\mathbf{7^{\bullet+}}$, $\mathbf{9^{2+}}$ and the *p*-xylene $\mathbf{6^{2+}}$ are small, the spectral features of the "dimers" $\mathbf{4^{2+}}$ and $\mathbf{6^{2+}}$ can be explained by exciton coupling of two "monomers" $\mathbf{8^{\bullet+}}$.

The combination of AM1-CISD computed transition moments connecting the two excited CT_{bridge} states μ_{ab}(calc.) with experimental transition moments μ_{ga}(exp.) and transition energies $\tilde{\nu}_a$ (exp.) allows to apply a GMH analysis. Within this GMH three-level model, the coupling $V_{23}^{(d)}$ between the first and the second excited state -which were described as mixed-valence states- were calculated. These couplings are a direct measure for the electronic interactions of the excited bridge states (a) and (b). The trends of the couplings $V_{23}^{(d)}$ are in reasonable agreement with the exciton coupling model. On the one hand, this coupling decreases with increasing bridge size as demonstrated for $\mathbf{4^{2+}}$ and $\mathbf{9^{2+}}$ and, on the other hand, the coupling significantly increases when the bridge reveals direct π-conjugation as in compound $\mathbf{6^{2+}}$. The 60° orientation of the chromophores in $\mathbf{5^{2+}}$ results in a distinct lowering of the coupling. Compound $\mathbf{1^{2+}}$ is an exception, since the value estimated by the GMH is smaller than that of $\mathbf{4^{2+}}$ although $\mathbf{1^{2+}}$ has the smallest bridge. This discrepancy can be explained by steric hindrance which results in larger torsion angles at the biaryl axes of $\mathbf{1^{2+}}$ (59°) and, therefore, in reduced interactions of the π-systems. This assumption also explains the unusually large experimental shift of the CT_{bridge} absorption energy $\tilde{\nu}_a$ of $\mathbf{1^{2+}}$ versus $\tilde{\nu}_a$ of its corresponding molecular half $\mathbf{3^{\bullet+}}$ (torsion angle 46°).

A modification to the diabatic states of the GMH theory was done by applying a *Jacobi* transformation to the adiabatic matrices. A 45° *Jacobi* rotation of the adiabatic matrices results in block diagonalized diabatic matrices. These two matrices (12) and (13) represent the starting point of the exciton coupling model, because their matrix elements consist of values which correspond to the monomeric subunits. The exciton coupling model starts off with the monomeric subunits, while the GMH starts with the dimer and, thus, the modified GMH can

be regarded as an inversion of exciton coupling and vice versa. An additional outcome of this modified GMH is that the transition moments μ_{ab} connecting the two excited states (a) and (b) of the dimer equals the adiabatic dipole moment difference $\Delta\mu_{12}^{(m)} = \mu_{11}^{(m)} - \mu_{22}^{(m)}$ between the ground state (1) and the CT_{bridge} excited state (2) of the monomer. This dipole moment difference was determined by semiempirical AM1-CISD computations. The comparison of the transition moments μ_{ab} with the dipole moment differences of the monomers $\Delta\mu_{12}^{(m)}$ leads to the conclusion that the adequate monomers for the [2.2]paracyclophanes $\mathbf{1^{2+}}$, $\mathbf{4^{2+}}$, $\mathbf{5^{2+}}$ and $\mathbf{9^{2+}}$ are the corresponding cyclophanes $\mathbf{2^{\bullet+}}$, $\mathbf{7^{\bullet+}}$ and $\mathbf{10^{\bullet+}}$ whereas the p-xylene $\mathbf{6^{2+}}$ can be related to the monomer $\mathbf{8^{\bullet+}}$. Although the exciton coupling is suitable for the interpretation of the shifts, the relation between $\Delta\mu_{12}^{(m)}$ and μ_{ab} shows the limits of the simple exciton coupling model. The dipole moment differences of the monomers $\Delta\mu_{12}^{(m)}$ were used for the GMH analysis to calculate $V_{23}^{(m)}$. These couplings $V_{23}^{(m)}$ are somewhat larger than $V_{23}^{(d)}$ but the trends of $V_{23}^{(m)}$ and $V_{23}^{(d)}$ are similar with the exception that $V_{23}^{(m)}$ of $\mathbf{1^{2+}}$ is smaller than $V_{23}^{(m)}$ of $\mathbf{5^{2+}}$ and $\mathbf{9^{2+}}$.

In conclusion, this study demonstrates a close similarity of exciton and GMH model. Since exciton coupling can be viewed as a coherent energy transfer process, a close analogy of charge transfer and energy transfer processes results.

4   Experimental Section

4.1   UV/Vis/NIR spectroscopy

The UV/Vis/NIR spectra of the radical cations and dications in MeCN were obtained by stepwise addition of 10^{-2}-10^{-3} M NOBF$_4$/MeCN via a microliter syringe to a solution of the compounds (3 to $7 \cdot 10^{-5}$ M). Because the oxidation process is rather slow using NOBF$_4$ in MeCN, one has to wait approximately 30 min before the spectrum after each addition could be recorded. The extinction coefficients obtained in MeCN are too small due to the slight instability of the radical cations under the conditions employed. The spectra in CH$_2$Cl$_2$ were obtained by dropwise addition of 10^{-2}-10^{-3} M SbCl$_5$/CH$_2$Cl$_2$ in the same way. The quick oxidation process in CH$_2$Cl$_2$ allows very short periods between the addition of oxidation agent and spectrum measurement. The Vis/NIR region of the absorption spectra recorded in CH$_2$Cl$_2$ were fitted by three *Gaussian* functions, while a single function was fitted to the CT$_{bridge}$ band two *Gaussian* functions were fitted to the π-π* absorption signal. For the radical cation **3**$^{\bullet+}$ in CH$_2$Cl$_2$ two functions were fitted to each absorption signal. Equation 14 was used to calculate the experimental transition moments from the integrals of the reduced (divided by $\widetilde{\nu}$) *Gaussian* functions.

$$\mu_{\mathrm{exp}} = \sqrt{\frac{3\,h\,c\,\varepsilon_0\,\ln 10}{2000\,\pi^2\,N} \cdot \frac{9\,n}{(n^2+2)^2} \cdot \int \frac{\varepsilon(\widetilde{\nu})}{\widetilde{\nu}}\,\mathrm{d}\widetilde{\nu}} \qquad (14)$$

4.2   AM1-CISD calculations

All calculation were carried out using the AM1 parameterization implemented in the MOPAC97 program.[83] The optimization of all bis-triarylamine diradical dications **1**$^{2+}$, **4**$^{2+}$, **6**$^{2+}$ and **9**$^{2+}$ were performed with symmetry restrictions (C$_2$ for **5**$^{2+}$ and C$_i$ for the remaining) by the BFGS method. The configuration interaction included singles and doubles excitations (CISD) within an active orbital window comprising the three highest doubly occupied, the two highest singly occupied and the two lowest unoccupied orbitals. The structures of the

mono-triarylamine radical cations $2^{\bullet+}$, $3^{\bullet+}$, $7^{\bullet+}$, $8^{\bullet+}$, $10^{\bullet+}$ and $11^{\bullet+}$. were optimized without symmetry restrictions in Cartesian coordinates by the BFGS method. Here the active orbital space consisted of the four highest doubly occupied, one singly occupied and the two lowest unoccupied orbitals. The *Pulay*'s procedure was used as the self consistent field (SCF) converger of all calculations. In order to improve the calculation results larger active orbitals windows have been used (see Table 2) and a single SCF cycle was computed. The values of c.i.(n,m) in Table 2 are specified as n the number of orbitals in the active space, m the number of doubly filled levels and the values of the open(n_1,n_2) keyword consists of n_1 as the number of electrons in n_2 levels. The used open(2,2) keyword adds two more electrons to the two lowest unoccupied levels of the active space defined by the c.i. keyword and, thus, the doubly charged bis-triarylamines are described as diradical dications. For the single SCF cycle of the radical cation $10^{\bullet+}$ a c.i.(9,6) and for $11^{\bullet+}$ a c.i.(8,5) was used.

5   References

(1)   Tang, C. W. *Appl. Phys. Lett.* **1986**, *48*, 183-185.

(2)   Tang, C. W.; van Slyke, S. A. *Appl. Phys. Lett.* **1987**, *51*, 913-915.

(3)   Borsenberger, P. M.; Weiss, D. S. *Organic Photoreceptors for Imaging Systems*; Marcel Dekker: New York, 1993.

(4)   Kolb, E. S.; Gaudiana, R. A.; Mehta, P. G. *Macromolecules* **1996**, *29*, 2359-2364.

(5)   Fujikawa, H.; Tokito, S.; Taga, Y. *Synth. Met.* **1997**, *91*, 161-162.

(6)   Thelakkat, M.; Fink, R.; Haubner, F.; Schmidt, H.-W. *Macromol. Symp.* **1998**, *125*, 157-164.

(7)   Giebeler, C.; Antoniadis, H.; Bradley, D. D. C.; Shirota, Y. *Appl. Phys. Lett.* **1998**, *72*, 2448-2450.

(8)   Redecker, M.; Bradley, D. D. C.; Inbasekaran, M.; Wu, W. W.; Woo, E. P. *Adv. Mater.* **1999**, *11*, 241-246.

(9)   Braig, T.; Müller, D. C.; Groß, M.; Meerholz, K.; Nuyken, O. *Macromol. Rapid Commun.* **2000**, *21*, 583-589.

(10)   Thelakkat, M. *Macromol. Mater. Eng.* **2002**, *287*, 442-461.

(11) Takeuchi, M.; Kobayashi, M.; Shishikawa, R.; Sakai, T.; Nakamura, H.; Konuma, H. *Jpn. Kokai Tokkyo Koho* **1986**.

(12) Kaeriyama, K.; Suda, M.; Sato, M.; Osawa, Y.; Ishikawa, M.; Kawai, M. *Jpn. Kokai Tokkyo Koho* **1988**.

(13) Moerner, W. E.; Silence, S. M. *Chem. Rev.* **1994**, *94*, 127-155.

(14) Nishikitani, Y.; Kobayashi, M.; Uchida, S.; Kubo, T. *Electrochim. Acta* **2001**, *46*, 2035-2040.

(15) Stolka, M.; Yanus, J. F.; Pai, D. M. *J. Phys. Chem.* **1984**, *88*, 4707.

(16) Bonvoisin, J.; Launay, J.-P.; Van der Auweraer, M.; De Schryver, F. C. *J. Phys. Chem.* **1994**, *98*, 5052-5057, **Erratum: 1996,** *100(45)*, 18006.

(17) Bonvoisin, J.; Launay, J.-P.; Verbouwe, W.; Van der Auweraer, M.; De Schryver, F. C. *J. Phys. Chem.* **1996**, *100*, 17079-17082.

(18) Stickley, K. R.; Blackstock, S. C. *Tetrahedron Lett.* **1995**, *36*, 1585-1588.

(19) Lambert, C.; Nöll, G. *Angew. Chem., Int. Ed.* **1998**, *37*, 2107-2110.

(20) Lambert, C.; Nöll, G.; Schmalzlin, E.; Meerholz, K.; Bräuchle, C. *Chem.-Eur. J.* **1998**, *4*, 2129-2135.

(21) Lambert, C.; Nöll, G. *J. Am. Chem. Soc.* **1999**, *121*, 8434-8442.

(22) Lambert, C.; Nöll, G.; Hampel, F. *J. Phys. Chem. A* **2001**, *105*, 7751-7758.

(23) Coropceanu, V.; Malagoli, M.; Andre, J. M.; Brédas, J.-L. *J. Chem. Phys.* **2001**, *115*, 10409-10416.

(24) Lambert, C.; Nöll, G. *Chem.-Eur. J.* **2002**, *8*, 3467-3477.

(25) Coropceanu, V.; Malagoli, M.; Andre, J. M.; Brédas, J.-L. *J. Am. Chem. Soc.* **2002**, *124*, 10519-10530.

(26) Lambert, C.; Nöll, G.; Schelter, J. *Nat. Mater.* **2002**, *1*, 69–73.

(27) Lambert, C.; Nöll, G. *J. Chem. Soc., Perkin Trans. 2* **2002**, 2039-2043.

(28) Nelsen, S. F.; Konradsson, A. E.; Weaver, M. N.; Telo, J. P. *J. Am. Chem. Soc.* **2003**, *125*, 12493-12501.

(29) Lambert, C.; Nöll, G.; Zabel, M.; Hampel, F.; Schmalzlin, E.; Bräuchle, C.; Meerholz, K. *Chem.-Eur. J.* **2003**, *9*, 4232-4239.

(30) Lambert, C. *ChemPhysChem* **2003**, *4*, 877-880.

(31) Coropceanu, V.; Lambert, C.; Nöll, G.; Brédas, J.-L. *Chem. Phys. Lett.* **2003**, *373*, 153-160.

(32) Yano, M.; Ishida, Y.; Aoyama, K.; Tatsumi, M.; Sato, K.; Shiomi, D.; Ichimura, A.; Takui, T. *Synth. Met.* **2003**, *137*, 1275-1276.

(33) Yano, M.; Aoyama, K.; Ishida, Y.; Tatsumi, M.; Sato, K.; Shiomi, D.; Takui, T. *Polyhedron* **2003**, *22*, 2003-2008.

(34) Jones, S. C.; Coropceanu, V.; Barlow, S.; Kinnibrugh, T.; Timofeeva, T.; Brédas, J. L.; Marder, S. R. *J. Am. Chem. Soc.* **2004**, *126*, 11782-11783.

(35) Coropceanu, V.; Gruhn, N. E.; Barlow, S.; Lambert, C.; Durivage, J. C.; Bill, T. G.; Nöll, G.; Marder, S. R.; Brédas, J.-L. *J. Am. Chem. Soc.* **2004**, *126*, 2727-2731.

(36) Lambert, C.; Amthor, S.; Schelter, J. *J. Phys. Chem. A* **2004**, *108*, 6474-6486.

(37) Szeghalmi, A. V.; Erdmann, M.; Engel, V.; Schmitt, M.; Amthor, S.; Kriegisch, V.; Nöll, G.; Stahl, R.; Lambert, C.; Leusser, D.; Stalke, D.; Zabel, M.; Popp, J. *J. Am. Chem. Soc.* **2004**, *126*, 7834-7845.

(38) Heckmann, A.; Lambert, C.; Goebel, M.; Wortmann, R. *Angew. Chem., Int. Ed.* **2004**, *43*, 5851-5856.

(39) Low, P. J.; Paterson, M. A. J.; Puschmann, H.; Goeta, A. E.; Howard, J. A. K.; Lambert, C.; Cherryman, J. C.; Tackley, D. R.; Leeming, S.; Brown, B. *Chem.-Eur. J.* **2004**, *10*, 83-91.

(40) Lambert, C.; Risko, C.; Coropceanu, V.; Schelter, J.; Amthor, S.; Gruhn, N. E.; Durivage, J.; Brédas, J.-L. *J. Am. Chem. Soc.* **2005**, *127*, 8508-8516.

(41) Barlow, S.; Risko, C.; Coropceanu, V.; Tucker, N. M.; Jones, S. C.; Levi, Z.; Khrustalev, V. N.; Antipin, M. Y.; Kinnibrugh, T. L.; Timofeeva, T.; Marder, S. R.; Brédas, J. L. *Chem. Commun.* **2005**, 764-766.

(42) Chiu, K. Y.; Su, T. H.; Huang, C. W.; Liou, G. S.; Cheng, S. H. *J. Electroanal. Chem.* **2005**, *578*, 283-287.

(43) Dümmler, S.; Roth, W.; Fischer, I.; Heckmann, A.; Lambert, C. *Chem. Phys. Lett.* **2005**, *408*, 264-268.

(44) Lockard, J. V.; Zink, J. I.; Trieber, D. A.; Konradsson, A. E.; Weaver, M. N.; Nelsen, S. F. *J. Phys. Chem. A* **2005**, *109*, 1205-1215.

(45) J. V. Lockard, J. I. Zink, A. E. Konradsson, M. N. Weaver, S. F. Nelsen, *J. Am. Chem. Soc.* **2003**, *125*, 13471-13480.

(46) Lambert, C.; Schelter, J.; Fiebig, T.; Mank, D.; Trifonov, A. *J. Am. Chem. Soc.* **2005**, *127*, 10600-10610.

(47) Hreha, R. D.; George, C. P.; Haldi, A.; Domercq, B.; Malagoli, M.; Barlow, S.; Brédas, J.-L.; Kippelen, B.; Marder, S. R. *Adv. Funct. Mater.* **2003**, *13*, 967-973.

(48) Albota, M.; Beljonne, D.; Brédas, J.-L.; Ehrlich, J. E.; Fu, J.-Y.; Heikal, A. A.; Hess, S. E.; Kogej, T.; Levin, M. D.; Marder, S. R.; McCord-Maughon; Dianne, P.; Joseph, W.; Rockel, H.; Rumi, M.; Subramaniam, G.; Webb, W. W.; Wu, X.-L.; Xu, C. *Science* **1998**, *281*, 1653-1656.

(49) Reinhardt, B. A.; Brott, L. L.; Clarson, S. J.; Dillard, A. G.; Bhatt, J. C.; Kannan, R.; Yuan, L. X.; He, G. S.; Prasad, P. N. *Chem. Mater.* **1998**, *10*, 1863-1874.

(50) Rumi, M.; Ehrlich, J. E.; Heikal, A. A.; Perry, J. W.; Barlow, S.; Hu, Z.; McCord-Maughon, D.; Parker, T. C.; Roeckel, H.; Thayumanavan, S.; Marder, S. R.; Beljonne, D.; Brédas, J.-L. *J. Am. Chem. Soc.* **2000**, *122*, 9500-9510.

(51) Chung, S. J.; Lin, T. C.; Kim, K. S.; He, G. S.; Swiatkiewicz, J.; Prasad, P. N.; Baker, G. A.; Bright, F. V. *Chem. Mater.* **2001**, *13*, 4071-4076.

(52) Cho, B. R.; Piao, M. J.; Son, K. H.; Lee, S. H.; Yoon, S. J.; Jeon, S. J.; Cho, M. H. *Chem.-Eur. J.* **2002**, *8*, 3907-3916.

(53) Pond, S. J. K.; Rumi, M.; Levin, M. D.; Parker, T. C.; Beljonne, D.; Day, M. W.; Brédas, J. L.; Marder, S. R.; Perry, J. W. *J. Phys. Chem. A* **2002**, *106*, 11470-11480.

(54) Strehmel, B.; Amthor, S.; Schelter, J.; Lambert, C. *ChemPhysChem* **2005**, *6*, 893-896.

(55) Chapter II of this doctoral thesis.

(56) Heilbronner, E.; Maier, J. P. *Helv. Chim. Acta* **1974**, *57*, 151-159.

(57) Bazan, G. C.; Oldham Jr., J.; Lachicotte, R. J.; Tretiak, S.; Chernyak, V.; Mukamel, S. *J. Am. Chem. Soc.* **1998**, *120*, 9188-9204.

(58) Verdal, N.; Godbout, J. T.; Perkins, T. L.; Bartholomew, G. P.; Bazan, G. C.; Kelley, A. M. *Chem. Phys. Lett.* **2000**, *320*, 95-103.

(59) Bartholomew, G. P.; Bazan, G. C. *Acc. Chem. Res.* **2001**, *34*, 30-39.

(60) Zyss, J.; Ledoux, I.; Volkov, S.; Chernyak, V.; Mukamel, S.; Bartholomew, G. P.; Bazan, G. C. *J. Am. Chem. Soc.* **2000**, *122*, 11956-11962.

(61) Bartholomew, G. P.; Bazan, G. C. *J. Am. Chem. Soc.* **2002**, *124*, 5183-5196.

(62) Moran, A. M.; Bartholomew, G. P.; Bazan, G. C.; Kelley, A. M. *J. Phys. Chem. A* **2002**, *106*, 4928-4937.

(63) Bartholomew, G. P.; Rumi, M.; Pond, S. J. K.; Perry, J. W.; Tretiak, S.; Bazan, G. C. *J. Am. Chem. Soc.* **2004**, *126*, 11529-11542.

(64) Hong, J. W.; Woo, H. Y.; Liu, B.; Bazan, G. C. *J. Am. Chem. Soc.* **2005**, *127*, 7435-7443.

(65) Woo, H. Y.; Hong, J. W.; Liu, B.; Mikhailovsky, A.; Korystov, D.; Bazan, G. C. *J. Am. Chem. Soc.* **2005**, *127*, 820-821.

(66) Salhi, F.; Collard, D. M. *Adv. Mater.* **2003**, *15*, 81-85.

(67) Salhi, F.; Lee, B.; Metz, C.; Bottomley, L. A.; Collard, D. M. *Org. Lett.* **2002**, *4*, 3195-3198.

(68) Creutz, C.; Newton, M. D.; Sutin, N. J. *J. Photochem. Photobiol. A* **1994**, *82*, 47-59.

(69) Cave, R. J.; Newton, M. D. *Chem. Phys. Lett.* **1996**, *249*, 15-19.

(70) Newton, M. D. *Adv. Chem. Phys.* **1999**, *106*, 303-375.

(71) Amthor, S.; Noller, B.; Lambert, C. *Chem. Phys.* **2005**, *316*, 141-152.

(72) Brunschwig, B. S.; Sutin, N. In *Electron Transfer in Chemistry*; 1 ed.; Balzani, V., Ed.; VCH: Weinheim, 2001; Vol. 2, pp 583-617.

(73) Brunschwig, B. S.; Creutz, C.; Sutin, N. *Chem. Soc. Rev.* **2002**, *31*, 168-184.

(74) Kasha, M. In *Physical Processes in Radiation Biology*; Augenstein, L., Mason, R., Rosenberg, B., Eds.; Academic Press: New York, 1964.

(75) McRae, E. G.; Kasha, M. In *Physical Process in Radiation Biology*; Augenstein, L., Mason, R., B, R., Eds.; Academic Press: New York, 1964; pp 23-42.

(76) Kasha, M.; Rawls, H. R.; El-Bayoumi, M. A. *Pure Appl. Chem.* **1965**, *11*, 371-392.

(77) Hayashi, M.; Shiu, Y. J.; Chang, C. H.; Liang, K. K.; Chang, R.; Yang, T. S.; Islampour, R.; Yu, J.; Lin, S. H. *J. Chin. Chem. Soc.* **1999**, *46*, 381-393.

(78) Beenken, W. J. D.; Dahlbom, M.; Kjellberg, P.; Pullerits, T. *J. Chem. Phys.* **2002**, *117*, 5810-5820.

(79) The interactions between the ground and the excited states which result in a energy lowering are neglected as they are supposed to be small.

(80) M. Kasha, H. R. Rawls, M. A. El-Bayoumi, *Pure Appl. Chem.* **1965**, *11*, 371-392. Equation (14) of this paper was corrected by us.

(81) Mank, D.; Raytchev, M.; Amthor, S.; Lambert, C.; Fiebig, T. *Chem. Phys. Lett.* **2003**, *376*, 201-206.

(82) This thesis acts on the assumption that the distances $r_{m1, m2}$ and the transition moments are similar [see Eq. (2)].

(83) Stewart, J. J. P. MOPAC97; Fujitsu Limited: 1997.

(84) Newton, M. D. *Chem. Rev.* **1991**, *91*, 767-792.

(85) Although we imply the tight-binding approximation to the GMH model with the assumption that the excited states do not interact directly the GMH analysis yields values for the coupling between these two excited CT_{bridge} states.

(86) Kryachko, E. S. *J. Phys. Chem. A* **1999**, *103*, 4368-4370.

(87) This would be more obvious if the indices 1 and 2 of the matrix elements were exchanged.

Synthesis and Ligand Properties of Thianthrenophane

CONTENTS

1. Introduction

Over the last years the focus in cyclophane chemistry has changed from pure electronic and structural properties to the investigation of the function and application of cyclophanes.[1-7] In particular, the host-guest chemistry,[8] the use of cyclophanes as ligands in metal clusters,[9] as chiral auxiliaries in asymmetric synthesis,[10, 11] for chemical vapour deposition polymerisation[12] and polymeric transition-metal cyclophane complexes[13] are of recent interest.
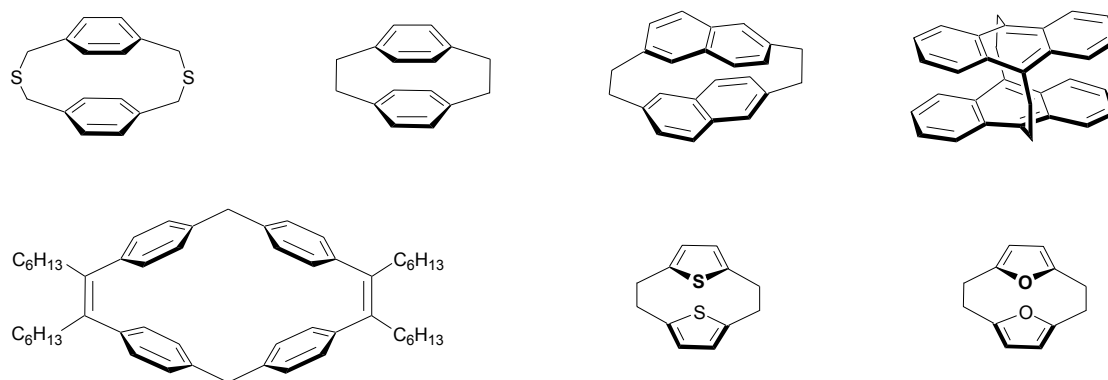
Cyclophanes containing heterocycles, e.g. [2.2]-(2,5)-furanophane[14] and [2.2]-(2,5)-thiophenophane[15] as well as annelated cyclophanes such as [2.2]-(2,6)-naphthalenophane[16] and [2.2]-(9,10)-anthracenophane[17] have been described in the literature (see above). The most well-known cyclophanes containing sulphur are thia-bridged cyclophanes.[5] The possibility of sulphur atoms to coordinate to soft metal ions has already been demonstrated for 2,11-dithia[3.3]paracyclophane which yields polymeric structures with silver(I) and copper(I).[13] Thianthrene has also been used as a ligand for transition metals such as silver[18, 19], palladium[18], platinum[18] and mercury[18]. Therefore, a cyclophane (**1**) was designed that is built up from two thianthrene units and which might have enough room between the butterfly-like thianthrene moieties to accommodate small ions or molecules. This thianthrenophane should be able to offer both exohedral sulphur coordination sites to soft metal ions and endohedral π-face coordination.

In the present study the ligand properties of this new thianthrenophane to silver(I) ions will be probed by UV/Vis titration experiments as well as by testing the transport capabilities through liquid membranes in comparison with other soft metal ions and in comparison with

thianthrene parent compound and 1,4,8,11-tetrathiacyclotetradecane (14-ane-S4). In addition the X-ray crystal structure determination of a polymeric [Ag(**1**)]ClO₄•(dioxane)₇ complex will be presented.

2. Results and Discussion

2.1. Synthesis and Crystal Structure of **1**

Cyclophane **1** was synthesised by *McMurry* coupling using high-dilution technique analogous to *Yamato* et al. (Scheme 1).[20, 21] The starting material for the *McMurry* cyclisation, 2,7-diacetylthianthrene, can be obtained by *Friedel-Crafts* acylation of thianthrene with two equivalents of acetyl chloride in high quantities[22], which is necessary because the yield in the subsequent cyclisation reaction was very low. Nevertheless, thanks to the easy availability of 2,7-diacetylthianthrene it was possible to synthesise several hundreds of milligrams of **1**.
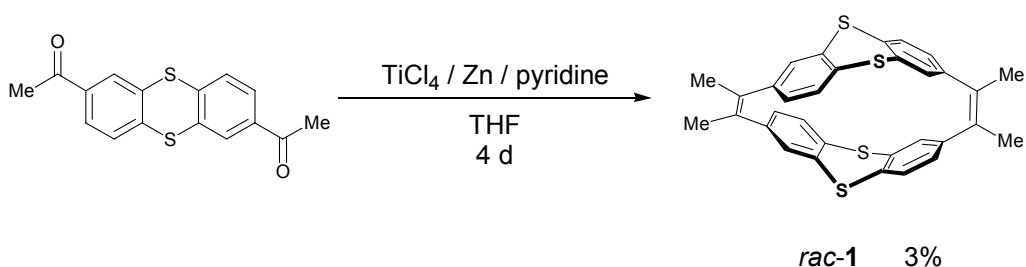
Scheme 1 Synthesis of thianthrenophane **1**.

Because thianthrenophane **1** has two stereogenic planes three possible stereoisomers exist. One isomer is the achiral *meso*-form with C_{2h} symmetry and the others represent a pair of enantiomers with D_2 symmetry (Fig. 1).

The IR-spectrum of 2,7-diacetylthianthrene shows a very intense carbonyl band at 1683 cm^{-1} which is replaced by a strong band due to the C=C double bond stretching at 1736 cm^{-1} in **1**. The ^{1}H-NMR of the product **1** shows only one set of signals indicating that a single isomer was formed, either the *meso* form or a racemic mixture of the two enatiomers (see Fig. 1).

Fig. 1 Possible isomers of thianthrenophane **1**.

An X-ray crystal structure analysis of **1** (Fig. 2) indeed demonstrates that the cyclophane crystallises as a conglomerate of the two D_2 enantiomers. The crystal structure analysis reveals a crossed orientation of the two thianthrene units with an angle of 42.7° between the S(1)-S(2) / S(3)-S(4) axes. As a consequence of the twisted thianthrene units the two ethene bridges are also not arranged parallel but are crossed with an angle of 58.0° between the C(13)-C(15) / C(31)-C(29) axes.

Fig. 2 Solid state structure of the asymmetric unit (50% probability level) and space filling model of thianthrenophane **1**.

The ethene bridges of **1** show distinct deviation from planarity with torsion angles of 7.7° between the C(10)-C(13)-C(14) plane and the C(17)-C(15)-C(16) plane and of 2.7° between

the C(1)-C(31)-C(32) plane and the C(26)-C(29)-C(30) plane. These distortions are similar to the one in (Z)-2,3-diphenyl-2-butene (3.9°) which is assumed to be strainless.[23]

The bond lengths and angles as well as the butterfly structure of the thianthrene rings in **1** are similar to common thianthrenes.[24-26] The folded structure of each thianthrene subunit has an interplanar angle of 129.3° and 129.9°, respectively, which is also comparable to the corresponding angle of known thianthrene structures.[24-26] Nevertheless, the cyclophane **1** is a somewhat strained molecule with the following structural characteristics: a) all planes of the folded thianthrene units show a slight deviation out of planarity. b) the mean bond angle $\delta =$ 119.5° of the (Z)-stilbene units in **1** is smaller than $\delta = 122.8°$[23] of (Z)-2,3-diphenyl-2-butene c) the average angle $\eta = 124.7°$ is large compared with $\eta = 114.6°$[23] of (Z)-2,3-diphenyl-2-butene.

The size of the cavity of cage compound **1** is limited by the distance from the centroid between S(1) and S(2) to the centroid between S(3) and S(4) which is 5.95 Å. Subtraction of the *van-der-Waals* radii of two sulphur atoms (3.60 Å)[27] yields a distance of 2.35 Å. Thus, thianthrenophane **1** should provide enough room between both thianthrene units in order to serve as a host for small metal ions such as Ag^+ ($r = 1.15$ Å, see space filling model, Fig. 2).

2.2. Redox Properties of **1**

Although thianthrene radical cation $\mathbf{2}^+$ is widely used as a one-electron oxidant the electrochemistry of thianthrene itself is complicated. The one-electron oxidation of thianthrene under superdry conditions is followed by a planarisation of the ring system (butterfly angle of **2** in the gas phase 131°[28] and in the solid state 128°[26], $\mathbf{1}^+ AlCl_4^-$ 174°[29]) and a dimerisation via the sulphur atoms to give $(\mathbf{2})_2^{2+}$ in polar solvents such as MeCN (see Scheme 2).[30]
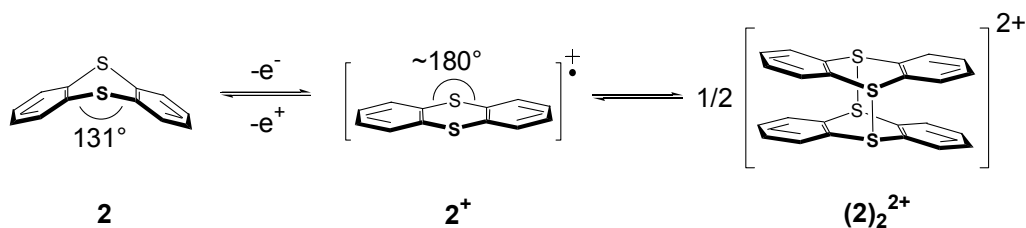
Scheme 2 Oxidation of thianthrene **2** and reversible dimerisation of the monoradical cation.

The redox behaviour of thianthrenophane **1** was investigated by cyclic voltammetry (CV) in butyronitrile. At high scan rate ($v > 5000$ mV/s) the CV shows two chemically reversible oxidation signals (Fig. 3).
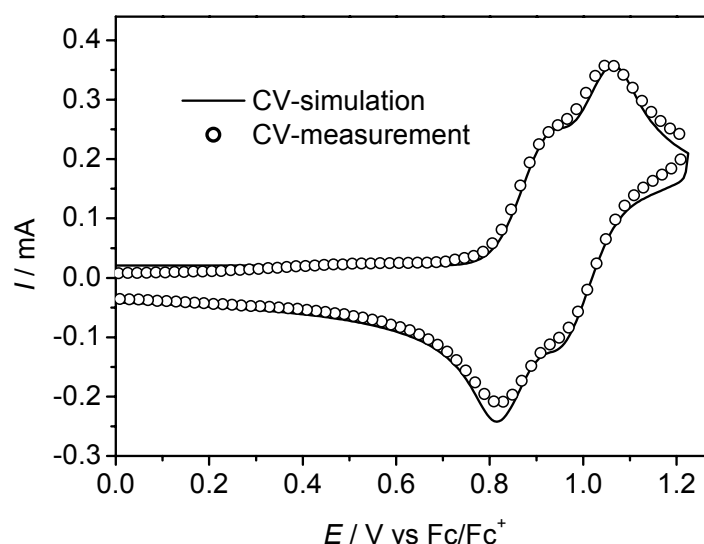
Fig. 3 CV of thianthrenophane **1** in PrCN / 0.1 M TBAH (v = 5000 mV/s).

Digital simulation of the CV (with DigiSim)[31] yields a peak potential difference ΔE of 126 mV between the two oxidation signals with $E_{1/2}(I) = 872$ mV and $E_{1/2}(II) = 998$ mV versus ferrocene as internal reference. The oxidation of **1** is chemically reversible at high scan rates only. At lower scan rates chemical follow up reactions take place and the back reduction signal allmost disapears. It is supposed that the generated radical cations of **1** are unstable due to the existence of strained double bonds which may lead to irreversible oligomerization reactions. But as mentioned above, cyclic voltammetry of thianthrene itself reveals two reversible oxidation signals only in the case of aprotic solvents under superdry conditions. Although the CV experiments were carried out under argon inert gas with rigorously dried solvents traces of water can not be excluded which might lead to the irreversible formation of sulfoxides as final products.[32]

2.3. Stability Constants for the Complexation of Silver(I) with Thianthrenophane **1** and Thianthrene **2**.

In order to probe the ligand properties of thianthrenophane **1** to soft metal ions the complex formation constant of the appropriate silver complex was measured and for comparison that of thianthrene **2** was measured similarly.

The complex stability constants K were determined by UV/Vis titration experiments with thianthrenophane **1** (K_1) and thianthrene **2** (K_2) as ligands in silver(I) complexes. In both cases a solution of the ligand in CH_2Cl_2 was titrated by a silver(I)perchlorate solution in $MeCN/CH_2Cl_2$ 1:9. The UV/Vis spectra obtained were analysed by global least squares data fitting by the *Levenberg-Marquardt* method using SPECFIT/32™-software.[33] The "singular value decomposition" (SVD) analysis of the experimental absorbance data for both ligands shows that only two spectroscopically distinguishable species are present, i.e. the free ligand and one complex are in equilibrium. The compositions of the complexes were determined by *Job's* method.[34] The resulting *Job's* plots indicate that thianthrenophane forms a 1:1 complex [Ag(**1**)]ClO$_4$ with silver(I) while a 1:2 aggregate [Ag(**2**)$_2$]ClO$_4$ is formed in the case of thianthrene.

The resulting logarithmic complex stability constants $\log K_1 = 5.45 \pm 0.13$ and $\log K_2 = 9.16 \pm 0.10$ were obtained by the global analysis fits. If one assumes that the complexation of silver with the first and the second thianthrene ligand has the same heat of formation the complex stability constant of a hypothetical 1:1 [Ag(**2**)]$^+$ complex will be $\log K_2/2 = 4.58$ which is somewhat smaller than $\log K_1$. This discrepancy indicates a different type of Ag$^+$ complexation by thianthrene and by cyclophane **1**.

The UV/Vis spectra of **1** and of **2** are given in Fig. 4. Both compounds show a distinct absorption maximum at ca. 260 nm which is comparable in molar absorptivity if a factor of two is applied for **2**. At $\lambda > 280$ nm there is a broad and less intense shoulder for both compounds. The main difference of both spectra is that the bands in **1** are much broader and less resolved. This broadening might be due to exciton coupling[35-37] of the two thianthrene subunits in **1**.
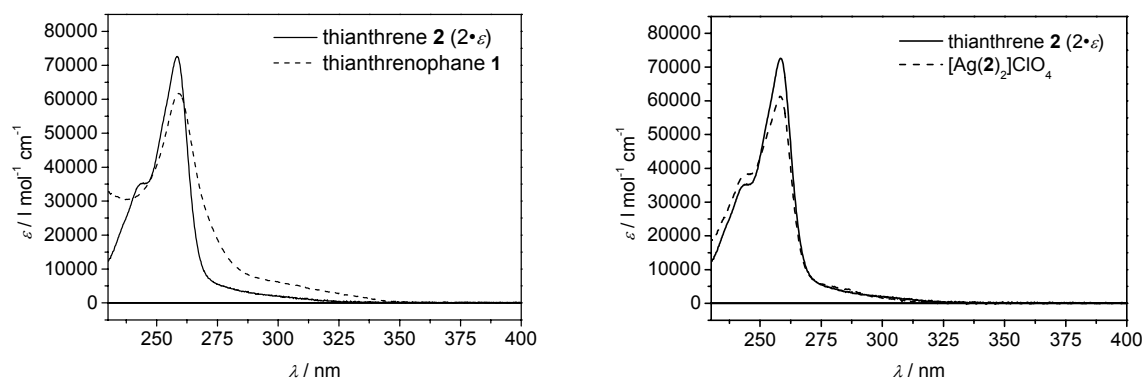
Fig. 4 UV/Vis spectra of the ligands (**1** and **2**) and the silver(I) complex [Ag(**2**)$_2$]ClO$_4$ in CH$_2$Cl$_2$ after deconvolution by global analysis.

Upon silver ion complexation the spectra of **1** and of **2** retain their shape but the molar absorbtivity at the peak maximum decreases significantly and the spectral features become somewhat broader.

The 1:1 stoichiometry of [Ag(**1**)]ClO$_4$ and the distinct difference between logK_1 and logK_2/2 suggests an endohedral coordination of Ag$^+$ by **1**, whereas the 1:2 stoichiometry of [Ag(**2**)$_2$]ClO$_4$ suggests a coordination of Ag$^+$ by the sulphur atoms on the convex side of thianthrene.

2.4. Transport Properties of 1 as a Carrier in Liquid Membranes

In order to further elucidate the complex formation of thianthrenophane **1** as well as its application in ion transport processes in liquid membranes single competition transport experiments with ten metal salts were carried out.[38-40]

Thianthrenophane **1** was used as the carrier in comparison with thianthrene **2** and 1,4,8,11-tetrathiacyclotetradecane (14-ane-S$_4$). Bulk liquid membranes as they were used here comprise of an aqueous source phase and a receiving phase separated by a CH$_2$Cl$_2$ phase as the membrane (Scheme 3).[41]
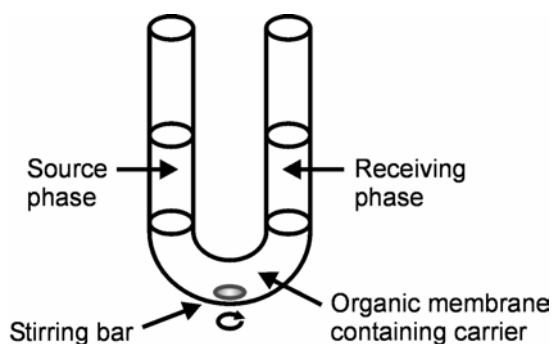
Scheme 3 Bulk liquid membrane cell with source phase and receiving phase separated by an organic membrane phase.

The aqueous source phase contained nine nitrate salts and mercury acetate at concentrations given in Table 1. The receiving phase was analysed by AAS for Ca^{2+}, K^+, Mg^{2+}, Na^+ and Hg^{2+}, and all remaining metals by ICP-OES after 120 h to determine the transport rates J for each metal ion (Table 1).

Under the conditions employed **1** transports silver(I) with a much higher rate and selectivity than thianthrene does. The ion flux of silver(I) was about thirteen times higher than that of mercury(II) and more than thousand times higher than that of cadmium(II), zinc(II) and lead(II) for **1**. For thianthrene as the carrier which was used in the same equivalent concentration per sulphur atoms (Table 1) the transport is also selective for silver(I) but the selectivity is lower than for cyclophane **1**. In the case of thianthrene silver(I) was transported only about five times faster than mercury(II). Furthermore, the transport rate of silver(I) is four times higher for cyclophane **1** compared to the thianthrene.

Macrocyclic polythioethers such as 14-ane-S_4 are extraction reagents which are known to be selective for soft metal ions such as silver(I).[43] In fact the selectivity for the silver(I) transport of 14-ane-S_4 at the same carrier concentration as for cyclophane **1** is similar to that of thianthrene although the ion fluxes for 14-ane-S_4 are distinctly smaller than those of thianthrene and **1**.

Table 1 Transport rates J^a (10^{-8} mol m^{-2} s^{-1}) for three carrier molecules.

	Source phase concentration /10^{-3} M	**1** (10^{-3} M)	**2** ($2 \cdot 10^{-3}$ M)	14-ane-S$_4$ (10^{-3} M)
Pb^{2+}	172	0.02	0.01	0.01
Zn^{2+}	158	0.01	0.05	0.05
Al^{3+}	151	-^{b}	-	-
Ca^{2+}	95	-	0.61	0.61
K$^+$	153	-	-	-
Mg^{2+}	127	-	-	-
Na$^+$	146	-	-	-
Cd^{2+}	161	0.02	-	0.003
Ag$^+$	166	37.53	8.93	1.51
Hg^{2+}	150	2.85	1.58	0.33

^{a} Calculated from $J = c\,V\,t^{-1}\,A^{-1}$, with c = concentration receiving phase after time t = 120 h, V = 5.0 ml (volume receiving phase) and A = 7.09 10^{-5} m^2 (effective exchange area).[42] ^{b} All missing data lie below the detection limit of the used device.

According to a simplified equation reported by Reusch and Cussler[44] the transport rate J_M depends on the diffusion coefficient of the carrier-metal complex D, the complex formation constant for the carrier-metal complex K, and a partition coefficient k for the metal ion partitioning between aqueous and membrane phase, the cation concentration in the source phase C_M, and the carrier concentration C_C as well as the transport length l: $J_M = D \cdot k \cdot K \cdot C_M^2 \cdot C_C / l$. However, in practice a decrease of J_M for higher complexation constants was observed experimentally and described theoretically by Lamb et al..[45] Without additional information about the above mentioned quantities it is impossible to give definite conclusions about the transport rate and selectivity of the three carriers. Tentatively, both the high selectivity of the silver(I) transport by thianthrenophane **1** and the high transport rate can be explained by the formation of an endohedral [Ag(**1**)]$^+$ complex. Because of the smaller size this endohedral [Ag(**1**)]$^+$ complex should have a higher diffusion coefficient than [Ag(**2**)$_2$]$^+$. The formation of an endohedral [Ag(**1**)]$^+$ complex also is supported by the analysis if the UV titration which suggests a 1:1 carrier-metal ratio and a complex stability constant which would be unlikely for an exohedral complex formation.

2.5. Crystal Structure of [Ag(1)]ClO₄•(dioxane)₇

Reaction of **1** with one equivalent of silver(I) perchlorate in THF affords a colourless solid which was recrystallised from dioxane to obtain colourless needles of complex [Ag(**1**)]ClO$_4$•(dioxane)$_7$. The X-ray structure analysis reveals a coordination polymer of silver(I) and thianthrenophane **1** in which thianthrenophane acts as a pure S ligand to Ag$^+$ (see Fig. 5). This contrasts the structure of many other cyclophane-Ag$^+$ complexes where silver(I) sits endohedrally in the cage coordinated by the arene π-systems.[9, 46]

The complex shows a one-dimensional polymeric structure where each silver ion is coordinated by two ligands. Regarding the [Ag(**1**)$_2$] substructure the metal ion is coordinated by two sulphur atoms of each bidentate ligand part. The bond angles S(1')-Ag(1)-S(2') and S(3)-Ag(1)-S(4) are 68° and the mean Ag-S bond length is 2.81 Å. These values are comparable to the S-Ag-S bond angle of 70.9° and Ag-S bond lengths of 2.63 and 2.79 Å in the dinuclear [Ag$_2$(thianthrene)$_2$ClO$_4$)$_2$] complex described by *Munakata et al.*.[19] In contrast to the structure of [Ag(**1**)]ClO$_4$•(dioxane)$_7$ this dimeric thianthrene complex not only shows the coordination of sulphur atoms to silver(I) but also a complexation by the π system of phenylene rings to silver(I). Due to the complexation the interplanar angles of the folded thianthrene units of the ligand show a narrowing from 129.3° (**1**) and 129.9° (**1**) to 121.8° and 122.0°, respectively. Thus, the distance from the centroid between S(1) and S(2) to the centroid between S(3) and S(4) is enlarged to 6.32 Å. After subtraction of the *van-der-Waals* radius of two sulphur atoms the size of the cavity is specified by the resulting distance of 2.72 Å. The twist angles of the uncoordinated cyclophane **1** mentioned above are comparable to the ligand structure in the [Ag(**1**)]ClO$_4$•(dioxane)$_7$ complex. Although the solid state structure of [Ag(**1**)]ClO$_4$•(dioxane)$_7$ is polymeric it is unlikely that fragments of this structure constitute the entities present in solution. In fact [Ag(**1**)]ClO$_4$•(dioxane)$_7$ is insoluble in moderately polar solvents such as CH$_2$Cl$_2$ or THF and can only be dissolved upon addition of, for example, MeCN from which silver-free **1** could be isolated.
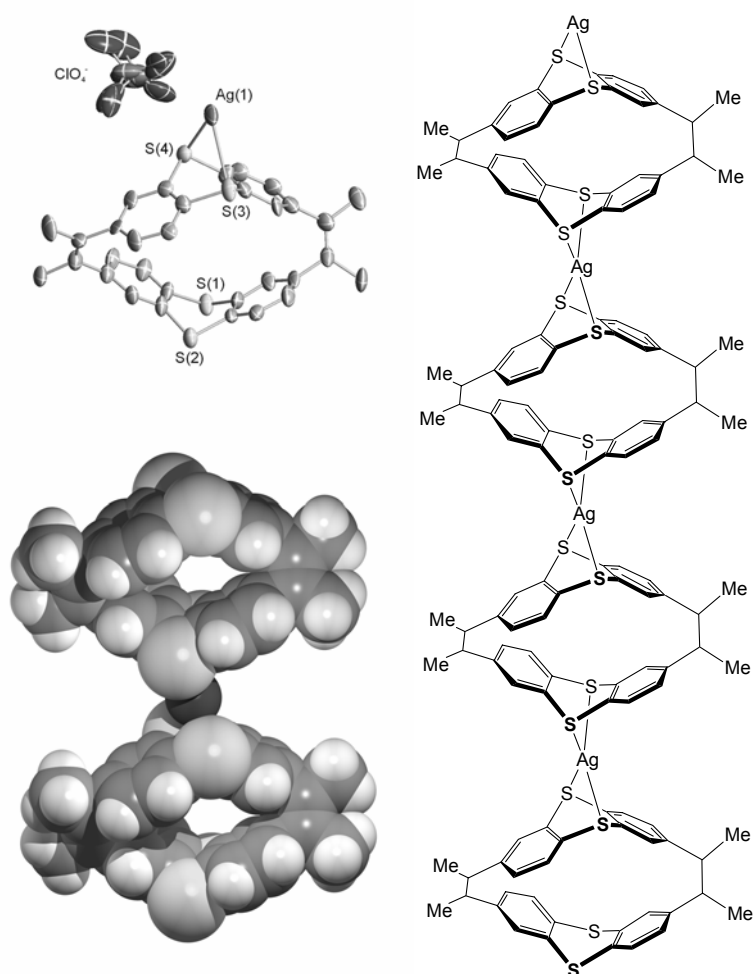
Fig. 5 Solid state structure (50% probability level) of the asymmetric unit, polymeric representation of [Ag(**1**)]ClO$_4$•(dioxane)$_7$ (the solvent molecules and hydrogen atoms are omitted) and space filling model of dimeric subunit.

3. Conclusions

In this study it was shown that [Ag(**1**)]$^+$ form a 1:1 complex in CH$_2$Cl$_2$ solution with a stability constant of 5.45 ± 0.13. Competitive membrane phase transport experiments with ten metal salts and two alternative carriers (thianthrene and 14-ane-S$_4$) demonstrate the high selectivity of **1** as a carrier for silver(I) compared to, for example, Hg^{2+} as well as its distinctly higher transport rates compared to the other carriers. An endohedral [Ag(**1**)]$^+$ complex is suggested to be the active unit in the transport experiments at very low concentrations while [Ag(**1**)]$^+$ forms a polymeric exohedral coordination structure in the solid state.

4. Experimental Section

4.1. Synthesis of rac-1,4(2,7)-bisthianthrenediyl-2,3,5,6-tetramethylcyclohexanophane-2,5-diene (1)

Titanium tetrachloride (23.8 g, 13.8 ml, 125 mmol) was added slowly to 500 ml of dry THF at 0°C under nitrogen atmosphere. After warming up to room temperature zinc dust (18.0 g, 275 mmol) was added in small portions. The yellow suspension changes colour over green to purple and finally to black. A solution of 2,7-diacetylthianthrene (2.71 g, 9.00 mmol) in 250 ml dry THF and dry pyridine (22.5 ml, 200 mmol) was added to the black mixture of the *McMurry* reagent within four days under continuous reflux and stirring (with a 250 ml funnel-constant-addition with glass needle valve from Normag®). After additional 12 h of reflux the reaction mixture was cooled to room temperature and hydrolysed with 200 ml of 10% aqueous potassium carbonate solution. Most of the solvent was destilled off (~500-600 ml) and CH_2Cl_2 (250 ml) was added to the suspension. The black precipitate was filtered off, hydrolysed with hydrochloric acid (400 ml, 2 N) and the insoluble solid was filtered off. This solid was extracted with CH_2Cl_2 (100 ml). Both aqueous phases were extracted with CH_2Cl_2 (200 ml) each. The combined organic phases were washed twice with water (200 ml), dried over sodium sulphate and concentrated. The residue was purified by flash-chromatography over silica gel with petroleum/CH_2Cl_2 6:1 as the eluent to give the crude product **1**. This was recrystallised twice from EtOAc/CH_2Cl_2 1:9 to yield colourless crystals (135 mg, 3%). mp 263 °C (from EtOAc/CH_2Cl_2 1:9); δ_H(250 MHz; CDCl$_3$) 7.19 (4 H, d, J 7.93 Hz, Ar 4-H, 9-H), 6.97 (4 H, dd, J 7.93 and 1.83 Hz, Ar 3-H, 8-H), 6.55 (4 H, d, J 1.53 Hz, Ar 1-H, 6-H), 2.09 (12 H, s, CH$_3$); δ_H(62.90 MHz; CDCl$_3$) 144.6, 134.5, 134.5, 134.3, 130.8, 127.5, 127.4, 19.9 (CH$_3$); v_{max}/cm^{-1} 1736s (C=C), 1448vs, 1376s, 1234s, 881s, 821vs, 728m; m/z (EI) 536.0763 (M$^+$,100%. C$_{32}$H$_{24}$S$_4$ requires 536.0761), 268 (M^{2+}, 23%).

*4.2. Synthesis of [Ag(**1**)]ClO$_4$•(dioxane)$_7$*

Silver(I) perchlorate (31.5 mg, 140 μmol) in THF (1 ml) was added to a solution of **1** (75.0 mg, 140 μmol) in THF (12 ml). The mixture was stirred for 20 min at room temperature. The colourless precipitate was filtered off, washed with THF and dried in vacuum to yield the crude product (156 mg). The product was recrystallised from dioxane to give colourless needles.

4.3. Cyclic Voltammetry

The electrochemical experiments were performed in superdry, argon-saturated PrCN with 0.2 M tetrabutylammoniumhexafluorophosphate (TBAH) as supporting electrolyte and 0.002 M substrate using a conventional three-electrode set-up with platinum disk electrode (0.12 cm^2). The solution was dried in situ by addition of activated (at 300°C and 10^{-3} mbar) aluminium oxide. The potentials are referenced against ferrocene (Fc/Fc$^+$). Digital fits of the experimental CV were done with DigiSim.[31]

4.4. UV/Vis Titration

The complexation of silver(I) with ligands **1** and **2** was done by stepwise adding a 0.006 M silver(I)perchlorate solution with a microlitre syringe into a 10^{-5} M solution of **1** or **2**, respectively, in 1:9 MeCN/CH$_2$Cl$_2$ in an UV quartz cell. The spectra obtained were analysed by global analysis using SPECFIT/32^{TM} software.[33] Taking into account that silver(I) forms [Ag(MeCN)$_4$]ClO$_4$[47] with MeCN a value of 5.19 ± 0.25 for log$K$([Ag(**1**)]ClO$_4$) and 9.04 ± 0.14 for log$K$([Ag(**2**)$_2$]ClO$_4$) were determined which are marginally lower than the values mentioned above which were obtained without consideration of MeCN complexation.

4.5. Application of Job's method[34]

The UV/Vis spectra obtained from the titration of ligands **1** and **2** with silver(I) were analysed with *Job's* method. Therefore, for each ligand, the difference between the extinction at a certain wavelength of the pure ligand E_0 (of the first spectrum before silver salt was added) and the following spectra E_x was divided by the total concentration of silver(I) and ligand. Thus, one yields the normalised extinction coefficient difference $\Delta\varepsilon$ (see Eq. (1)) which then was plotted versus the mole fraction of silver(I) $x(Ag^+)$ (see Eq. 2).

$$\Delta\varepsilon = \frac{E_x - E_0}{c(Ag^+) + c(L)} \tag{1}$$

$$x(Ag^+) = \frac{n(Ag^+)}{n(Ag^+) + n(L)} \tag{2}$$

The *Job's* plots resulting from the UV/Vis titration experiments of ligand **1** as well as of ligand **2** are presented in Fig. 6. For both ligands two plots at two different wavelengths were generated in order to prove the findings.
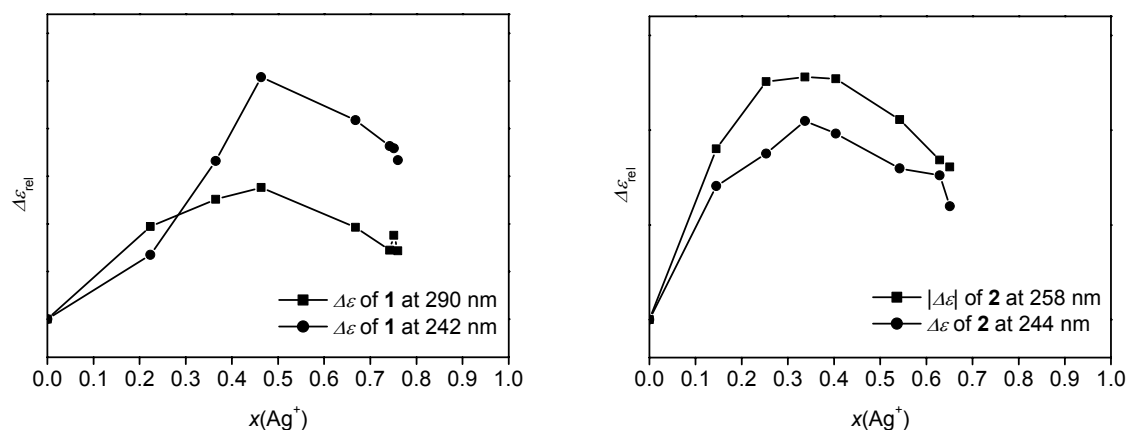
Fig. 6 *Job's* plots obtained from the UV/Vis titration experiments of ligands **1** and **2** with silver(I).

The *Job's* plots of ligand **1** show a maximum at a mole fraction of about $^1/_2$ while the maximum of the plots of ligand **2** is located at a mole fraction of circa $^1/_3$. These results indicate that thianthrenophane **1** forms a 1:1 complex [Ag(**1**)]ClO$_4$ with silver(I) while a 1:2

aggregate [Ag(**2**)$_2$]ClO$_4$ is formed in the case of thianthrene **2** as already mentioned in the text.

4.6. Membrane Transport Experiments

The nitric acid and all metal salts have been used in p.a. quality without further purification. Thianthrene was purchased from Fluka and 1,4,8,11-tetrathiacyclotetradecane from Aldrich, both were used without further purification. In order to obtain reliable results identical experimental setup consisting of a horseshoe bend standard glass tube with identical source phase (metal salts in 5 ml 10% aqueous nitric acid), receiving phase (5 ml pure 10% aqueous nitric acid) separated by the CH$_2$Cl$_2$ membrane (5 ml) and stirring bar (50 rpm) was used for all experiments. The period of transportation was 120 h and the effective exchange area was 7.09 10^{-5} m^2 in all cases. For the quantitative determinations of Ca^{2+}, K$^+$, Mg^{2+} and Na$^+$ an Unicam Solar 939 atomic absorption spectrometer was used. The content of Hg^{2+} was measured with a Seefelder Hg-254 NE analyser. The concentrations of all remaining metal salts were measured with a Spectroflame ICP-OES.

4.7. X-Ray Measurement of **1** and of [Ag(**1**)]ClO$_4$•(dioxane)$_7$

All data were collected from shock-cooled crystals on an Bruker Smart Apex D8 3 circle diffractometer (graphite-monochromated Mo-Kα radiation, $\lambda = 71.073$ pm) equipped with a low temperature device at 173(2) K.[48] An empirical absorption correction was employed for structure **1**.[49] The structures **1** and [Ag(**1**)]ClO$_4$•(dioxane)$_7$ were solved by direct methods (SHELXS-97[50]) and refined by full-matrix least squares procedure against F^2 (SHELXL-97[51]). R values: $RI = \Sigma||F_o|-|F_c||/\Sigma|F_o|$, $wR2 = [\Sigma w(F_o^2-F_c^2)^2/\Sigma w(F_o^2)^2]^{0.5}$, $w = [\sigma^2(F_o^2)+(g_1P)^2+g_2P]^{-1}$, $P = 1/3[\max(F_o^2,0)+2F_c^2]$. **1**: C$_{32}H_{24}S_4$, orthorhombic, space group P2$_1$2$_1$2$_1$, $Z = 4$, $a = 1183.13(10)$ pm, $b = 1478.32(13)$ pm, $c = 1595.19(14)$ pm, $\alpha = 90.00°$, $\beta = 90.00°$, $\gamma = 90.00°$, $V = 2.7901(4)$ nm^3, $\rho_c = 1.278$ Mg m^{-3}, 27669 reflections measured, 5746 unique, $RI[I>2\sigma(I)] = 0.0546$, $wR2$(all data) $= 0.1200$, $g_1 = 0.0397$,

g_2 = 1.7844 for 329 parameters. The Flack parameter refined to 0.10(8), therefore the absolute structure was determined correctly. All non-hydrogen atoms were refined anisotropically and all hydrogen atoms isotropically. [Ag(**1**)]ClO$_4$•(dioxane)$_7$: C$_{30}$H$_{40}$Ag$_{0.5}$Cl$_{0.5}$O$_9$S$_2$, monoclinic, space group P2$_1$/c^{52}, Z = 8, a = 2875.0(5) pm, b = 1096.8(2) pm, c = 2056.2(4) pm, α = 90.00°, β = 90.104(5)°, γ = 90.00°, V = 6.48(1) nm^3, ρ_c = 1.394 M g m^{-3}, 16989 reflections measured, 6242 unique, $R1[I>2\sigma(I)]$ = 0.0962, $wR2$(all data) = 0.1895, g_1 = 0.0843, g_2 = 0.0000 for 622 parameters and 669 restraints. Due to the unsatisfying crystal quality (three of the seven dioxane molecules were disordered as well as the ClO$_4^-$ anion) and the resulting decay of intensities at higher scattering angles the data had to be cut at the d=1.0Å resolution limit. All non-hydrogen atoms were refined anisotropically with exception of the dioxane molecules. The hydrogen atoms were refined isotropically. The disordered molecules were refined with different occupation factors. All disordered fragments were refined with SAME- and SADI-restraints implemented in SHELXL. Crystallographic data (excluding structure factors) for the structure reported in this chapter have been deposited with the Cambridge Crystallographic Data Centre as supplementary publication no. CCDC-238344 (**1**) and CCDC-238345 ([Ag(**1**)]ClO$_4$•(dioxane)$_7$). Copies of the data can be obtained free of charge on application to CCDC, 12 Union Road, Cambridge CB2 1EZ, UK [fax: (internat.) + 44(1223)336-033; e-mail: deposit@ccdc.cam.ac.uk.

5. References

(1)   H. Hopf, 'Classics in Hydrocarbon Chemistry', Wiley-VCH, Weinheim, 2000, p. 337.

(2)   B. König, *Topics Curr. Chem.*, 1998, **196**, 89.

(3)   G. J. Bodwell, *Angew. Chem.*, 1996, **108**, 2221.

(4)   H. Hopf, *Naturwiss.*, 1983, **70**, 349.

(5)   V. Boekelheide, *Topics Curr. Chem.*, 1983, **113**, 87.

(6)   F. Vögtle and P. Neumann, *Topics Curr. Chem.*, 1974, **48**, 67.

(7)   D. J. Cram and J. M. Cram, *Acc. Chem. Res.*, 1971, **4**, 204.

(8)   F. Diederich, 'Cyclophanes: A Monograph in Supramolecular Chemistry', Royal Society of Chemistry, London, 1991.

(9)   F. R. Heirtzler, H. Hopf, P. G. Jones, P. Bubenitschek, and V. Lehne, *J. Org. Chem.*, 1993, **58**, 2781.

(10)   K. Rossen, P. J. Pye, A. Maliakal, and R. P. Volante, *J. Org. Chem.*, 1997, **62**, 6462.

(11)   P. J. Pye, K. Rossen, R. A. Reamer, N. N. Tsou, R. P. Volante, and P. J. Reider, *J. Am. Chem. Soc.*, 1997, **119**, 6207.

(12)   T. Itoh, *Prog. Polym. Sci.*, 2001, **26**, 1019.

(13)   M. Munakata, L. P. Wu, T. KurodaSowa, M. Maekawa, Y. Suenaga, and S. Nakagawa, *J. Chem. Soc.-Dalton Trans.*, 1996, 1525.

(14)   D. J. Cram, C. S. Montgomery, and G. R. Knox, *J. Am. Chem. Soc.*, 1966, **88**, 515.

(15)   J. R. Fletcher and I. O. Sutherland, *Chem. Commun.*, 1969, 1504.

(16)   M. Haenel and H. A. Staab, *Tetrahedron Letters*, 1970, **11**, 3585.

(17)   J. H. Golden, *J. Chem. Soc.*, 1961, 3741.

(18)   U. Behrens, P. Berges, R. Bieganowski, W. Hinrichs, C. Schiffling, and G. Klar, *J. Chem. Res., (M)*, 1986, 2801.

(19)   M. Munakata, S. G. Yan, I. Ino, T. Kuroda-Sowa, M. Maekawa, and Y. Suenaga, *Inorg. Chim. Acta*, 1998, **271**, 145.

(20)   T. Yamato, K. Fujita, K. Futatsuki, and H. Tsuzuki, *Can. J. Chem.*, 2000, **78**, 1089.

(21)   H. F. Grützmacher, A. Mehdizadeh, and A. Muelverstedt, *Chem. Ber.*, 1994, **127**, 1163.

(22) K. Niume, K. Nakamichi, R. Takatuka, F. Toda, K. Uno, and Y. Iwakura, *J. Polym. Sci, Polym. Chem. Ed.*, 1979, **17**, 2371.

(23) F. R. Fronczek, A. M. Swan, J. A. Corkern, and R. D. Gandour, *Acta Crystallogr., Sect. C: Cryst. Struct. Commun.*, 1984, **C40**, 1875.

(24) I. Rowe and B. Post, *Acta Crystallogr.*, 1958, **11**, 372.

(25) C. H. Wei, *Acta Crystallogr., Sect. B: Struct. Sci.*, 1971, **B27**, 1523.

(26) S. Larson, O. Simonsen, G. E. Martin, K. Smith, and S. Puig-Torres, *Acta Crystallogr., Sect. C: Cryst. Struct. Commun.*, 1984, **C40**, 103.

(27) A. Bondi, *J. Phys. Chem.*, 1964, **68**, 441.

(28) K. L. Gallaher and S. H. Bauer, *J. Chem. Soc., Faraday Trans. 2*, 1975, **71**, 1173.

(29) W. Hinrichs, P. Berges, and G. Klar, *Z. Naturforsch.*, 1987, **42b**, 169.

(30) P. Huebler and J. Heinze, *Ber. Bunsenges. Phys. Chem.*, 1998, **102**, 1506.

(31) M. Rudolph and S. W. Feldberg, DigiSim V 3.03a (CV), Cyclic Voltammetric Simulator, 2000, Bioanalytical Systems, Inc., West Lafayette (U.S.A.).

(32) A. Domenech, I. Casades, and H. Garcia, *J. Org. Chem.*, 1999, **64**, 3731.

(33) R. A. Binstead, B. Jung, and A. D. Zuberbühler, SPECFIT/32™ V3.0.33, Program for Multivariate Data Analysis, 1993, Spectrum Software Associates, Marlborough (U.S.A.).

(34) Z. D. Hill and P. Maccarthy, *J. Chem. Educ.*, 1986, **63**, 162.

(35) E. G. McRae and M. Kasha, 'Physical Process in Radiation Biology', Academic Press, New York, 1964, p. 23.

(36) M. Kasha, H. R. Rawls, and M. A. El-Bayoumi, *Pure Appl. Chem.*, 1965, **11**, 371.

(37) M. Kasha, 'Physical Processes in Radiation Biology', Academic Press, New York, 1964.

(38) M. A. Ahearn, J. Kim, A. J. Leong, L. F. Lindoy, O. A. Matthews, and G. V. Meehan, *J. Chem. Soc.-Dalton Trans.*, 1996, 3591.

(39) J. Kim, A. J. Leong, L. F. Lindoy, J. Nachbaur, A. Nezhadali, G. Rounaghi, and G. Wei, *J. Chem. Soc.-Dalton Trans.*, 2000, 3453.

(40) B. König, M. Müller, H. Wichmann, and M. Bahadir, *J. Chem. Res., (M)*, 1998, 401.

(41) F. DeJong and H. C. Visser, 'Comprehensive Supramolecular Chemistry', Elsevier, Oxford, UK, 1996, p. 13.

(42) B. König, T. Fricke, U. Luning, M. Hagen, M. Müller, and M. Bahadir, *J. Prakt. Chem.*, 1999, **341**, 218.

(43)   K. Saito, S. Murakami, A. Muromatsu, and E. Sekido, *Polyhedron*, 1993, **12**, 1587.

(44)   C. F. Reusch and E. L. Cussler, *AIChE Journal*, 1973, **19**, 736.

(45)   J. D. Lamb, J. J. Christensen, J. L. Oscarson, B. L. Nielsen, B. W. Asay, and R. M. Izatt, *J. Am. Chem. Soc.*, 1980, **102**, 6820.

(46)   A. García Martínez, J. Osío Barcina, M. del Rosario Colorado Heras, Á. de Fresno Cerezo, and M. del Rosario Torres Salvador, *Chem.-Eur. J.*, 2003, **9**, 1157.

(47)   K. Nilsson and A. Oskarsson, *Acta Cham Scand A* , 1984, **38**, 79.

(48)   a) T. Kottke, D. Stalke*, J. Appl. Crystallogr*. **1993**, *26*, 615; b) T. Kottke, R. J. Lagow, D. Stalke, *J. Appl. Crystallogr*. **1996**, *29*, 465; c) D. Stalke, *Chem. Soc. Rev.* **1998**, *27*, 171.

(49)   G. M. Sheldrick, SADABS 2.05, Program for the Absorption Correction of Crystal Structures, 2000, University of Göttingen, Göttingen (Germany).

(50)   G. M. Sheldrick, *Acta Crystallogr.*, 1990, **A46**, 467.

(51)   G. M. Sheldrick, SHELXL-97 – Program for Structure Refinement, Universität Göttingen, 1997.

(52)   The β angle close to 90° and the systematic absences suggested a possible orthorhombic space group Pbcn (with the origin shifted to 0,0,0). Nevertheless, the structure could exclusivley solved and successfully refined (with the limitations due to the poor data quality) using the monolinic space group $P2_1/c$.

SUMMARY

Triarylamines themselves present a two-dimensional propeller structure which may be used to assemble three π-electron systems in a regular way. In chapter I of this thesis the one electron oxidation potential of ten triarylamines with all permutations of chloro-, methoxy- and methyl-substituents in the three *para*-positions were determined by cyclic voltammetry. The half wave potential $E_{1/2}(I)$ of the first oxidation wave correlates linearly with the number of chloro- and methoxy-substituents. A high long-term stability of the first oxidation wave for all triarylamines was observed by multi-cycle thin-layer measurements. AM1-CISD derived values of the absorption energies are in good agreement with the experiments but differ strongly for the oscillator strengths as well as for neutral compounds and their corresponding mono radical cations. The small solvent dependence of the experimental UV/Vis spectra in CH_2Cl_2 and MeCN reflects a minor charge transfer character of the electronic transitions of neutral and cationic compounds. The UV/Vis/NIR spectra of the series of triarylamines and their corresponding radical cations and the AM1 computations reveal that even small substituents may lead to strong symmetry breaking and to a modified electronic structure.

In chapter II the spectroscopic properties of a series of four bistriarylamine donor-π-bridge-donor X-B-X compounds (dimers), composed of two asymmetric triarylamine chromophores (monomers) were investigated. UV/vis-, fluorescence and transient absorption spectra were recorded and compared with those of the corresponding X-B monomers. Bilinear *Lippert-Mataga* plots indicate a major molecular reorganization of the excited state in polar media for all compounds. The excited states of the dimers are described as mixed-valence states which show, depending on the chemical nature of the π-bridge, a varying amount of interactions (couplings). It was found that superradiant emission, that is, an enhancement of fluorescence rate, only proceeds in the case of weak and medium coupling. Whether the first excited state potential energy surface of the dimers is a single minimum or a double minimum potential depends on the solvent polarity and the electronic coupling. In the latter case, the dimer relaxes in a symmetry broken CT state with partial positive charge at the triarylamine donor and negative charge at the π-bridge. The [2.2]paracyclophane bridged dimer is an example for a weakly coupled system, because the spectroscopic behavior is very similar to the corresponding *p*-xylene monomer. In contrast, anthracene as well as *p*-xylene bridges

mediate a stronger coupling and reveal a significant cooperative influence on the optical properties.

In chapter III a series of [2.2]paracylophane bridged bis-triarylamine mixed-valence (MV) radical cations X-B-X$^+$ were analyzed by a generalized *Mulliken-Hush* (GMH) three-level model which takes two transitions into account: the inter-valence charge transfer (IV-CT) band which is assigned to an optically induced hole transfer (HT) from one triarylamine unit to the second one, and a second band associated with a triarylamine radical cation to bridge (in particular [2.2]paracyclophane bridge) hole transfer. From the GMH analysis , one can conclude that the [2.2]paracyclophane moiety is not the limiting factor which governs the intramolecular charge transfer. AM1-CISD calculations reveal that both through-bond as well as through-space interactions of the [2.2]paracyclophane bridge play an important role for hole transfer processes. These electronic interactions are of course smaller than direct π-conjugation but from the order of magnitude of the couplings of the [2.2]paracyclophane MV species it can be assumed that this bridge is able to mediate significant through-space and through-bond interactions and that the cyclophane bridge acts more like an unsaturated spacer rather than a saturated one. From the exponential dependence of the electronic coupling V between the two triarylamine localized states on the distance r between the two redox centers, it was inferred that the hole transfer proceeds via superexchange mechanism. The analysis reveals that even significantly longer π-conjugated bridges should still mediate significant electronic interactions, because the decay constant β of a series of π-conjugated MV species is small.

In chapter IV, the absorption properties of a series of bis-triarylamino-[2.2]paracyclophane diradical dications X$^+$-B-X$^+$ were presented. The set of compounds is similar to that in chapter III, only the redox state differs. The localized π-π* and the charge-transfer (CT) transitions of these dications are explained and analyzed by an exciton coupling model which also considers the photophysical properties of the "monomeric" triarylamine radical cations. Together with AM1-CISD calculated transition moments, experimental transition moments and transition energies of the bis-triarylamine dications were used to calculate electronic couplings by a generalized *Mulliken-Hush* (GMH) approach. These couplings are a measure for interactions of the excited mixed-valence CT states. The modification of the diabatic states reveals similarities of the GMH three-level model and the exciton coupling model. Comparison of the two models shows that the transition moment between the excited mixed-

valence states μ_{ab} of the dimer equals the dipole moment difference $\Delta\mu_{12}^{(m)}$ of the ground and the excited bridge state of the corresponding monomer.

In chapter V, the multidimensional π-electron system thianthrenophane (**1**), a cyclophane which consists of two thiathrene units was presented. This thianthrenophane has a cavity which offers enough room to potentially enable endohedral coordination to small ions or molecules. For the complexation of silver(I) perchlorate, the complex stability constants of thianthrenophane $\log K_1 = 5.45 \pm 0.13$ and of thianthrene $\log K_2 = 9.16 \pm 0.10$ were determined by UV/Vis titration. Single competition transport experiments with ten metal salts demonstrate a very high selectivity of thianthrenophane as a carrier for silver(I) and a distinctly higher transport rate compared to carriers such as thianthrene and 1,4,8,11-tetrathia-cyclotetradecane (14-ane-S_4). Although the X-ray crystal structure analysis of the polymeric $[Ag(\mathbf{1})]ClO_4 \bullet (dioxane)_7$ complex shows an exohedral coordination to silver(I), the formation of an endohedral $[Ag(\mathbf{1})]^+$ complex is suggested to be the explanation for the unusual carrier selectivity of silver(I) by **1** in bulk liquid membrane.

Appendix

ZUSAMMENFASSUNG

Triarylaminverbindungen weisen eine dreiflüglige Propellerstruktur auf welche eine räumlich vordefinierte Verknüpfung von drei π-Systemen ermöglicht. Im ersten Kapitel dieser Doktorarbeit wurden zehn verschiedene Triarylamine mit allen möglichen Permutationen der Substituenten Chlor, Methoxy und Methyl in allen drei *para*-Position zum zentralen Stickstoff untersucht. Die cyclovoltammetrisch bestimmten Halbstufenpotentiale dieser Verbindungen zeigen eine lineare Korrelation zur Anzahl der Chlor- und Methoxysubstituenten. Eine hohe Reversibilität der ersten Oxidation aller Triarylamine konnte durch Dünnschicht CV Messungen belegt werden. Es wurden semiempirische AM1-CISD Berechnungen der neutralen Triarylamine und deren Monokationen durchgeführt, dabei wurden gute Übereinstimmungen für die Absorptionsenergien festgestellt, es zeigen sich jedoch große Abweichungen bei den entsprechenden Oszillatorstärken. Die geringe Solvensabhängigkeit der Absorptionsspektren, sowohl der neutralen Triarylamine, als auch der entsprechenden Monokationen verdeutlicht den geringen Ladungstransfercharakter der optischen Übergänge. Die UV/Vis-Spektren und die semiempirischen Berechnungen der Triarylamine und Triarylamin-Radikalkationen zeigen auf, dass selbst kleine Substituenten zu einem Symmetriebruch in Lösung führen können, welcher einen bedeutenden Einfluss auf die elektronischen Zustände hat.

Im zweiten Kapitel dieser Arbeit wurden zwei Triarylamin-Chromophore über verschiedene Brückeneinheiten miteinander zu Donor-Brücke-Donor Dimere (X-B-X) verknüpft. Absorptions-, Fluoreszenzeigenschaften und die Transientenabsorption des ersten angeregten Zustandes der Dimere wurden mit denen der entsprechenden X-B Triarylamin-Monomere verglichen. Sowohl für die Monomere, als auch für die Dimere erhält man bilineare *Lippert-Mataga*-Diagramme. Dieser Sachverhalt deutet darauf hin, dass es, nach der Anregung, im ersten angeregten Zustand aller Verbindungen zu einer signifikanten Strukturänderung im polaren Medium kommt. Die angeregten Zustände der Dimere können als gemischtvalente Zustände verstanden werden, welche in Abhängigkeit der Brücke, unterschiedliche Wechselwirkungen (Kopplungen) aufweisen. Beim Vergleich der Fluoreszenzquantenausbeuten Φ der Monomere mit denen der entsprechenden Dimere stellt sich heraus, dass es nur im Falle schwacher und mittlerer elektronischen Kopplung zu einer starken Erhöhung von Φ im Dimer kommt (sog „superradiance"). Die Potentialhyperfläche

des ersten angeregten Zustandes der Dimere hat, in Abhängigkeit von der Kopplung und der Lösungsmittelpolarität, entweder nur ein Minimum oder zwei Minima. Im Falle eines Doppleminimums kommt es nach der optischen Anregung zu einer Relaxation in einen symmetriegebrochenen ladungsgetrennten Zustand. Dieser Zustand ist charakterisiert durch partielle Ladungsumverteilung vom Triarylamindonor zur Brücke und hat demzufolge partielle positive Ladung am Triarylamin und partielle negative Ladung an der Brücke. Das Dimer mit einer [2.2]Paracyclophan-Brücke zeigt eine geringe Kopplung, weshalb die optischen Eigenschaften dieses Dimers denen des entsprechenden *p*-Xylol-Monomers sehr ähnlich sind. Im Gegensatz dazu vermitteln die Anthracen- und auch die p-Xylol-Brücke stärkere Wechselwirkungen zwischen den beiden Triarylamin-Chromophoren, welche sich in dem signifikanten Einfluss auf die optischen Eigenschaften dieser Dimere widerspiegeln.

Im dritten Kapitel wurden die Absorptionseigenschaften von gemischtvalenten [2.2]Paracyclophanverbrückten Bis-triarylaminen X-B-X^{+} mit Hilfe eines GMH-Dreiniveau-modells (generalized *Mulliken-Hush*) ausgewertet. Dieses Modell berücksichtigt zum einen die Intervalenzladungstransferbande (IV-CT) welche auf einen optisch induzierten Lochtransfer von einem Triarylaminredoxzentrum, zum zweiten Redoxzentrum zurückzuführen ist. Zum anderen wird ein zweiter elektronischer Übergang berücksichtigt welcher durch den Lochtransfer vom Triarylamin zur entsprechenden Brücke (u.a. [2.2]Paracyclophan) charakterisiert ist (Brückenbande). Aus der GMH-Analyse ist zu schließen, dass bezüglich des intramolekularen Ladungstransfers die [2.2]Paracyclophan-einheit nicht der limitierende Faktor ist. Durch semiempirischen (AM1-CISD) Rechnungen stellte sich heraus, dass im [2.2]Paracyclophane Wechselwirkungen sowohl durch die σ-Bindungen (through-bond) als auch über die π-Systeme durch den Raum (through-space) für den Lochtransfer von Bedeutung sind. Diese elektronischen Wechselwirkungen sind zwar schwächer als im Falle von direkter π-Konjugation, aber die Größenordnung der elektronischen Kopplung lässt darauf schließen, dass „through-bond" und „through-space" Wechselwirkungen signifikant sind. Das bedeutet, dass die [2.2]Paracyclophaneinheit sich nicht wie eine gesättigte Brücke verhält, sondern eher wie eine ungesättigte Brücke. Es wurde ein exponentieller Zusammenhang zwischen der elektronischen Kopplung V und dem Abstand zwischen den beiden Redoxzentren gefunden. Daraus lässt sich zum einen folgern, dass der Lochtransfer über einen Superaustauschmechanismus erfolgt. Zum anderen lässt sich aufgrund der kleinen Abklingkonstante β für eine Reihe von π-konjugierten gemischtvalenten

Verbindungen erwarten, dass selbst bedeutend längere π-konjugierte Brücken noch eine signifikante Kopplung aufweisen.

Das Kapitel IV dieser Arbeit zeigt die Absorptionseigenschaften von den Dikationen der [2.2]Paracyclophanverbrückten Bis-triarylamine X^+-B-X^+ („Dimere"), welche bereits in Kapitel III in Form ihrer Monokationen vorgestellt wurden. Für die Interpretation der lokalen π-π* Anregungen und der elektronischen Ladungstransferübergänge (Brückenbande) wurde ein „Exciton-Coupling"-Modell verwendet, welches von den optischen Eigenschaften der entsprechenden „Molekülhälften" („Monomere") ausgeht. Mit Hilfe der experimentellen Übergangsmomente und Anregungsenergien und semiempirisch (AM1-CISD) berechneten Übergangsmomenten zwischen den beiden angeregten Zuständen μ_{ab} wurde eine Auswertung mit einem GMH-Dreiniveaumodell durchgeführt. Die daraus resultierende elektronische Kopplung ist ein Maß für die Wechselwirkungen innerhalb der angeregten gemischtvalenten CT-Zustände. Das GMH-Dreiniveaumodell konnte dahingehend modifiziert werden um klare Analogien zwischen GMH-Modell und Exciton-Coupling-Modell zu verdeutlichen. Dabei konnte gezeigt werden, dass das Übergangsmoment zwischen den beiden gemischtvalenten angeregten Zuständen des Dimers μ_{ab} der Dipolmomentsdifferenz $\Delta\mu_{12}^{(m)}$ des Grundzustandes und des CT-Zustandes des entsprechenden Monomers entspricht.

Im letzten Kapitel dieser Arbeit wurden die Ligandeneigenschaften von Thianthrenophan (**1**) bezüglich der Komplexierung von Silber(I)ionen untersucht. Eine Röntgenstrukturanalyse hat gezeigt, dass der Raum zwischen den beiden Thianthrenuntereinheiten groß genug ist, um Platz sowohl für kleine Moleküle als auch für kleine Ionen zu bieten. Die Komplexierung von Silber(I)perchlorat mit Thianthrenophane ergab eine Komplexierungskonstante von $\log K_1 = 5.45 \pm 0.13$ und die Komplexierung von Silber(I)perchlorat mit Thianthrene ergab $\log K_2 = 9.16 \pm 0.10$. Es wurden Ionentransportexperimente durch Flüssigmembranen mit jeweils zehn verschiedenen Metallsalzen gleichzeitig durchgeführt. Damit konnte gezeigt werden, dass Thianthrenophan eine hohe Selektivität bezüglich des Transports von Silber(I)ionen hat. Des Weiteren zeigte sich, dass die Transportraten von Thianthrenophan deutlich größer sind als die von Molekülen wie Thianthren und 1,4,8,11-Tetrathiacyclotetradecane. Eine Röntgenstrukturanalyse des Polymerkomplexes $[Ag(\mathbf{1})]ClO_4\bullet(dioxane)_7$ zeigt, dass Silber(I) von außen koordiniert (exohedral). Nichtsdestotrotz wird davon ausgegangen, ein endohedraler $[Ag(\mathbf{1})]^+$-Komplex (Ag^+ innen) ist die Erklärung für die ungewöhnliche Transportselektivität und für die außerordentlich hohe Transportrate von Silber(I)ionen in den Transportexperimenten mit Thianthrenophan als Carrier.

LEBENSLAUF

PERSÖNLICHE DATEN

Stephan Amthor

geboren am 04.08.1976 in Schweinfurt

verheiratet

SCHULE

07/1995	**Allgemeine Hochschulreife** am Regiomontanus-Gymnasium Haßfurt, Note 1.7

ZIVILDIENST

09/1995 - 09/1996	Kreiskrankenhaus Haßfurt, Internistische Station, Zivildienstleistender im Pflegedienst

STUDIUM

10/1996 – 12/2001	Studium der Chemie an der Universität Würzburg
10/1998	**Vordiplom**, Note 1.65
04/2001 – 12/2001	Diplomarbeit bei Prof. Dr. C. Lambert am Institut für Organische Chemie der Universität Würzburg: „Synthese und Charakterisierung Redoxaktiver Cyclophane"
12/2001	**Diplom**, Note 1.33
Seit 01/2002	Doktorarbeit bei Prof. Dr. C. Lambert am Institut für Organische Chemie der Universität Würzburg: „Redox Properties of Bis-triarylamines and Ligand Properties of Thianthrenophane"

AUSLANDSERFAHRUNG

03/2000 – 05/2000	Arbeitskreis Prof. Dr. Florin Dan Irimie, Institut für Chemie und Verfahrenstechnik, Babeş-Bolyai Universität, Klausenburg, Rumänien, Praktikum für Fortgeschrittene im Fach Biochemie: „Horseradish Peroxidase-Catalysed Oxidation of Penothiazines"

WEITERBILDUNG

11/1990 – 12/1990	Bayrisches Rotes Kreuz, Haßfurt, Sanitätsdienstausbildung
04/2002 – 07/2003	Zentrum für Sprachen, Universität Würzburg, Sprachkurs Rumänisch

PUBLIKATIONEN

Femtosecond Probing of the Excited State Absorption and Structural Relaxation in Biphenyl Derivatives, D. Mank, M. Raytchev, S. Amthor, C. Lambert, T. Fiebig, *Chem. Phys. Lett.* **2003**, *376*, 201-206.

Horseradish Peroxidase-Catalyzed Oxidation of Water-Insoluble Phenothiazines, R. Silaghi-Dumitrescu, S. Amthor, C. Paizs, C. Majdik, M. Tosa, P. Moldovan, A. Sas, L. Tamas, F. D. Irimie, *Studia Universitatis Babes-Bolyai, Chemia* **2003**, *48*, 165-170.

✶ **Synthesis and Ligand Properties of Thianthrenophane**, S. Amthor, C. Lambert, B. Graser, D. Leusser, C. Selinka, D. Stalke, *Org. Biomol. Chem.* **2004**, *2*, 2897-2901.

From Valence Trapped to Valence Delocalized by Bridge State Modification in Bis(triarylamine) Radical Cations: Evaluation of Coupling Matrix Elements in a Three-Level System, C. Lambert, S. Amthor, J. Schelter, *J. Phys. Chem. A* **2004**, *108*, 6474-6486.

How Delocalized is *N,N,N',N'*-Tetraphenylphianylenediamine Radical Cation? An Experimental and Theoretical Study on the Electronic and Molecular Structure, A. V. Szeghalmi, M. Erdmann, V. Engel, M. Schmitt, S. Amthor, V. Kriegisch, G. Nöll, R. Stahl, C. Lambert, D. Leusser, D. Stalke, M. Zabel, J. Popp, *J. Am. Chem. Soc.* **2004**, *126*, 7834-7845.

Two-Photon Absorption of Bis[4-(*N,N*-diphenyl-amino)phenylethynyl]arenes, B. Strehmel, S. Amthor, J. Schelter, C. Lambert, *ChemPhysChem* **2005**, *6*, 893-896.

✶ **UV/Vis/NIR Spectral Properties of Triarylamines and their Corresponding Radical Cations**, S. Amthor, B. Noller, C. Lambert, *Chem. Phys.* **2005**, *316*, 141-152.

Electronic Coupling in Tetra-anisylarylendiamin Mixed-Valence Systems: The Interplay between Bridge Energy and Geometric Factors, C. Lambert, C. Risko, V. Coropceanu, J. Schelter, S. Amthor, N. E. Gruhn, J. Durivage, J.-L. Brédas, *J. Am. Chem. Soc.* **2005**, *127*, 8508-8516.

✶ **[2.2]Paracyclophane Bridged Mixed-Valence Compounds: Application of a GMH Three-Level Model**, S. Amthor, C. Lambert, 2005, manuscript submitted to *J. Phys. Chem. A*.

✶ **Dications of Bis-triarylamino-[2.2]paracyclophanes: Evaluation of Excited State Couplings by GMH Analysis**, S. Amthor, C. Lambert, 2005, manuscript submitted to *J. Phys. Chem. A*.

✶ **Excited Mixed-Valence States of Symmetrical Donor-Acceptor-Donor π-Systems**, S. Amthor, S. Dümmler, I. Fischer, C. Lambert, J. Schelter, 2005, manuscript submitted to *J. Phys. Chem. A*.

DANKSAGUNG

Besonderer Dank gebührt den Mitgliedern des Arbeitskreises Lambert für das angenehme Arbeitsklima, insbesondere gilt mein Dank:

Hongchao Li, für die Vermittlung chinesischer Kultur.

Jürgen Schelter, für die Bereitstellung der Anthracenverbindungen in Kapitel II, für die Unterstützung bei Problemen mit Messungen aller Art und für die Hilfe bei auftretenden Computerproblemen.

Volker Kriegisch, für seine stete Hilfsbereitschaft, für die Organisation unserer AK-Ausflüge, für die Grillabende bei ihm, bzw. natürlich auch unseren AK-Feiern, für die er wohl auch meist einen großen organisatorischen Beitrag geleistet hat.

Rainer Stahl, für Hilfestellung bei elektrochemischen Problemen jeglicher Art und unter anderem für die Diskussion über das Exciton-Coupling Modell, welche letzten Endes zu einem besseren Verständnis der Theorie beigetragen hat.

Marco Holzapfel, unserem skeptischen „Ex-Lehrämtler", für die Unterstützung bei Problemen mit dem Fluoreszenzspektrometer, das Korrekturlesen und die gute Zusammenarbeit.

Sascha Heckmann, für das Korrekturlesen und für sein stetiges Bedürfnis uns im AK auf amüsante Weise zu unterhalten; er hatte jederzeit einen lehrreichen Schwank aus seinem Leben auf Lager. Ich bin mir sicher, er konnte fast alle davon überzeugen, dass Mett einfach besser ist als Tofu.

Barbara Geiß, für die Organisation vieler AK-Feiern sowie für die erfolgreiche „Fortsetzung" des Institutsausflug 2005. Ohne sie wären wir sicher nach dem offiziellen Ende der Weinprobe schnell auf dem Trockenen gesessen.

Dirk Rausch, für die zusätzliche Steigerung des Institutsausflugs 2005 in seiner WG, ich hoffe, er darf dort noch etwas wohnen bleiben und bekommt keine Probleme mit dem Vermieter wegen Beschwerden wegen des „Rufens" aus seinem Fenster.

Simone Krakert, unserer Lehrämtlerin, für die Kneipentour in Friedberg und natürlich für die badischen Weine, die sie für unsere Weinprobe mitgebracht hat. Ich hoffe, sie bringt aus ihrem australischen Exil auch ein paar gute Tropfen mit.

Christian Müller, *Dörte Nowak*, *Conrad Kaiser*, unseren Diplomanden, für die gute Zusammenarbeit im AK.

Roswitha Scheblein, für die Synthese unter anderem von Katalysatoren und Leitsalz für die Elektrochemie und natürlich für die Destillation von Hektolitern an Lösungsmitteln.

Ganz besonders danke ich an dieser Stelle meiner Familie und insbesondere meiner Frau *Patricia* für ihre volle Unterstützung und das Korrekturlesen.

ERKLÄRUNG

Hiermit erkläre ich an Eides statt, dass ich die Dissertation „Redox Properties of Bis-triaryl-amines and Ligand Properties of Thianthrenophane" selbstständig angefertigt und keine anderen als die von mir angegebenen Quellen und Hilfsmittel benutzt habe.

Ich erkläre außerdem, dass diese Dissertation weder in gleicher oder anderer Form bereits in einem anderen Prüfungsverfahren vorgelegen hat.

Ich habe früher außer den mit dem Zulassungsgesuch urkundlich vorgelegten Graden keine weiteren akademischen Grade erworben oder zu erwerben versucht.

Würzburg, den 11. Oktober 2005